

Novel Therapeutic Approaches for Cancer Therapy Based on Targeting the Human
DNA Repair Enzyme Polynucleotide Kinase/Phosphatase

by

Zahra Shire

A thesis submitted in partial fulfillment of the requirements for the degree of

Doctor of Philosophy

in

Experimental Oncology

Department of Oncology
University of Alberta

© Zahra Shire, 2018

Abstract

The relentless growth of tumors is triggered by a complex array of molecular changes such as DNA damage, disruption of cell-cycle progression, uncontrolled proliferation and escaping cell death. Various therapies have been developed to treat cancer, many of which kill cancer cells by damaging their DNA. DNA damage in cells, including DNA strand breaks, are caused by endogenous agents, mainly reactive oxygen species (ROS), and exogenous sources such as ionizing radiation (IR) and topoisomerase poisons, such as irinotecan. Clinical evidence indicates that DNA repair is a major cause of cancer resistance. Therefore, attack on DNA repair processes renders cancer cells more sensitive to radiotherapy and DNA damage chemotherapy.

Targeting DNA repair enzymes is one approach to overcome resistance in cancer. DNA strand breaks, major lesions generated by ROS, IR and irinotecan, are lethal to cells if not repaired. The 3'- and 5'- termini of the DNA strand breaks are often modified and do not present the correct termini for completion of DNA repair. Among the frequently generated modifications are 3'-phosphate and 5'-hydroxyl termini. Human polynucleotide kinase/phosphatase (PNKP), a bifunctional DNA repair enzyme which phosphorylates DNA 5'-termini and dephosphorylates DNA 3'-termini, can process the unligatable DNA termini. Moreover, cancer cells depleted of PNKP show significant sensitivity to ionizing radiation and chemotherapeutic drugs such as irinotecan. Initial screening for the first generation of small molecule inhibitors of PNKP phosphatase activity identified A12B4C3, an imidopiperidine compound, which enhanced the radio- and chemosensitivity of lung and breast cancer cells. Based on these findings, we intended to identify more potent

PNKP phosphatase inhibitors than A12B4C3 and design suitable nanoparticles to target inhibitors to cancer cells.

First, we developed a novel fluorescence-based assay in order to screen a second generation of imidopiperidine compounds. This resulted in the identification of A12B4C50 and A83B4C63, which are more potent inhibitors than A12B4C3. In addition, we screened new compounds from a natural derivative library, which resulted in the identification of two new promising 3'-phosphatase inhibitors, N12 and O7. The novel assay was used to determine the IC₅₀ values of the newly identified inhibitors. Kinetic analysis revealed that A83B4C63 acts as a non-competitive inhibitor, whereas N12 acts as an uncompetitive inhibitor.

To test the hypothesis that nano-encapsulation would enhance the effectiveness of the newly identified imidopiperidine-based 3'-phosphatase inhibitors in a cellular context, a series of experiments was carried out with A12B4C50 and A83B4C63. First we examined the retention of the inhibitors by polymeric micelles of different poly(ethylene oxide)-*b*-poly(ester) based structures to determine suitable encapsulation media for each inhibitor. Cellular studies revealed that encapsulated A12B4C50 and A83B4C63 sensitized HCT116 cells to γ -radiation and irinotecan. Furthermore, the encapsulated inhibitors were capable of inducing synthetic lethality in phosphatase and tensin homolog (PTEN)-deficient HCT116 cells. In addition, actively targeted delivery of nano-encapsulated inhibitors to colorectal cancer cells overexpressing epidermal growth factor receptor (EGFR) was achieved by attachment of the peptide GE11 on the surface of polymeric micelles. Preliminary studies with a human xenograft model in nude mice indicated that

encapsulated A83B4C63 has the capacity to treat PTEN deficient tumors as a monotherapeutic agent.

Finally, investigation of the potential site of binding of 3'-phosphatase inhibitors to PNKP was determined by photoaffinity crosslinking method coupled with liquid chromatography-mass spectrometry technique (LC/MS/MS). The photoactivatable PNKP inhibitors A95B4C50, A95B4C3 and A12B4C67 revealed three distinct binding sites located in both the kinase and phosphatase domain of PNKP.

PREFACE

- Chapter 1 provides a brief introduction about PNKP mechanisms and characteristics, DNA double and single strand break repair pathways, synthetic lethality and targeted drug delivery using polymeric micelles.
- Chapter 2 describes original work performed by Zahra Shire. No part of this thesis has been previously published. Most of the experiments and manuscript preparation were designed and conducted by Zahra Shire under the supervision of Dr. Michael Weinfeld. Dr. Linda Reha-Krantz provided valuable advice as well as phage T4 DNA polymerase. Synthesis of the imidopiperidine compounds was performed by Dr. Timothy Morgan in Dr. Dennis Hall's laboratory. Binding assays were performed by Dr. Rajam S. Mani (Figure 2.9). The inhibitors' *in vitro* specificity analysis was performed by Dr. Phuwadet Pasarj in Dr. Charles Holmes' laboratory (Figure 2.11). Finally, the DNA kinase assay was performed by Mr. Mesfin Fanta (Figure 2.12).
- Chapter 3 describes original work conducted by Zahra Shire and recently submitted to Molecular Pharmaceutics, "Nano-encapsulation of novel inhibitors of PNKP for selective sensitization to ionizing radiation and irinotecan and induction of synthetic lethality". All the experiments and manuscript preparation were designed and performed by Zahra Shire under the supervision of Dr. Michael Weinfeld and Dr. Afsaneh Lavasanifar. Synthesis of the imidopiperidine compounds was performed by Dr. Timothy Morgan in Dr. Dennis Hall's laboratory. Dr. Vakili assisted in the synthesis of functionalized PEG.
- Chapter 4 describes original work conducted by Zahra Shire. No part of this chapter has been previously published. All the experiments and manuscript preparation were

designed and conducted by Zahra Shire under the supervision of Dr. Michael Weinfeld. Synthesis of the imidopiperidine compounds was performed by Dr. Timothy Morgan in Dr. Dennis Hall's laboratory. Dr. Rajam S. Mani conducted the binding assays (Figure 4.1). Dr. Mark Glover assisted in generating the structural analysis figure displaying the binding sites of the photoactivatable PNKP inhibitors (Figure 4.11).

- In Chapter 5, we summarize the three main topics of this thesis (i) the significance of developing small molecule inhibitors of DNA repair enzymes including PNKP, (ii) synthetic lethality and its role in personalized treatment, (iii) targeted delivery of small molecule inhibitors. We also discuss future experimental procedures required to optimize and complement work done in this thesis. Finally, we mention briefly a preliminary collaborative pre-clinical study in mice carried out by Zahra Shire and Sams Sadat under the supervision of Dr. Afsaneh Lavasanifar and Dr. Michael Weinfeld.

Dedication

All thanks and praises are due to Allah the most gracious the most merciful for granting me patience and strength. For my father Jama Hussein Shire and my mother Halimo Abdullah Arshe for all their support and patience during my PhD studies

Acknowledgments

To my family, especially my parents, I am grateful for your patience and great support over the past 5 years. Achieving a PhD degree would not have been possible without your help and encouragement.

Furthermore, I would like to thank Dr. Feridoun Karimi-Busheri, Dr. Rajam Mani, Dr. Aghdass Rasouli-Nia, Dr. Mohammad Reza Vakili, Mr. Mesfin Fanta and Mrs. Xiaoyan Yang for their guidance and technical support throughout my research project. Without your help this project would not have been easy. In addition, I would like to thank Mr. Ed Fu and Mr. Bela Reiz, Department of Chemistry, for their great technical support.

I would also like to thank the Alberta Cancer Foundation, Canadian Institutes of Health Research and EIRR21 Fellowship for their tremendous help in funding our research, which is focused on enhancing the treatment of colon cancer to benefit cancer patients and make an impact here in Alberta and Canada.

Finally, I would like to express my special gratitude for my advisors Dr. Michael Weinfeld and Dr. Afsaneh Lavasanifar. I am very grateful to be part of your wonderful team, and I am grateful for your guidance and support on my projects. You are humble, patient and great scientists. I couldn't have asked for better mentors. I would also like to thank my supervisory committee members, Dr. Mary Hitt and Dr. Armin Gamper for their continued advice and guidance throughout my studies.

Table of Contents

Chapter 1: Introduction	1
1.1 DNA damage and repair	3
1.1.1 Single-strand break repair (SSBR)	5
1.1.1.1 Base excision repair pathway (BER)	8
1.1.1.2 Topoisomerase-I poisoning induces SSBs	8
1.1.2 Double-strand break repair (DSBR)	9
1.1.2.1 Nonhomologous end-joining (NHEJ): classic and alternative pathways....	10
1.2 Polynucleotide kinase / phosphatase (PNKP): structure and key interactions	12
1.2.1 Catalytic activities of PNKP	13
1.2.2 Physiological importance of PNKP increased its clinical interest.....	18
1.3 Small molecule inhibitors, novel drugs to overcome resistance of conventional cancer treatment	19
1.4 A12B4C3: a first-generation inhibitor of the DNA repair enzyme PNKP	22
1.5 Synthetic lethality: The application of PNKP inhibitors as monotherapeutic in the context of cancer therapy	24
1.6 The role of nanoparticles in drug delivery.....	32
1.6.1 Polymeric micelles.....	34
1.7 Epidermal growth factor receptor (EGFR), a clinical target for anti-cancer therapy	39
1.7.1 GE11: a novel peptide ligand targeting EGFR.....	41
1.8 Colorectal cancer: the role of damage and repair of DNA in disease progression and treatment.....	43
1.9 Hypothesis and scope of the thesis	46
Chapter 2: Identification and characterization of new inhibitors of the 3'-phosphatase activity of human polynucleotide kinase/phosphatase	49
2.1. Introduction	53
2.2. Experimental procedures.	55
2.2.1 Materials.....	55
2.2.2. Synthesis of polysubstituted imidopiperidine compounds	56
2.3. Methods	60

2.3.1. Fluorescence-based assay for screening small molecules inhibitors of the 3'-phosphatase activity of PNKP	60
2.3.2. Determination of binding constants to PNKP.....	60
2.3.3. Mechanism of inhibition-Lineweaver-Burk Plot.....	61
2.3.4. Testing possible protein phosphatase inhibition by PNKP inhibitors	62
2.3.5. Conventional radio-gel assay to detect PNKP 5'-kinase activity.....	62
2.3.6. Statistical analysis	63
2.4. Results	63
2.4.1. Test for the exonuclease and phosphatase activities of the DNA polymerase and PNKP with the 2-Ap hairpin probes.....	63
2.4.2. Screening small molecule inhibitors with the fluorescence-based assay.....	67
2.4.3. Measurement of IC ₅₀ values	70
2.4.4. Measurements of K _d values.....	74
2.4.5. Mechanism of inhibition of PNKP phosphatase activity by inhibitors.....	74
2.4.6. Specificity of inhibitors.....	77
2.4.7. The effect of PNKP phosphatase inhibitors on the kinase activity.....	77
2.5. Discussion.....	80
2.6. Acknowledgements	82
Chapter 3: Nano-encapsulation of novel inhibitors of PNKP for selective sensitization to ionizing radiation and irinotecan and induction of synthetic lethality.....	83
3.1. Introduction	87
3.2. Materials and methods.....	91
3.2.1. Materials.....	91
3.2.2. Cell lines.....	91
3.2.3. Synthesis of polysubstituted imidopiperidine compounds	92
3.2.4. Synthesis of block copolymers	92
3.2.5. Synthesis and characterization of GE11-PEO- <i>b</i> -PBCL conjugates.....	93
3.2.6. Characterization of the prepared block copolymers and polymeric micelles	94

3.2.7. <i>In vitro</i> release of encapsulated PNKP inhibitors.....	95
3.2.8. Cell proliferation assay	95
3.2.9. Clonogenic survival assay	96
3.2.10. Determination of polymeric micellar uptake by different colorectal cancer cells.....	96
3.2.11. Statistical analysis	98
3.3. Results	99
3.3.1. Polymer synthesis and micelle characterization	99
3.3.2. <i>In vitro</i> release of PNKP inhibitors from polymeric micelles	99
3.3.3. Inhibition of cell growth by the hit PNKP inhibitors and their polymeric micellar formulations.....	101
3.3.4. Cellular radio- and chemosensitization by PNKP inhibitors.....	101
3.3.5. <i>In vitro</i> release of PNKP inhibitors from GE11-conjugated polymeric micelles	104
3.3.6. Cellular uptake of encapsulated compounds.....	104
3.3.7. Cellular radio- and chemosensitization by PNKP inhibitors encapsulated in GE11-conjugated micelles.	107
3.3.8. Synthetic lethal targeting of PTEN-deficient cancer cells using encapsulated PNKP inhibitors.....	108
3.4. Discussion.....	112
3.5. Acknowledgements	116
Chapter 4: Identification of binding sites of small molecule inhibitors of polynucleotide kinase/phosphatase by photoaffinity labeling-mass spectrometry	117
4.1. Introduction	122
4.2. Experimental procedures	126
4.2.1. Materials.....	126
4.2.2. Methods.....	126
4.2.2.1. Synthesis of components of photoactivatable PNKP inhibitors A95 component	126
4.2.2.2. Determination of binding constants of PNKP photolabelled inhibitors	131

4.2.2.3. Fluorescence-based assay for detecting activity of photoactivatable inhibitors of the 3'-phosphatase activity of PNKP	132
4.2.2.4. Photocrosslinking of ligand-PNKP mixture	132
4.2.2.5. In-solution digestion of ligand-modified PNKP	133
4.2.2.6. Purification of ligand-modified PNKP	133
4.2.2.7. LC-MS/MS analysis	133
4.3. Results	134
4.3.1. Measurement of K_d values	134
4.3.2. Biochemical evaluation of the photoaffinity probes.....	135
4.3.3. Identification of the binding sites by tandem mass spectrometry	140
4.3.3.1. A95B4C50	140
4.3.3.2. A95B4C3	145
4.3.3.3. A12B4C67	149
4.4. Discussion	153
4.5. Acknowledgements	157
Chapter 5: Discussion and future work	158
5.1. Discussion	160
5.1.1. The promise of targeted therapy: small molecule inhibitors	160
5.1.2. Synthetic lethality, a revolution in the era of personalized treatment.....	162
5.1.3. Targeted delivery of small molecule inhibitors.....	164
5.2. Future work	167
5.2.1. Optimization of lead compounds, A12B4C50 and A83B4C63.....	167
5.2.2. Purification of N12 mixture is needed to identify the active component.....	167
5.2.3. Monitoring the interaction of small molecule inhibitors with PNKP inside living cells	168
5.2.4. Identification of the mechanism responsible of the synthetic lethality partnership between PTEN and PNKP	170
5.2.5. Identification of binding sites of inhibitors to PNKP	171
5.2.6. Pre-clinical study of PNKP 3'-phosphatase inhibitors: preliminary results and future work	172
5.3. Significance	174

References	177
Appendix: Supplementary material	241

List of Schemes

2.1	Mechanism of synthesis of polysubstituted imidopiperidines	58
4.1	Photochemistry of benzophenone	124
4.2	Photoactivatable PNKP inhibitors used in this study	125

List of Tables

1.1	Chemical structure of the three poly(ethylene glycol)- <i>block</i> -poly(ester)s used in this thesis	38
2.1	Chemical structure of the newly found PNKP inhibitors	59
3.1	Characteristics of the polymeric micelles under study (n=3) determined by dynamic light scattering.....	90
4.1	Induced fragments of unmodified and modified peptides after photoreaction with A95B4C50	143
4.2	Induced fragments of unmodified and modified peptides after photoreaction with A95B4C3.....	147
4.3	Induced fragments of unmodified and modified peptides after photoreaction with A12B4C67	151

List of Figures

1.1	DNA damage and repair mechanisms	4
1.2	The mechanism of BER	7
1.3	Classical NHEJ pathway	11
1.4A	Crystallographic structure of a murine PNKP	14
1.4B	DNA binding modes to murine PNKP	16
1.5	Catalytic reactions of PNKP	17
1.6	The causes of resistance to anti-cancer drugs	21
1.7	Drug design and development stages	23
1.8	The structure of the first generation PNKP inhibitor, A12B4C3	25
1.9	The concept of synthetic lethality	26
1.10	Synthetic lethal partnership between PARP and BRCA	28
1.11	The role of PTEN in the cytoplasm and nucleus	29
1.12	Clonogenic survival assay of HCT116 cells deficient in PTEN	31
1.13	Enhanced permeability and retention (EPR) effect	33
1.14	Different shapes and designs of nanoparticles currently used in cancer therapy	35
1.15	Micellization and drug loading by self-assembly of block-copolymers in aqueous solution	36
1.16	EGFR biology	40
1.17	The chemical structure of GE11 peptide	42
1.18	Multiple major mutations occur in CRC that lead to disease progression	44
2.1	(A) The structure of the hairpin probes used for the screening assay (B) The structure of 2-Amino-9-(β -D-2-deoxyribofuranosyl purine) (2-Ap)	57
2.2	Schematic diagram of the function of the novel fluorescence assay for the 3'-phosphatase activity of PNKP	64
2.3	The hydrolysis of hairpin probes treated with DNA polymerases and PNKP	66
2.4	The effect of A12B4C3 and A70B4C3 on PNKP activity	68
2.5	The effect of A12B4C50 and A83B4C63 on PNKP activity	69

2.6	The effect of different small molecules from library of 200 natural product derivatives on PNKP activity	71
2.7	The effect of N12 and O7 on PNKP activity	72
2.8	Dose dependent inhibition of PNKP by inhibitors	73
2.9	A plot of fluorescence intensities of titration of PNKP.....	75
2.10	Lineweaver-Burk analysis of the inhibition of PNKP phosphatase activity using varying concentrations of A83B4C63, N12 and 20-mer 3'-phosphorylated substrate ...	76
2.11	A ctivity of PNKP inhibitors against three protein phosphatases, PP-1c, aspartate-based ubiquitous Mg ²⁺ -dependent phosphatase (AUM) and calcineurin (CAN).....	78
2.12	DNA kinase assay	79
3.1	TEM of loaded polymeric micelles.....	100
3.2	<i>In vitro</i> release from dialysis tubing (MWCO 3.5 kDa) for free versus encapsulated (A) A12B4C50 and (B) A83B4C63 in aqueous solution at 37°C	102
3.3	<i>In vitro</i> cytotoxicity of (A) A12B4C50 and (B) A83B4C63 measured by MTS assay after 72 h of drug incubation at 37°C	103
3.4	Radio/chemosensitization by free and encapsulated A12B4C50 or A83B4C63 .	105
3.5	<i>In vitro</i> release from dialysis tubing (MWCO 3.5 kDa) of (A) A12B4C50, (B) A83B4C63 and (C) Dil.....	106
3.6	Cellular uptake of Dil-encapsulated polymeric micelles.....	109
3.7	Radio/chemosensitization of HCT116 wild-type cells by A12B4C50 and A83B4C63 encapsulated in GE11-PEO- <i>b</i> -PCCL and GE11-PEO- <i>b</i> -PBCL, respectively	110
3.8	Clonogenic survival assays of PTEN-deficient cells treated with encapsulated PNKP inhibitors.....	111
4.1	A plot of fluorescence intensities of titration of PNKP with (A) A95B4C50, (B) A95B4C3 and (C) A12B4C67.....	136
4.2	The effect of A95B4C50 on PNKP activity. (A) Hairpin HPP was incubated with both PNKP (25 nM) and T4 pol	137
4.3	The effect of A95B4C3 on PNKP activity. (A) hairpin HPP was incubated with both PNKP & T4 pol	138
4.4	The effect of A12B4C67 on PNKP activity. (A) hairpin HPP was incubated with both PNKP & T4 pol	139

4.5	Sequence coverage of PNKP in the presence or absence of A95B4C50 determined by ProteinScape software	141
4.6	Mass spectra of digested-PNKP peptide PANWAPGR	144
4.7	Sequence coverage of PNKP in the presence or absence of A95B4C3 determined by ProteinScape software	146
4.8	Mass spectrum of digested-PNKP peptide LLVFTAAGVK modified by A95B4C3	148
4.9	Sequence coverage of PNKP in the presence or absence of A12B4C67 determined by ProteinScape software	150
4.10	Mass spectra of digested-PNKP peptide STFLK.....	152
4.11	The structure of PNKP catalytic domains and the location of the target-binding sites of A95B4C50 (294-301), A95B4C3 (153-162) and A12B4C67 (379-383).....	156
5.1	PTEN is a predictive biomarker for the outcome of monoclonal antibodies targeting EGFR therapy in mCRC patients	165
5.2	Schematic diagram of approaches suggested to monitor PNKP-inhibitor interactions inside living cells	169
5.3	Tumor volume curve.....	175
5.4	Mean body weight–time profile of NIH-III nude mice	176
A1	Time course for monitoring the activity of T4 polymerase by varying the concentration of enzyme from 0.005 to 0.2 μ M.....	242
A2	Time course for monitoring the activity of PNKP by varying the concentration of enzyme from 0.005 to 0.2 μ M	243
A3	Fluorescence Intensities of 200 nM 2-Ap (open circles) and 200 nM HPOH (filled circles).....	244
A4	Dose dependent inhibition of PNKP by inhibitor A12B4C3	245
A5	Chromatogram of N12 dissolved in DMSO under storage of room temperature	246
A6	NMR Spectra of A12B4C50	247
A7	NMR Spectra of A83B4C63	249
A8	¹ H NMR spectrum of PEO- <i>b</i> -PCL block copolymer in CDCl ₃ and peak assignments	251

A9	^1H NMR spectrum of PEO- <i>b</i> -PBCL block copolymer in CDCl_3 and peak assignments	252
A10	^1H NMR spectrum of PEO- <i>b</i> -PCCL block copolymer in CDCl_3 and peak assignments	253
A11	^1H NMR spectrum of act-PEO- <i>b</i> -PCCL block copolymer in CDCl_3 and peak assignments	254
A12	^1H NMR spectrum of act-PEO- <i>b</i> -PBCL block copolymer in CDCl_3 and peak assignments	255
A13	Life cell fluorescence microscopy images of A12B4C50 accumulation in HCT116 after 4 h incubation.....	256

List of Abbreviations

AML	Acute myeloid leukemia
AOA4	Ataxia-ocular motor apraxia 4
AP	Abasic (apurinic/aprimidinic)
2-Ap	2-Amino-9-(β -D-2-deoxyribofuranosyl) purine
APC	Adenomatous polyposis coli
APE-1	AP endonuclease-1
APTX	Aprataxin
ATM	Ataxia telangiectasia mutated
ATXN3	Ataxin-3
AUM	Aspartate-based ubiquitous Mg^{2+} -dependent phosphatase
BER	Base excision repair
Bp	Benzophenone
CAN	Calcineurin
CIMP	CpG island methylator phenotype
CIN	Chromosomal instability
CK2	Casein kinase 2
CMC	Critical micelle concentration
CML	Chronic myeloid leukemia
CRC	Colorectal cancer
CsA	Cyclosporine A
DDR	DNA damage response
Dil	1,1'-Dioctadecyl-3,3,3',3'-tetramethylindocarbocyanine perchlorate
DLS	Dynamic light scattering
DNA PKcs	DNA-dependent protein kinase catalytic subunit
DSBs	Double-strand breaks
DSBR	Double-strand break repair
DTT	Dithiothreitol
EGFR	Epidermal growth factor receptor
EPR	Enhanced permeability and retention

EtOAc	Ethyl acetate
FHA	Forkhead associated domain
FRET-FLIM	Fluorescence resonance energy transfer - fluorescence lifetime imaging microscopy
HAD	Haloacid dehalogenase superfamily
HPLC	High-performance liquid chromatography
HR	Homologous recombination
IC ₅₀	the concentration of an inhibitor which causes 50% reduction of enzyme activity
IR	Ionizing radiation or infrared spectroscopy
iRGD	Tumor-internalizing RGD peptide
K _d	The measurement of the affinity constant
LC/MS	Liquid chromatography-mass spectrometry
LET	Linear energy transfer
Lig3/4	DNA ligase 3/4
MCSZ	Microcephaly, seizures and developmental delay
mCRC	Metastatic colorectal cancer
MDR	Multiple drug resistance
MGMT	O ⁶ -methylguanine-DNA methyltransferase
MH	Microhomology
MMR	Mismatch repair
MSI	Microsatellite instability
MWCO	Molecular weight cut-off
NEIL	Endonuclease VIII-like
NHEJ	Nonhomologous end-joining
NIS	Sodium iodide symporter
NMR	Nuclear magnetic resonance
PARP-1/2	Poly(ADP-ribose) polymerase-1/2
PDI	Polydispersity index
PEG	Polyethylene glycol

PEG- <i>b</i> -PBCL	Poly(ethylene glycol)- <i>block</i> -poly(α -benzyl carboxylate- ϵ -caprolactone)
PEG- <i>b</i> -PCL	Poly(ethylene glycol)- <i>block</i> -poly(ϵ -caprolactone)
PEG- <i>b</i> -PCCL	Poly(ethylene glycol)- <i>block</i> -poly(α -carboxyl- ϵ -caprolactone)
PEI-PEG	Polyethyleneimine-polyethyleneglycol
PIP2	Phosphatidylinositol 4,5-bisphosphate
PIP3	Phosphatidylinositol (3,4,5)-trisphosphate
PLGA	Poly(lactide-co-glycolide)
PNKP	Polynucleotide kinase/phosphatase
PP-1c	Protein phosphatase 1 catalytic subunit
Pol	Polymerase
PTEN	Phosphatase and tensin homolog
PUA	Phosphor- α,β -unsaturated aldehyde
RES	Reticuloendothelial system
ROS	Reactive oxygen species
SCA3	Spinocerebellar ataxia type 3 SCA3
SHP-1	Protein tyrosine phosphatase
SSBs	Single-strand breaks
SSBR	Single-strand break repair
Tdp1	Tyrosyl-DNA phosphodiesterase
TEM	Transmission electron microscopy
Top I	Topoisomerase I
UV	Ultraviolet
XLF	XRCC4-like factor
XRCC1/4	X-ray repair cross-complementing group

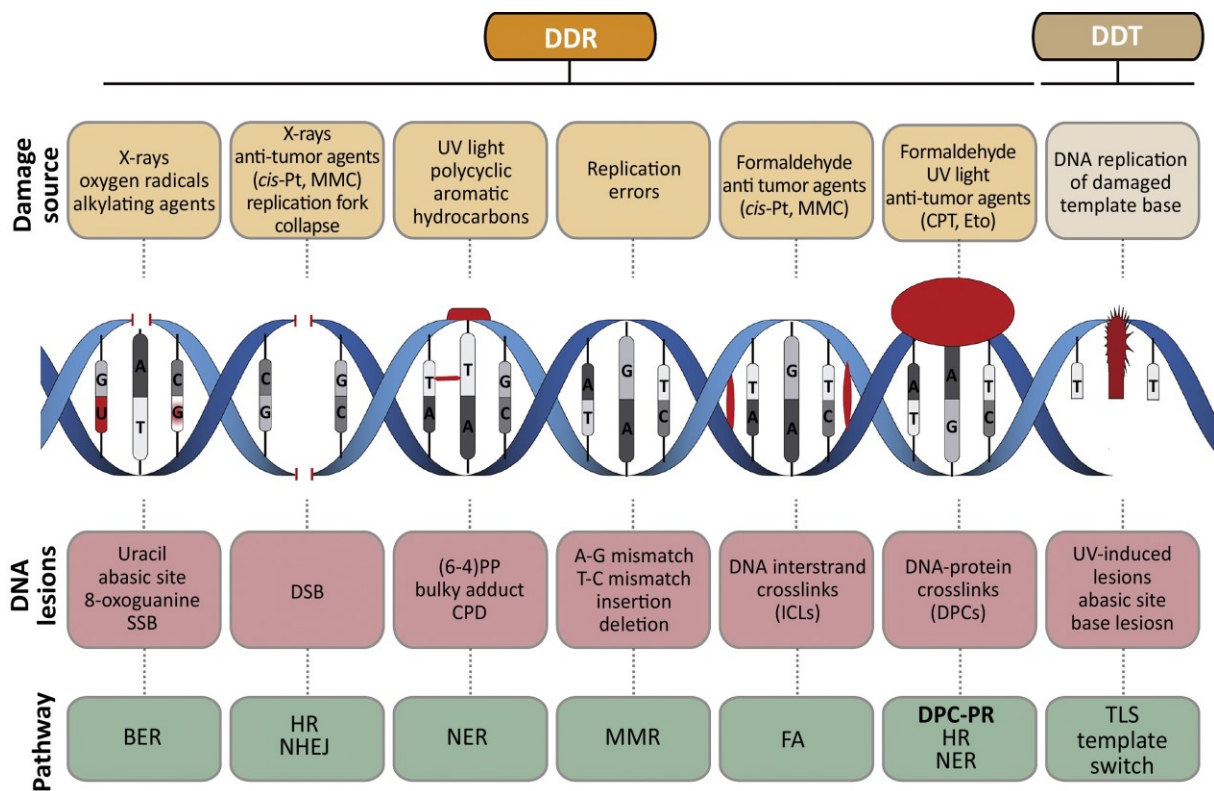
Chapter 1: Introduction

Overview:

In this chapter we provide a summary of PNKP structural analysis, mechanisms and characteristics, DNA double and single strand break repair pathways, the benefits of using small molecule inhibitors for cancer therapy, synthetic lethality and targeted drug delivery using polymeric micelles.

1.1. DNA damage and repair

Daily exposure to environmental stressors, radiation, chemotherapeutic drugs, inflammation, and DNA metabolism all lead to the production of cytotoxic and mutagenic DNA lesions¹⁻³. Fortunately, efficient DNA repair mechanisms protect the DNA by either removing or tolerating the damage to ensure overall survival (Fig. 1.1). Deficiency in the repair of DNA damage is known to lead to elevated cancer risk, neurological disorders and aging⁴⁻⁶. The DNA damage response (DDR) is a complex of protein networks responsible for the identification and repair of disruptions in DNA structure⁷. This organized complex network senses and responds to these DNA lesions by inducing cell-cycle arrest, DNA repair or apoptosis⁸. In this thesis, single-strand break repair (SSBR) via base excision repair (BER), and topoisomerase I (Top I) inhibitor single-strand break repair and double-strand break repair (DSBR) via the nonhomologous end-joining (NHEJ) pathway will be discussed with an emphasis on the enzyme, human polynucleotide kinase/phosphatase (PNKP). This protein plays an important role in restoring the chemical structure at DNA ends, so that they can serve as substrates for DNA polymerases and ligases to allow the extension and ligation of the broken strand(s).



Trends in Biochemical Sciences

Figure 1. 1. DNA damage and repair mechanisms. Upper panel, different endogenous and exogenous agents that generate different types of DNA damage. Lower panel, DNA repair mechanisms needed to repair the different types of DNA lesions. **Vaz et al. Trends Biochem Sci. 2017 Jun;42(6):483-495. Reused with permission from Trends in Biochemical Sciences**

1.1.1. Single-strand break repair (SSBR)

Single-strand breaks (SSBs) often encompass the disintegration of a single nucleotide, and damaged 5'- and/or 3'-termini ⁹. Typical sources of SSBs include spontaneous hydrolysis, leading to the formation of abasic (or apurinic/aprimidinic, AP) sites and further hydrolysis, and oxidative damage by endogenous reactive oxygen species (ROS) and ionizing radiation ¹⁰. SSBs can also be generated as intermediates of Endonuclease VIII-like (NEIL) - mediated BER and they can also arise as a result of chemical inhibition of cellular enzymes such as Top I ^{2, 10-14}. IR and free radicals generate two primary end groups at the 3'-termini, phosphate, which is processed by PNKP ¹⁵, and phosphoglycolate, which is usually handled by AP endonuclease (APE1) ^{2, 15}. The primary end group at the 5'-termini is phosphate, but up to 15% is 5'-hydroxyl groups, which are handled by PNKP ¹⁵. On the other hand, damage by Top I inhibitors generates 3'-phosphate and 5'-OH termini. The removal of damaged bases by DNA glycosylases, which possess an AP lyase activity, can also generate 3'-phosphate and 5'-phosphate termini ¹⁵.

SSBs are considered a serious threat to genetic stability and cell survival. If not repaired rapidly, SSBs occur at a substantially higher frequency than double-strand breaks (DSBs) ¹⁶. Most SSBs are repaired by a global SSBR process that can be divided into four basic steps; SSB detection, DNA end processing, DNA gap filling, and DNA ligation: (i) SSB detection is primarily mediated by poly(ADP-ribose) polymerase-1 (PARP-1) and (PARP-2), which are critical for recruitment of X-ray repair cross-complementing group 1 protein, XRCC1 and PNKP ¹⁶⁻¹⁹. XRCC1 is a scaffold protein required for the assembly of the other proteins at the site of DNA damage within the cell

such as PNKP, DNA polymerase β (Pol β), and DNA ligase III (Lig3). It has been shown previously that XRCC1 can stimulate both the 3'-phosphatase and 5'-kinase activities of PNKP and this stimulation is triggered by phosphorylation of a cluster of three CK2 phosphorylation sites at Ser518, Thr519, Thr523 in XRCC1 and high-affinity binding to the forkhead associated (FHA) domain of PNKP²⁰⁻²³. Non-phosphorylated XRCC1 can also stimulate PNKP activity through a lower-affinity interaction with the catalytic domain of PNKP, and recent data have led to speculation that in cells XRCC1 is initially tethered to PNKP through the phosphorylation-dependent interaction followed by a shift to the low-affinity interaction to stimulate activity^{24, 25}. (ii) DNA end processing of the 3'- and/or 5'-termini, which are often modified, must be carried out to restore the correct 3'-OH and 5'-phosphate required for gap filling and DNA ligation to occur. As mentioned earlier, PNKP plays critical roles in processing the damaged ends. (iii) The DNA gap is filled once damaged termini have been restored to their suitable configuration. Gap filling can occur by two different mechanisms. The insertion of the single nucleotide that is missing at most SSBs (short-patch repair) can be catalyzed by Pol β . But at some SSBs, gap filling may continue for multiple nucleotides and this is done by Pol δ/ϵ (long-patch repair)²⁶. (iv) DNA ligation is the final step of SSBR. Lig1 and Lig3 α appear to be the enzymes of choice during nuclear long patch repair and short patch SSBR, respectively²⁷⁻²⁹, but there is some controversy regarding the role of Lig3 in the repair of nuclear DNA. Lig3 is present in both nuclei and mitochondria. A study has shown that mitochondrial Lig3 is required for cellular viability independent of the XRCC1 repair pathway³⁰. Figure 1.2 shows a model depicting the steps involved in the BER pathways.

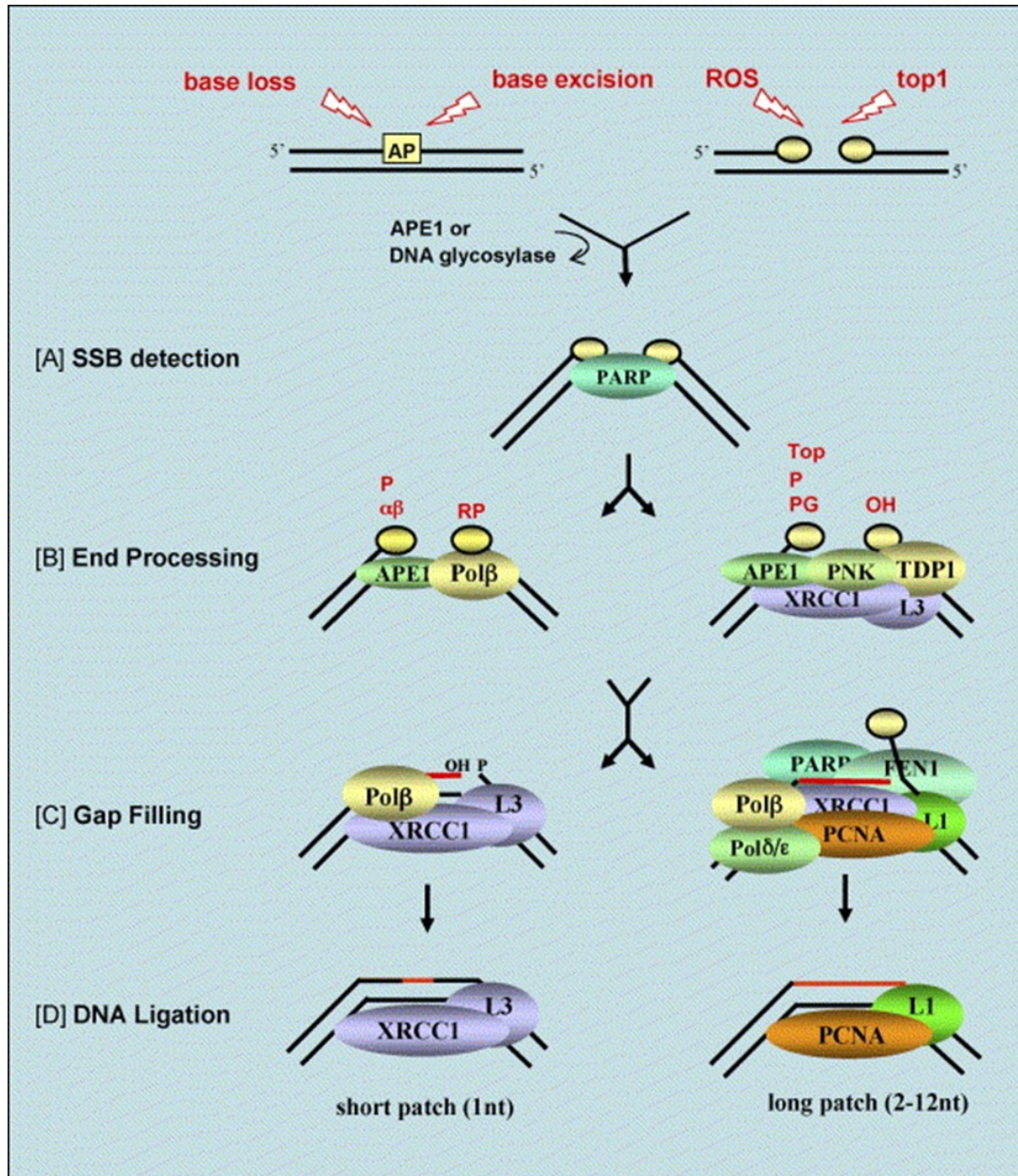


Figure 1.2. The mechanism of BER/SSBR. BER/SSBR model describing the steps involved in both short patch and long patch repair as described in section 1.1.1. The yellow circles indicate the damage on each terminus, AP indicates an abasic (apurinic/aprimidinic) site, FEN-1 is Flap endonuclease 1 and PCNA is proliferating cell nuclear antigen. Caldecott. *DNA Repair (Amst)* 6, 443-453 (2007). Re-used with permission from Elsevier

1.1.1.1. Base excision repair pathway (BER)

BER is responsible for the removal of oxidative and alkylation base damage^{31, 32}. The first step in this pathway is catalyzed by one of several DNA glycosylases such as the Neil glycosylases^{33, 34}. Mono-functional DNA glycosylases, which lack lyase activity, excise the damaged base and must rely on APE1 to hydrolyze the phosphate backbone^{15, 26}. On the other hand, bi-functional DNA glycosylases cleave the N-glycosyl bond, releasing the base and leaving an abasic site in the DNA, and can also cleave the DNA backbone on the 3' side of the abasic site via a lyase reaction^{26, 35}. There are two processes by which the cleavage of the phosphodiester backbone of DNA can occur, β -elimination or by two consecutive elimination steps (β,δ -elimination). Either of these processes create a DNA nick with "unclean" 3'-termini, a phospho- α,β -unsaturated aldehyde (PUA) or phosphate, respectively, which requires further processing by a specific enzyme to provide a suitable substrate for a DNA polymerase^{26, 35, 36}. Endo-glycosylases (NEIL1, NEIL2, and NEIL3) carry out a β,δ -elimination to generate 3'-phosphate and 5'-phosphate termini^{37, 38}. The removal of the 3'-phosphate is dependent on PNKP and not APE1^{36, 39-41}.

1.1.1.2. Topoisomerase I poison induces SSBs

Top I relieves torsional strain in DNA by nicking and then resealing a single strand of DNA during replication, transcription and other cellular processes^{11, 42}. The cleavage occurs via a transesterification reaction in which a Tyr molecule located in the active site acts as a nucleophile causing a SSB (a nick), which results in linking the enzyme covalently via a 3'-phosphotyrosyl DNA bond^{43, 44}. The complex retains the enzyme at the nick while the strain on the DNA is relieved prior to rejoining of the DNA. However, several factors

can stall the enzyme at the cleavage site, including DNA lesions in close proximity to the site of Top I cleavage ⁴⁵⁻⁴⁷, and the use of Top I inhibitors, such as camptothecin or one of its derivatives irinotecan ⁴⁸. The inhibitor prevents re-ligation and release of Top I from DNA ⁴⁹⁻⁵². The inhibition of TOP I is particularly deleterious at replication forks as this can lead to DSB. The inhibitor binds to Top I, creating a bulky adduct that is recognized as a DNA lesion. First, Spartan, a protease that resolves DNA-protein crosslinks, digests the TOP I leaving a small peptide fragment covalently attached to the DNA ^{53, 54}. Then this fragment is acted upon by tyrosyl-DNA phosphodiesterase (Tdp1), which releases the fragment from DNA by hydrolyzing the 3'-phosphotyrosyl DNA bond creating a single-strand break with a nick flanked by a 3'-phosphate and a 5'-hydroxyl, which are resolved by PNKP ⁵⁵⁻⁵⁷.

1.1.2. Double-strand break repair (DSBR)

DNA damaging agents such as ionizing radiation, topoisomerase II inhibitors, antitumor antibiotics, such as bleomycin, and cellular recombination processes can induce DSBs directly ⁵⁸, while other agents, such as ultraviolet (UV) light, and oxidative free radicals can cause DSBs when the replication fork encounters unrepaired SSB ⁵⁹. DSBs pose a major threat to cell survival and, unless repaired, lead to chromosomal rearrangements (translocations or deletions) or cell death. These detrimental effects help accelerate aging and promote carcinogenesis ⁶⁰. There are three main DSBR pathways: homologous recombination (HR), NHEJ and alternative NHEJ (alt-NHEJ) pathway. HR, an error free repair pathway, requires the homologous strand at the time of repair to use as a template and is active during DNA replication (S phase) and G₂ phase ⁶¹⁻⁶³. On the other hand, NHEJ functions in all phases of the cell cycle and does not require homology between

DNA strands, and is considered an error prone repair pathway⁶¹⁻⁶³. For the purpose of this thesis, we will only focus on NHEJ and alt-NHEJ because PNKP participates in DNA end processing in these pathways⁶⁴.

1.1.2.1. Nonhomologous end-joining (NHEJ): classic and alternative pathways

NHEJ is a major mechanism of DSB⁶⁵. The Ku complex, a heterodimer of two protein subunits Ku70 and Ku80, acts as a sensor for DSBs. The presence of Ku complex at the DNA ends of DSB is essential for subsequent DNA end processing and ligation^{66, 67}. DNA-dependent protein kinase catalytic subunit (DNA-PKcs) is recruited to Ku at DNA ends of DSB, becomes activated and catalyzes synapsis of the DNA ends by dimerization^{66, 67}. Another core complex, XRCC4-lig4-XRCC4 like factor (XLF), is also recruited to sites of damage. XRCC4-lig4-XLF induces DNA-PKcs autophosphorylation, dissociation, translocation of the Ku heterodimer along the DNA away from the ends, and recruitment of end processing factors⁶⁷. A number of end processing enzymes and polymerases are recruited to the site of damage by interacting with the core complex^{59, 67, 68}. PNKP is one of the key enzymes required for the processing of radiation-induced DSBs. PNKP is recruited to the site of damage by interacting with phosphorylated XRCC4 via the PNKP FHA domain⁶⁹. Ligation of DNA ends is catalyzed by lig4. Finally, the Ku complex is removed from DNA ends by proteasomal degradation mediated by ubiquitination by Cullin and RNF8⁶⁷. Figure 1.3 shows a model delineating the steps involved in the conventional NHEJ pathway.

A substitute of classical NHEJ, alt-NHEJ, is available when the cell is deficient in NHEJ components and relies on microhomology (MH), the tendency of the two DNA ends to align themselves at short regions of homology within the two ends⁷⁰⁻⁷². The main

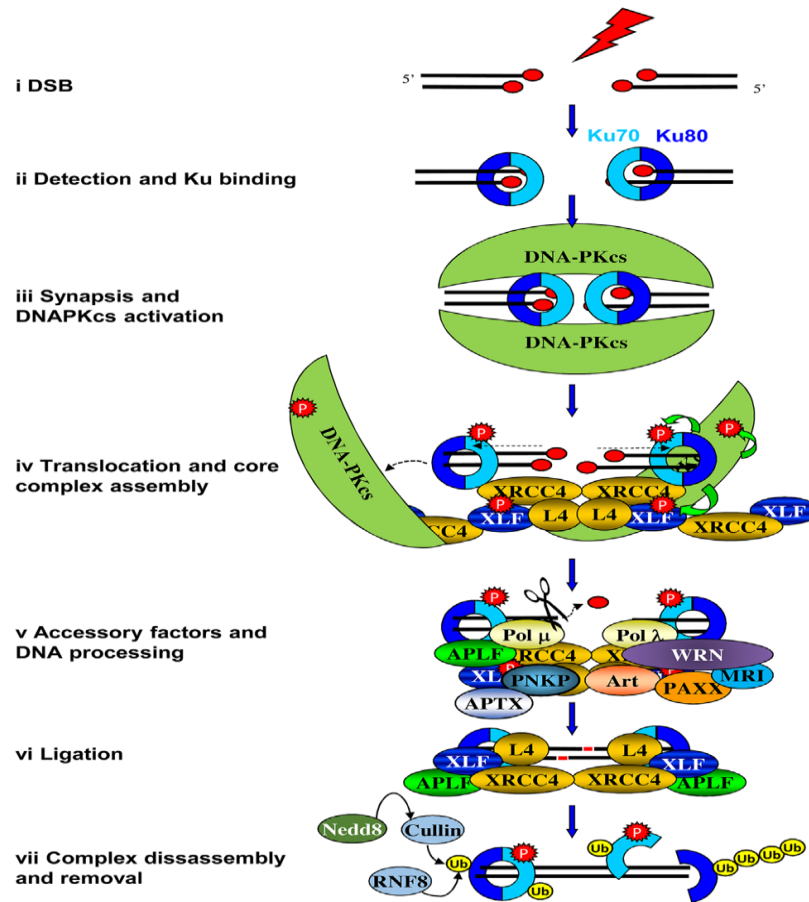


Figure 1.3. Classical NHEJ pathway. The DSB is first detected by the Ku70/Ku80 heterodimer, the complex binds and encircles DNA ends. The DNA-PKcs is then recruited to the site of damage. Activation of DNA-PKcs occurs and the recruitment of subsequent end-processing enzymes is required to produce ligatable ends. PNKP is one of the key enzymes for the processing of DSBs. The final stage of NHEJ repair process is the removal of Ku complex by proteasomal degradation. **Rulten and Grundy. BioEssays. 2017;39(3). doi: 10.1002. Re-used with permission from BioEssays**

attributes of alt-NHEJ are large deletions, insertions and a high frequency of chromosomal translocations ⁷³. The damage is detected in this situation by PARP-1, which facilitates the recruitment of the MRN complex to bridge the DNA ends, following the loading of CtIP to facilitate MH searches ⁷⁴⁻⁷⁶. The ligation process is mainly driven by the activity of the XRCC1/lig3 complex and on some occasions lig1, where MH is not required ⁷⁷. In recent studies, it was shown that polymerase θ (Pol θ) performs terminal transferase activity at the 3'-termini of resected DSBs to mediate MH ^{78, 79}. PNKP is also involved in this process and is likely partially regulated by IR-induced phosphorylation of PNKP by Ataxia telangiectasia mutated (ATM) and DNA-PKcs ^{80, 81}. An *in vivo* study showed that the inactivation of DNA-PKcs and/or ATM led to reduced PNKP levels at DNA damage sites ⁸¹. Based on the observation that depletion of PNKP does not alter the level of sister chromatid exchanges, it was surmised that PNKP does not participate in HR, the other major DSB repair pathway ⁸².

1.2. Polynucleotide kinase/ phosphatase (PNKP): structure and key interactions

PNKP, a 57-kDa protein, is a dual function enzyme that possesses DNA 3'-phosphatase and DNA 5'-kinase activities ^{83, 84}. The location of the gene for PNKP was found to be at chromosome 19q13.4 ⁸⁵. PNKP is found in both the nucleus and mitochondria. PNKP participates in the BER/SSBR pathway to process the damaged ends of nuclear and mitochondrial DNA caused by oxidative damage ⁸⁶. Under normal conditions, PNKP is regulated by a balance between PNKP transcription and CUL4A-DDB1-STRAP-dependent protein degradation ⁸⁷. However, the activation of ATM upon cellular exposure to radiation and oxidative stress prevents PNKP ubiquitylation and degradation by

phosphorylation at serines 114 and 126 in the linker region between the FHA and catalytic domains of PNKP ⁸⁸.

The phosphatase activity of PNKP supersedes the kinase activity ⁸⁹. Phage T4 PNK, another bifunctional enzyme, shares similar catalytic activity to PNKP but lacks an FHA domain ⁹⁰. T4 PNK does not repair DNA, but instead acts on RNA ^{90,91}. Identified proteins of *Caenorhabditis elegans* and *Schizosaccharomyces pombe* have ~ 30% similarity to human PNKP ^{85, 92-94}. The murine PNKP is ~80% identical to human PNKP ⁹⁰.

A crystal structural of murine PNKP (Figure 1.4A) revealed that the enzyme consists of three domains, the kinase domain at the C-terminus, the phosphatase domain in the centre and an FHA domain at the N-terminus ^{95,96}. The kinase and phosphatase domains together make up the catalytic segment of PNKP, once separated they lose activity ⁹⁷. The flexibility of the kinase and phosphatase domains of PNKP may allow this enzyme to work on either the 5'-OH or 3'-phosphate termini, or both if present at the same DNA strand break ⁹⁶. The FHA domain, a phosphothreonine-binding signaling module, is attached to the catalytic fragment by a flexible linker. The FHA domain recognizes the phosphorylated forms of XRCC1/4, key components of BER and NHEJ pathways, respectively, to direct PNKP to the site of DNA damage. This recognition occurs via FHA-dependent interaction with CK2-phosphorylated regions of XRCC 1/4 ^{98, 99}.

1.2.1. Catalytic activities of PNKP

PNKP is essential for maintaining genomic stability. To date, PNKP is the only DNA repair enzyme that has been identified as possessing 5'-kinase activity ⁵⁶. In addition, the 3'-phosphatase activity of PNKP supersedes that of APE1 and aprataxin (APTX), which

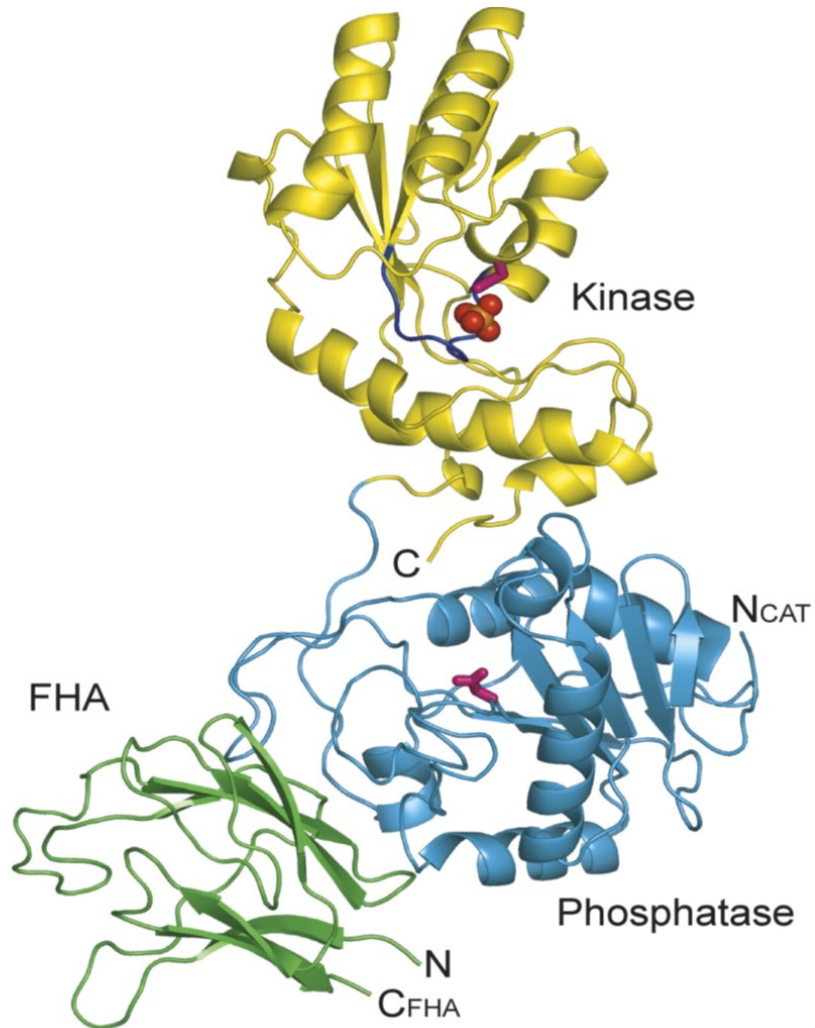


Figure 1.4A. Crystallographic structure of murine PNKP. The model shows the three major subdomains: kinase in yellow, phosphatase in blue and FHA domain in green. The catalytic active sites (Asp 396 in the kinase and Asp 170 in the phosphatase) are represented in pink. The navy blue in the kinase domain shows the ATP binding site, the orange and red spheres represent the sulfate bound at the P loop. **Bernstein *et al.* Mol. Cell 17, 657-670 (2005). Re-used with permission from Elsevier**

have been identified as being able to dephosphorylate 3'-phosphate⁵⁶. Previous studies revealed major differences in substrate type between the kinase and phosphatase domains, and it also showed that both act independently of one another, with the phosphatase being more active than the kinase¹⁰⁰. The kinase domain, which is selective for DNA, preferentially phosphorylates nicks, small gaps and recessed 5'-hydroxyl ends with a 3'-overhang^{3, 95, 101}. Furthermore, the kinase domain can bind to double-stranded 5'-termini without base pair disruption (Figure 1.4B)¹⁰². This domain belongs to the adenylate kinase family and includes both DNA and ATP binding sites. The ATP binding site consists of Walker A (P-loop) and B motifs^{95, 103, 104}. The Walker A motif binds the β - and γ -phosphates of ATP, while the Walker B motif coordinates Mg^{2+} ion. The DNA end is sequestered in a pocket of PNKP kinase domain with access to the 5'-OH terminus and the reaction is catalyzed by the Asp397 residue (Figure 1.5A)¹⁰⁵.

The phosphatase domain is a member of the haloacid dehalogenase (HAD) superfamily and adopts the Dx DGT motif^{90, 102, 106}. This domain is dependent on Mg^{2+} , which catalyzes the removal of 3'-phosphate of DNA and stabilizes the negative charge on the substrate phosphate during the process¹⁰⁷. The phosphatase domain functions in a two-step mechanism, the nucleophilic attack is first carried out on the substrate phosphate by the Asp171 carboxylate to produce the covalent phospho-aspartate intermediate. In the following step, the intermediate is hydrolyzed by Asp172 which deprotonates the attacking water molecule (Figure 1.5B)^{90, 107}. The dephosphorylation process acts in the same manner on nicked and gapped double-stranded substrates and single-stranded substrates as small as 3 nucleotides (Figure 1.4B)^{83, 90, 102, 105, 107}. However, the binding of double-stranded DNA to the PNKP phosphatase domain destabilizes base pairing in

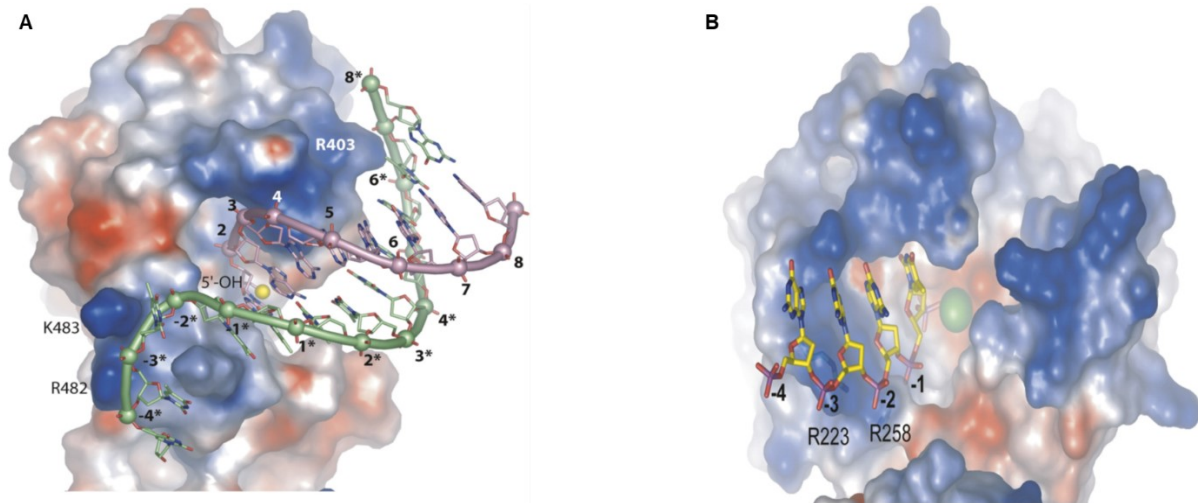


Figure 1.4B. DNA binding modes to murine PNKP. (A) The kinase domain acts preferentially on a double-stranded DNA substrate with 8 base pairs, which contains a 5'-hydroxyl recessed by 4-5 nucleotides to catalyze the phosphorylation process. **(B)** The phosphatase domain requires a minimum of trinucleotide single-stranded DNA to catalyze the dephosphorylation process. **Bernstein *et al.* Mol. Cell 17, 657-670 (2005). Re-used with permission from Elsevier**

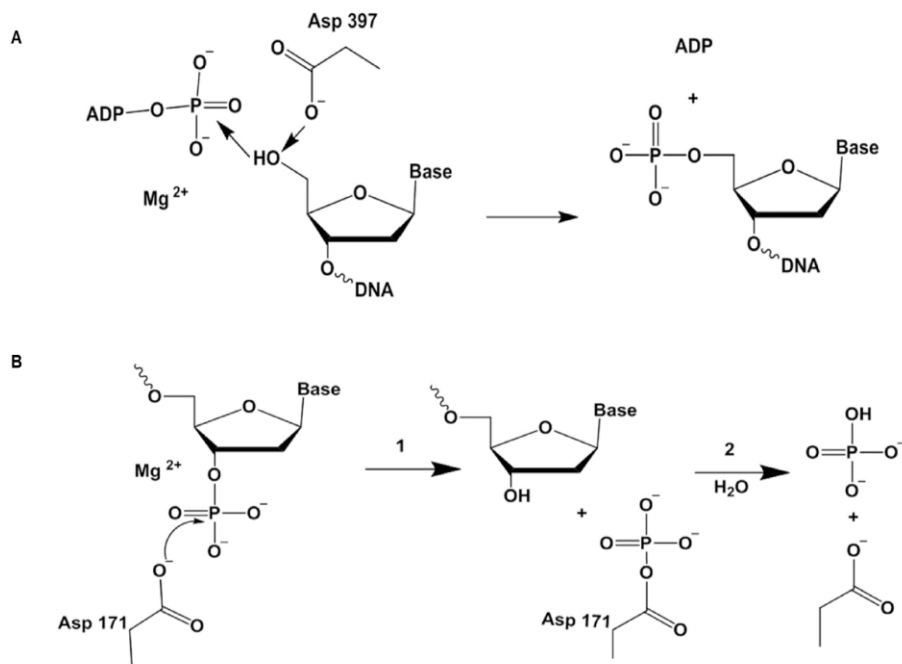


Figure 1.5. Catalytic reactions of PNKP. (A) The mechanism of action of PNKP kinase activity is catalyzed by Asp397, which is believed to provide base assistance by activating the 5'-OH for nucleophilic attack on the ATP γ -phosphate and is dependent on Mg^{2+} ion. **(B)** The 3'-DNA dephosphorylation mechanism of PNKP phosphatase subdomain involving nucleophilic attack by Asp171 carboxylate dependent on Mg^{2+} ion, followed by activating a water molecule to serve as a nucleophile in an S_N2 attack on the phosphorus atom to release the cleaved phosphate from the aspartate residue. **Shire et al. Processing strand break termini in the DNA single-strand break repair pathway. In: Wilson III DM, editor. The Base Excision Repair Pathway: Molecular Mechanisms and Role in Disease Development and Therapeutic Design. London: World Scientific; 2017. p. 281-321**

the two or three terminal base pairs of double-stranded substrates closest to the 3'-phosphate by electrostatic interactions between a positively charged surface of PNKP and the DNA strand ¹⁰².

PNKP kinase and phosphatase activities are active on DNA and inactive on RNA. Mammalian cells have distinct DNA-specific and RNA-specific polynucleotide kinase functions. The mammalian DNA kinase has a pH optimum of 5.5, while the RNA kinase has an alkaline pH optimum ¹⁰⁸⁻¹¹¹. Moreover, the human RNA kinase does not have an associated 3'-phosphatase, whereas DNA kinases do have an inherent DNA-specific 3'-phosphatase function ^{112, 113}.

1.2.2. Physiological importance of PNKP increased its clinical interest

Although there has not been any study confirming that PNKP is mutated in cancer cells, shRNA mediated knock down of PNKP increases the spontaneous mutation frequency ¹¹⁴. The following examples highlight the risks resulting from PNKP mutations in neuronal cells. Several studies have linked defects in BER/SSBR proteins to hereditary neurodegenerative diseases ¹¹⁵. Moreover, recent studies have highlighted that mutations in the gene coding for PNKP can cause neurological disorders ¹¹⁶⁻¹²⁰. Neuronal cells live longer, which makes them more prone to endogenous DNA damage. PNKP is a DNA end processing enzyme that can process endogenous DNA damage. Therefore, it is not surprising that PNKP mutations are associated with the severe neurodevelopmental disorder, microcephaly, seizures and developmental delay (MCSZ) ^{116, 121-123}. Most of the PNKP mutations identified in the MSCZ patients are in the phosphatase and kinase domains ¹²⁴. To date, there is no indication of ataxia, immunodeficiency or cancer in individuals affected with MCSZ ¹¹⁶. On the other hand, the

neurodegenerative disorder ataxia-ocular motor apraxia 4 (AOA4), a complex movement disorder that causes eye movement abnormalities, polyneuropathy and obesity¹²⁵, is also caused by mutations of PNKP, which to date appear to be located only in the kinase domain¹²⁴. Spinocerebellar ataxia type 3 (SCA3), is a disease characterized by CAG repeat expansion of the polyglutamine protein, ataxin-3 (ATXN3). In recent studies, it has been shown that there is an association of ATXN3 with PNKP. The purified wild-type ATXN3 stimulates the 3'-phosphatase activity of PNKP, and ATXN3-deficient cells show decreased 3'-phosphatase activity of PNKP^{123, 126-129}.

1.3. Small molecule inhibitors, novel drugs to overcome resistance of conventional cancer treatment

The conventional therapeutic approaches to cancer treatment include surgery, radiotherapy and chemotherapy¹³⁰⁻¹³². Chemotherapy can be delivered as a single drug or a combination of drugs that mainly target rapidly dividing cancer cells¹³³. Unfortunately, chemotherapy also harms normal cells that proliferate rapidly such as cells in the gut, bone marrow and hair follicles, thus resulting in side effects such as fatigue, nausea, vomiting, immune suppression and hair loss¹³⁴⁻¹³⁶. Surgery, a primary treatment to prevent cancer spread, is very efficient in dealing with early localized stages of disease and less advanced tumors but is rarely curative for metastasized cancers. Despite the introduction of techniques such as image-guided adaptive radiotherapy, there is still the potential for radiation-induced normal tissue damage to surrounding healthy tissue. Moreover, although tumors often respond to a range of conventional and advanced treatments, tumor resistance frequently develops through several mechanisms such as

multidrug resistance, defects in cell death pathways, incomplete drug activation and enhanced DNA repair (Figure 1.6) ¹³⁷.

Thus, the development of new targeted small molecule inhibitors is needed to overcome the drawbacks of traditional cancer therapies. These molecules should conceptually be more specific to cancer than the traditional non-targeted therapy. Small molecule inhibitors can penetrate tissues and tumors easily and interact with targets on the cell surface and/or within the cells ^{138, 139}. Examples of successful small molecule inhibitors in clinical use are Glivec, a kinase inhibitor of the BCR-ABL fusion protein in chronic myeloid leukemia (CML), and Gefitinib, an epidermal growth factor receptor (EGFR) inhibitor ¹⁴⁰⁻¹⁴². DNA repair pathways enable tumors to survive DNA damage that is induced by radiation or chemotherapeutic agents; therefore, inhibitors of specific DNA repair enzymes, such as PARP-1, O⁶-methylguanine-DNA methyltransferase (MGMT) and ATM, have been generated and have undergone, or are currently undergoing, clinical trials ¹⁴³⁻¹⁴⁷. Olaparib (Trade name - Lynparza), a PARP-1 inhibitor has been approved by the FDA for treatment of ovarian cancer patients carrying germline mutations in BRCA1 or BRCA2 ¹⁴⁸.

The discovery of new small molecule cancer drugs remains challenging and may take several years to gain success clinically. The major steps for small molecule inhibitor discovery are target validation, the discovery of chemical hits and lead compounds, optimizing lead drug candidates for preclinical tests to predict how potent and selective targeted drugs will function in future clinical applications (Figure 1.7) ^{149, 150}. To continue the discovery of potential future targets and identify successful novel treatments of

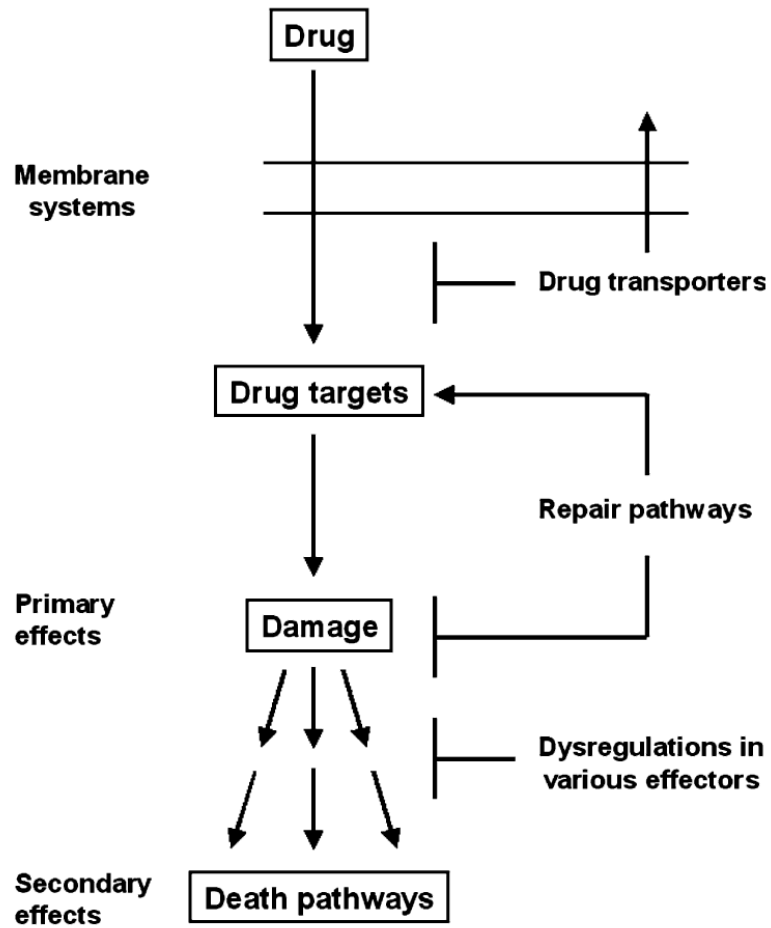


Figure 1.6. The causes of resistance to anti-cancer drugs. Cellular mechanisms responsible for cancer cells resistance to chemotherapy. *Lage. Cell. Mol. Life Sci.* 65 (2008) 3145 - 3167. Re-used with permission from Springer

cancer, my focus in this thesis is the development of new small molecule inhibitors of the DNA repair enzyme PNKP.

1.4. A12B4C3: a first-generation inhibitor of the DNA repair enzyme PNKP

PNKP plays important roles in both SSBR and DSBR repair, and cancer cells depleted of PNKP are more sensitive to ionizing radiation and the Top I inhibitor camptothecin^{82, 151-154}, making PNKP a suitable target for inhibition^{56, 97}. Several reasons led to the choice of targeting the PNKP phosphatase activity rather than the kinase. First, studies have indicated that the phosphatase activity of PNKP takes precedence over the kinase activity^{155, 156}. Second, 3'-phosphate termini are produced more frequently than 5'-OH by IR and ROS. Third, targeting the PNKP phosphatase (especially by competitive inhibitors) is more specific than targeting the kinase activity. Although the phosphatase belongs to the HAD superfamily, there are very few enzymes with true similarity to mammalian PNKP (Dr. Mark Glover, personal communication, Department of Biochemistry, University of Alberta)¹⁵, while the kinase domain belongs to a superfamily with many similar structures to the PNKP kinase^{56, 97, 157}.

Several members of a small chemical library of imidopiperidine derivative compounds synthesized by Dr. Dennis Hall's group (Dept. of Chemistry, University of Alberta) were shown to inhibit the phosphatase activity of PNKP^{158, 159}. A12B4C3, Figure 1.8, was the first PNKP phosphatase inhibitor discovered in our lab. A12B4C3 is able to enhance the radio/chemosensitivity of human A549 lung adenocarcinoma, MDA-MB-231 breast carcinoma and acute myeloid leukemia cells (AML)¹⁶⁰⁻¹⁶². In addition, a recent study showed that A12B4C3 can sensitize PC3 cells, which are radioresistant, to high linear

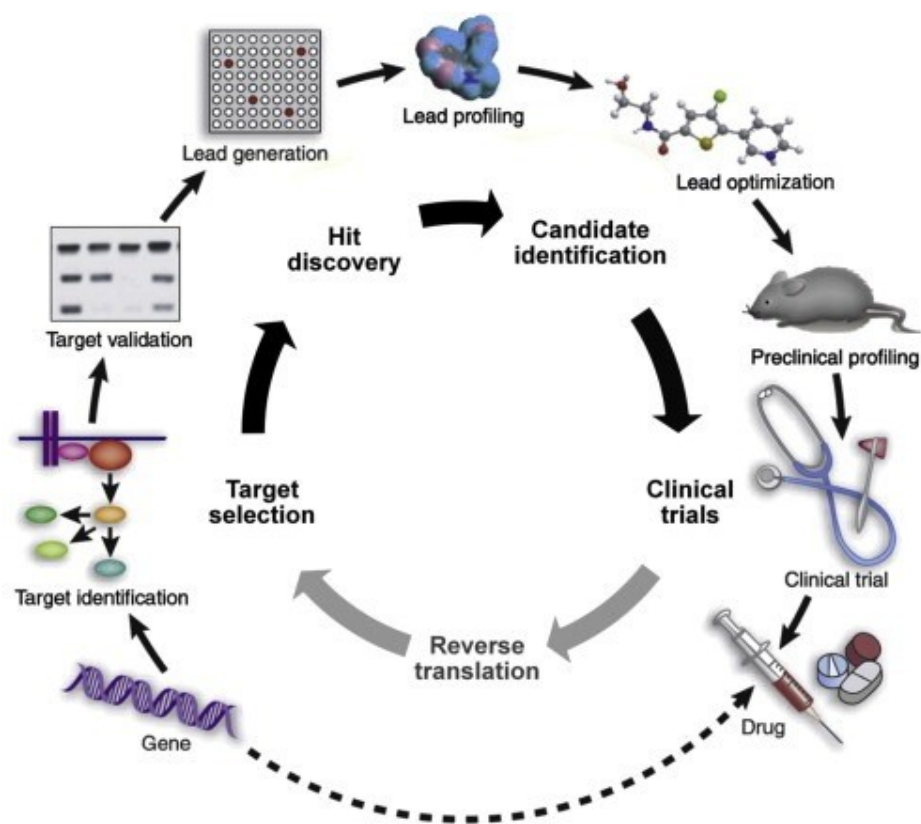


Figure 1.7. Drug design and development stages. The main steps of cancer drug discovery that are featured in this scheme are: target identification, discovery of lead compound, performance of preclinical studies to determine efficacy and finally performance of clinical trials. **Hoelder *et al.* Mol Oncol. 2012; (2): 155 - 176**

energy transfer (LET) radiation ¹⁶³. Further kinetic analysis of A12B4C3 showed it to be a non-competitive inhibitor ¹⁶¹.

This thesis discusses attempts to optimize the lead compound A12B4C3 by identifying second generation compounds that are more potent, and to design novel nanocarriers for targeted delivery of the newly found inhibitors to cancer cells.

1.5. Synthetic lethality: The application of PNKP inhibitors as a monotherapeutic in the context of cancer therapy

Synthetic lethality delineates the phenomenon whereby a defect or loss of a non-essential gene or its coded protein allows for cell survival under normal circumstances but results in cell death when associated with mutation or loss of another non-essential gene or its coded protein (Figure 1.9) ¹⁶⁴. Synthetic sickness, in contrast to synthetic lethality, is a situation where combinations of defective genes can engender non-lethal weakness and hence greater susceptibility to stressors ^{165, 166}. The concept of synthetic lethality has been successfully employed to identify new drug targets for personalized therapies by exploiting weaknesses present in tumor cells ¹⁶⁷. The selective targeting of cancer via synthetic lethality is a smart approach that can spare normal cells from the toxicity of anti-cancer therapy. Tumor suppressors are major targets for synthetic lethality ¹⁶⁸. Through both chemical and genetic screens, it is possible to identify potential genes or proteins that are synthetic lethal partners with defective tumor suppressors ¹⁶⁹. The tumor suppressor proteins BRCA1 and BRCA2 play key roles in the repair of DNA DSBs by HR ^{170, 171}. BRCA1 and BRCA2 have been found to be mutated in 5-10% of ovarian and breast cancer patients ¹⁷². While both alleles of BRCA1 or BRCA2 are defective in the tumor, the

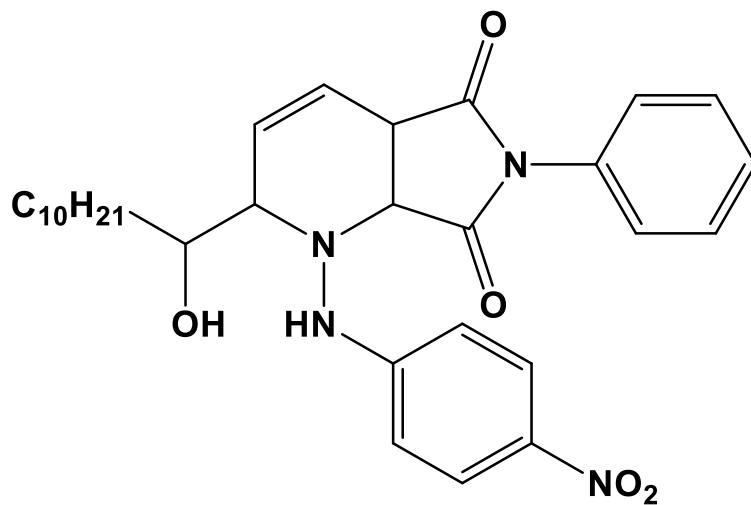


Figure 1.8. The structure of the first generation PNKP inhibitor, A12B4C3.

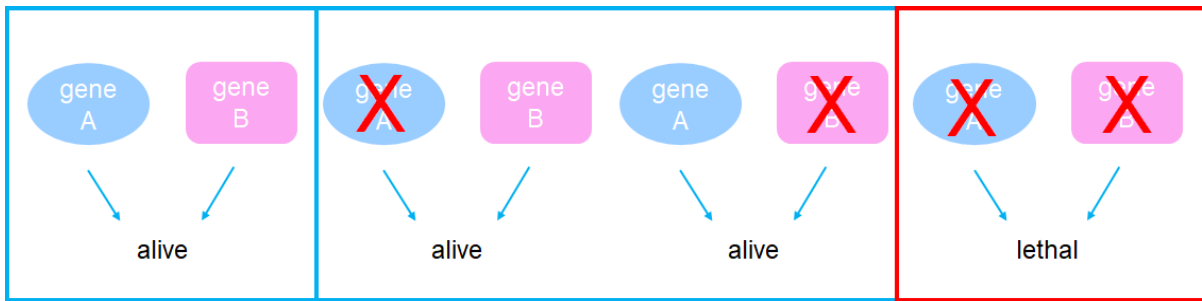


Figure 1.9. The concept of synthetic lethality. Non-essential genes A and B are not lethal to cells if inactivated individually. However, cell death occurs when both genes or their coded proteins are inactivated. **Adapted from Nijman. FEBS Lett. 2011 Jan 3; 585(1): 1- 6**

patients' normal cells carry a wild-type allele and therefore retain BRCA1 or BRCA2 activity. Inhibiting PARP-1 in cancer cells with defective BRCA1 or 2 genes was found to be lethal to these cells ¹⁷³⁻¹⁷⁵. The lethality in these situations is a result of the disruption of two main repair pathways. Figure 1.10 illustrates one proposed mechanism of synthetic lethality between PARP and BRCA.

The tumor suppressor gene, phosphatase and tensin homolog (PTEN), which is located on human chromosome 10q23, is one of the most commonly mutated genes in several cancer types ^{176, 177}. PTEN regulates many cellular processes via its lipid phosphatase activity such as cell survival, metabolism, microenvironment and proliferation (Figure 1.11). Mechanisms controlling PTEN expression and its activity, including transcription factors and phosphorylation, are often poorly regulated in cancer ¹⁷⁷⁻¹⁷⁹. Recent evidence also indicates that PTEN is important for the maintenance of genome stability ¹⁸⁰. Similar to BRCA, PTEN was found to be a synthetic lethal partner of PARP ¹⁸¹. A combination of the PARP inhibitor, Olaparib, and cisplatin showed a synergistic effect in PTEN-deficient lung cancer and endometrial adenocarcinoma ^{182, 183}. In another study, it was suggested that PTEN deficiency causes an HR defect in tumor cells ^{184, 185}. In PTEN-deficient cells, inhibition of ATM, a key player in DDR, by a small molecule exhibited synthetic lethality. It was concluded that the reason behind this lethality is that elevated levels of ROS due to absence of PTEN, increased endogenous DNA damage, and therefore ATM inactivation led to accumulation of drastic DNA damage¹⁸⁶.

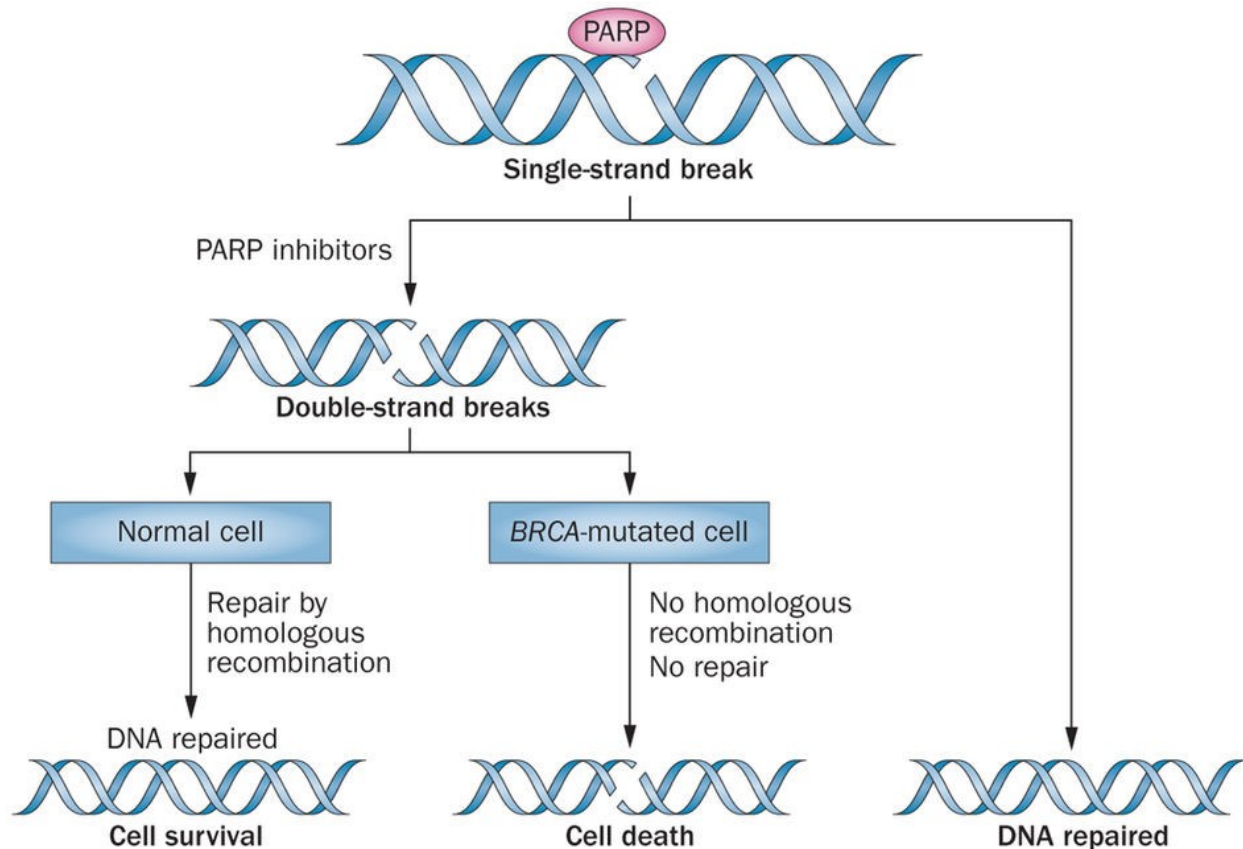


Figure 1.10. Synthetic lethal partnership between PARP and BRCA. PARP participates in SSBR. Inhibiting PARP chemically leads to stalled replication forks creating DSBs. However, cells with inactivated BRCA are sensitive to PARP inhibitors due to the inactivation of both SSBR and HR resulting in cell death. **Sonnenblick *et al.* Nat Rev Clin Oncol. 2015;12(1):27-41. Re-used with permission from Nature Publishing Group**

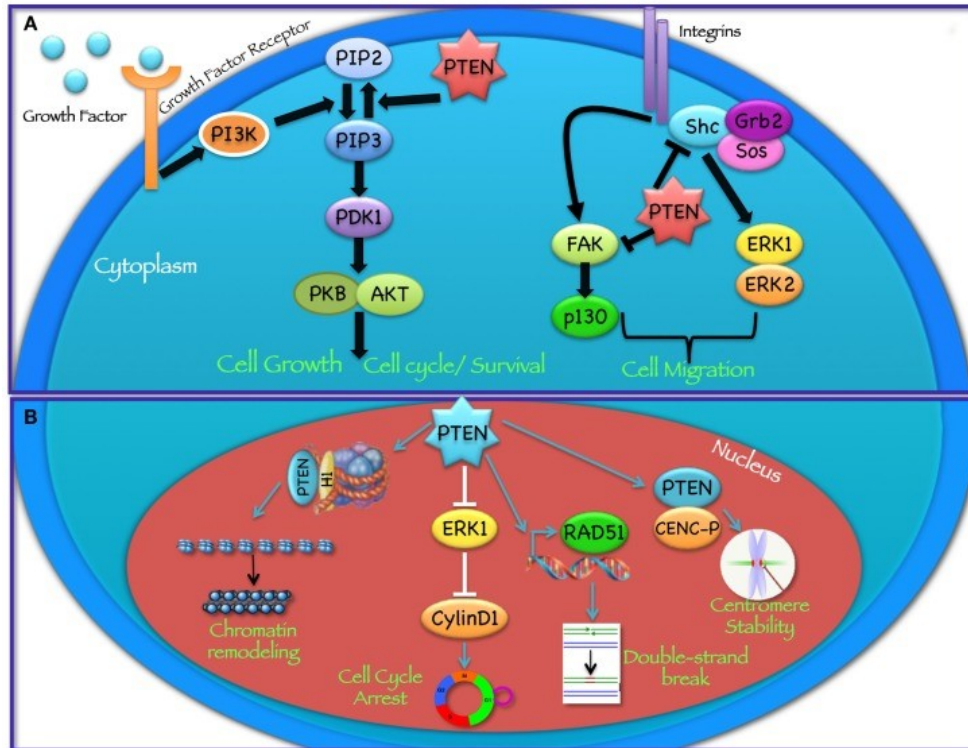


Figure 1.11. The role of PTEN in the cytoplasm and nucleus. (A) PTEN dephosphorylates phosphatidylinositol (3,4,5)-trisphosphate (PIP3) to the diphosphate phosphatidylinositol 4,5-bisphosphate (PIP2) in the cytoplasm obstructing downstream pathways regulated by PDK and AKT, such as cell-cycle progression, survival, proliferation and regulation of cell migration through controlling FAK and Shc pathways. **(B)** PTEN is also present and functional in the nucleus, it protects genomic integrity, maintains DNA double strand break repair and regulates cell-cycle progression. **Milella et al. Front Oncol. 2015 Feb 16;5:24**

In recent years, PNKP has emerged as a new synthetic lethal partner of PTEN. An siRNA-based screen of the ~7000-gene “druggable genome” led to the identification of PTEN (and another tumor suppressor, protein tyrosine phosphatase SHP-1) as a synthetic lethal partner of PNKP in A549 lung cancer cells ¹⁸⁷. Subsequent work showed that PTEN-deficient HCT116 colon cancer cells were sensitive to A12B4C3 (Figure 1.12), and also dramatically sensitized PTEN-deficient cells to ionizing radiation ¹⁸⁸. The mechanism responsible for the synthetic lethal partnership between PTEN and PNKP has not yet been fully elucidated.

PTEN is of interest clinically for synthetic lethality in many cancers including colorectal cancer (CRC). Monoallelic mutations at position 10q23 are found in 50-80% of sporadic cancers such as glioblastoma and prostate cancer and 30-50% in colon and lung cancers ¹⁷⁶. One study demonstrated that PTEN alteration through genetic or epigenetic mechanisms, such as mutations and promoter hypermethylation, causes biallelic inactivation of PTEN in 20-30% of CRC patients ¹⁸⁹. Another group reported that PTEN is inactivated either by loss or reduction of expression in ~70% of CRCs, and this is frequently caused by microsatellite instability (MSI) ¹⁹⁰. MSI in CRC contributes to loss, reduction or inactivation of PTEN protein levels, thus resulting in tumor progression ¹⁹¹⁻¹⁹³. In a recent study, it was found that microRNA-26b promotes CRC metastasis by down-regulating PTEN ¹⁹⁴. In addition, mutations or loss of PTEN leads to upregulation of the oncogenic PI3K/AKT pathways ^{195, 196}, and knockdown of PTEN induces invasion and migration of HCT116 cells through epithelial mesenchymal transition (EMT) ¹⁹⁷. Failure of anti-EGFR treatment, a prominent targeted therapy, in metastatic CRC (mCRC)

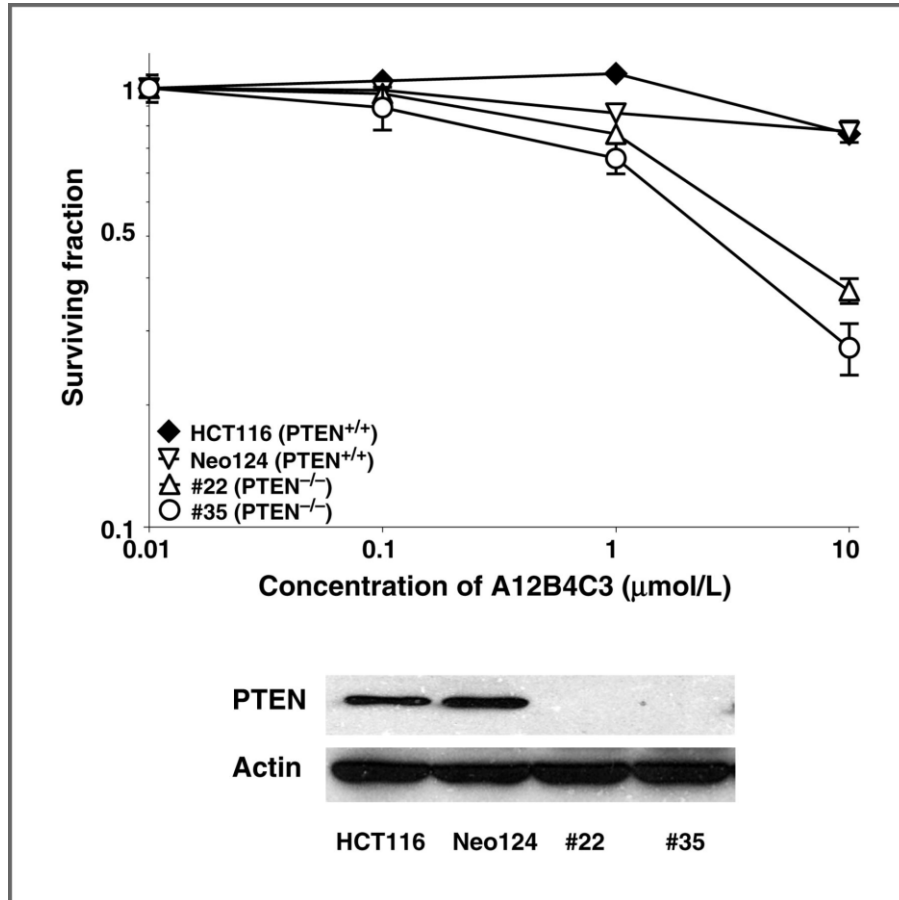


Figure 1.12. Clonogenic survival assay of HCT116 cells deficient in PTEN. Data represented here indicate that inhibition of PNKP 3'-phosphatase activity, chemically by addition of A12B4C3, is synthetically lethal to PTEN deficient cancer cells. Western blot indicates the expression of PTEN in HCT116- PTEN wildtype (wt), Neo124 vector only control cells and two PTEN^{-/-} HCT116 strains, #22 and #35. **Mereniuk *et al.* Mol Cancer Ther. 2013;12(10):2135-44. Re-used with permission from American Association for Cancer Research**

has been attributed to the loss of PTEN¹⁹⁸⁻²⁰⁰. The studies mentioned above all highlight that irregular or absent functions of PTEN probably contribute significantly to CRC progression and metastasis, therefore we investigated if the newly identified PNKP inhibitors could elicit synthetic lethality in CRC cells lacking PTEN.

1.6. The role of nanoparticles in drug delivery

Disadvantages of traditional cancer chemotherapeutics include toxicity, poor solubility and bioavailability. Nanoparticles have been designed with optimal size and synthesized with multi-functionality surfaces to improve solubility and enhance biodistribution, escape the reticuloendothelial system (RES) and increase drug circulation time in the bloodstream²⁰¹⁻²⁰³. Nanoparticles have the capability to penetrate tumors passively because of the enhanced permeability and retention effect (EPR) and the tumor microenvironment^{204, 205}. Tumor blood vessel walls have big intercellular gaps between endothelial cells. In addition, the absence of lymphatic drainage will allow particles to accumulate in the tumor interstitial space²⁰⁶. Figure 1.13 shows the differences between leaky and normal vasculature in the tumor microenvironment. Furthermore, nanoparticles can avoid recognition by P-glycoprotein, one of the main mechanisms of multiple drug resistance (MDR), and are frequently sheathed inside endosomes when entering cells, resulting in increased intracellular concentration of drugs. Active targeting approaches using ligands or antibodies specific for tumors also reduce toxicity and eliminate resistance to these therapeutic nanoparticles²⁰⁷. Receptor-targeting ligands facilitate the uptake of nanoparticles via receptor-mediated endocytosis to overcome drug resistance²⁰⁸.

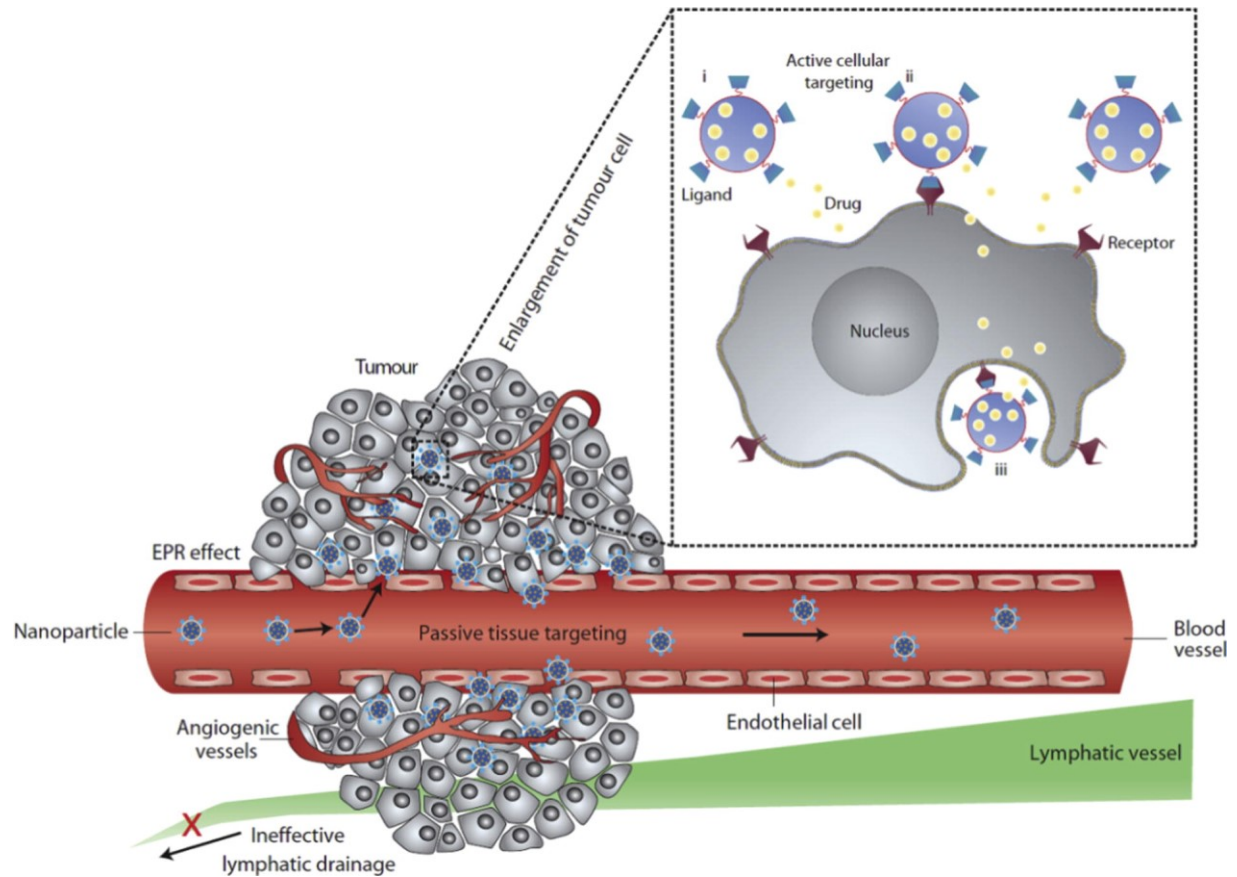


Figure 1.13. Enhanced Permeability and Retention (EPR) effect. Tumor tissues have destabilized vasculature and the effectiveness of lymphatic drainage is greatly reduced, which helps nanoparticles internalize in tumors by the EPR effect. Actively-targeted nanoparticles further enhance drug accumulation inside cells by receptor-mediated endocytosis. Pérez-Herrero and Fernández-Medarde. *Eur J Pharm Biopharm.* 2015; 93:52-79. Re-used with permission from Elsevier

Forms of nanoparticles used for delivery of cancer therapeutics include polymeric micelles, dendrimers, liposomes, gold carriers, nanotubes and magnetic carriers ^{209, 210}.

Figure 1.14 summarizes the design of various nanoparticles and their unique physical and chemical properties.

1.6.1. Polymeric micelles

Polymeric micelles are established through self-assembly of amphiphilic block copolymers in an aqueous environment, due to the large solubility difference between hydrophilic and hydrophobic segments ²¹¹. Figure 1.15 shows the micellization process in aqueous media. Polymeric micelles usually form a spherical core/shell structure in which the hydrophobic core encapsulates poorly water-soluble drugs, proteins or DNA, whereas the hydrophilic shell of the copolymer protects the drug from the aqueous environment and stabilizes polymeric micelles against recognition by the RES *in vivo* ²¹¹⁻²¹³. The chemical structure and physicochemical properties of the core/shell-forming blocks of polymeric micelles can be easily modified to lead to sustained, pulsed or delayed mode of drug release depending on the delivery purpose ²¹⁴. Some intrinsic properties of polymeric micelles include, size in the nm range, stability in plasma, prolonged blood circulation times and release of the loaded drug in a controlled manner at target sites ²¹⁵⁻²¹⁹. Moreover, polymeric micelles reduce the clearance of drugs from the body via metabolism or kidney excretion ²²⁰. Their size (> 50 kDa) is large enough to avoid renal excretion and small enough (< 200 nm) to bypass filtration by the spleen ²²¹.

Polymeric micelles are stable due to the polymeric nature of the hydrophobic core. The long hydrophobic chain of the core segment in polymeric micelles supports the formation

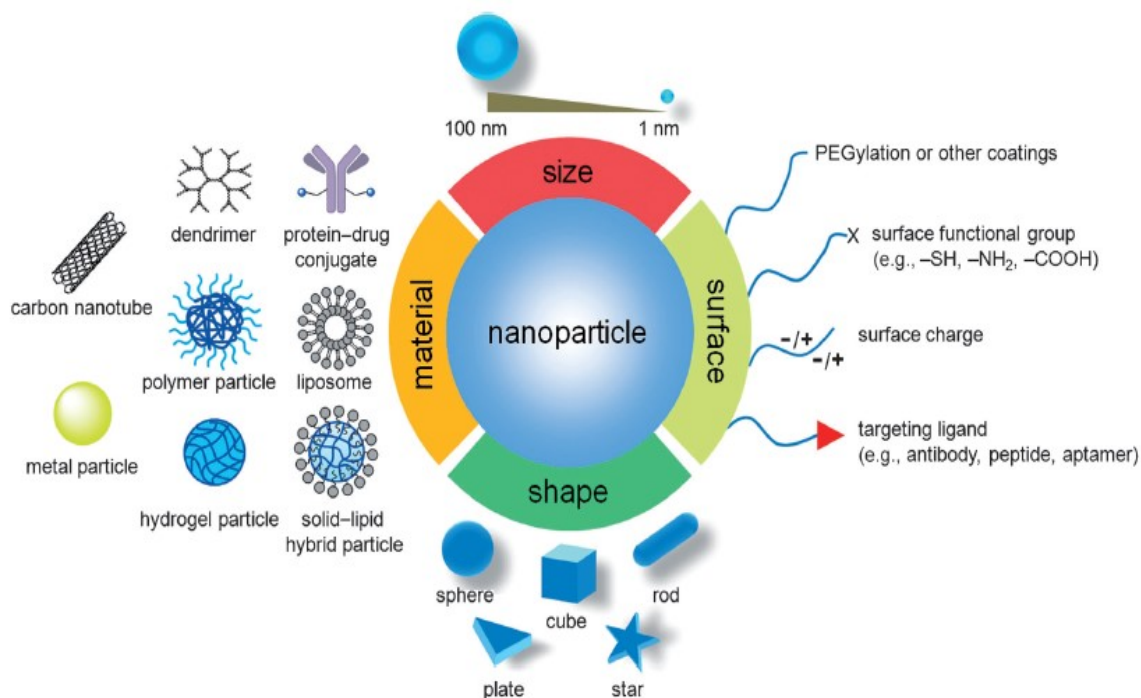


Figure 1.14. Different shapes and designs of nanoparticles currently used in cancer therapy. Nanoparticles can be constructed from a variety of materials, compositions and structures to assist in loading different anticancer drugs, with their sizes being < 100 nm. Sun *et al.* *Angew Chem Int Ed Engl.* 2014 Nov 10;53(46):12320-64. Re-used with permission from John Wiley and Sons

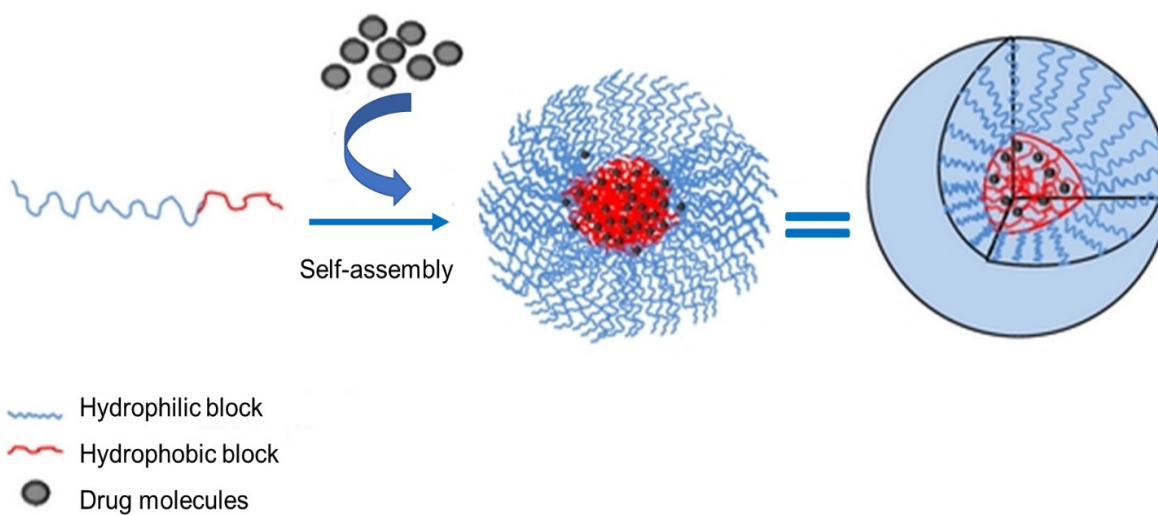


Figure 1.15. Micellization and drug loading by self-assembly of block-copolymers in aqueous solution. First, the drug and the polymer are dissolved in an organic solvent (acetone). The mixture is then added dropwise to an aqueous solution to form micelles.

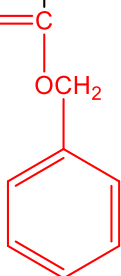
Reproduced from Xu *et al.* *J Drug Deliv.* 2013;2013:340315

of micelles, resulting in a critical micellar concentration (CMC) as low as 10^{-6} M. As a result, polymeric micelles may stay above the CMC for longer periods after dilution in the blood stream ^{212, 220}. In addition, optimizing factors like the structure of the hydrophobic core of polymeric micelles and the micellization process can aid in optimizing drug loading capacity ²²².

The work represented in this thesis is focused on the use of poly(ethylene glycol)-*block*-poly(ϵ -caprolactone) (PEG-*b*-PCL) based polymeric micelles. The PEG segment is a neutral water-soluble polymer, which is non-toxic, non-immunogenic and FDA approved to be used *in vivo* ^{223, 224}. PEG-*b*-PCL has been successfully used previously to encapsulate indomethacin, cyclosporine A (CsA), a STAT3 inhibitor, paclitaxel, doxorubicin and siRNA ²²⁵⁻²³⁰. New modifications of PEG-*b*-PCL were applied to enhance the encapsulation and release of a variety of drugs ²³¹. We have used PEG-*b*-PCL bearing side groups of benzyl carboxylate, poly(ethylene glycol)-*block*-poly(α -benzyl carboxylate- ϵ -caprolactone) (PEG-*b*-PBCL), or free carboxyl, poly(ethylene glycol)-*block*-poly(α -carboxyl- ϵ -caprolactone) (PEG-*b*-PCCL), on the PCL backbone to encapsulate the newly found inhibitors of PNKP as we will describe in detail in Chapter 3. Table 1.1 shows the chemical structures of PEG-*b*-PCL, PEG-*b*-PBCL and PEG-*b*-PCCL.

As mentioned previously, the nanoscale size of polymeric micelles aids in passive drug targeting and their preferential accumulation in solid tumors due to leaky vasculature by the EPR effect. However, accumulation of polymeric micelles at the tumor site does not guarantee effective drug delivery to target cells. A second generation of polymeric micelles for active drug targeting, in the form of polymeric micelles with tumor specific ligands attached on the surface, have been synthesized previously ²³². Ligands such as

Table 1.1. Chemical structure of the three poly(ethylene glycol)-*block*-poly(ester)s used in this thesis.

$\text{CH}_3\text{O}-(\text{CH}_2\text{CH}_2\text{O})_x-\overset{\text{O}}{\parallel}{\text{C}}-\underset{\text{H}}{\text{C}}-\text{H}-(\text{CH}_2)_4-\text{O}-\text{H}$ <p>(PEG-<i>b</i>-PCL)</p>
$\text{CH}_3\text{O}-(\text{CH}_2\text{CH}_2\text{O})_x-\overset{\text{O}}{\parallel}{\text{C}}-\underset{\text{H}}{\text{C}}-\text{H}-(\text{CH}_2)_4-\text{O}-\text{H}$  <p>(PEG-<i>b</i>-PBCL)</p>
$\text{CH}_3\text{O}-(\text{CH}_2\text{CH}_2\text{O})_x-\overset{\text{O}}{\parallel}{\text{C}}-\underset{\text{COOH}}{\text{C}}-\text{H}-(\text{CH}_2)_4-\text{O}-\text{H}$ <p>(PEG-<i>b</i>-PCCL)</p>

monoclonal antibodies, aptamers, peptides and folate ligands have been attached on the micellar shell to improve drug targeting by specific recognition by cancer cells ²³³. For the purpose of this thesis, we will focus on targeting colorectal cancer (CRC) taking advantage of the overexpression of the epidermal growth factor receptor (EGFR).

1.7. Epidermal growth factor receptor (EGFR), a clinical target for anti-cancer therapy

EGFR, a transmembrane protein receptor, belongs to the ErbB family of tyrosine kinase receptors. EGFR is activated by interacting with its associated ligands resulting in autophosphorylation and activation of downstream signaling pathways that are involved in regulating cellular growth, cell motility, angiogenesis and survival (Figure 1.16) ²³⁴. Mutations in EGFR activity or enhanced expression levels are found in many cancers such as colon, lung, breast and head and neck ²³⁵⁻²³⁸. Changes in EGFR structure and/or expression contribute to the causes of hallmark properties of malignant behavior such as cell proliferation, anti-apoptosis, metastasis and uncontrolled angiogenesis ^{239, 240}. As a result, EGFR mutations have provided opportunities for the development of anti-EGFR therapeutics such as antibody-based approaches including Cetuximab and Trastuzumab, and small molecule ligands such as Erlotinib and Gefitinib. These approaches have been used for the treatment of several cancers including colon, lung and breast ²⁴¹⁻²⁴⁵. EGFR overexpression in cancer is also attracting attention clinically as a significant candidate for targeted nanoparticle delivery. In CRC, several targeted delivery approaches to enhance drug accumulation in tumor and efficacy have been applied. Immunoliposomes,

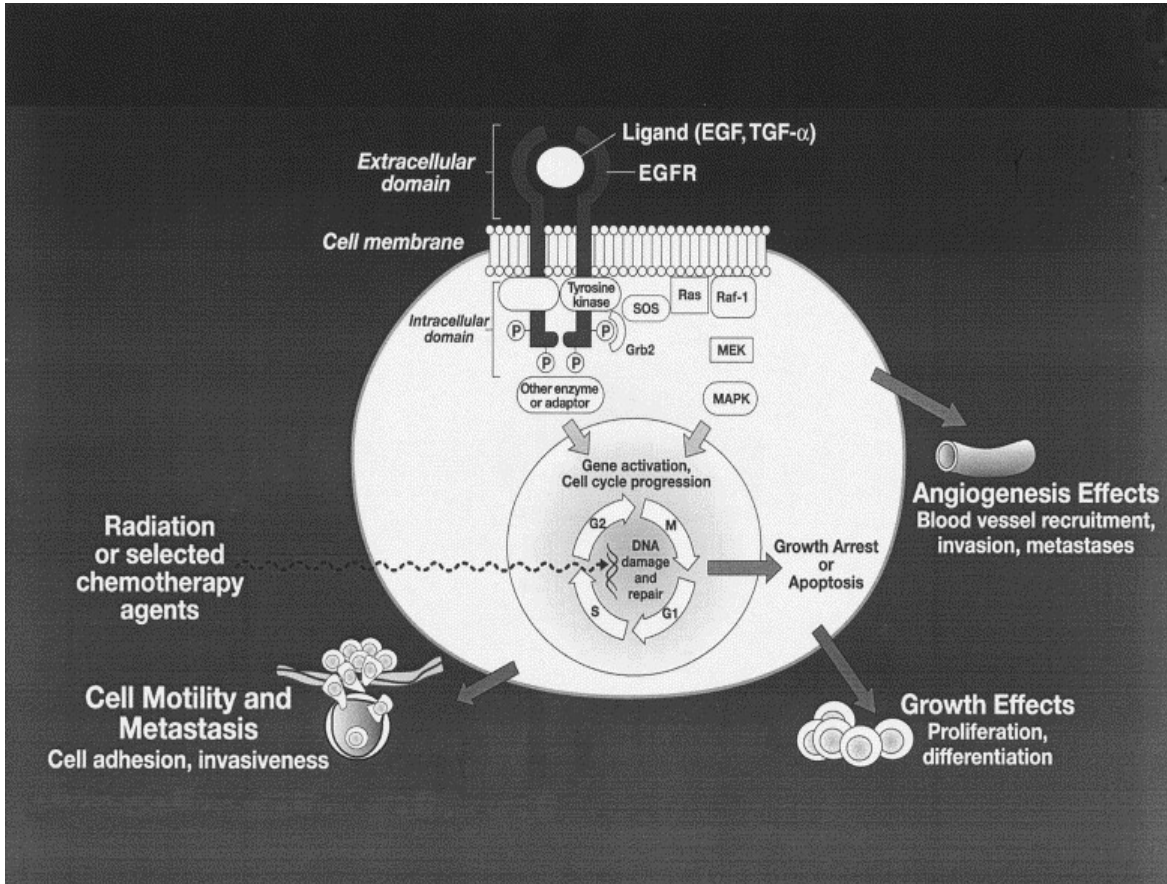


Figure 1.16. EGFR biology. Interaction of EGFR with its cognate ligands leads to the activation of several downstream signaling pathways responsible for regulating cell proliferation, motility and angiogenesis. **Herbst. Int J Radiat Oncol Biol Phys. 2004; 59:21-6. Re-used with permission from Elsevier**

prepared by attaching the Fab fragment of a humanized anti-EGFR monoclonal antibody, and a formulation consisting of antibody-conjugated nanotubes loaded with SN38, an active metabolite of irinotecan, have been used to target CRC ^{246, 247}.

Peptides are more suitable than antibodies and antibody fragments to be used for active targeting, because antibodies are large molecules that can interfere with nanoparticle dimensions and can elicit immunogenicity. On the other hand, peptides have lower manufacturing costs and better tumor penetration ²⁴⁸.

1.7.1. GE11: a novel peptide ligand targeting EGFR

A phage-display screening of peptides resulted in the identification of GE11, a potent peptide that can specifically target EGFR in a manner that mimics the natural ligand of EGFR, EGF ²⁴⁹. GE11, 12-mer peptide YHWYGYTPQNV (Figure 1.17), binds efficiently to EGFR with a dissociation constant of ~22 nM, but does not activate the receptor ²⁵⁰. GE11 internalizes preferentially into EGFR highly expressing tumor cells and has minimal to no effect on healthy tissue ²⁵¹. The use of GE11 as a targeted ligand enhanced the internalization of nanocarriers. For example, polyethyleneimine-polyethyleneglycol (PEI-PEG) conjugated to GE11 and GE11-targeted polylactide-co-glycolide (PLGA) showed high affinity to EGFR overexpressing MDA-MB-468 and A549 tumors, respectively ^{252, 253}. Another study showed that GE11-conjugation increased the effectiveness of an oncolytic adenovirus carrying the sodium iodide symporter gene ²⁵⁴. Doxorubicin-loaded liposomes with GE11 attached on their surface showed higher A549 cell killing than the unconjugated counterpart ²⁵⁵. Liposomes loaded with a combination of docetaxel and siRNA molecules against the ABCG2 gene that regulates multidrug resistance in laryngeal cancers showed enhanced anti-tumor efficacy and specificity when conjugated

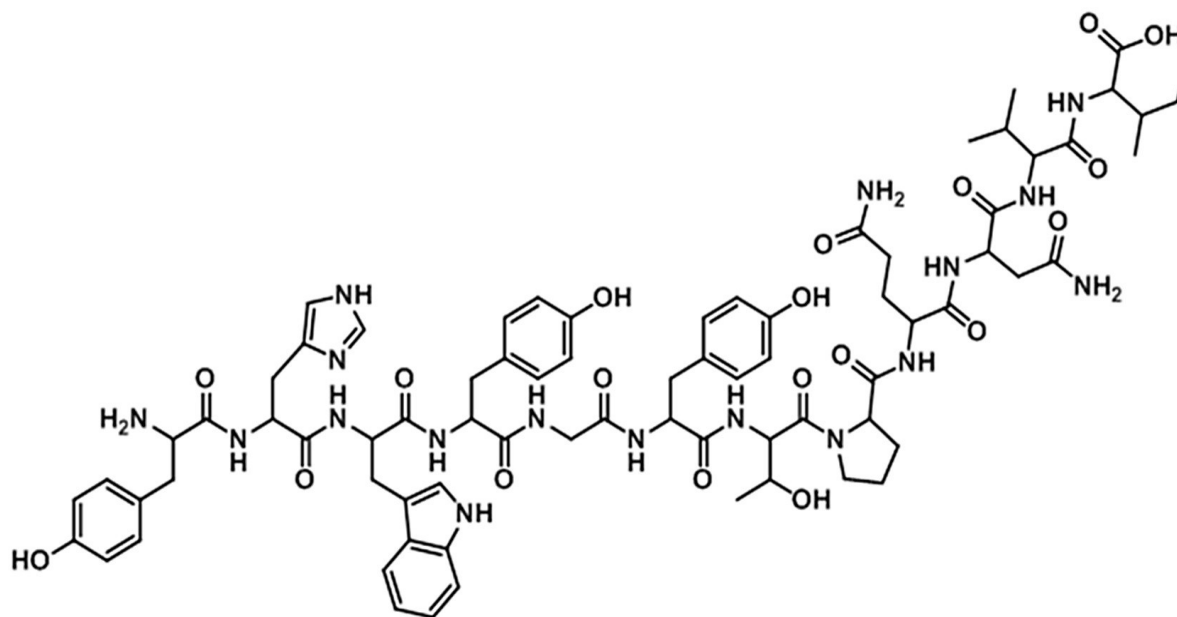


Figure 1.17. The chemical structure of GE11 peptide. **Colzani et al.** *Int J Pharm.* 2016;511(2):1112-23. Re-used with permission from Elsevier

with GE11 ²⁵⁶. The above-mentioned trials indicate that GE11 peptide might be a successful and suitable targeting moiety to actively deliver the newly found PNKP inhibitors to EGFR-overexpressing CRCs.

1.8. Colorectal cancer: the role of damage and repair of DNA in disease progression and treatment

CRC is classified as the 4th leading cause of cancer-related death globally ^{257, 258}. CRC is the 2nd most diagnosed cancer in Canada, 2nd leading cause of death in men and the 3rd leading cause of death in women (Canadian Cancer Society, 2017). According to the Canadian Cancer Society, Public Health Agency of Canada and Statistics Canada, the percent distribution estimated for male CRC patients was 12% of the total 42,600 deaths of all cancer types in 2017 and 11.3% for female CRC patients of total 38,200 deaths.

There are three molecular features that characterise CRC progression: (i) chromosomal instability (CIN), the majority of CRCs develop via CIN, which leads to mutations in tumor suppressors, cell cycle genes, epigenetic and genetic alterations (Figure 1.18) ^{259, 260}; (ii) defective mismatch repair (MMR) genes, which lead to DNA microsatellite instability (MSI), short repeat DNA sequences, and (iii) CpG island methylator phenotype (CIMP) ²⁶¹⁻²⁶³.

The first choice of treatment in CRC often involves surgery followed by chemotherapy such as FOLFIRI (5-FU/irinotecan/folinic acid) or FOLFOX (5-FU/leucovorin/oxaliplatin) and radiation ²⁶⁴⁻²⁶⁸. There are different approaches to administer the different treatment options. In a phase II study, radiation was performed on patients first, then surgery followed by FOLFOX treatment post-surgery ²⁶⁹. In another phase II trial, FOLFIRI was

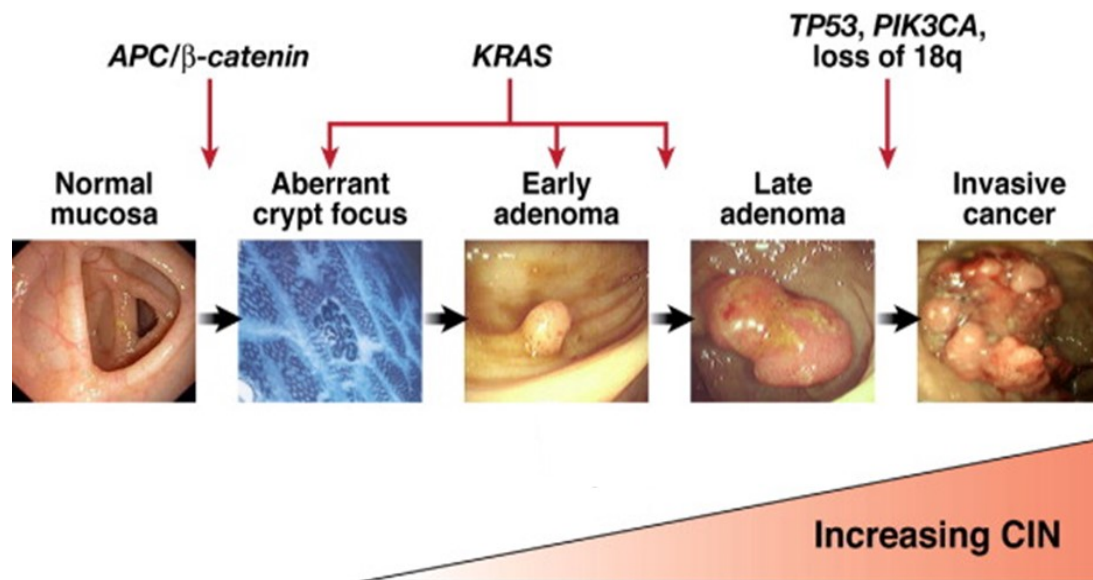


Figure 1.18. Multiple major genetic mutations occur in CRC that lead to disease progression. First, inactivation of the adenomatous polyposis coli (APC) tumor suppressor gene occurs, followed by activating mutations of *KRAS*. Finally, mutations in the transforming growth factor- β , *PIK3CA*, and *TP53* pathways. **Pino and Chung. Gastroenterology. 2010;(6):2059-72. Re-used with permission from Elsevier**

administered in parallel with low-dose radiotherapy²⁷⁰. All these attempts aim to improve overall survival for CRC and increase treatment efficacy. However, the harsh treatment could cause other toxic complications.

DNA repair mechanisms, such as BER and mismatch repair MMR, may not only influence tumor characteristics and prognosis but also dictate chemotherapy response. For example, defective MMR contributes to chemoresistance in CRC²⁷¹. Similarly, efficient BER enhances cellular survival by repairing genotoxic base damage generated from treatment²⁷².

CRC is one of the most common malignancies and has a relatively poor prognosis due to high metastasis and tumor recurrence. In addition, side effects often hinder the success of some chemotherapy and, as in the case of FOLFOX, some patients suffer from renal failure due to oxaliplatin, and there is also a risk of causing female fertility problems^{273, 274}. Accordingly, the integration of targeted small molecules inhibitors with conventional therapy (combination therapy) could reduce toxicity of conventional treatment and improve treatment outcome. Therefore, there is a need to expand personalised therapy to overcome metastatic CRC, increase the survival gains and reduce toxicity in healthy tissues. However, targeting DNA repair pathways may not improve the therapeutic index because there is the increased risk of harming normal cells. We can overcome this problem by targeting small molecule inhibitors to CRC utilizing nanoparticles and/or inducing synthetic lethality in CRC with the targeted small molecule inhibitors (monotherapy) taking advantage of certain deficiencies and weaknesses present in CRC.

1.9. Hypotheses and scope of the thesis

The overarching hypothesis for the work described in this thesis is that small molecule inhibitors of the 3'-phosphatase activity of PNKP can provide an effective means by which to enhance cytotoxicity conferred by ionizing radiation and chemotherapeutic agents targeting topoisomerase 1 and/or elicit cytotoxicity as single agents when used in a synthetic lethal setting. The other hypotheses are as follows:

- 1) To date the small molecule inhibitors of PNKP 3'-phosphatase that have been identified belong to an imidopiperidine family of chemical compounds. We hypothesize that other chemical structures exist that can inhibit PNKP and that these may act by a different mechanism to the imidopiperidine molecules.
- 2) Nano-encapsulation of small molecule inhibitors of the 3'-phosphatase activity of PNKP will enhance the efficacy of the inhibitors by improving solubilization and cellular uptake, thereby enhancing cell killing.
- 3) Given the tight structural interrelationship between the kinase and phosphatase domains of PNKP, the binding of phosphatase inhibitors to the protein may not be confined to the phosphatase domain.

In Chapter 2, we describe in detail the design and development of a novel fluorescence-based assay employing 2-aminopurine that was utilized to screen two libraries of small molecules, a library of natural derivative compounds from which we identified N12 and O7 as inhibitors of PNKP, and a library of polysubstituted imidopiperidine compounds from which A12B4C50 and A83B4C63 were identified. This was followed by characterizing the inhibitors by determining their equilibrium dissociation constant (K_d), and the concentration of the inhibitor which causes 50% reduction of enzyme activity

(IC₅₀) and illustrating the mechanism of action of the new PNKP inhibitors using biophysical and molecular methods.

We have also developed nano-delivery systems for the newly identified hit compounds with potent PNKP inhibitory activity (described in Chapter 3). The inhibitors were encapsulated in polymeric micelles of different poly(ethylene glycol)-*b*-poly(ϵ -caprolactone) (PEG-*b*-PCL) -based structures having various modifications on the PCL block. The amount of encapsulated compounds and the *in vitro* release of inhibitors were measured by high-performance liquid chromatography (HPLC). Targeted delivery to EGFR-expressing cells following conjugation of GE11 peptide to the polymeric micelles was investigated by cellular uptake of an encapsulated dye. The cells that overexpress EGFR showed higher internalization of GE11-modified polymeric micelles. The cytotoxicity of the PNKP inhibitors towards HCT116 colorectal cancer cells was assessed, and, at non-toxic doses, both free and encapsulated inhibitors were tested for their capacity to sensitize HCT116 cells to radiation and irinotecan by colony forming assay. Furthermore, free and encapsulated inhibitors were also tested for their ability to cause synthetic lethality in PTEN-deficient HCT116 cells.

In addition, we investigated the possible binding sites that are involved in the interaction between novel inhibitors and PNKP (described in Chapter 4). Photoactivatable benzophenone derivatives of the newly found inhibitors were synthesized to generate, through photoreaction, an irreversibly labelled PNKP-inhibitor complex. The photolabelled inhibitors were characterized and tested for their ability to bind and inhibit the 3'-phosphatase activity of PNKP. The site of covalent addition to PNKP by the inhibitor

was identified by proteolytic digestions and characterization of the resulting peptides by liquid chromatography - tandem mass spectrometry LC/MS/MS method.

The data we present in this thesis show that the DNA repair enzyme PNKP is a useful target for enhancing CRC treatment. We have also demonstrated the potential of nano-encapsulated inhibitors of PNKP to be used as either mono or combined therapeutic agents for CRC in the future.

Chapter 2: Identification and characterization of new inhibitors of the 3'-phosphatase activity of human polynucleotide kinase/phosphatase

Overview:

In this chapter we discuss the first step of this project, which is the development of a novel fluorescence-based assay utilizing 2-aminopurine to screen two distinct libraries of small molecules. A library of natural derivative compounds from which we identified N12 and O7 as new inhibitors of PNKP, and a library of polysubstituted imidopiperidine compounds from which A12B4C50 and A83B4C63, derivatives of the parent compound A12B4C3, were identified. We also discuss the potency of the inhibitors by determining their K_d and IC_{50} values and investigating the mechanism of action of the new PNKP inhibitors using biophysical and molecular methods.

Identification and characterization of new inhibitors of the 3'-phosphatase activity of
human polynucleotide kinase/phosphatase

Zahra Shire¹, Rajam S. Mani¹, Mesfin Fanta¹, Timothy D R Morgan², Phuwadet Pasarj³,
Charles Holmes³, Dennis G Hall² and Michael Weinfeld^{1*}

¹Department of Oncology, University of Alberta, Edmonton, AB, Canada

²Department of Chemistry, University of Alberta, Edmonton, AB, Canada

³Department of Biochemistry, University of Alberta, Edmonton, AB, Canada

* Corresponding author: Michael Weinfeld, PhD

Experimental Oncology, Cross Cancer Institute 11560 University Ave

Edmonton, AB, T6G 1Z2

Tel: +1 780 432 8438

Fax: +1 780 432 8428

E-mail: michael.weinfeld@albertahealthservices.ca

Abstract

Human polynucleotide kinase/phosphatase (PNKP), which possesses DNA 5'-kinase and 3'-phosphatase activities, plays an essential role in DNA strand break repair by rendering strand-break termini suitable for DNA polymerases and ligases. Inhibition of PNKP increases the sensitivity of cells to ionizing radiation and topoisomerase-I poisons, such as camptothecin. We have developed a rapid fluorescence-based assay to identify small molecule inhibitors of the 3'-phosphatase activity of PNKP. The main components of this assay are two oligonucleotide hairpin probes, PNKP enzyme, and T4 DNA polymerase. T4 DNA polymerase has a powerful 3'→5' exonuclease activity that digests oligonucleotides that have a 3'-OH terminus but is blocked by the presence of a 3'-phosphate terminus. We detect the inhibition of PNKP by monitoring the fluorescence signal of 2-aminopurine (2-Ap) embedded in the stem of the hairpin probes. The fluorescence of 2-Ap is highly quenched when it is incorporated in duplex DNA. One hairpin probe, which has a 3'-OH terminus (HPOH), is used as a control, and the test probe (HPP) is a hairpin with the same sequence as HPOH but has a 3'-PO₄ terminus. In the presence of PNKP, the 3'-PO₄ terminus of the HPP probe is converted to 3'-OH allowing T4 DNA polymerase to hydrolyze the probe, thereby releasing 2-Ap as a highly fluorescent mononucleotide. However, the presence of small molecule inhibitors of PNKP, such as the natural derivative compounds N12 and O7, or the polysubstituted imidopiperidine compounds A12B4C50 and A83B4C63 results in the retention of the 3'-PO₄ terminus of HPP and prevents the increase in the fluorescence signal caused by the release of 2-ApMP. HPOH is used to ensure that the small molecules under investigation do not inhibit the exonuclease activity of T4 DNA polymerase.

2.1. Introduction

Cells in our body are exposed to both endogenous and exogenous agents that cause DNA strand breaks ^{275, 276}, including reactive oxygen species (ROS), inadvertent action by nuclear enzymes on DNA, DNA glycosylases, ionizing radiation, topoisomerase poisons, and physical or mechanical stress on the DNA duplex ^{59, 277-279}. The DNA strand breaks produced by these agents often possess 3'-phosphate termini and 5'-hydroxyl termini ^{280, 281}. The presence of these abnormal termini block DNA polymerisation and ligation ²⁸², and DNA repair mechanisms are required to process such termini, thereby maintaining the stability of the genome and ensuring cell survival.

Human polynucleotide kinase/phosphatase (PNKP), a 57 kDa enzyme, plays an important role in the repair of DNA strand breaks ²⁸³, and as such contributes to several DNA repair pathways including single-strand break repair (SSBR), base excision repair (BER), the nonhomologous end-joining (NHEJ) double-strand break repair pathway, and the repair of topoisomerase-I dead-end complexes ^{96, 154, 284}. Human PNKP possesses two activities, a DNA 5'-kinase activity that catalyzes the phosphorylation of 5'-hydroxyl termini and 3'-phosphatase activity that converts 3'-phosphate termini to 3'-hydroxyl termini ^{84, 280}. If this repair process is deficient or absent, cells accumulate increased levels of strand breaks and thereby become sensitized to genotoxic agents including ionizing radiation, alkylating agents and the topoisomerase-I poison camptothecin ¹¹⁴.

Reducing DNA repair in cancer cells by inhibiting specific DNA repair enzymes is emerging as a new therapeutic strategy to improve cancer treatment, either in combination with radiation or chemotherapy or as monotherapy targeting cells expressing severely reduced levels of a synthetic lethal partner protein of the DNA repair enzyme ²⁸⁵.

We have previously identified several molecules from a relatively small library of polysubstituted imidopiperidine compounds that effectively inhibit the phosphatase activity of PNKP¹⁶⁰. One of these compounds, A12B4C3, was shown to sensitize cells to ionizing radiation and camptothecin^{160, 161} and to induce cell death in cells lacking synthetic lethal partners of PNKP such as SHP-1 and PTEN^{188, 286}. Several methods have been employed to detect inhibitors of DNA 3'-phosphatases^{158, 287}. However, these methods have some limitations with regards to their ease of use, for example the need for radiolabeled substrates, or their requirement for relatively substantial quantities of enzyme (colorimetric assays).

Here we describe the development of a radiolabel free, reliable and rapid fluorescence-based assay for inhibitors of 3'-DNA phosphatase activity based on the release of 2-aminopurine monodeoxynucleotide (2-ApMP). We have used this assay to screen new derivatives of A12B4C3 (A12B4C50 and A83B4C63) as well as a series of 200 natural compounds or derivatives of natural compounds, from which we identified novel inhibitors of PNKP (N12 and O7).

2.2. Experimental procedures

2.2.1. Materials

Synthetic oligonucleotides hairpin probes were obtained from Integrated DNA Technologies, Inc. (Coralville, IA, USA). See Figure 2.1A for the oligonucleotide sequences, 5'-GTGTCGTCCTTGGAAAAACCAAGG(2-Ap)CGACAC-OH-3' is the control sequence and 5'-GTGTCGTCCTTGGAAAAACCAAGG(2-Ap)CGACAC-PO₄-3' is the test sequence. 2-Amino-9-(β-D-2-deoxyribofuranosyl)purine (2-Ap), Figure 2.1B, was purchased from Berry & Associates (Dexter, MI, US). PiColorLock Gold reagent was purchased from Innova Biosciences Ltd. (San Diego, CA, US). Magnesium chloride was obtained from EMD Chemicals Inc. (Gibbstown, NJ, US), sodium chloride from ACP Chemicals Inc. (Montreal, QC, CA), ultrapure Tris from ICN Biomedical Inc. (Aurora, OH, US), dithiothreitol (DTT) from Gold Biotechnology (St. Louis, MO, USA), HEPES and EDTA from Fisher Scientific Company (Fairlawn, NJ, US). All chemicals were used as received without further purification. Oligonucleotide test samples were dissolved in Tris-buffer (10 mM Tris (pH 7.5), 50 mM NaCl, 3 mM MgCl₂, 1 mM EDTA) to a concentration of 2 μM. Samples were kept frozen at -20 °C until needed. The hairpin probes were dissolved in Tris-buffer, and then annealed by heating in a water bath to 80 °C, followed by cooling to room temperature.

Recombinant PNKP, produced in *E.coli*, was purified as described previously^{280, 288} and stored in 50 mM Tris-HCl (pH 7.4), 100 mM NaCl, 5 mM MgCl₂, and 0.5 mM DTT. T4 DNA polymerase was prepared as previously described²⁸⁹, T7 DNA polymerase and Klenow fragment were purchased from New England Biolabs Inc. (Ipswich, MA, US). Biomol Green was purchased from Enzo Life Sciences Inc. (Farmingdale, NY, US). Myria

screen II and natural derivative compounds were purchased from Time Tec Inc. (Newark, DE, US).

2.2.2. Synthesis of polysubstituted imidopiperidine compounds

Compounds A12B4C50 and A83B4C63 (Table 2.1) were prepared by Dr. Timothy Morgan (Department of Chemistry, University of Alberta) according to the previously reported procedure ²⁹⁰. The heterodiene (1 equiv) and maleimide (1.5-2 equiv) were dissolved in toluene in a screw-cap reaction vial. The aldehyde (2 equiv) was added and the vial was sealed and heated to 85 °C for three days. After cooling to room temperature, the solvent was removed under reduced pressure. The residue was purified by flash column chromatography (ethyl acetate (EtOAc)/Hexane solvent system) to afford yellow solids (40-70% yield). The compounds were further purified by semi-prep high-performance liquid chromatography (HPLC) to purities of 95-99%. Pure compounds were characterized by nuclear magnetic resonance (NMR), infrared spectroscopy (IR) and mass spectrometry (refer to appendix Figs. A7-A8).

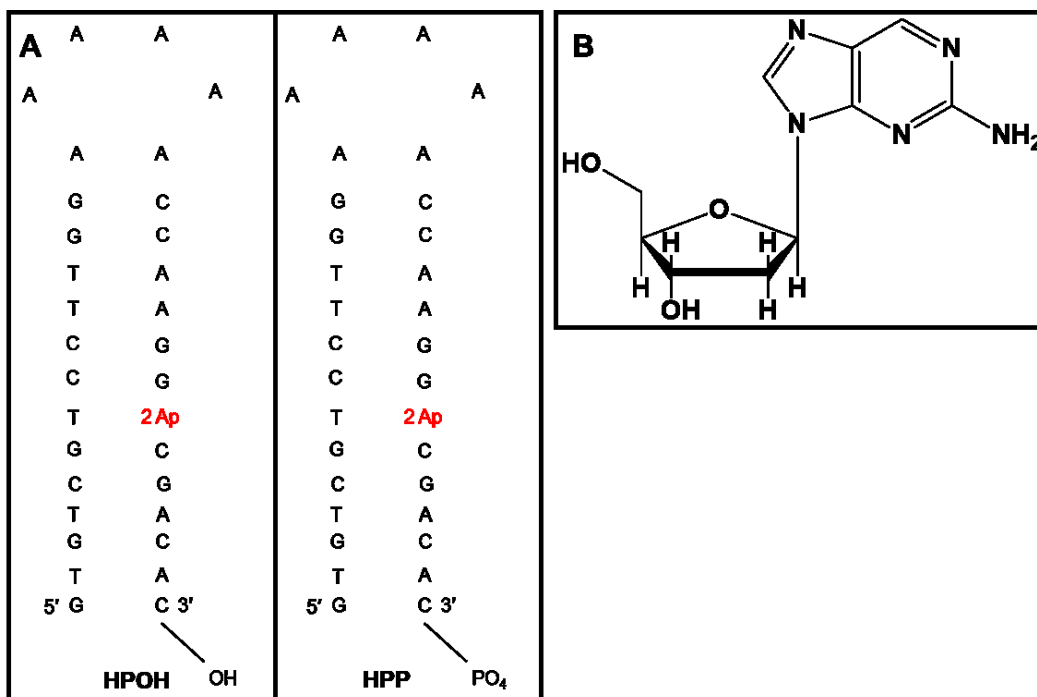
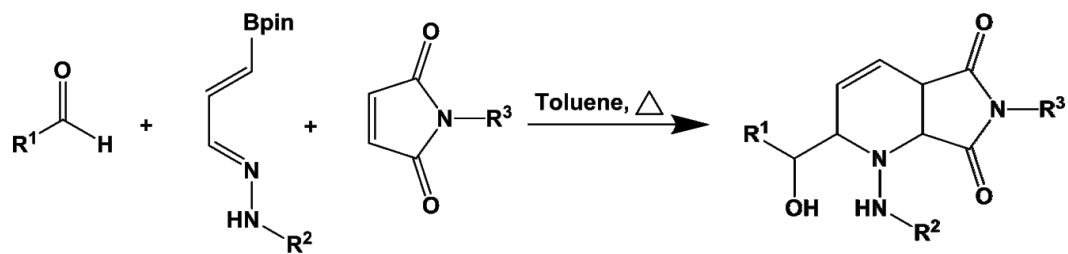
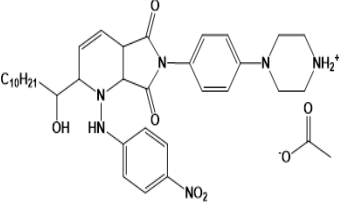
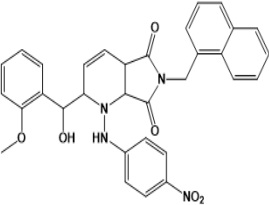
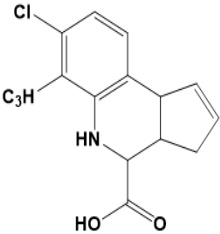
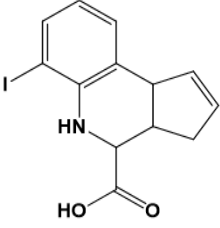


Figure 2.1. (A) The structure of the hairpin probes used for the screening assay. (B) The structure of 2-Amino-9-(β -D-2-deoxyribofuranosyl purine) (2-Ap).



Scheme 2.1. Mechanism of synthesis of polysubstituted imidopiperidines.

Table 2.1. Chemical structures of newly found PNKP inhibitors

Compound	Structure
A12B4C50	 <p>The structure of A12B4C50 is a complex heterocyclic molecule. It features a central bicyclic core consisting of a piperidine ring fused to a five-membered ring containing two carbonyl groups and a nitrogen atom. This core is substituted with a C₁₀H₂₁ group, a hydroxyl group, and a 4-nitrophenyl group. Additionally, it is linked to a piperazine ring which is further substituted with an acetate group.</p>
A83B4C63	 <p>The structure of A83B4C63 is a complex heterocyclic molecule. It features a central bicyclic core consisting of a piperidine ring fused to a five-membered ring containing two carbonyl groups and a nitrogen atom. This core is substituted with a 4-methoxyphenyl group, a hydroxyl group, and a 4-nitrophenyl group. Additionally, it is linked to a naphthalene ring system.</p>
N12	 <p>The structure of N12 is a complex heterocyclic molecule. It features a central bicyclic core consisting of a piperidine ring fused to a five-membered ring containing a nitrogen atom and a carbonyl group. This core is substituted with a chlorine atom, a C₃H group, and a hydroxyl group. Additionally, it is linked to a cyclopentadiene ring system.</p>
07	 <p>The structure of 07 is a complex heterocyclic molecule. It features a central bicyclic core consisting of a piperidine ring fused to a five-membered ring containing a nitrogen atom and a carbonyl group. This core is substituted with an iodine atom and a hydroxyl group. Additionally, it is linked to a cyclopentadiene ring system.</p>

2.3. Methods

2.3.1. Fluorescence-based assay for screening small molecules inhibitors of the 3'-phosphatase activity of PNKP

The assays (100 μ L total volume) were performed in Corning 3573 black, flat bottom 384-well microplates, purchased from Corning Life Sciences (Tewksbury, MA, US), and prepared in 100 mM HEPES (pH 7.5), 50 mM NaCl, 10 mM MgCl₂, and 1mM DTT. Several DNA polymerases were tested for this assay including Klenow fragment I of *E. coli* DNA polymerase, T4 and T7 phage DNA polymerases. Initially 25 nM PNKP (2.5 μ L) was preincubated with 10 μ M test compound (2 μ L) or DMSO vehicle for 5-15 min at room temperature. Then HPP (10 μ L) or HPOH (10 μ L) and 80 nM T4 DNA polymerase (4 μ L) were added.

The phosphatase activity of PNKP was monitored by first treating HPP (10 μ L) with 25 nM PNKP (2.5 μ L) to convert all 3'-P to 3'-OH, then adding 80 nM T4 DNA polymerase (4 μ L) to hydrolyse the recovered hairpins. Finally, the released 2-Ap led to an increase in the fluorescence signal. However, the fluorescence signal of 2-Ap was reduced after incubating PNKP with 10 μ M and 25 μ M inhibitor (2 μ L) for 5-15 min. Fluorescence (320 nm excitation and 405 nm emission) of each well was read in a FLUOstar Optima (BMG Labtech Inc., Guelph, ON, CA). Data were analyzed using Graphpad Prism software.

2.3.2. Determination of binding constants to PNKP

Fluorescence titrations of PNKP with small molecule inhibitors were measured by Dr. Rajam Mani (Department of Oncology, University of Alberta) at 25 °C using a PerkinElmer Life Sciences LS-55 spectrofluorometer with 3 nm spectral resolution for excitation and emission as previously described²⁸⁸. PNKP fluorescence was excited at 295 nm, and

fluorescence emission was recorded at 340 nm. In this experimental design a single concentration of the receptor (PNKP) was used and varied the concentration of the ligand (inhibitor). Binding of the inhibitor to PNKP was analyzed using the equation:

$$[LR] = \frac{([X] + [R_{tot}] + kd) \pm \sqrt{([X] + [R_{tot}] + kd)^2 - 4[X][R_{tot}]}}{2}$$

$L = X - LR$.

Where, X is the total Ligand concentration and R_{tot} : is the total receptor concentration (Same units as X). LR refers to ligand bound to the receptor and the L is the free ligand concentration. Binding data were analyzed using Prism (GraphPad Software Inc., La Jolla, CA).

2.3.3. Mechanism of inhibition, Lineweaver-Burk plot

PNKP phosphatase activity was determined by the PiColorLock Gold reagent. This protocol is modified from a previously described method ¹⁶¹. Briefly, the phosphatase reactions (20 μ L total volume) were prepared as follows: 3 μ L of PNKP (100 ng), 2 μ L of 10 X phosphatase buffer (100 mM Tris HCl, pH 7.4, 500 mM NaCl, and 100 mM Mg_2Cl), 2 μ L of 0, 100, 200, 400, or 800 μ M 3'-phosphorylated 20-mer oligonucleotide, 15 μ L of distilled H_2O , and 2 μ L of PNKP inhibitors to a final concentration of 1, 5, 10, or 20 μ M. The assays were performed in a clear polystyrene colorimetric 384-well plate, purchased from Corning Life Sciences (Tewksbury, MA, US), and incubated at 25 °C for 5-10 min. Finally, PiColorLock Gold reagent was prepared by the addition of 1:100 volume of accelerator to the Gold reagent. The reagent mixture was then added to the reaction samples in a volume ratio of 1:4 (incubated at 37 °C for 30 min) and absorbance was

read at 620 nm using a FLUOstar Optima (BMG Labtech Inc., Guelph, ON, CA). Data were analyzed using Graphpad Prism software.

2.3.4. Testing possible protein phosphatase inhibition by PNKP inhibitors

The phosphatase activity of aspartate-based ubiquitous Mg²⁺-dependent phosphatase (AUM), protein phosphatase 1 catalytic subunit (PP-1c) and calcineurin (CAN) were tested (Dr. Phuwadet Pasarij, Department of Biochemistry, University of Alberta) using a colorimetric *p*-nitrophenol phosphate assay as described previously^{160, 291}. The reactions were performed in a 96-well microplate in a final volume of 60 µL containing 40 µL of *p*-nitrophenol phosphate assay buffer [50 mM Tris (pH 7.4), 0.1 mM EDTA, 30 mM MgCl₂, 0.5 mM MnCl₂, 1 mg/mL BSA, and 0.2% β-mercaptoethanol], 0.03 µg PP-1c (specific activity of >30 units per mg) or a catalytically equivalent quantity of CAN and AUM. A12B4C50, A83B4C63, N12 and O7 dissolved in DMSO (10 µL of 0.5 mM or 10 µL of 50 µM) or control solvent were added to the reaction. After a 10-min incubation at 37°C, 10 µL of 30 mM *p*-nitrophenol phosphate was added to each well and incubated for an additional 60 and 45 min for AUM, PP-1c and CAN, respectively. The absorbance at 405 nm was measured using a SOFTmax 2.35 kinetic microplate reader (Molecular Devices).

2.3.5. Conventional radio-gel assay to detect PNKP 5'-kinase activity

This experiment was conducted by Mesfin Fanta (Department of oncology, University of Alberta). PNKP (0.02 nmol) was premixed with 0.2 nmol of the inhibitors (O7, N12, A12B4C50 and A83B4C63) and incubated at 37°C for 5 min. Kinase buffer (80 mM succinic acid (pH5.5), 10 mM MgCl₂, and 1 mM dithiothreitol), 0.2 nmol of 24-mer DNA substrate (Integrated DNA Technologies), and 3.3 pmol of [γ-³²P]ATP (PerkinElmer Life Sciences) were added to the mixtures, and incubated for 20 min. 4 µl samples were mixed

with 2 μ l of 3X sequencing gel loading dye (Fisher), boiled for 10 min and run on a 12% polyacrylamide sequencing gel which contains 7 M urea at 200 V. Gels were scanned on a Typhoon 9400 variable mode imager (GE Healthcare, Bucks, UK) and the resulting bands were quantified using Image Quant 5.2 (GE Healthcare, Bucks, UK). This assay was performed by Mesfin Fanta (Department of Oncology, University of Alberta).

2.3.6 Statistical analysis

Each experimental group was compared with a control group using a two-tailed unpaired Student's *t*-test. The software used was GraphPad Prism5 software (La Jolla, CA, USA). A value of $P < 0.05$ was considered as statistically significant in all experiments. Error bars represent mean \pm SD.

2.4. Results

2.4.1. Test for the exonuclease and phosphatase activities of the DNA polymerase and PNKP with the 2-Ap hairpin probes

The basis of the novel fluorescence assay for the 3'-phosphatase activity of PNKP is shown schematically in Figure 2.2. The fluorescence is generated as a result of digestion of an oligonucleotide to release the fluorescent mononucleotide (2-ApMP) of 2-aminopurine (2-Ap). 2-Ap is an analog of adenine and guanine that pairs with both thymine and cytosine. It has been used previously for probing the dynamic structure of DNA polymerases ²⁹²⁻²⁹⁵. The fluorescence of 2-Ap is highly quenched when incorporated in double-stranded DNA due to base stacking, slightly fluorescent in single-stranded DNA, while the maximum fluorescence is detected for the free base or nucleotide ^{296, 297}. Figure 2.1A shows the structure of the two hairpin probes that we designed for this assay. The test probe (HPP) bears a 2-Ap in the stem of the hairpin

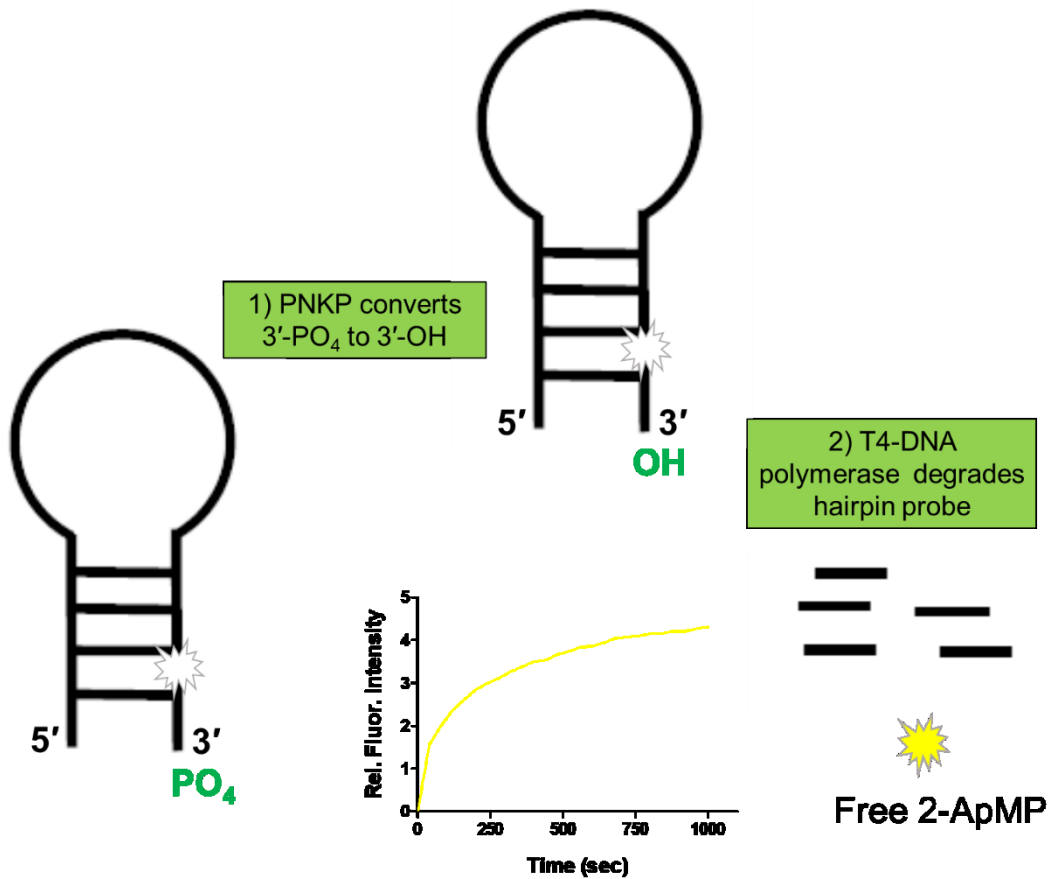


Figure 2.2. Schematic diagram of the function of the novel fluorescence assay for the 3'-phosphatase activity of PNKP. First, PNKP will convert 3'-PO₄ group to 3'-OH group. Second, T4 DNA polymerase will be able to digest the probe. Finally, the fluorescence signal will develop due to release of 2-ApMP.

and a 3'-PO₄ terminus that is resistant to the 3'→5' exonuclease activity of many DNA polymerases unless first removed by the PNKP 3'-phosphatase. The second probe (HPOH) has the same structure as HPP but has a 3'-hydroxyl terminus and is used as a control to ensure that failure to generate a fluorescent signal is not due to inhibition of the exonuclease rather than inhibition of PNKP phosphatase activity.

Several DNA polymerases were examined for this assay including Klenow fragment I of *E. coli* DNA polymerase, phage T4 and T7 DNA polymerases. The 3'→5' exonuclease activity of these enzymes is dominant in the absence of deoxynucleotide triphosphates. We have optimized the amount of the oligonucleotides hairpin probes, DNA polymerase and PNKP to be used in this assay (Figs. A1-A3) (refer to Appendix). Initially, we tested the ability of the three different DNA polymerases to hydrolyze the hairpin probes. Figure 2.3 shows the change in the fluorescence intensity over time after incubating the probes with each polymerase. While phage T4 (Figure 2.3A) and T7 (Figure 2.3B) DNA polymerases both readily hydrolyzed HPOH, thereby releasing 2-ApMP, Klenow fragment (Figure 2.3C), which has a weaker exonuclease activity, generated no increase in fluorescence. The latter observation is not surprising, because previous studies showed that the 3'→5' exonuclease activity of the Klenow fragment is faster and more efficient with single-stranded than double-stranded DNA ²⁹⁸. In contrast, incubation of the 3'-phosphorylated substrate, HPP, with T4 and T7 DNA polymerases elicited no increase in fluorescence signal (Figures 2.3A and 2.3B), but an increase in fluorescence was observed when HPP was incubated with PNKP and T4 or T7 DNA polymerase (Figures 2.3B and 2.3C), due to 3'-dephosphorylation followed by digestion of the probes. As a

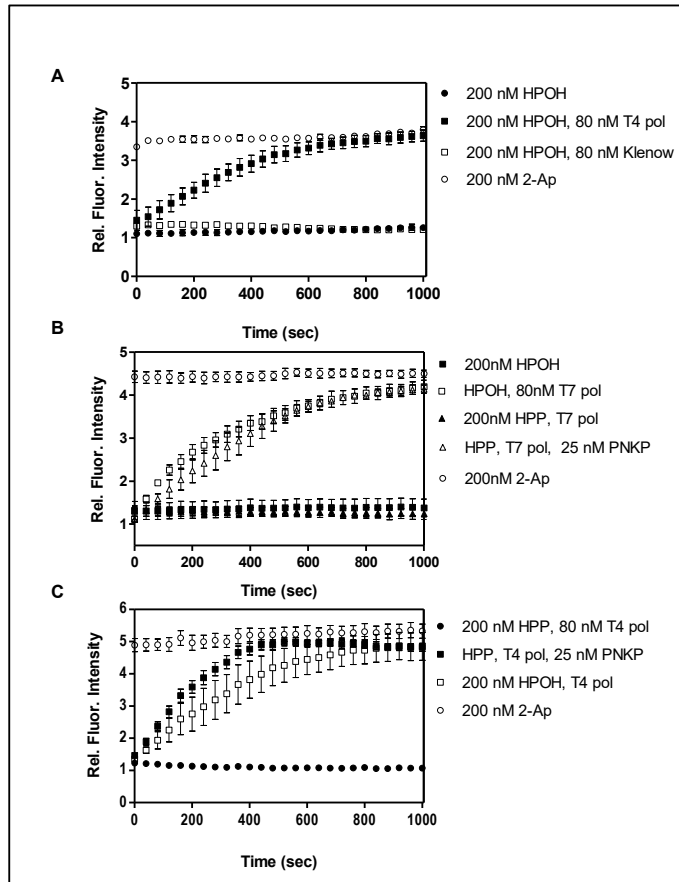


Figure 2.3. The hydrolysis of hairpin probes treated with DNA polymerases and PNKP. (A) 200 nM HPOH (filled circles), 200 nM HPOH treated with 80 nM T4 pol (filled squares). 200 nM HPOH treated with 80 nM Klenow (open squares) and 200 nM 2-Ap (open circles), which was used as a control for 2-ApMP because the base and mononucleotide display the same fluorescence. **(B)** 200 nM HPOH treated with 80 nM T7 pol (open squares). 200 nM HPP treated with 80 nM T7 pol (filled triangles), 200 nM HPP treated with 80 nM T7 pol and 25 nM PNKP (open triangles). **(C)** 200 nM HPP treated with 80 nM T4 pol (filled circles), 200 nM HPP treated with 80 nM T4 pol and 25 nM PNKP (filled squares). Each point represents the mean \pm SD ($n = 3$).

result of these data, we chose to carry out further measurements using T4 DNA polymerase.

2.4.2. Screening small molecule inhibitors with the fluorescence-based assay

Prior to using the assay for screening, we examined its applicability by testing compounds previously shown ¹⁶⁰ to inhibit (A12B4C3) and not inhibit (A70B4C3) PNKP 3'-phosphatase using a conventional radiolabeled based approach. As is evident from Figure 2.4, the presence of A12B4C3 reduced the expected increase in the fluorescence signal, while A70B4C3 elicited no effect.

Next, we tested two new derivatives of A12B4C3 for inhibition of PNKP phosphatase activity, A12B4C50 and A83B4C63 (Table 2.1). Figure 2.5A and C show the fluorescence signal obtained with PNKP treated with 10 μ M A12B4C50 and A83B4C63. A decrease in the fluorescence signal is observed in comparison to the PNKP free of drug, which indicates a possible blocking effect of the phosphatase activity of PNKP by A12B4C50 and A83B4C63. To further confirm this observation, we treated T4 pol with the same amount of the drugs to check if the exonuclease activity of the polymerase is targeted by A12B4C50 and A83B4C63. As shown in Figure 2.5B and D, there was no inhibitory effect on the exonuclease activity of T4 pol in the presence of 10 μ M A12B4C50 and A83B4C63, which indicates that the reduced fluorescence signal was indeed due to the inhibition of PNKP only.

We also tested a small library of 200 natural product derivatives for inhibition of PNKP phosphatase activity, and one compound N12 (7-chloro-6-methyl-3,4,5,3a,9b-pentahydrocyclopenta [1,2-c] quinolone-4-carboxylic acid, Table 2.1) gave a positive result.

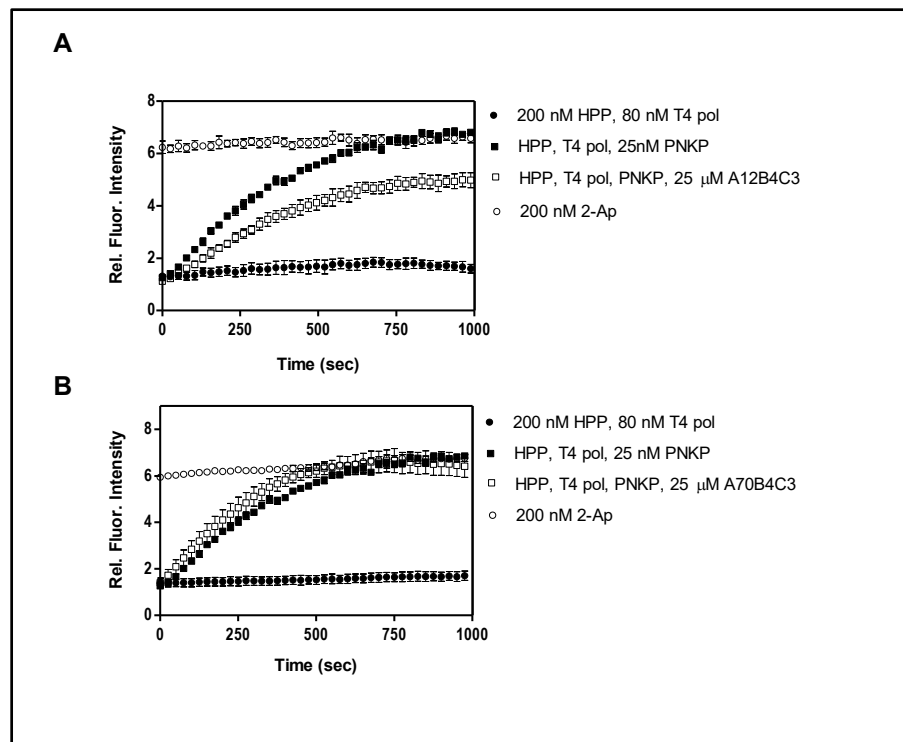


Figure 2.4. The effect of A12B4C3 and A70B4C3 on PNKP activity. (A) Incubation of hairpin HPP with both PNKP and T4 pol causes an increase in the fluorescence signal (filled squares), indicating release of 2-ApMP from the hairpin. In the presence of A12B4C3, the fluorescence signal is partially reduced (open squares), indicating partial inhibition of PNKP phosphatase activity. (B) There was no reduction of 2-ApMP release in the presence of A70B4C3 (open squares), indicating poor inhibition. Each point represents the mean \pm SD ($n = 3$).

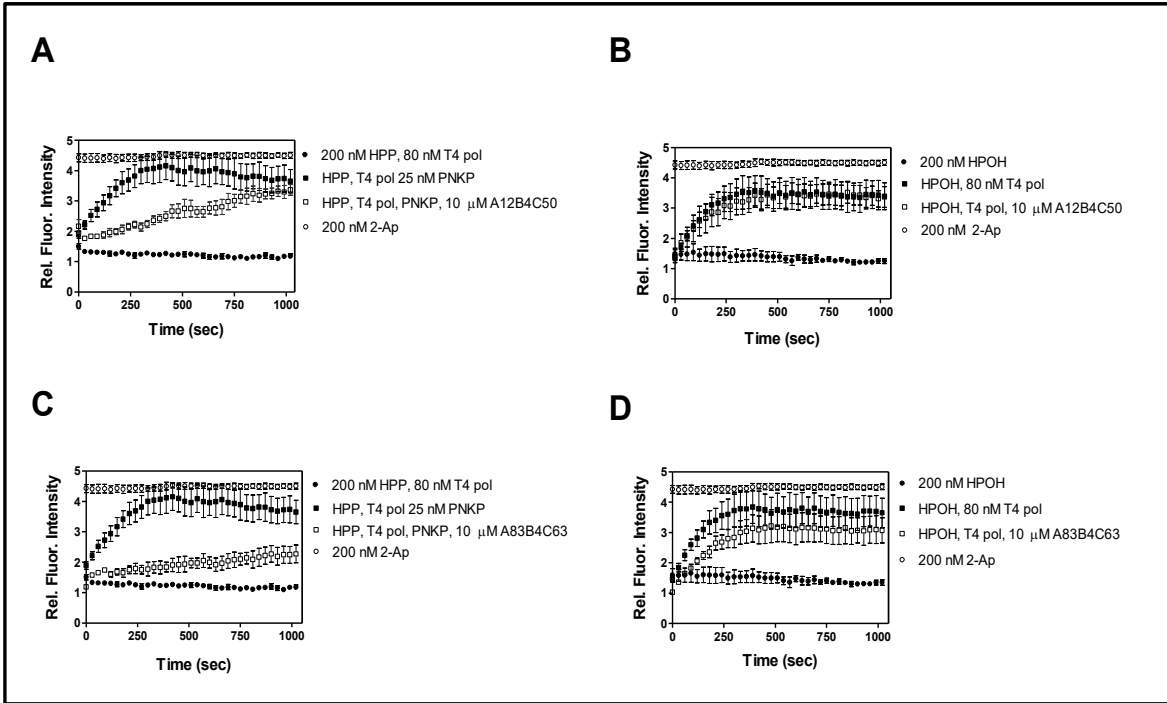


Figure 2.5. The effect of A12B4C50 and A83B4C63 on PNKP activity. (A and C)

Incubation of hairpin HPP with both PNKP and T4 pol caused an increase in the fluorescence signal (filled squares), indicating release of 2-ApMP from the hairpin. In the presence of A12B4C50 and A83B4C63, the fluorescence signal was reduced (open squares), indicating inhibition of PNKP phosphatase activity. **(B and D)** Incubation of hairpin HPOH to assess if T4 pol is inhibited by A12B4C50 or A83B4C63. There was no reduction of 2-ApMP release in the presence of A12B4C50, however, A83B4C63 caused a small reduction of 2-ApMP release (open squares), indicating a low level of inhibition of T4 pol. Each point represents the mean \pm SD ($n = 3$).

Figure 2.6 shows the clear difference between N12 and a group of compounds from the same library showing a negative response.

Figure 2.7A shows the fluorescence signal obtained with PNKP treated with 10 μ M N12. A decrease in the fluorescence signal is observed in comparison to the PNKP free of inhibitor, which indicates a possible blocking effect of the phosphatase activity of PNKP by N12. To further confirm this observation, we treated T4 pol with the same amount of N12 to check if the exonuclease activity of the polymerase is targeted by N12. As shown in Figure 2.7B, there was no inhibitory effect on the exonuclease activity of T4 pol in the presence of 10 μ M N12, which indicates that the reduced fluorescence signal was indeed due to the inhibition of PNKP only.

Since N12 has a radically different structure to our previously identified PNKP inhibitor, the polysubstituted imidopiperidine A12B4C3, we tested another compound with a similar basic structure to N12 (6-iodo-6-methyl-3,4,5,3a,9b-pentahydrocyclopenta [1,2-c] quinolone-4-carboxylic acid (O7), Table 2.1), which was not in the original 200 compounds screened. The fluorescence assay indicates that O7 also inhibits PNKP phosphatase (Figure 2.7C), although it also displays a modest inhibition of the exonuclease activity of T4 pol (Figure 2.7D).

2.4.3. Measurement of IC₅₀ values

The 2-Ap-based assay was used to determine IC₅₀ values for the newly identified compounds by incubating PNKP with concentrations ranging from 0.1 to 10 μ M. Figure 2.8 shows that the phosphatase activity of PNKP is affected significantly at concentrations

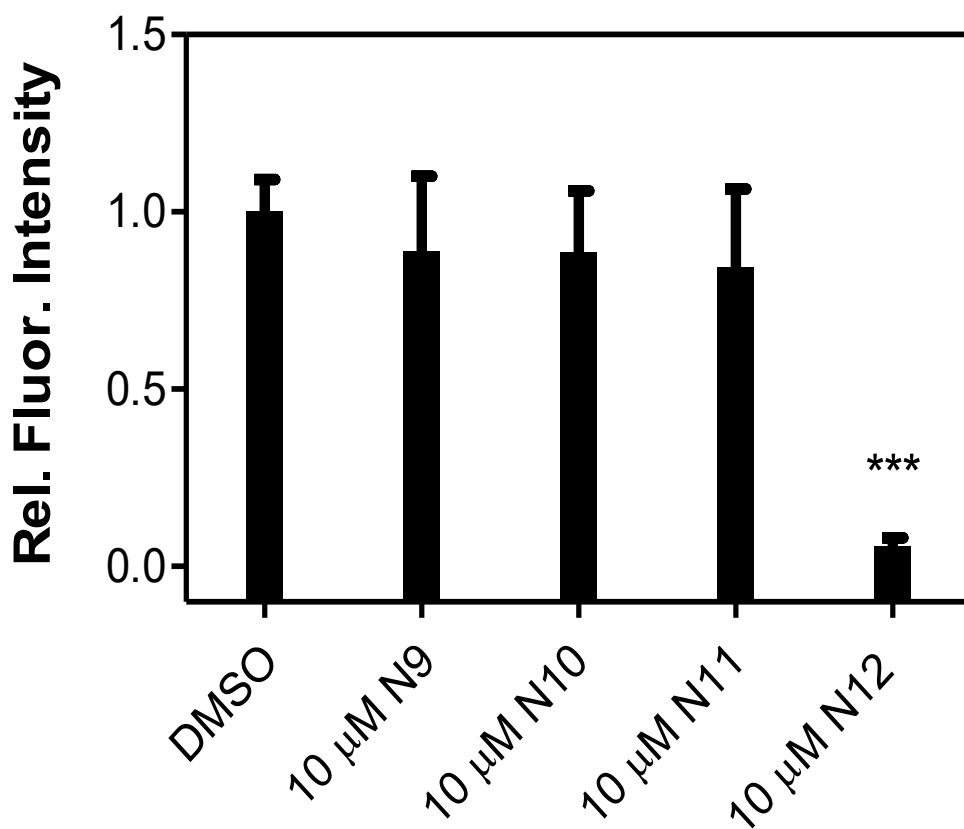


Figure 2.6. The effect of different small molecules from library of 200 natural product derivatives on PNKP activity. The initial screening of the compounds showed that N12 is a positive hit for PNKP phosphatase activity inhibition. Each point represents the mean \pm SD (n = 3). Marked points were compared to control group and are statistically significant at (***) $P \leq 0.001$.

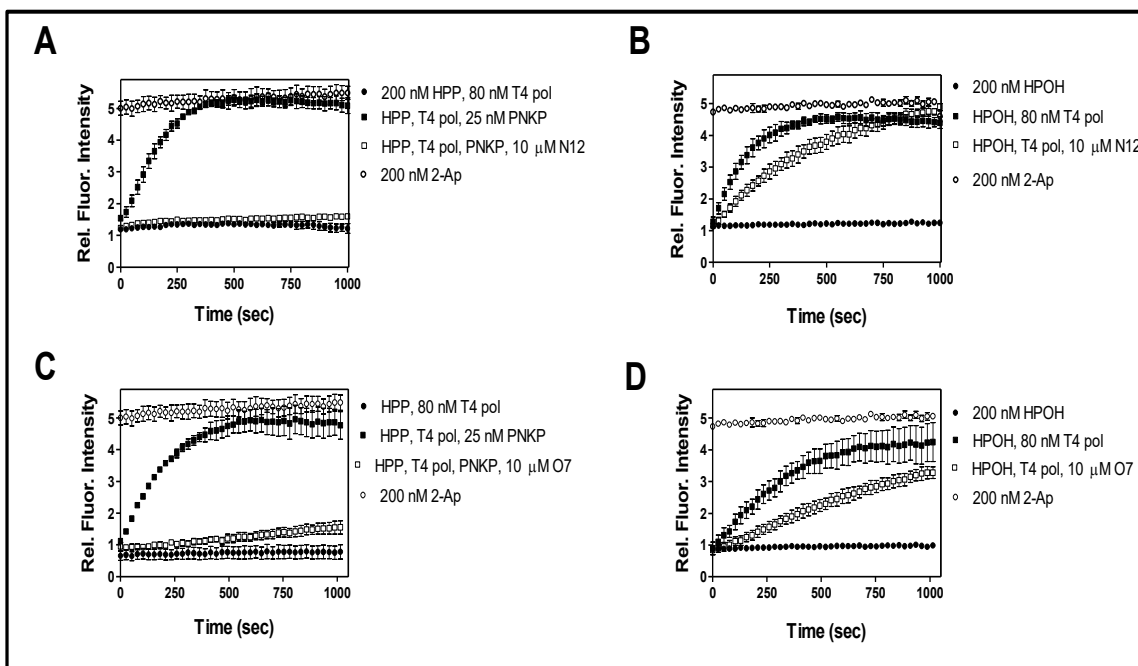


Figure 2.7. The effect of N12 and O7 on PNKP activity. (A and C) Incubation of hairpin HPP with both PNKP and T4 pol caused an increase in the fluorescence signal (filled squares), indicating release of 2-ApMP from the hairpin. In the presence of N12 and O7, the fluorescence signal was significantly reduced (open squares), indicating inhibition of PNKP phosphatase activity. **(B and D)** Hairpin HPOH was used to assess if N12 or O7 inhibit T4 pol. There was a slight reduction of 2-ApMP release in the presence of N12 and O7 (open squares), indicating a low level of T4 pol inhibition by these compounds. Each point represents the mean \pm SD ($n = 3$).

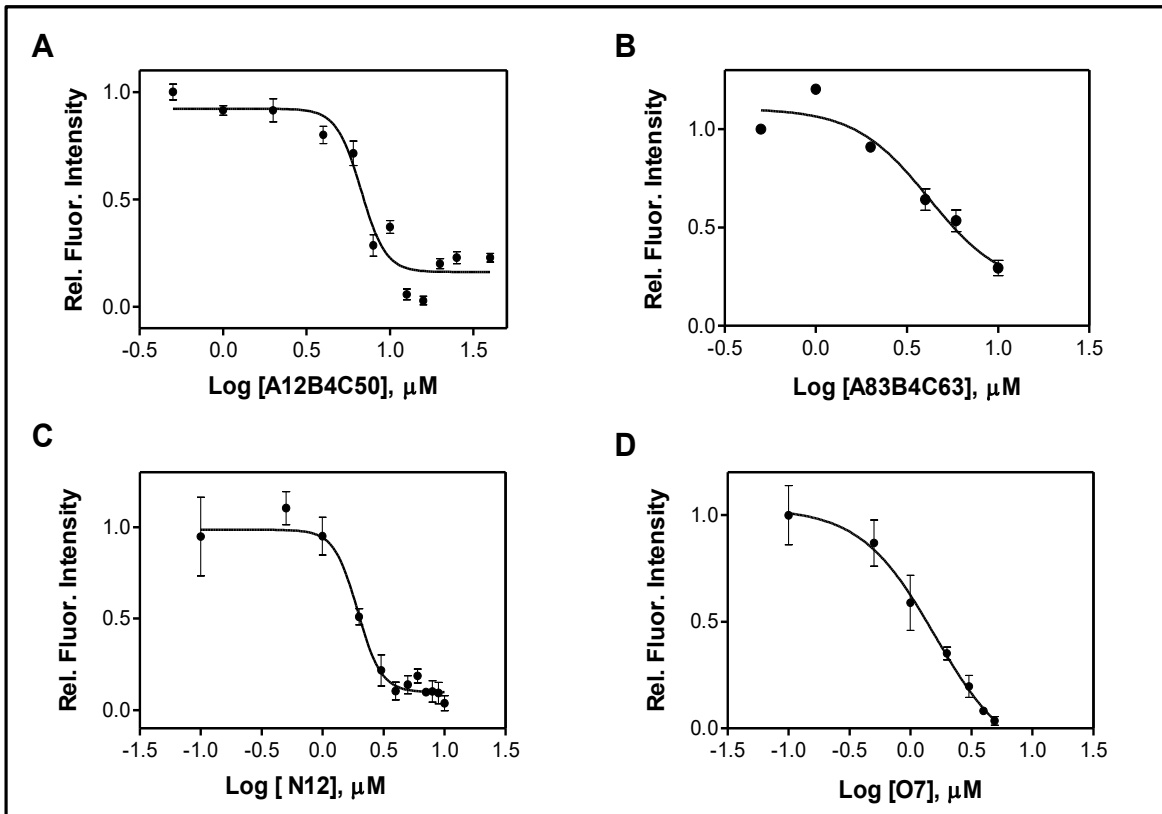


Figure 2.8. Dose dependent inhibition of PNKP by inhibitors. The IC₅₀ values were determined using Graphpad Prism software. Each point represents the mean \pm SD (n = 3).

higher than 2 μM of PNKP inhibitors. The IC_{50} values of N12 and O7 were determined to be $\sim 1.6 \mu\text{M}$ and $1.9 \mu\text{M}$, respectively.

2.4.4. Measurements of K_d values

Binding constants of the inhibitors to PNKP were obtained by fluorescence spectroscopy. Since binding of the inhibitor to PNKP partially quenches the intrinsic protein fluorescence due to tryptophan residues at 340 nm following excitation at 295 nm, the binding affinity (K_d) can be determined by following fluorescence quenching as a function of ligand concentration. Figure 2.9 shows the fluorescence intensities versus the concentrations of A12B4C50, A83B4C63, N12 and O7. Nonlinear regression analysis of the binding data revealed unimodal binding with a K_d value of $0.1 \pm 0.05 \mu\text{M}$ for A12B4C50, $0.09 \pm 0.05 \mu\text{M}$ for A83B4C63, $0.14 \pm 0.02 \mu\text{M}$ for N12 and $0.1 \mu\text{M} \pm 0.02$ for O7.

2.4.5. Mechanism of inhibition of PNKP phosphatase activity by inhibitors

The mechanism of inhibition of PNKP phosphatase activity by the newly found inhibitors was determined by a Lineweaver-Burk analysis of the substrate concentration dependence on the reaction. We chose A83B4C63 as a representative of polysubstituted imidopiperidine compounds and N12 from the natural compound hits to be tested for their mechanism of inhibition.

Phosphatase activity was determined using a Pi-Colorlock assay in which the substrate is a 20-mer single-stranded oligonucleotide bearing a terminal 3'-phosphate group. To determine the mode of inhibition, the assay was carried out using a fixed enzyme concentration while varying the concentration of the inhibitors and the substrates. A plot of $1/[S]$ versus $1/V$ is shown in Figure 2.10. Figure 2.10A, the observed velocity V , which

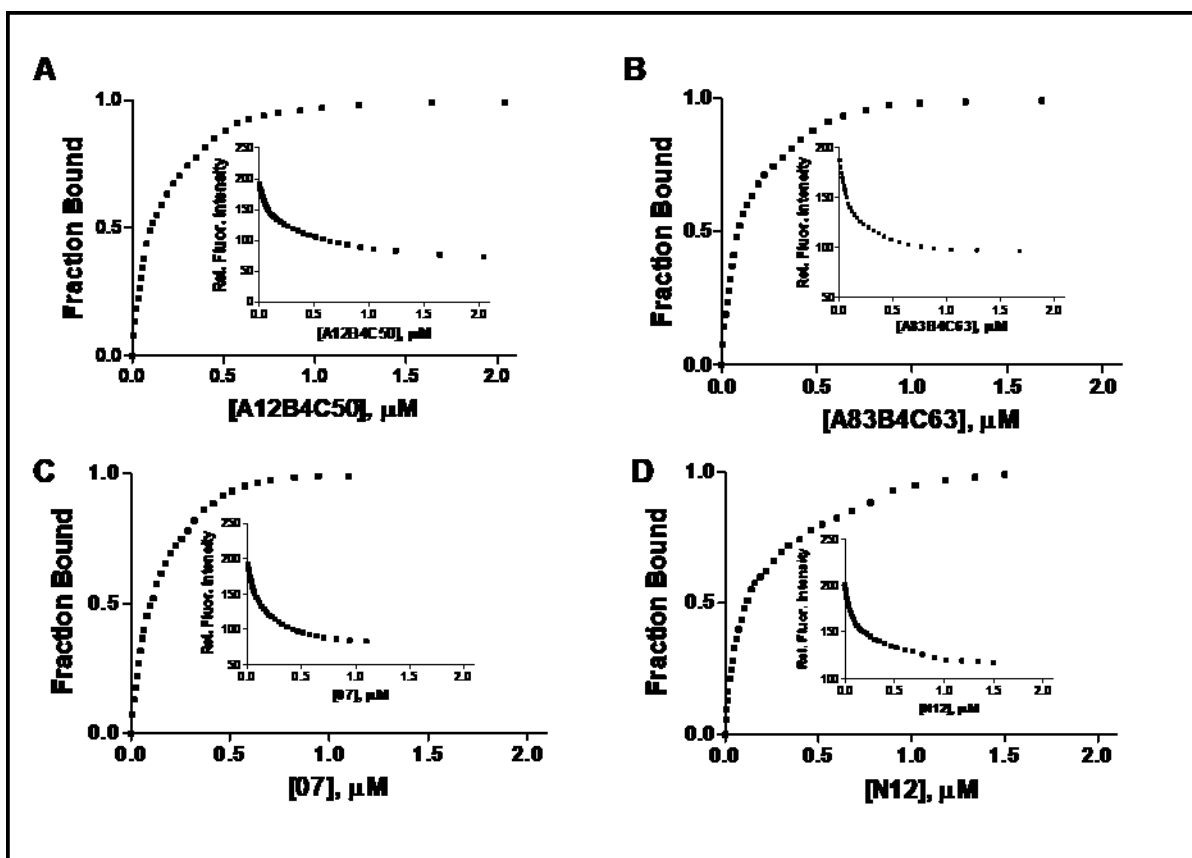


Figure 2.9. A plot of fluorescence intensities of titration of PNKP. (A) A12B4C50, (B) A83B4C63, (C) N12 and (D) O7. PNKP (0.3 μM) in 50 mM Tris HCl (pH 7.5), 100 mM NaCl, 5 mM MgCl_2 was excited at 295 nm, and fluorescence intensity was monitored at 340 nm. Data presented in this figure were generated by Dr. Rajam S. Mani.

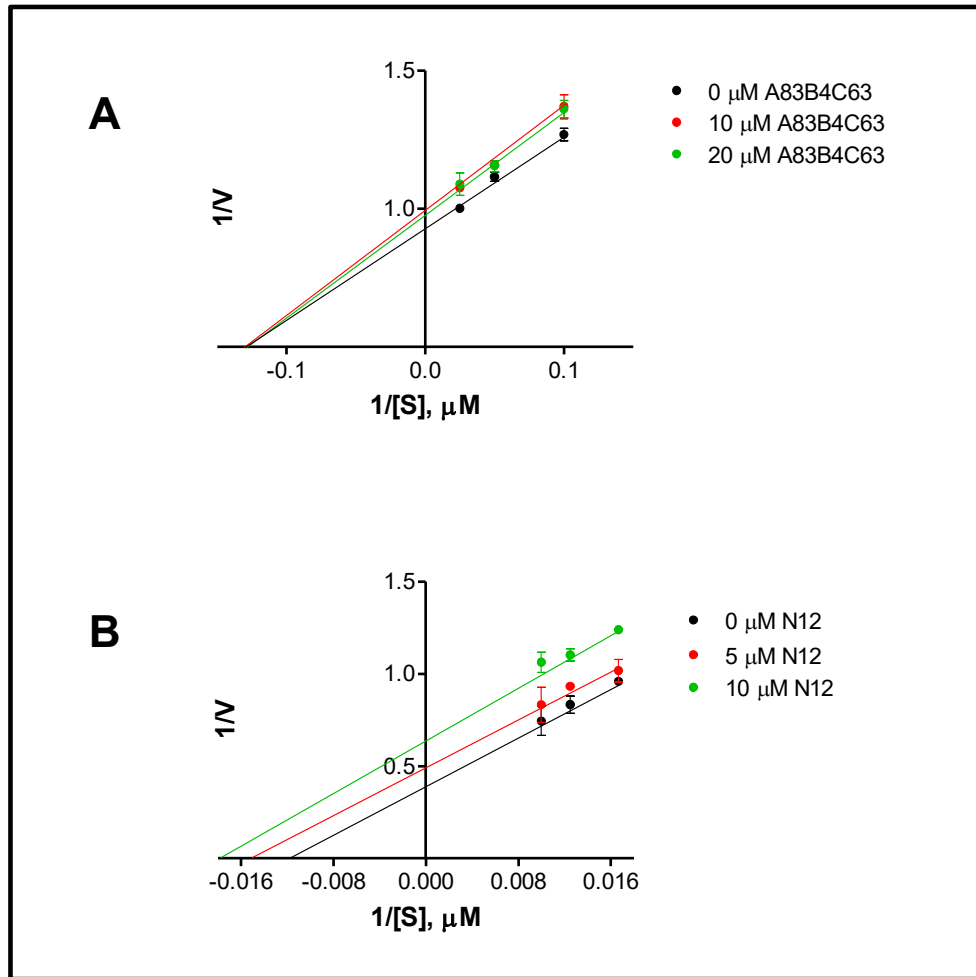


Figure 2.10. Lineweaver-Burk analysis of the inhibition of PNKP phosphatase activity using varying concentrations of A83B4C63, N12 and 20-mer 3'-phosphorylated substrate. Each point represents the mean \pm SD ($n = 3$).

is a measure of the color change, decreased as A83B4C63 concentrations were increased, whereas the K_m (the substrate concentration at which the reaction rate is half of V_{max}) value remained the same. This type of response is the hallmark of a non-competitive inhibitor. This result is in accordance with what was previously observed for the parent compound A12B4C3¹⁶¹. On the other hand, the observed velocity V as well as the K_m values decreased as N12 concentrations were increased. This type of response is the hallmark of an *uncompetitive* inhibitor (Figure 2.10B).

2.4.6. Specificity of inhibitors

To determine the specificity of inhibitors for PNKP phosphatase activity, we examined a number of protein phosphatases such as calcineurin and PP-1c. We also broadened our examination to include aspartate-based ubiquitous Mg^{2+} -dependent phosphatase (AUM), which like PNKP belongs to the HAD superfamily. Figure 2.11 shows the effect of inhibitors on the three protein phosphatases. We detected a slight decrease in the proteins' phosphatase activity when incubated with 100 μ M of PNKP inhibitors, which is higher than the effective doses we observed for PNKP inhibition. These results indicate that the newly found PNKP inhibitors are more specific to PNKP than PP-1c, CAN or AUM.

2.4.7. The effect of PNKP phosphatase inhibitors on the kinase activity

The effect of A83B4C63, A12B4C50, O7 and N12 on the kinase activity of PNKP was tested by monitoring the transfer of ³²P-labeled phosphate from radiolabeled ATP to an oligonucleotide. As shown in Fig. 2.12A, neither A83B4C63 nor A12B4C50 inhibit the PNKP kinase activity, as confirmed by the successful transfer of ³²P-labeled phosphate

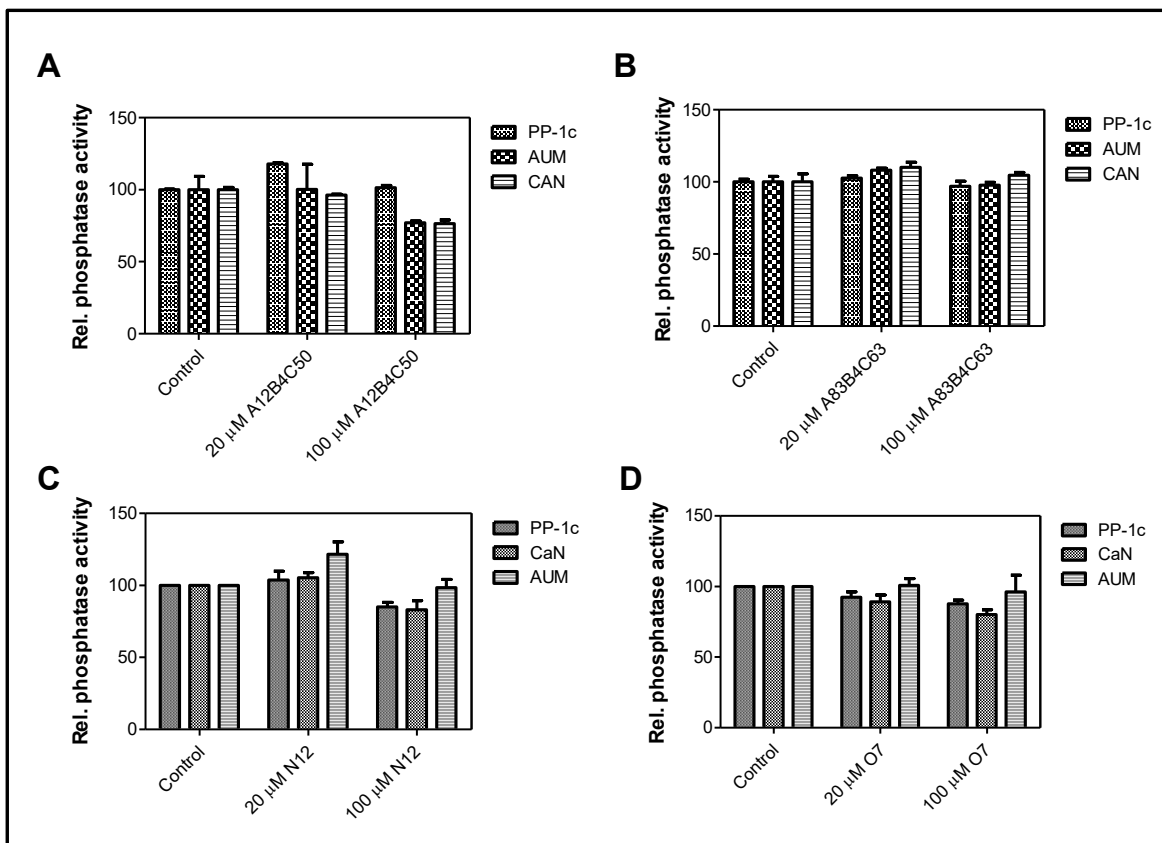


Figure 2.11. Activity of PNKP inhibitors against three protein phosphatases, PP-1c, aspartate-based ubiquitous Mg^{2+} - dependent phosphatase (AUM) and calcineurin (CAN). The protocol for this assay is described in detail in section 2.3.4. Each point represents the mean \pm SD (n = 3). **Data presented in this figure were generated by Dr. Phuwadet Pasarj.**

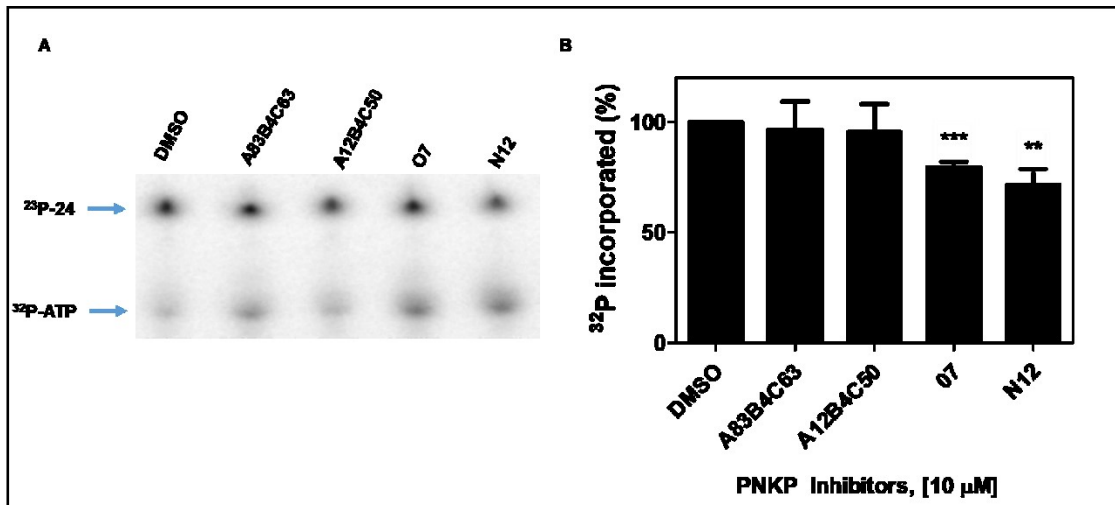


Figure 2.12. DNA kinase assay. Inhibition of PNKP DNA kinase activity by A83B4C63, A12B4C50, O7 and N12 measured by the transfer of radiolabeled phosphate from [γ - ^{32}P] ATP as described in Materials and Methods. **(A)** Representative of DNA gel showing the band of ^{23}P -24 (upper row) and ^{32}P -ATP (lower row). **(B)** The quantified values obtained from DNA gels show that A83B4C63 and A12B4C50 did not affect the kinase activity. However, there is a modest inhibition of the kinase activity by O7 and N12. Each point represents the mean \pm SD ($n = 3$). All marked points were compared to control group and are statistically significant at (** $P \leq 0.01$) and (***) $P \leq 0.001$). **Data presented in this figure were generated by Mesfin Fanta**

from radiolabeled ATP to the 24-mer oligonucleotide substrate compared to the control (DMSO). However, there was a slight decrease of the kinase activity by O7 and N12. This was confirmed by the lower percentage of ^{32}P -labeled phosphate incorporated into the 24-mer oligonucleotide compared to the control.

2.5. Discussion

Several methods have been previously devised to monitor the activity of PNKP²⁹⁹⁻³⁰¹, all of which have their own advantages in monitoring the PNKP activity, however they suffer from some shortcomings such as cost and complexity. Furthermore, most have focused on the kinase rather than the phosphatase activity of PNKP. To overcome these disadvantages, we have designed an assay to provide us with a rapid mix-and-read sensitive approach for screening a library of small molecule inhibitors, which will be used later to target PNKP in cells.

The 2-Ap hairpin probes were specifically designed to screen a library of small molecule inhibitors for PNKP and test the inhibitory activity of the second generation of imidopiperidine compounds in comparison to the earlier inhibitor A12B4C3^{160, 161}. A12B4C50 and A83B4C63 proved to be more effective than A12B4C3 (Figures 2.4 and 2.5). Our screening of a library of 200 natural compounds or derivatives of natural compounds led to the identification of N12 and O7. These two compounds exhibit stronger inhibition on PNKP phosphatase activity than the imidopiperidine compounds (Figure 2.7). Unfortunately, the natural compounds are not pure but rather are mixtures of several related compounds that need to be separated and extracted (refer to Appendix Fig. A5). Each component of the mixture will need to be checked for its activity to determine which is responsible for the inhibition of PNKP phosphatase activity.

Fortunately, the T4 DNA polymerase is not a significant target for these inhibitors. The presented assay suggests that 2-Ap hairpin probes are robust and cheap and provide a selective method to be used for *in vitro* screening of potential inhibitors of PNKP.

A12B4C50, A83B4C63, N12 and O7 exhibit strong affinity (K_d value of $0.1 \pm 0.05 \mu\text{M}$ for A12B4C50, $0.09 \pm 0.05 \mu\text{M}$ for A83B4C63, $0.14 \pm 0.02 \mu\text{M}$ for N12 and $0.1 \mu\text{M} \pm 0.02$ for O7) for PNKP and the IC_{50} values obtained were 6.7, 4.2, 1.9 and 1.6 μM , respectively in comparison to A12B4C3, $K_d = 0.37 \pm 0.03 \mu\text{M}$, $IC_{50} = 22 \mu\text{M}$, (Fig. A4) (refer to Appendix).

We have further characterized the mechanism of inhibition of PNKP by the second generation imidopiperidine compounds represented by A83B4C63 and the natural derivative compound N12, showing them to be a non-competitive and uncompetitive inhibitor, respectively. The mechanism of enzyme inhibition was determined by a Lineweaver-Burk analysis of the substrate concentration dependence on the reaction. The Lineweaver-Burk plot (Figure 2.10A) shows a non-competitive nature of A83B4C63, which matches what was previously observed for A12B4C3¹⁶¹. In non-competitive inhibition, the binding of the inhibitor reduces enzyme activity, but does not affect the binding of substrate. As a result, V_{max} is reduced, but K_m is unaffected. On the other hand, N12 showed an uncompetitive inhibition behavior, because V_{max} as well as the K_m values decreased as N12 concentrations were increased (Figure 2.10B). A characteristic feature of uncompetitive inhibitors is that they bind only to the enzyme-substrate complex³⁰².

To determine the specificity of the newly found inhibitors for PNKP phosphatase activity, we examined a number of phosphatases such as calcineurin and PP-1c. We also broadened our examination to include AUM, aspartate-based ubiquitous Mg^{2+} -dependent

phosphatase, which like the PNKP phosphatase domain belongs to the HAD superfamily^{106, 303}. Figure 2.11 shows that the PNKP inhibitors slightly affect calcineurin, PP-1c and AUM at ~100 μ M concentration. This concentration is much higher than the effective concentrations for inhibiting PNKP, indicating that A12B4C50, A83B4C63, N12 and O7 have a much greater affinity for PNKP than calcineurin, PP-1c and AUM.

Finally, A83B4C63 and A12B4C50 do not inhibit the kinase activity of PNKP, but O7 and N12 do (Figure 2.12A). These data are not surprising, because A12B4C3 was found to have only a slight inhibitory effect on PNKP kinase activity¹⁶⁰, which is probably due to the proximity of the two catalytic domains of PNKP.

In conclusion, we have identified potent inhibitors of PNKP phosphatase activity utilizing a newly developed screening tool, and upon further drug development, these inhibitors may hold clinical value against tumors and could be used in the future either as a monotherapeutic or in combined treatments.

2.6. Acknowledgements

We would like to extend our appreciation to Dr. Linda Reha-Krantz for providing us with T4 DNA polymerase. This work was supported by grants funded by the Canadian Institutes of Health Research (MOP 15385) to MW and the Alberta Cancer Foundation Transformative Program Project (26603) to DH, AL and MW.

Chapter 3: Nano-encapsulation of novel inhibitors of PNKP for selective sensitization to ionizing radiation and irinotecan and induction of synthetic lethality

Overview:

In the previous chapter, we discussed the screening of two different libraries for small molecule inhibitors of PNKP phosphatase activity, in vitro using a method developed in our lab, which resulted in the finding of four potential inhibitors of PNKP, A12B4C50, A83B4C63, N12 and O7. The second step in our project is a study of the effect of PNKP inhibition by A12B4C50 and A83B4C63 on cell survival following exposure to radiation and irinotecan. We also describe the development of appropriate nano-carriers to dissolve the hydrophobic inhibitors A12B4C50 and A83B4C63, and the ability of free and encapsulated inhibitors to sensitize HCT116 cells to radiation and irinotecan. Finally, we investigate the ability of the encapsulated inhibitors to trigger synthetic lethality in PTEN-deficient HCT116 cell.

Nano-encapsulation of novel inhibitors of PNKP for selective sensitization to ionizing radiation and irinotecan and induction of synthetic lethality¹

Zahra Shire^{1, 2}, Mohammad Reza Vakili², Timothy D R Morgan³, Dennis G Hall³,
Afsaneh Lavasanifar² and Michael Weinfeld¹

¹Department of Oncology, Faculty of Medicine and Dentistry, University of Alberta,
Edmonton, AB, Canada

²Faculty of Pharmacy and Pharmaceutical Sciences, University of Alberta, Edmonton,
AB, Canada

³Department of Chemistry, Faculty of Science, University of Alberta, Edmonton, AB,
Canada

* Corresponding authors: Michael Weinfeld, PhD
Experimental Oncology, Cross Cancer Institute
Edmonton, AB Canada T6G 1Z2
Tel: +1 780 432 8438
Fax: +1 780 432 8428
E-mail: michael.weinfeld@ahs.ca

Afsaneh Lavasanifar, Pharm D, PhD
Faculty of Pharmacy and Pharmaceutical Sciences
Edmonton, AB Canada T6G 2E1
Tel: +1 780 492 2742
Fax: +1 780 492 1217
E-mail: afsaneh@ualberta.ca

Conflict of Interest Statement: Material in this manuscript has been included in recent US patent applications. Dr. Lavasanifar is Vice-President of Meros Polymer

¹ A version of this chapter was submitted to Molecular Pharmaceutics

Abstract

There is increasing interest in developing and applying DNA repair inhibitors in cancer treatment to augment the efficacy of radiation and conventional genotoxic chemotherapy. However, targeting the inhibitor is required to avoid reducing the repair capacity of normal tissue. The aim of this study was to develop nano-delivery systems for the encapsulation of novel imidopiperidine-based inhibitors of the DNA 3'-phosphatase activity of polynucleotide kinase/phosphatase (PNKP), a DNA repair enzyme that plays a critical role in rejoining DNA single- and double-strand breaks. For this purpose, newly identified hit compounds with potent PNKP inhibitory activity, A12B4C50 and A83B4C63, were encapsulated in polymeric micelles of different poly(ethylene oxide)-*b*-poly(ϵ -caprolactone) (PEO-*b*-PCL)-based structures. Our results showed efficient loading of A12B4C50 and A83B4C63 in PEO-*b*-PCLs with pendent carboxyl and benzyl carboxylate groups, respectively, and relatively slow release over 24 h. Both free and encapsulated inhibitors were able to sensitize HCT116 cells to radiation and the topoisomerase I poison, irinotecan. In addition, the encapsulated inhibitors were capable of inducing synthetic lethality in Phosphatase and tensin homolog (PTEN)-deficient cells. We also established the validity of the peptide GE11 as a suitable ligand for active targeted delivery of nano-encapsulated drugs to colorectal cancer cells overexpressing epidermal growth factor receptor (EGFR). Our results show the potential of nano-encapsulated inhibitors of PNKP as either mono or combined therapeutic agents for colorectal cancer.

3.1. Introduction

DNA termini with 5'-phosphate and 3'-hydroxyl groups are a prerequisite for DNA strand rejoining by DNA ligases. Polynucleotide kinase/phosphatase (PNKP), which catalyzes the phosphorylation of DNA 5'-hydroxyl termini and removes DNA 3'-phosphate groups, is therefore required for the repair of strand breaks with unligatable DNA ends that can be generated by certain DNA-damaging agents, including reactive oxygen species, ionizing radiation and topoisomerase I (Top I) poisons, and by the Endonuclease VIII-like (NEIL1 and NEIL2) DNA glycosylases that remove oxidized bases in the base excision repair pathway ^{2, 3, 90-92, 304}. As a result, reducing PNKP activity, either by genetic means or by chemical inhibition, renders cells more sensitive to therapeutic agents that cause single or double strand breaks with these incompatible termini ^{152, 160, 161}. We previously identified compound A12B4C3 as an inhibitor of the PNKP 3'-phosphatase activity from a library of polysubstituted imidopiperidines ^{160, 161}. Further modification of this scaffold structure has led to the synthesis of two more potent inhibitors of PNKP, A12B4C50 and A83B4C63 (Table 3.1). However, since these inhibitors have low water solubility, we investigated the use of polymeric micelles as solubilizers for these compounds. Polymeric micelles can provide the additional benefits of protecting their constituents from metabolism by serum factors until they are delivered to cells and have the potential to enhance delivery of the encapsulated compound to cancer cells over normal tissues ³⁰⁵⁻³⁰⁷.

Polymeric micelles are self-assembled amphiphilic block copolymers that are used for encapsulation, sustained-release and targeted drug delivery of poorly soluble drugs ^{231, 308-311}. In aqueous solution, polymeric micelles consist of a hydrophobic core that can

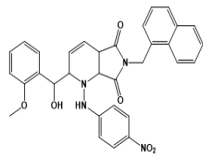
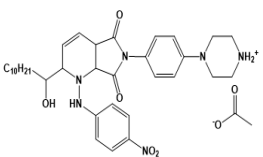
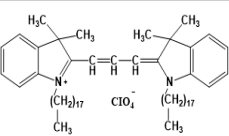
serve as a reservoir for encapsulation and delivery of hydrophobic compounds and a hydrophilic shell that can make the nano-carrier stealthy, i.e. prevent its recognition and early elimination by mononuclear phagocytes^{231, 312}. The diameter of polymeric micelles (20-100 nm) is a critical feature of these formulations for tumor accumulation by enhanced permeability and retention (EPR) effect^{313, 314}.

To further enhance the selectivity for tumor cells, targeting ligands specifically interacting with receptors overexpressed on cancer versus normal cells, can be attached to the surface of polymeric micelles^{315, 316}. Epidermal growth factor receptor (EGFR) overexpression is frequently found in tumors such as colorectal, breast and lung cancer³¹⁷⁻³¹⁹. It is a cellular transmembrane receptor with tyrosine kinase enzymatic activity that plays a key role in cell proliferation, survival and differentiation²³⁴. A dodecapeptide, (YHWYGYTPQNVI), identified by phage display screening and designated as GE11, has been found to be a selective and efficient EGFR allosteric ligand³²⁰⁻³²². GE11 binds specifically to EGFR with a dissociation constant of ~22 nM, and with much lower mitogenic activity than EGF, the natural ligand of EGFR, itself³²³.

Another strategy to selectively target tumors is the application of synthetic lethality. Synthetic lethality is defined as a condition where the simultaneous disruption of two genes or their cognate proteins, but not either gene/protein alone, leads to cell death^{324, 325}. Phosphatase and tensin homolog (PTEN), which is one of the most frequently disrupted tumor suppressors in cancer, has been studied extensively as a synthetic lethal partner for several proteins including PNKP^{187, 326-328}.

Here we describe the encapsulation and characterization of A12B4C50 and A83B4C63 in polymeric micelles for the purpose of lead solubilization and tumor targeted drug delivery assisting accelerated development of PNKP inhibitors for cancer therapy. To provide a range of different core structures for efficient accommodation of hit molecules under study in the micellar system, a series of micelle-forming block copolymers based on methoxy poly(ethylene oxide)-b-poly(ϵ -caprolactone) (PEO-*b*-PCL), methoxy poly(ethylene oxide)-b-poly(α -benzyl carboxylate- ϵ -caprolactone) (PEO-*b*-PBCL), and methoxy poly(ethylene oxide)-b-poly(α -carboxyl- ϵ -caprolactone) (PEO-*b*-PCCL) were used^{231, 233}. For A12B4C50 and A83B4C63, optimum formulations were achieved using PEO-*b*-PCCL and PEO-*b*-PBCL micelles, respectively. We examined the ability of the encapsulated inhibitors to radiosensitize and chemosensitize cancer cells or engender a synthetic lethal response in PTEN-deficient cells, *in vitro*. We have also developed GE11 modified polymeric micelles and assessed the potential of these nano-carriers for active targeting of EGFR-overexpressing colorectal cancer cells. We also evaluated the effect of GE11 modification of polymeric micelles in potentiating the cytotoxic effects of encapsulated PNKP inhibitors in EGFR-overexpressing colorectal cancer cells.

Table 3.1. Characteristics of the polymeric micelles under study (n = 3) determined by dynamic light scattering.

Compound	Structure	Formulation	Size ± SD (nm)	*PDI ± SD	^a EE %	^b DL %
A83B4C63		PEO- <i>b</i> -PCL-A83B4C63	62 ± 3.4	0.37 ± 0.01	93.8 ± 0.51	4.9
		PEO- <i>b</i> -PBCL-A83B4C63	99.9 ± 0.8	0.23 ± 0.02	48.3 ± 1.0	9.1
		GE11-PEO- <i>b</i> -PBCL-A83B4C63	47.5 ± 0.3	0.26 ± 0.00	89.2 ± 9.3	8
A12B4C50		PEO- <i>b</i> -PCL-A12B4C50	71.3 ± 0.1	0.18 ± 0.00	91.9 ± 2.3	5
		PEO- <i>b</i> -PCCL-A12B4C50	33.8 ± 0.3	0.25 ± 0.00	92 ± 16.0	5
		GE11-PEO- <i>b</i> -PCCL-A12B4C50	58.8 ± 0.4	0.29 ± 0.00	81.6 ± 1.8	7.5
Dil		PEO- <i>b</i> -PBCL-Dil	70.7 ± 0.9	0.23 ± 0.01	38.9 ± 0.4	1.7
		GE11-PEO- <i>b</i> -PBCL-Dil	62.7 ± 0.6	0.19 ± 0.00	51 ± 5.6	1.7

* PDI, polydispersity index, the distribution of molecular masses of the micelles

$$^a \text{ Encapsulation Efficiency (EE \%)} = \frac{\text{the amount of encapsulated inhibitor}}{\text{the initial amount of inhibitor added}} \times 100$$

$$^b \text{ Drug Loading (DL \%)} = \frac{\text{the amount of encapsulated inhibitor}}{\text{the total amount of polymer}} \times 100$$

3.2. Materials and Methods

3.2.1. Materials

Methoxy-polyethylene oxide (PEO) (average molecular weight of 5000 g/mol), and palladium on charcoal were purchased from Sigma (St. Louis, MO). ϵ -Caprolactone was purchased from Lancaster Synthesis (Lancashire, UK). α -Benzyl carboxylate- ϵ -caprolactone monomer was synthesized by Alberta Research Chemicals Inc. (Edmonton, AB). Stannous octoate was purchased from MP Biomedicals Inc. (Tuttlingen, Germany). GE11 peptide was kindly provided by Dr. Rania Soudy (Faculty of Pharmacy and Pharmaceutical Sciences, University of Alberta). Fluorescent probes, 1,1'-Dioctadecyl-3,3,3',3'-tetramethylindocarbocyanine perchlorate (Dil) and Hoechst 33342, were purchased from Molecular Probes (Waltham, MA, USA). Antibodies used included monoclonal antibodies against PNKP ³²⁹, anti-EGFR antibodies [EP38Y] (cat. # ab52894 and ab193244, Abcam Inc., Toronto, CA), lamin B (cat. # sc-6127, Santa Cruz Biotechnology, Santa Cruz, CA) and actin (cat. # sc-1616, Santa Cruz Biotechnology, Santa Cruz, CA).

3.2.2 Cell lines

HCT116, HT29 and SW620 cells were purchased from the American Type Culture Collection (ATCC). HCT116 PNKP knock-out cells were prepared by CRISPR technology by Dr. Yaping Yu (Molecular Biology Services, University of Calgary). The identity of HCT116 cells, both in their original and modified forms, was confirmed by ATCC. The correct identity of HCT116 cells was last confirmed by STR testing on March 13th, 2017. The HCT116 PTEN knock-out variants were generously provided by Dr. Todd Waldman

(Georgetown University, Washington DC)³³⁰. The presence or absence of PNKP, PTEN and EGFR expression was confirmed by western blot. Cell lines were cultured at 37°C in 5% CO₂ in a humidified incubator in a 1:1 mixture of Dulbecco's modified Eagle medium and F12 (DMEM/F12) supplemented with 10% FBS, 50 U/mL penicillin, 50 mg/mL streptomycin, 2 mmol/L L-glutamine, 0.1 mmol/L nonessential amino acids, and 1 mmol/L sodium pyruvate. All culture supplements were purchased from Invitrogen (Burlington, ON, CA).

3.2.3. Synthesis of polysubstituted imidopiperidine compounds

Compounds A12B4C50 and A83B4C63 (Table 3.1) were prepared by Dr. Timothy Morgan (Department of Chemistry, University of Alberta) according to the previously reported one-pot procedure²⁹⁰. The heterodiene (1 equiv) and maleimide (1.5-2 equiv) were dissolved in toluene in a screw-cap reaction vial. The aldehyde (2 equiv) was added and the vial was sealed and heated to 85 °C for three days. After cooling to room temperature, the solvent was removed under reduced pressure. The residue was purified by flash column chromatography (ethyl acetate/hexane solvent system) to afford yellow solids (40-70% yield). The compounds were further purified by semi-preparative HPLC to purities of 95-99%. Purified compounds were characterized by NMR, IR, and mass spectrometry (refer to appendix Figs. A6-A7).

3.2.4. Synthesis of block copolymers

Block copolymers of PEO-*b*-PCL (degree of polymerization 20 and 30) and PEO-*b*-PBCL (degree of polymerization 30) were synthesized by ring-opening polymerization of ϵ -caprolactone or α -benzyl carboxylate- ϵ -caprolactone, respectively, using methoxy-PEO (MW: 5000 g/mol) as an initiator and stannous octoate as catalyst according to a method

described previously³³¹⁻³³⁴. Block copolymers of PEO-*b*-PCCL (degree of polymerization 21) were synthesized by catalytic debenzoylation of PEO-*b*-PBCL in the presence of H₂ according to a method described previously³³⁴.

3.2.5. Synthesis and characterization of GE11-PEO-*b*-PBCL conjugates

We followed a previously reported method for the preparation of GE11-PEO-*b*-PBCL conjugates^{335, 336}. To prepare aldehyde-PEO-*b*-PBCL, acetal-PEO-*b*-PBCL was first synthesized by one-pot anionic ring-opening polymerization of ethylene oxide using the initiator 3,3 diethoxy-1-propanol (DEP) and potassium naphthalenide solution in THF under argon at room temperature, followed by ϵ -caprolactone addition. Acetal-PEO-*b*-PBCL was then added to a water/acetone mixture to form micelles, and acetone was then removed by evaporation under vacuum. The acetal groups on the surface of the micelles were converted to aldehyde by adjusting the pH of the solution to 2.0 using HCl (0.5 mol/L). The mixture was stirred at room temperature for 2 h, after which it was neutralized with NaOH (0.5 mol/L) to stop the reaction. In the final step of the reaction, GE11 peptide was conjugated to the aldehyde-PEO-*b*-PBCL micelles. The peptide was added and stirred with the polymeric micelles at a 1:3 molar ratio (peptide: CHO-PEO-*b*-PBCL) at room temperature for 2 h. Finally, to reduce the Schiff's base, NaBH₃CN (10 equiv) was added to the micellar solution. After 24 h, the micellar solution was purified by dialysis against water (molecular weight cut-off (MWCO), 3.5 kDa). The relative amount of un-conjugated peptide was determined using HPLC and subtracted from the total level of peptide used in the reaction to estimate the level of conjugated peptide. Reversed phase chromatography was carried out on a Microsorb-MV 5 μ m C18-100 Å column (4.6 mm \times 250 mm, Phenomenex, Torrance, CA, USA) with 20 μ L of sample injected and eluted using the following conditions: (1) 100% A (0.1% trifluoroacetic acid aqueous

solution) and 0% B (acetonitrile) over 1 min; (2) linear gradient from 100% A to 60% A and 0% B to 40% B over 21 min; (3) linear gradient from 60% A to 0% A and 40% B to 100% B over 25 min; (4) 0% A and 100%B over 27 min; (5) 100% A and 0%B over 31 min. Gradient elution was performed at a flow rate of 1 mL/min using a Varian Prostar 210 HPLC System. Detection was performed at 214 nm using a Varian 335 detector (Varian Inc., Palo Alto, CA, USA). The resulting GE11-PEO-*b*-PBCL conjugates were freeze-dried and stored at -20 °C until use.

3.2.6. Characterization of the prepared block copolymers and polymeric micelles

The prepared block copolymers were characterized for their average molecular weights by ¹H NMR (600 MHz Avance III – Bruker, East Milton, ON, CA) using deuterated chloroform (CDCl₃) as solvent and tetramethylsilane as an internal reference standard. Drug-loaded micelles were prepared by dissolving lead PNKP inhibitors (1 mg) and block copolymers (10-20 mg) in acetone. The solution was added to double distilled water (10 mL) in a dropwise manner and stirred overnight, the organic solvent was removed under vacuum. The obtained micellar solution was then centrifuged at 11,600 x g for 5 min to remove the free un-encapsulated inhibitors. The Z-average diameter of the prepared micelles were estimated by dynamic light scattering (DLS) using a Malvern Zetasizer 3000 (Malvern Instruments Ltd, Malvern, UK). An aqueous droplet (20 µL) of the micellar solution with a polymer concentration of 1 mg/mL was placed on a copper-coated grid. The polymeric micellar solution was negatively stained by 1% phosphotungstic acid (H₃PO₄ 12WO₃·24H₂O). After 5 min, the excess fluid was removed by filter paper and the grid was inserted in transmission electron microscopy (TEM) (FEI Morgagni 268, North America NanoPort, Oregon, USA) machine for image analysis.

3.2.7. *In vitro* release of encapsulated PNKP inhibitors

The *in vitro* release of encapsulated PNKP inhibitors was studied using dialysis method. Each dialysis bag (Spectrapor dialysis tubing, MWCO 3.5 kDa, Spectrum Laboratories, Rancho Dominguez, CA), containing 2 mL of the micellar formulation or free drug dissolved in acetone, was placed into 300 mL of distilled water maintained at 37°C in a shaking water bath (65 rpm, Julabo SW 22 shaking water bath, Seelbach, Germany). At selected time intervals, aliquots of 200 µL from the inside of the dialysis bag were collected. The amount of PNKP inhibitor was analyzed using a Varian Prostar 210 HPLC system. Reversed phase chromatography was carried out with a Microsorb-MV 5 µm C18-100 Å column (4.6 mm × 250 mm) with 20 µL of sample injected and eluted under isocratic conditions with a solution of 0.1% trifluoroacetic acid / acetonitrile (1:1 v/v) at a flow rate of 0.7 mL/min at room temperature. Detection was performed at 380 and 280 nm for A12B4C50 and A83B4C63, respectively using a Varian 335 Photodiode Array HPLC detector (Varian Inc., Palo Alto, CA, USA).

3.2.8. Cell proliferation assay

To determine the maximum dose of each PNKP inhibitor that did not affect cell growth rate, we used the CellTiter 96® Non-Radioactive Cell Proliferation Assay (MTS), (Promega). Approximately 1×10^5 HCT116 cells were plated in triplicate in a 96-well plate and allowed to adhere overnight before treatment with different concentrations of the inhibitors as free or polymeric micellar formulation. Free inhibitor was dissolved in DMSO in a way to keep the final concentration of DMSO < 1%. After 72 h, 11 µL of the pre-mixed optimized dye solution (tetrazolium dye) was added to each well and cells were incubated for 4 more hours at 37°C. The absorbance recorded at 490 nm on a FLUOstar Optima®

plate reader (BMG Labtech Inc., Durham, NC) was used as a representation of the relative number of metabolically active cells in the culture.

3.2.9. Clonogenic survival assay

Cells were seeded in 60-mm dishes 24 hours in advance and cultured for 9 - 14 consecutive days. Fresh PNKP inhibitor was added to cells every 3 days to ensure effective inhibition of PNKP was achieved at nontoxic concentrations defined by the above MTS assay. Colonies were then stained with a crystal violet (Sigma, Oakville, ON, CA) stain containing 25% methanol for 30 min, after which the plates were washed in warm water and left to dry overnight. Colonies consisting of 50 cells or more were counted using an automated colony counter (Oxford Optronix, Abingdon, UK).

To determine the radiation response, cells, plated at 500, 750, 1500 and 3000 cells per dish, were treated with 0, 2, 4, or 6 Gy γ -radiation, respectively (60Co Gammacell, AECL, Chalk River, ON, CA) in the absence or presence of PNKP inhibitors as free or polymeric micellar formulation added 24 h prior to treatment with radiation. Additionally, plated cells (500 per dish) were treated with 0 μ M irinotecan, 1500 per dish with 2 μ M irinotecan and 3000 per dish with 3 or 4 μ M irinotecan in the absence or presence of PNKP inhibitor as free or polymeric micellar formulation. The PNKP inhibitor, as free or encapsulated drug, was added 24 h prior to treatment with irinotecan.

3.2.10. Determination of polymeric micellar uptake by different colorectal cancer cells

The protocol for encapsulating Dil inside polymeric micelles for cellular uptake studies was described previously³³⁷. Dil (30 μ g) and the block copolymer (3 mg) were dissolved in acetone (0.5 mL) and then added to 3 mL of water in a dropwise manner. The acetone

was removed by evaporation under vacuum, and the micellar solution was then centrifuged at $11,600 \times g$ to remove the un-encapsulated Dil. The level of Dil encapsulation efficiency was determined by measuring the its fluorescence at 550/565 nm (excitation/emission) (using a FLUOstar Optima® plate reader (BMG Labtech Inc., Durham, NC). The release of Dil from micelles was evaluated in PBS buffer containing lipid vesicles as the receiver phase of the released Dil as described previously ³³⁸.

To determine cellular uptake by confocal microscopy, HCT116, HT29, and SW620 cells (1×10^5) were cultured on a coverslip at 37°C for 24 h. The medium was removed and replaced with 1 mL of fresh medium containing free Dil, PEO-*b*-PBCL-Dil and GE11-PEO-*b*-PBCL-Dil at a Dil concentration of 10 µg/mL. The cells were incubated for 3 h at 37°C. After incubation the medium was removed, and the cells were washed three times with 1 mL of PBS, and then fixed with ice cold methanol for 5 min. Methanol was removed by washing with PBS three times. The coverslips were put on slides containing anti-EGFR antibody to stain the membrane for 60 min. The cells were then washed three times with washing buffer and incubated with Hoechst 33342 to stain the nuclei for 5 min. The fixed cells were imaged by confocal laser scanning microscopy (Zeiss 510 LSMNLO, Jena, Germany) performed using a 40× oil immersion lens. Confocal stacks were processed using Carl Zeiss LSM 5 Image software.

Cellular uptake was also measured by determining the fluorescence of Dil using a well plate reader FLUOstar Optima (BMG Labtech Inc., Guelph ON, CA). HCT116, HT29 and SW620 cells were seeded into a 96-well plate (1×10^4 cells/well) containing 100 µL of media. 24 h later, Dil loaded polymeric micelles were added and incubated with the cells for 3 h at 37°C. For the competition experiments, HCT116 cells were pre-incubated with excess free GE11 peptide (1 mg/mL) for 30 min to

saturate receptors and to inhibit the binding and internalization of peptide conjugated micelles. Following the incubation period medium was removed and cells were washed with PBS three times. Internalized Dil levels were assessed by fluorescence emission intensity at 565 nm.

3.2.11. Statistical analysis

Plots show an average of at least three independent biological replicates. Each experimental group was compared with control group using a two-tail unpaired Student's *t*- test. The software used was GraphPad Prism5 software (La Jolla, CA, USA). A value of $P < 0.05$ was considered as statistically significant in all experiments. Error bars represent mean \pm SD.

3.3. Results

3.3.1. Polymer synthesis and micelle characterization

The structure of PEO-*b*-PCL, PEO-*b*-PBCL, PEO-*b*-PCCL, acetal-PEO-*b*-PBCL and acetal-PEO-*b*-PCCL were confirmed by NMR, which showed all of the characteristic peaks for PEO, PCL, PBCL, PCCL and acetal segments in their corresponding spectra (refer to appendix Figs. A8-A12). ¹H NMR was also used to characterize the degree of polymerization of the core forming block in prepared block copolymer micelles as 20, 30 and 21 for PCL, PBCL and PCCL, respectively. Further micelle characterization was accomplished by studying the size distribution and polydispersity index (PDI, the distribution of molecular masses) of empty or Dil or PNKP inhibitor loaded micelles using dynamic light scattering (DLS) measurements. The Z-average diameter of all micelles was < 100 nm. The highest PDI was seen for PEO-*b*-PCL micellar formulation of A83B4C63 (0.37) indicating a more dispersed size distribution of the micellar population. The encapsulation efficiency for all formulations was relatively high ranging between 75-100%. The characteristics of the developed polymeric micelles are summarized in Table 3.1. In addition, the morphology of the micelles was investigated by TEM confirming formation of the spherical shape for both plain and GE11-modified micelles (Fig. 3.1).

3.3.2. *In vitro* release of PNKP inhibitors from polymeric micelles

The results of the *in vitro* release of A12B4C50 and A83B4C63 from PEO-*b*-PCCL and PEO-*b*-PBCL micelles versus PEO-*b*-PCL micelles are presented in Figures 3.2A and 3.2B, respectively. Free A12B4C50 and A83B4C63 were released from the dialysis bag at a rapid rate, 94.8% and 59.4% within 6 h, respectively indicating the sink condition, a condition by which the release of drug is controlled by diffusion from regions of high

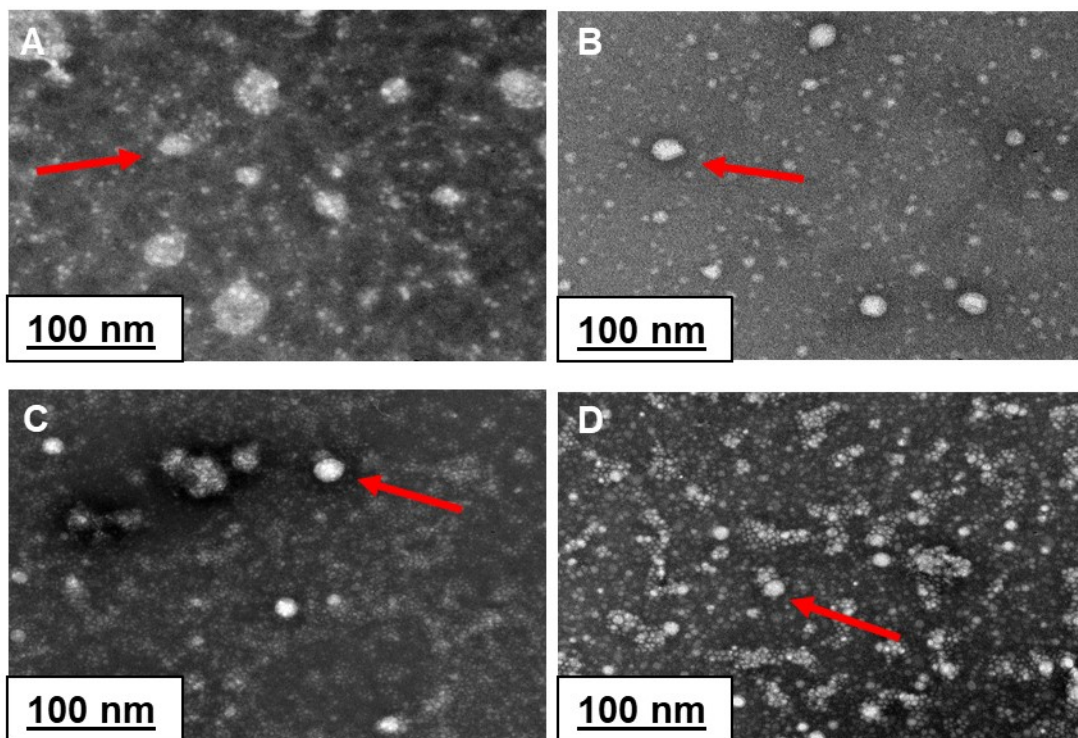


Figure 3.1. TEM of loaded polymeric micelles. (A) PEO-*b*-PCCL-A12B4C50 **(B)** PEO-*b*-PBCL A83B4C63 **(C)** GE11-PEO-*b*-PCCL-A12B4C50 and **(D)** GE11-PEO-*b*-PBCL-A83B4C63. An aqueous droplet (20 μ L) of the micellar solution with a polymer concentration of 1 mg/mL was placed on a copper-coated grid. Then a drop of 1% solution of phosphotungstic acid was added to provide the negative stain. After 5 min, the excess fluid was removed by filter paper and the grid was inserted in the TEM for image analysis.

concentration to regions of low concentration³³⁹. At the same time point, only 44.5% of A12B4C50 and 30.6% of A83B4C63 was released from PEO-*b*-PCCL and PEO-*b*-PBCL micelles, respectively. In contrast, PEO-*b*-PCL micelles released 67.2% and 66.5% of A12B4C50 and A83B4C63, respectively, within the same time frame. These observations indicate that polymeric micelles with a PCCL or PBCL core are better solubilizers of the imidopiperidine PNKP inhibitors than polymeric micelles with a PCL core.

3.3.3. Inhibition of cell growth by the hit PNKP inhibitors and their polymeric micellar formulations

To determine the maximum concentrations of the PNKP inhibitors that could be employed in the subsequent clonogenic survival assays, we used the MTS assay to assess non-specific inhibition of colorectal cancer cell growth/metabolism induced by the free and encapsulated PNKP inhibitors. HCT116 colorectal cancer cells were exposed to serial dilutions of empty polymeric micelles, free and encapsulated PNKP inhibitor for 72 h. As shown in Figure 3.3, free and encapsulated A12B4C50 affected cell growth at concentrations $> 5 \mu\text{M}$, thus limiting the usable concentration of this compound to $\leq 5 \mu\text{M}$ in the clonogenic survival assays. On the other hand, A83B4C63 could be used at concentrations $< 20 \mu\text{M}$. Furthermore, there was no toxicity associated with the empty PEO-*b*-PCCL and PEO-*b*-PBCL micelles.

3.3.4. Cellular radio- and chemosensitization by PNKP inhibitors

As shown in Figs. 3.4A, C, E and G, exposure of wild type HCT116 cells to encapsulated A12B4C50 and A83B4C63 significantly increased their sensitivity to radiation and irinotecan ($P \leq 0.05$, two-tail unpaired Student's *t*-test). This response was nearly identical to that seen with HCT116 PNKP-knock out cells treated with either radiation or

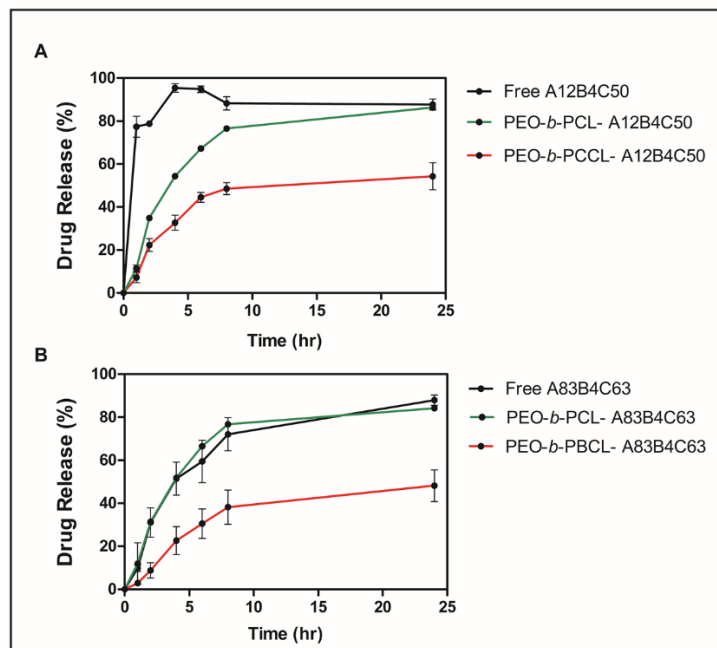


Figure 3.2. *In vitro* release from dialysis tubing (MWCO 3.5 kDa) for free versus encapsulated (A) A12B4C50 and (B) A83B4C63 in aqueous solution at 37°C. At fixed time intervals, a sample of 120 μ L was withdrawn from dialysis tube and was analyzed by HPLC to determine the amount of released drug. Each point represents the mean \pm SD ($n = 3$).

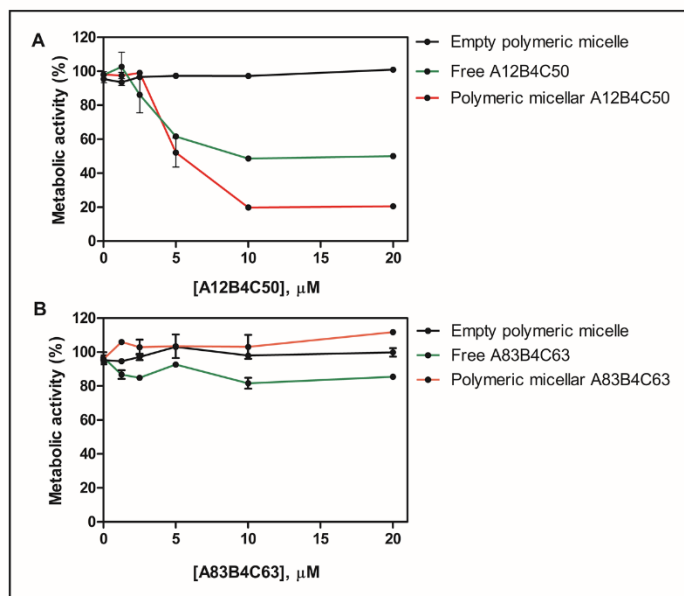


Figure 3.3. *In vitro* cytotoxicity of (A) A12B4C50 and (B) A83B4C63 measured by MTS assay after 72 h of drug incubation at 37°C. HCT116 cells (1×10^5) were plated in triplicate in a 96-well plate with different concentrations of inhibitors. After 72 h, a tetrazolium dye solution was added to each well and cells were incubated for 4 h at 37°C. Absorbance was recorded at 490 nm. Each point represents the mean \pm SD ($n = 3$).

irinotecan alone (without PNKP inhibitor). However, only free A83B4C63 was able to sensitize HCT116 cells to either radiation or irinotecan. Free A12B4C50 failed to sensitize HCT116 cells to either treatment. This could be due to the poor internalization of free A12B4C50 in HCT116 cells, which was confirmed by fluorescence microscopy (refer to appendix Fig. A14). Furthermore, A12B4C50 and A83B4C63 (free or encapsulated) failed to further sensitize the HCT116 PNKP-knock out cells to either radiation or irinotecan (Figs. 3.4B, D, F and H).

3.3.5. *In vitro* release of PNKP inhibitors from GE11-conjugated polymeric micelles

Figures 3.5A & 4B show that the attachment of the EGFR ligand GE11 on the surface of either PEO-*b*-PCCL or PEO-*b*-PBCL did not perturb the slow release of A12B4C50 and A83B4C63 seen with the unmodified micelles.

To study the influence of GE11 on cellular uptake in cells expressing different levels of EGFR, we encapsulated Dil dye in PEO-*b*-PBCL to be used as a general model for targeted polymeric micelles. Figure 3.5C shows that Dil dye has a slow controlled release from both plain and GE11-modified polymeric micelles. This further confirmed that GE11 attachment to the surface of the micelles did not alter the release of the encapsulated compounds.

3.3.6. Cellular uptake of encapsulated compounds

To evaluate the relationship between EGFR expression and the effectiveness of GE11-conjugated micelles, we monitored the cellular uptake of Dil by three colorectal cancer cell lines expressing different levels of EGFR. Western blot analysis revealed that HCT116 cells express relatively high levels of EGFR compared to HT29 cells, while the

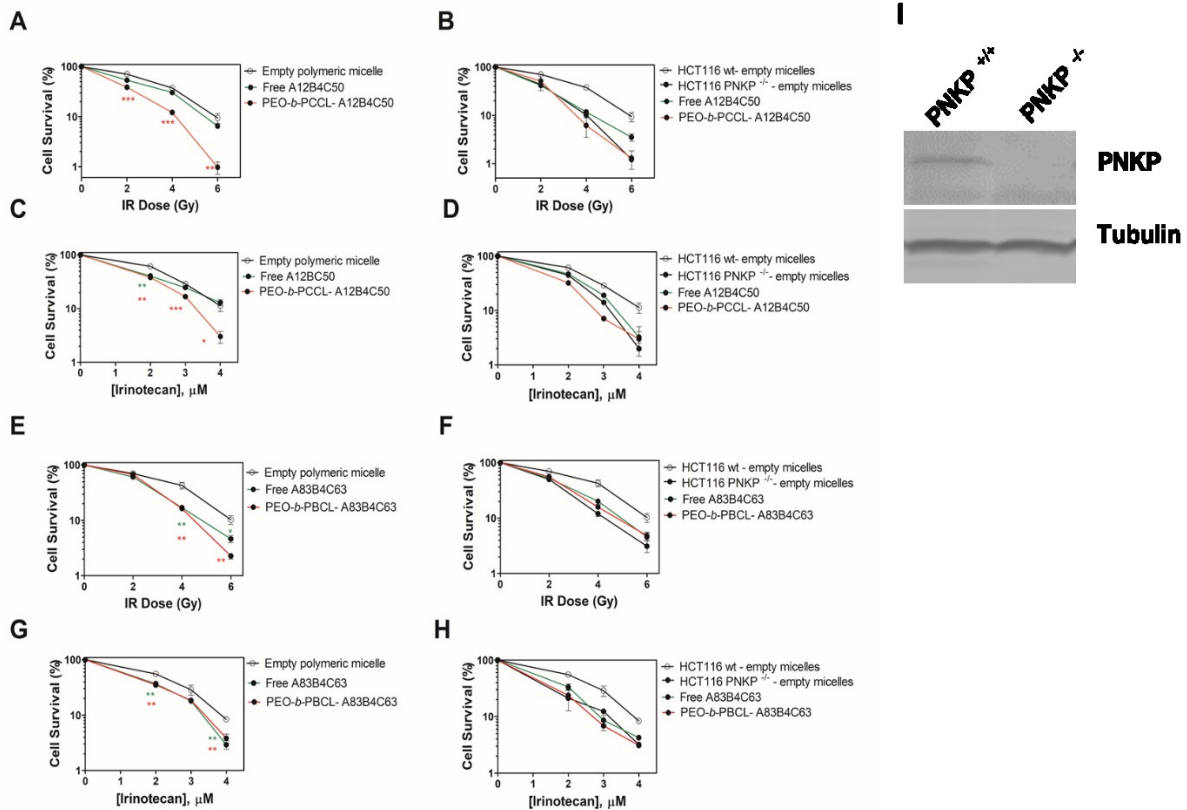


Figure 3.4. Radio/chemosensitization by free and encapsulated A12B4C50 or A83B4C63. Cells, treated with 4 μM A12B4C50 and 6 μM A83B4C63 24 hours in advance, were subjected to radiation or irinotecan and survival was assessed by clonogenic survival assay. **(A, C, E and G)** HCT116 wild-type cells were sensitized to radiation and irinotecan by encapsulated PNKP inhibitors. **(B, D, F and H)** PNKP inhibitors failed to sensitize HCT116 PNKP-knock out cells (HCT116PNKP^{-/-}) to radiation or irinotecan. **(I)** Western blot showing PNKP protein levels in wild-type and PNKP-knock out HCT116 cells. Each point represents mean \pm SD ($n = 3$). All marked points were compared to control group and are statistically significant at (* $P \leq 0.05$), (** $P \leq 0.01$) and (***) $P \leq 0.001$).

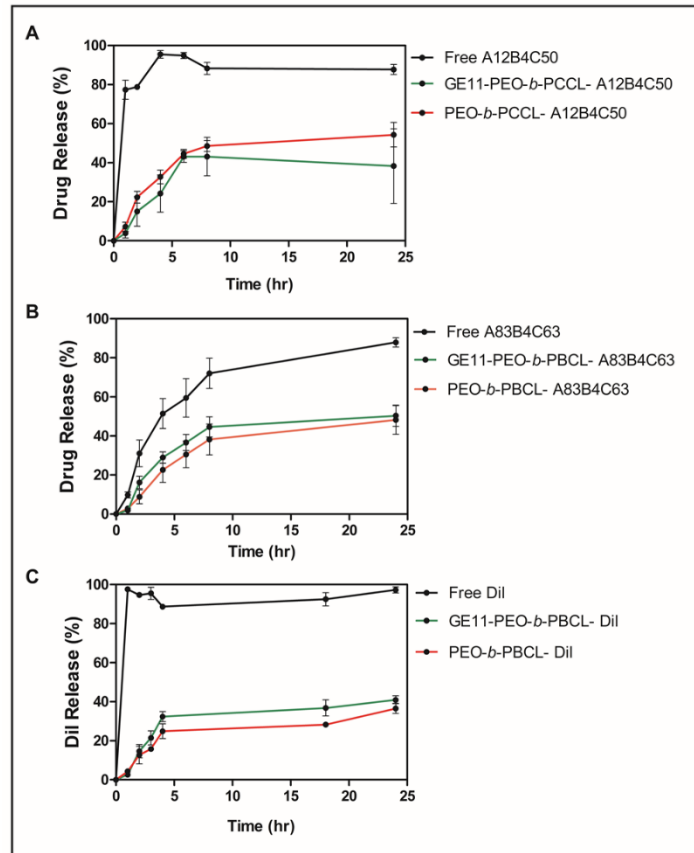


Figure 3.5. *In vitro* release from dialysis tubing (MWCO 3.5 kDa) of (A) A12B4C50, (B) A83B4C63 and (C) Dil, from GE11-conjugated polymeric micelles in comparison to plain micelles and free drug (reported previously in Fig. 3.2) in aqueous solution at 37°C. At fixed time intervals, a sample of 120 μ L was withdrawn and analyzed by HPLC to determine the amount of released drug. Each point represents the mean \pm SD ($n = 3$).

EGFR signal from SW620 cells was undetectable (Fig. 3.6A), in agreement with previous reports³⁴⁰. In line with the expression level of EGFR on HCT116, HT29 and SW620 cells, GE11-PEO-*b*-PBCL-Dil incubated with these cells, showed more intense intracellular fluorescence in HCT116 cells followed by HT29 and then SW620 cells following 3 h incubation (Fig. 3.6B). In addition, the study revealed that the Dil was mainly localized in the cytoplasmic compartment in all cells under study.

To obtain quantifiable data, fluorescence intensities of Dil uptake were measured using a plate reader. After 3 h incubation we observed enhanced cellular uptake of GE11-PEO-*b*-PBCL-Dil micelles by HCT116 cells in comparison to HT29 and SW620 cells (Fig. 3.6C). In addition, the cellular uptake by HCT116 cells of GE11-PEO-*b*-PBCL-Dil was higher than PEO-*b*-PBCL-Dil ($P \leq 0.05$, two-tail unpaired Student's *t*-test). These data are in accord with our cell imaging observations.

To investigate the possible role of receptor mediated cell uptake of GE11-PEO-*b*-PBCL-Dil, we pretreated HCT116 cells with 1 mg/mL free GE11 to compete with the conjugated micelles. As shown in Fig. 3.6D, the free GE11 significantly reduced the cellular uptake of GE11-PEO-*b*-PBCL-Dil by HCT116 cells. In comparison, the uptake of PEO-*b*-PBCL-Dil by HCT116 cells did not change significantly following pre-treatment with free GE11.

3.3.7. Cellular radio- and chemosensitization by PNKP inhibitors encapsulated in GE11-conjugated micelles

The survival curves (Fig. 3.7) indicated that both GE11-PEO-*b*-PCCL-A12B4C50 and GE11-PEO-*b*-PBCL-A83B4C63 significantly increased the sensitivity of HCT116 cells to radiation and irinotecan, and this response was almost identical to that seen with plain

PEO-*b*-PCCL-A12B4C50 and PEO-*b*-PBCL-A83B4C63. ($P \leq 0.05$, two-tail unpaired Student's *t*- test).

3.3.8. Synthetic lethal targeting of PTEN-deficient cancer cells using encapsulated PNKP inhibitors

To investigate whether the encapsulated PNKP 3'-phosphatase inhibitors could induce a synthetic lethal response in PTEN-deficient cells, we performed clonogenic survival assays with both HCT116 PTEN^{+/+} and HCT116 PTEN^{-/-} cells. As shown in Fig. 3.8, the combined disruption of both PTEN (genetically) and PNKP (by encapsulated inhibitors) led to a lethal response with increasing dose of PNKP inhibitor ($P \leq 0.05$, two-tail unpaired Student's *t*- test). However, the disruption of PNKP (chemically by inhibitors) or PTEN (genetically) individually was not lethal. These findings confirm our previous observation that a synthetic lethal relationship exists between PTEN and PNKP.

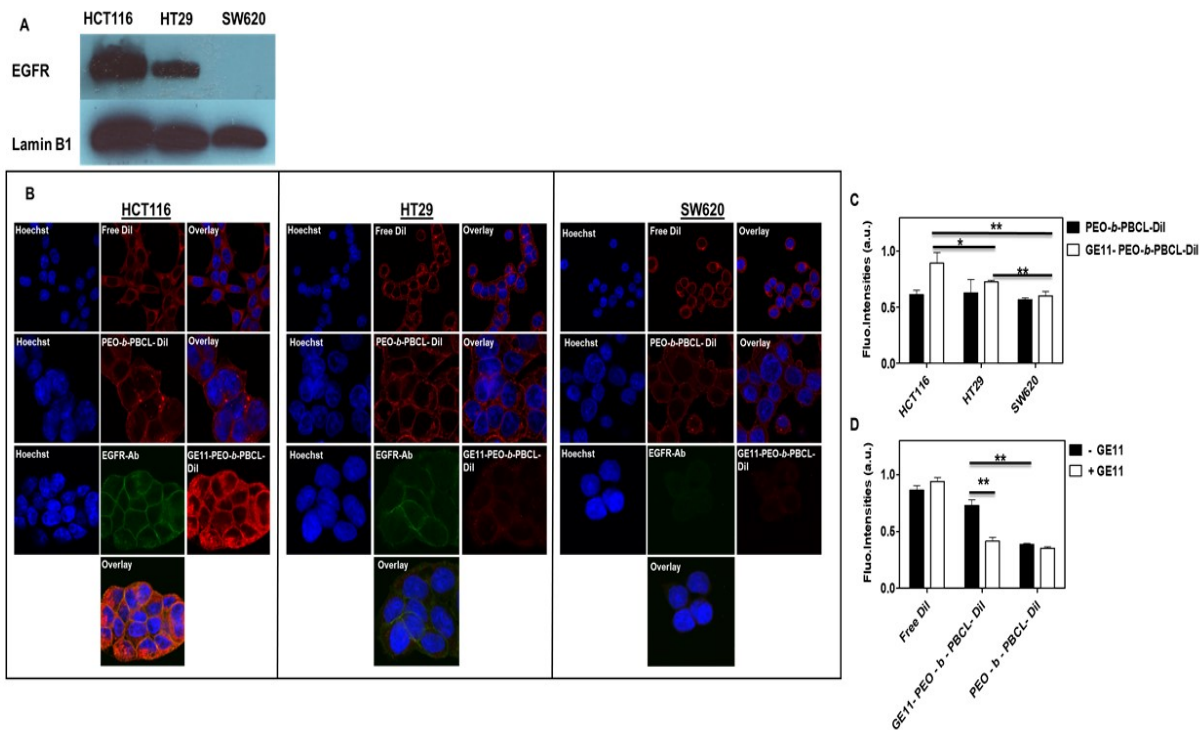


Figure 3.6. Cellular uptake of Dil-encapsulated polymeric micelles. (A) Western blotting shows different expression levels of EGFR in HCT116, HT29 and SW620 cells. **(B)** *In vitro* fluorescence microscopy images of Dil accumulation in HCT116, HT29 and SW620 cells. After 3 h incubation with free Dil, PEO-*b*-PBCL-Dil and GE11-PEO-*b*-PBCL-Dil. Red fluorescence indicates Dil. Blue fluorescence indicates Hoechst dye. Green fluorescence indicates EGFR immunostaining. Fluorescence intensity measurement of *in vitro* cell uptake of **(C)** PEO-*b*-PBCL-Dil and GE11-PEO-*b*-PBCL-Dil by HCT116, HT29 and SW620 cells, and **(D)** free Dil by HCT116 cells, GE11-PEO-*b*-PBCL-Dil and PEO-*b*-PBCL-Dil with (+) or without (-) pre-treatment with excess of free GE11 peptide. Each point represents mean \pm SD ($n = 3$). (* $P \leq 0.05$) and (** $P \leq 0.01$).

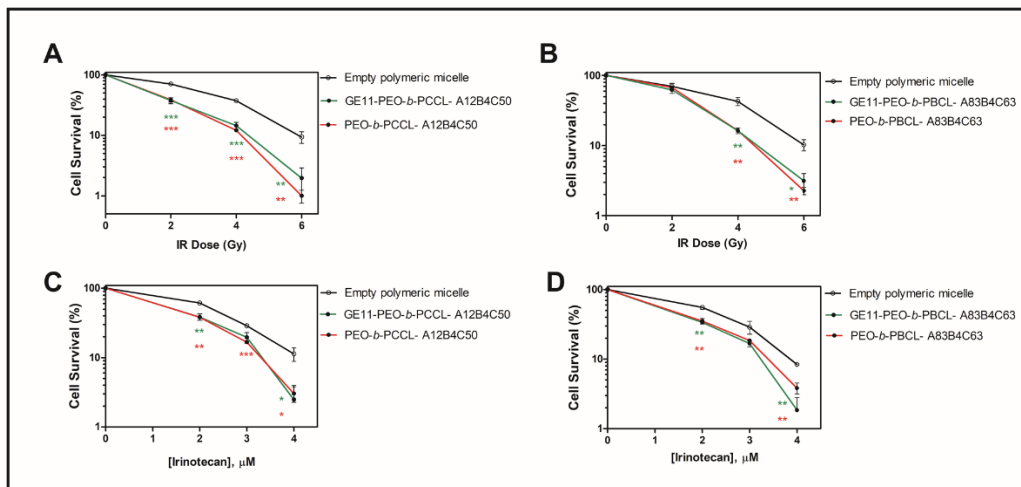


Figure 3.7. Radio/chemosensitization of HCT116 wild-type cells by A12B4C50 and A83B4C63 encapsulated in GE11-PEO-*b*-PCCL and GE11-PEO-*b*-PBCL, respectively. Cells, treated with 4 μM A12B4C50 and 6 μM A83B4C63 24 hours in advance, were subjected to radiation or irinotecan and survival was assessed by clonogenic survival assay. Data of empty polymeric micelles, PEO-*b*-PBCL-A83B4C63 and PEO-*b*-PCCL-A12B4C50 were reported previously in Fig. 3.4. Each point represents mean \pm SD ($n = 3$). All marked points were compared to control group and are statistically significant at (* $P \leq 0.05$), (** $P \leq 0.01$) and (***) $P \leq 0.001$).

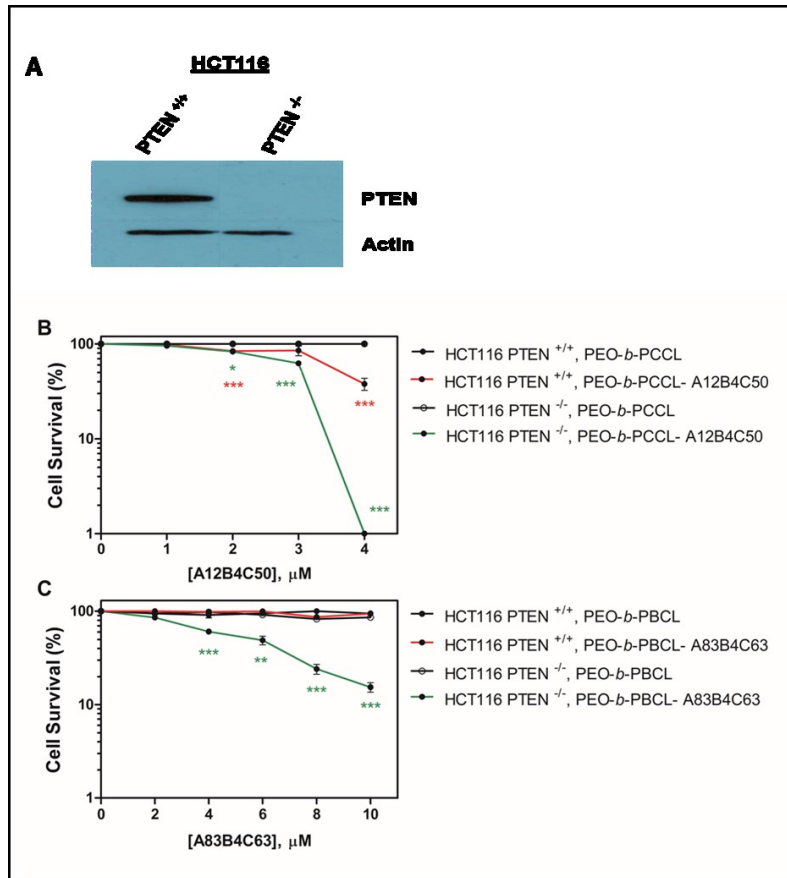


Figure 3.8. Clonogenic survival assays of PTEN-deficient cells treated with encapsulated PNKP inhibitors. (A) Western blot confirms disruption of PTEN in HCT116 cells. **(B & C)** Cells were subjected to increasing concentrations of PNKP inhibitors encapsulated in polymeric micelles as well as empty polymeric micelles for control sets for 9-14 consecutive days. Colonies consisting of 50 cells or more were counted using an automated colony counter. Each point represents mean \pm SD ($n = 3$). All marked points were compared to control (HCT116 PTEN ^{-/-}, PEO-*b*-PBCL / PEO-*b*-PCCL) group and are statistically significant at (* $P \leq 0.05$), (** $P \leq 0.01$) and (***) $P \leq 0.001$).

3.4. Discussion

Despite recent advances in radio- and chemotherapy, a large proportion of colorectal cancer patients do not achieve objective responses due to the existence of intrinsic and acquired resistance to these therapies. Identification of molecular mechanisms that reduce the efficacy of conventional therapy, and targeting these pathways, is essential for improving radiation and chemotherapy responses in cancer patients. DNA repair pathways play a major role in tumor resistance towards radiation and chemotherapy. Therefore, targeting DNA repair pathways by small molecule inhibitors should enhance the efficacy of traditional cancer therapies. Furthermore, tumor cells harboring specific genetic defects may be susceptible to the administration of DNA repair inhibitors as single therapeutic agents ³⁴¹. PNKP, a DNA repair enzyme that possesses DNA 5'-kinase and 3'-phosphatase activity represents a candidate target for achieving this goal. Our previous studies indicated that depletion of PNKP activity by shRNA or a small molecule inhibitor of its phosphatase activity sensitizes cells to ionizing radiation and camptothecin ^{152, 160, 161}. Moreover, reduction of PNKP increases the spontaneous mutation frequency, indicating that it is required for the repair of endogenous DNA damage induced by reactive oxygen species (ROS) ¹⁵². The imidopiperidine, A12B4C3, was the first PNKP phosphatase inhibitor discovered in our lab ^{160, 161}. A12B4C50 and A83B4C63 represent the development of second generation and more potent inhibitors of PNKP derived from the parent compound A12B4C3.

In this study, we describe the encapsulation of A12B4C50 and A83B4C63 inside polymeric micelles. Many emerging cancer drugs suffer from nonspecific distribution, rapid clearance and toxicity, which hinder their further pre-clinical evaluation and

advancement in drug development process. Specifically, since our molecules of interest aim to inhibit a DNA repair enzyme, it is essential to target these carriers to tumor tissue and spare normal tissue from their exposure and effects. The advantages of employing polymeric micelles as solubilizers for hydrophobic drugs include improved water solubility, prolonged drug circulation in blood, prevention of rapid renal clearance of drugs from the body and increased drug accumulation in tumor ³⁴². A series of block copolymers based on PEO-*b*-PCL, bearing side groups of benzyl carboxylate (PEO-*b*-PBCL) or free carboxyl (PEO-*b*-PCCL) on the PCL backbone were used for this study. A12B4C50 and A83B4C63 were efficiently loaded in PEO-*b*-PCCL and PEO-*b*-PBCL nanoparticles, respectively. These polymer formulations were found to be superior to the more commonly used PEO-*b*-PCL micelles because the release of the compounds was considerably slower from the new polymeric micelles with pendent groups on the PCL block; 54 and 48% drug release from polymeric micellar formulations of A12B4C50 and A83B4C63 within 24 h in comparison to 86 and 84% release of A12B4C50 and A83B4C63 from PEO-*b*-PCL formulations.

The newly synthesized inhibitors were tested for their ability to sensitize HCT116 cells to either radiation or irinotecan. While free A83B4C63 was able to sensitize HCT116 cells to both radiation and irinotecan, free A12B4C50 failed to sensitize HCT116 cells to either treatment. We investigated the internalization of A12B4C50 (4 μ M) by fluorescence microscopy by monitoring the fluorescence of A12B4C50 (excitation wavelength 380 nm and emission wavelength 405 nm) (refer to appendix A13) and found that there is poor cellular uptake of free A12B4C50 by HCT116 cells compared to PEO-*b*-PCCL-A12B4C50 and GE11-PEO-*b*-PCCL-A12B4C50. This could explain the poor sensitization effect of

free A12B4C50 compared to the encapsulated A12B4C50. Furthermore, PEO-*b*-PCCL-A12B4C50 and PEO-*b*-PBCL-A83B4C63 were able to effectively sensitize wild-type HCT116 cells to radiation and irinotecan, but importantly, failed to sensitize the HCT116 PNKP-knockout cells. This is an indication that the new inhibitors sensitize cells primarily through inhibition of PNKP 3'-phosphatase activity and not an alternative, unidentified protein.

Based on the above data, the PEO-*b*-PCCL and PEO-*b*-PBCL micelles are expected to provide A12B4C50 and A83B4C63, respectively, the capacity for so-called "passive" targeting of tumor by EPR effect due to a leaky vasculature and poor or absent lymphatic drainage, which allows particles of diameter ~20–200 nm to preferentially enter tumor tissue and accumulate there ³⁴². PEO-*b*-PCCL-A12B4C50 and PEO-*b*-PBCL-A83B4C63 hydrodynamic diameters are within this range as shown by DLS analysis.

To achieve active targeting of our polymeric micelles and enhance their interaction with cancer cells, we covalently attached GE11 peptide to the surface of PEO-*b*-PCCL and PEO-*b*-PBCL. GE11 has an affinity for EGFR, which is expressed at a high level by HCT116 cells in comparison to HT29 cells, while SW620 cells express no EGFR. Cellular uptake analysis showed higher cellular internalization of Dil dye encapsulated in GE11 modified polymeric micelles by HCT116 cells in comparison to HT29 and SW620 cells. In contrast, free Dil and PEO-*b*-PBCL-Dil internalization was similar in all cells. Furthermore, pre-treatment of HCT116 cells with an excess of free GE11, resulted in reduced internalization of GE11-PEO-*b*-PBCL-Dil, which confirmed the involvement of receptor mediated endocytosis as the mechanism of polymeric micellar cell uptake. Despite higher uptake of GE11 modified micelles compared to plain micelles by HCT116 cells, GE11-

PEO-*b*-PCCL-A12B4C50 and GE11-PEO-*b*-PBCL-A83B4C63 were able to sensitize HCT116 cells to radiation and irinotecan in a similar manner to that of the unmodified micelles. This is most likely due to the release of encapsulated drug from the micellar carrier during the incubation with the cells (9-14 days) undermining the effect of GE11 modification. Collectively, these data indicate that GE11 is a suitable ligand to target the EGFR overexpressing cancer cells potentially providing PNKP inhibitors with more selective targeting capabilities of cancer cells for future *in vivo* studies.

Since the discovery of a synthetic lethal partnership between PARP1 and BRCA1/2, synthetic lethality has become the most desired strategy clinically for targeting DNA repair inhibition³⁴³⁻³⁴⁶. Previously, genetic screening for possible synthetic lethal partners with PNKP led to the identification of two tumor suppressor proteins, SHP-1 and PTEN^{187, 326}. We have shown in this report that PEO-*b*-PCCL-A12B4C50 and PEO-*b*-PBCL-A83B4C63 cause synthetic lethality in HCT116 PTEN^{-/-} cells (Fig. 3.8). Interestingly, PEO-*b*-PCCL-A12B4C50 displayed a marked synthetic lethality response in the HCT116 PTEN^{-/-} cells at a dose coinciding with the onset of toxicity seen with the encapsulated compound in the wild type cells. This is probably indicative of a synthetic sickness response in which the additional stress arising from the A12B4C50 toxicity amplifies the synthetic lethality. Applying this synthetic lethality/sickness approach would allow us to use these PNKP inhibitors as single agents selectively targeting PTEN-deficient tumors.

In conclusion, we have demonstrated that potent and specific nano-encapsulated PNKP phosphatase inhibitors could further enhance radiation and irinotecan therapy in colorectal cancer cells, and that PTEN-deficient tumors may be susceptible to encapsulated PNKP inhibitors administered as single therapeutic agents. Our results also

pointed to the potential of GE11 modified polymeric micelles for active targeting of PNKP inhibitors to colorectal cancers overexpressing EGFR. Finally, in general terms, this paper provided proof of concept data for a positive role of nanoparticle delivery for the acceleration of drug development efforts in cancer therapy.

3.5. Acknowledgments

We thank Ed Fu, Department of Chemistry (University of Alberta), and Mesfin Fanta, Department of Oncology (University of Alberta) for their technical assistance. This work was supported by grants funded by the Canadian Institutes of Health Research (MOP 15385) to MW and the Alberta Cancer Foundation Transformative Program Project (26603) to DH, AL and MW.

Chapter 4: Identification of binding sites of small molecule inhibitors of polynucleotide kinase/phosphatase by photoaffinity labeling-mass spectrometry

Overview:

It has previously been shown that the imidopiperidine-based inhibitors of PNKP phosphatase activity act as non-competitive inhibitors. In Chapter 3 we described the activity of two new imidopiperidine compounds. Further refinement of the imidopiperidine structures would benefit from more information regarding the interaction between the protein and inhibitors to assist with rational drug design. In an effort to identify the binding site of the newly found inhibitors, we discuss in this chapter the use of benzophenone as a photo-crosslinking moiety attached to two PNKP inhibitors, A12B4C50 and A12B4C3, and analyzing the conjugated PNKP-inhibitor complex using liquid chromatography-mass spectrometry (LC/MS/MS). Since the kinase and the phosphatase domains of PNKP lose activity if separated the protein has to be regarded as a single unit, and, therefore, we predict that the interaction site(s) of the imidopiperidine inhibitors with PNKP may not be confined to the phosphatase domain.

Identification of binding sites of small molecule inhibitors of polynucleotide
kinase/phosphatase by photoaffinity labeling-mass spectrometry

Zahra Shire¹, Rajam Mani¹, Timothy D R Morgan², Dennis G Hall² and Michael
Weinfeld¹

¹Department of Oncology, University of Alberta, Edmonton, AB, Canada

²Department of Chemistry, University of Alberta, Edmonton, AB, Canada

* Corresponding authors: Michael Weinfeld, PhD

Experimental Oncology, Cross Cancer Institute

Edmonton, AB Canada T6G 1Z2

Tel: +1 780 432 8438

Fax: +1 780 432 8428

E-mail: michael.weinfeld@albertahealthservices.ca

Abstract

Human polynucleotide kinase/phosphatase (PNKP) is a 57-kDa enzyme that phosphorylates DNA 5'-termini and dephosphorylates DNA 3'-termini. PNKP is involved in both single- and double-strand break repair. A screen of a library of imidopiperidine-based compounds resulted in the identification of three compounds that significantly inhibited PNKP phosphatase activity. To investigate the protein binding sites of the PNKP inhibitors, we synthesized novel photoaffinity probes containing a benzophenone photoreactive group linked to the small molecule inhibitors. A95B4C3 and A12B4C67 are the benzophenone-containing derivatives of A12B4C3, a first-generation PNKP inhibitor, and A95B4C50 is the benzophenone-containing derivative of A12B4C50, a potent second-generation PNKP inhibitor. The binding affinity (K_d) values were $0.17 \pm 0.01 \mu\text{M}$ for A95B4C3, $0.23 \pm 0.02 \mu\text{M}$ for A12B4C67 and $0.14 \pm 0.01 \mu\text{M}$ for A95B4C50. The photoaffinity inhibitors were evaluated for their inhibitory reactivity toward PNKP using a 2-aminopurine (2-Ap) fluorescence-based assay. The photoaffinity ligands A95B4C3 and A12B4C67 were found to have a similar effect on PNKP phosphatase activity in comparison to their parent compound A12B4C3. However, A95B4C50 was less effective than its parent compound A12B4C50 but showed a response similar to A12B4C3. Photoreaction was initiated by irradiating the mixture of PNKP and inhibitors with UV light (365 nm), and then the photolabelled PNKP was subjected to trypsin digestion. Control and modified peptide sequences were identified by liquid chromatography/mass spectrometry. Results showed that A95B4C50 binds in the region between a.a: 294 - 301 and A95B4C3 between a.a: 153 - 162, these two regions are located in the phosphatase domain. However, A12B4C67 binds to PNKP between a.a: 379 - 383, a region that is

located in the kinase domain. Although it needs further optimization, this study provides an insight into the binding sites of PNKP inhibitors. Further investigation by computational analysis and site directed mutagenesis is needed to confirm these findings.

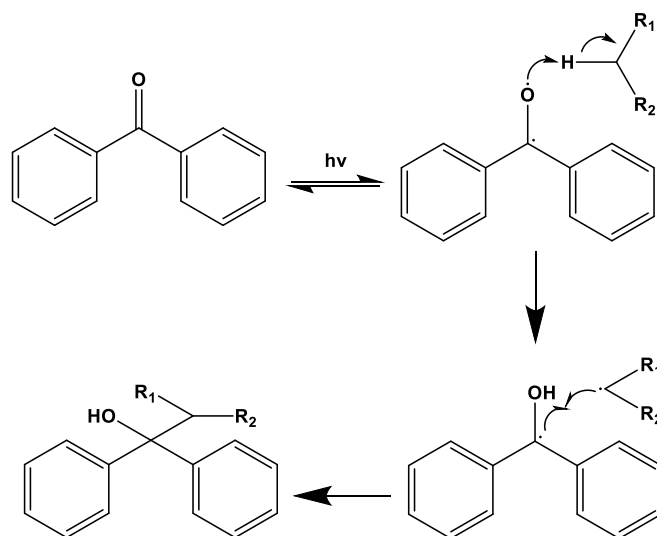
4.1. Introduction

DNA single-strand breaks (SSBs) can occur during DNA base excision repair (BER) or can arise from DNA damage by different genotoxic agents, which include ionizing radiation, and topoisomerase-I (Top-I) poisons³⁴⁷⁻³⁵⁰. Such damage often results in DNA strands with 3'-phosphate and 5'-hydroxyl termini. Neither terminus is a substrate for direct repair and ligation by DNA polymerases and ligases, which require 3'-hydroxyl and 5'-phosphate termini. Processing of DNA termini by polynucleotide kinase/phosphatase (PNKP), which possesses a DNA 5'-kinase and a 3'-phosphatase activity, has an important role in the restoration of DNA strand breaks with 5'-hydroxyl termini or 3'-phosphate termini^{64, 351-354}. PNKP is a key enzyme in the repair of both SSBs and double strand breaks (DSBs). RNAi-mediated knockdown of PNKP sensitizes cells to a variety of DNA-damaging agents. Small molecule inhibitors of PNKP have been generated that are able to sensitize cells to ionizing radiation and the Top-I poison, camptothecin^{97, 114, 158, 159}. A12B4C3, A12B4C50 and A83B4C63 are polysubstituted imidopiperidine compounds that effectively inhibit the phosphatase activity of PNKP (refer to Chapter 2). A12B4C3 was shown to be a non-competitive inhibitor^{158, 159} but its protein binding site(s), and that of the related inhibitors, has not been identified. Identifying the binding site would enable more rational design of new inhibitors.

One useful tool for the analysis of protein interactions is the use of a photoactivatable benzophenone (BP) group³⁵⁵⁻³⁵⁹. BP photoprobes have been used for drug discovery and development, identification of drug targets, determining the affinity and selectivity of drugs and identification of binding sites³⁶⁰. The attraction of using BP photoprobes can be accredited to three important features. First, BPs are chemically

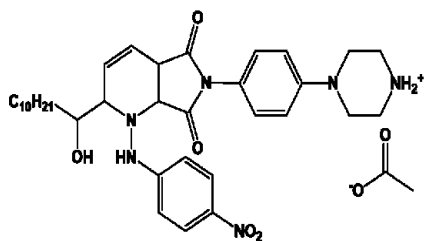
more stable than photoactivatable azide and diazirine groups. Second, BPs can be activated at wavelengths >310 nm, avoiding macromolecular-damaging wavelengths. Third, BPs react preferentially with sterically accessible C-H bonds, even in the presence of water and bulk nucleophiles (Scheme 4.1). Photoaffinity labeling in combination with mass spectrometric techniques such as liquid chromatography/mass spectrometry (LC/MS), can provide information regarding ligand-protein interaction sites³⁶¹. Once a ligand-protein complex is identified and isolated, the binding region can be identified by fragmentation of the protein into peptide fragments followed by MS-based sequencing. Finally, a BP adduct aids identification of the amino acids involved in interaction with the ligand in the binding pocket³⁶¹.

For this study, the BP was linked directly to the PNKP inhibitors A12B4C3 and A12B4C50. Activation of the BP group attached to the PNKP inhibitors with UV light resulted in its conjugation to accessible (C-H) groups in the binding pockets of PNKP. Finally, we determined the site of interaction of the inhibitors using liquid chromatography/tandem mass spectrometry (LC/MS/MS).

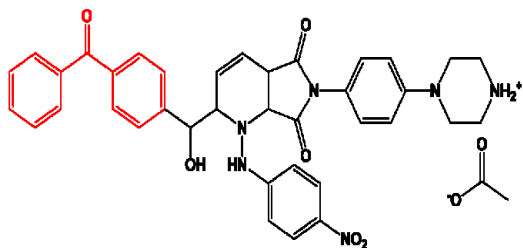


Scheme 4.1. Photochemistry of benzophenone. The reaction consists of three main steps: (i) excitation by UV light (>310 nm), (ii) H-abstraction, and (iii) radical combination to create covalent crosslinkage.

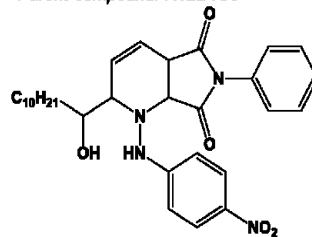
Parent compound: A12B4C50



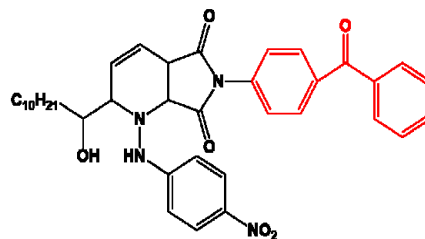
Photolabelled derivative: A95B4C50



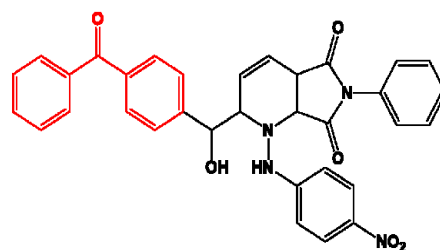
Parent compound: A12B4C3



Photolabelled derivative 1: A12B4C67



Photolabelled derivative 2: A95B4C3



Scheme 4.2. Photoactivatable PNKP inhibitors used in this study.

4.2. Experimental procedures

4.2.1. Materials

Magnesium chloride was obtained from EMD Chemicals Inc. (Gibbstown, NJ, US), sodium chloride from ACP Chemicals Inc. (Montreal, QC, CA), ultrapure Tris from ICN Biomedical Inc. (Aurora, OH, US), dithiothreitol (DTT) from Gold Biotechnology (St. Louis, MO, US). Urea was purchased from Fisher Scientific (Ottawa, ON, CA). Iodoacetamide, trifluoroacetic acid (TFA) and acetonitrile (ACN) were purchased from Sigma (Oakville, ON, CA). Trypsin/Lys-C Mix, Mass Spec Grade was purchased from Promega (Madison, WI, US). Macro Spin Columns, C18, were purchased from Harvard Apparatus (St. Laurent, Qu, CA). UVL-56 Handheld UV Lamp (6-watt, 365 nm) was purchased from The Science Company (Upland, CA, US).

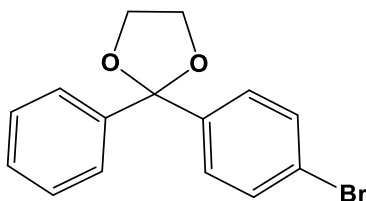
The protocol for PNKP purification was described previously^{280, 288}. PNKP is stored in 50 mM Tris-HCl (pH 7.4), 100 mM NaCl, 5 mM MgCl₂, and 0.5 mM DTT. T4 DNA polymerase was prepared as previously described²⁸⁹. All chemicals were used as received without further purification.

4.2.2. Methods

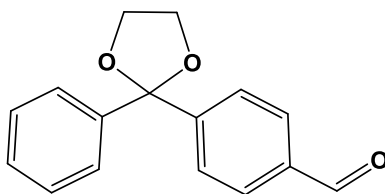
All compounds were prepared by Dr. Timothy Morgan (Department of Chemistry, University of Alberta).

4.2.2.1. Synthesis of components of photoactivatable PNKP inhibitors

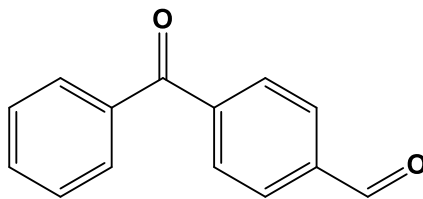
A95 component:



2-(4-Bromophenyl)-2-phenyl-1,3-dioxolane (S1): 4-Bromobenzophenone (8.4 mmol) was dissolved in benzene. *p*-TsOH·H₂O (0.4 mmol) and ethylene glycol (42.2 mmol) were added and the flask was equipped with a Dean-Stark apparatus and condenser. The reaction mixture was heated under reflux for 48 h. After cooling to room temperature, the reaction was quenched with 1 M NaOH (28 mL) and the mixture was extracted with Et₂O (x3). The combined organic extracts were washed with saturated NaCl, dried over MgSO₄, filtered and concentrated under reduced pressure. The crude product was purified by flash chromatography (40% CH₂Cl₂/hexane) to yield **S1** as a white crystalline solid (91%).

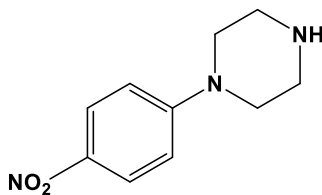


4-(2-Phenyl-1,3-dioxolan-2-yl) benzaldehyde (S2): **S1** (1.9 mmol) was dissolved in THF (5 mL) and cooled to -78°C . *n*-BuLi [2 M/hexane] (2 mmol) was added slowly and the mixture was stirred for 30 min at -78°C . DMF (2.6 mmol) was added dropwise and the reaction mixture was stirred for 15 min at -78°C before being warmed to room temperature. The reaction was quenched by the addition of saturated NH₄Cl and was diluted with EtOAc. The phases were separated, and the aqueous phase was extracted with EtOAc. The combined organic extracts were washed with saturated NaCl, dried over Na₂SO₄, filtered and concentrated under reduced pressure. The crude product (99% yield) was used without further purification.

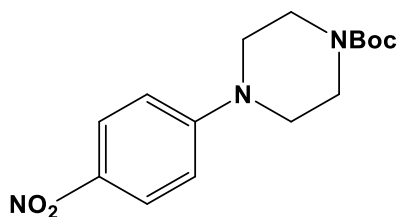


4-Benzoylbenzaldehyde (S3): **S2** (1.9 mmol) and *p*-TsOH•H₂O were combined in acetone/H₂O (10 mL, 4:1) and heated under reflux for 48 h. After cooling to room temperature, the mixture was diluted with EtOAc and washed with saturated NaHCO₃, H₂O, and saturated NaCl, dried over Na₂SO₄, filtered and concentrated under reduced pressure. The crude product was purified by flash chromatography (20% EtOAc/hexane) to yield **S3** as a white solid (70%).

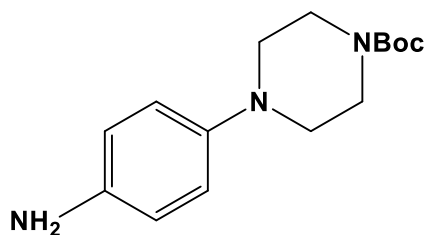
C50 component:



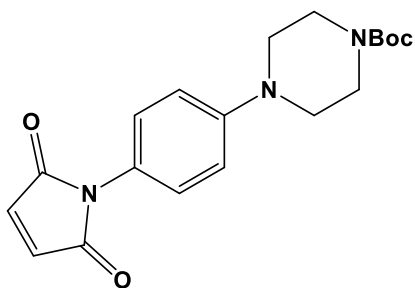
1-(4-Nitrophenyl) piperazine (S4): Prepared according to the procedure of Hepperle *et al.*³⁶². 1-Bromo-4-nitrobenzene (10.2 mmol), piperazine (13.1 mmol), K₂CO₃ (15.6 mmol) and tetrabutylammonium iodide (0.1 mmol) were combined in DMSO (20 mL) and heated to 120°C overnight. After cooling to room temperature, the reaction mixture was carefully poured into 40 mL of 1 M HCl at 0°C. The mixture was filtered to remove precipitate and the filtrate was extracted with EtOAc (x3). The aqueous phase was cooled to 0°C and basified with 6 M NaOH. The basic solution was extracted with CH₂Cl₂ (x5) and the combined extracts were dried over Na₂SO₄, filtered and concentrated under reduced pressure. The crude product (76% yield) was used without further purification.



tert-Butyl-4-(4-nitrophenyl) piperazine-1-carboxylate (S5): 1-(4-Nitrophenyl) piperazine (**S4**) (7.6 mmol) was dissolved in CH₂Cl₂ (20 mL) and cooled to 0 °C. Triethylamine (14 mmol) was added followed by the slow addition of di-*tert*-butyl dicarbonate (7.8 mmol) in CH₂Cl₂ (5 mL). The reaction mixture was warmed slowly to room temperature and stirred overnight. Water was added, and the phases were separated, the organic phase was washed successively with saturated solutions of NaHCO₃ and NaCl, dried over Na₂SO₄, filtered and concentrated under reduced pressure. The crude product (72% yield) was used without further purification.

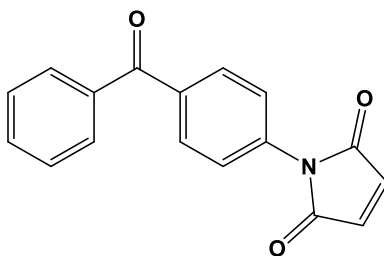


tert-Butyl-4-(4-aminophenyl) piperazine-1-carboxylate (S6): Compound **S5** (5.5 mmol) was dissolved in EtOH (50 mL) and 10% Pd/C (0.2 mmol) was added carefully. The reaction vessel was purged with N₂ then purged with H₂ and maintained under an atmosphere of H₂ for 24 h at room temperature. The reaction mixture was filtered through a plug of celite, the plug was washed with EtOAc and the filtrate was concentrated under reduced pressure. The crude product (93% yield) was used without further purification.



tert-Butyl-4-[4-(2,5-dioxo-2,5-dihydro-1H-pyrrol-1-yl)phenyl]piperazine-1-carboxylate (S7): Maleimide **S7** was prepared using a modified version of a published procedure ³⁶³. Maleic anhydride (5.6 mmol) was dissolved in EtOAc (10 mL) and **S6** (5.1 mmol) in EtOAc (5 mL) was added slowly. The reaction mixture was stirred overnight at room temperature. Stirring was halted and the mixture was cooled to 0°C, the precipitate was collected by suction filtration and transferred to an appropriately sized round bottom flask. NaOAc (10.3 mmol) and Ac₂O were added and the mixture was heated to 100°C for 5 h. After cooling to room temperature water (10 mL) and saturated NaHCO₃ (15 mL) were added and the mixture was stirred for 1 h. The mixture was extracted with EtOAc (x3), the combined extracts were washed with water (x3) and saturated NaCl, dried over Na₂SO₄ filtered and concentrated under reduced pressure. The crude material was purified by flash chromatography (30-50% EtOAc/hexane) to yield **S7** as an orange powder (52%).

C67 component:



1-(4-Benzoylphenyl)-2,5-dihydro-1H-pyrrole-2,5-dione (S8): Maleimide **S8** was prepared using a modified version of a previously published procedure ³⁶⁴. Aminobenzophenone (10 mmol) and maleic anhydride (10 mmol) were stirred in EtOAc (100 mL) for 24 h at room temperature. Solvent was removed under reduced pressure and AcOK (5 mmol) and Ac₂O (50 mL) were added. The reaction mixture was heated to 80 °C overnight. The reaction was quenched with ice cold water and the mixture was extracted with EtOAc (x3). The combined organic extracts were washed with water and saturated NaCl, dried over Na₂SO₄, filtered and concentrated under reduced pressure. The crude product was purified by flash chromatography (50-100% CH₂Cl₂/hexane) to yield **S8** as a white solid (62%).

4.2.2.2. Determination of binding constants of PNKP photolabelled inhibitors

This experiment was conducted by Dr. Rajam Mani (Department of Oncology, University of Alberta). Fluorescence titrations of PNKP with photoactivatable inhibitors were measured at 25°C using a PerkinElmer Life Sciences LS-55 spectrofluorometer with 3 nm spectral resolution for excitation and emission as previously described ²⁸⁸. PNKP fluorescence was excited at 295 nm, and fluorescence emission was recorded at 340 nm. In this experimental design, a single concentration of the receptor (PNKP) was used and the concentration of the inhibitor (Ligand) was varied. Binding of the inhibitor to PNKP was analyzed using the equation:

$$[LR] = \frac{([X] + [R_{tot}] + kd) \pm \sqrt{([X] + [R_{tot}] + kd)^2 - 4[X][R_{tot}]}}{2}$$

L = X – LR.

Where, X is the total Ligand concentration and R_{tot} is the total receptor concentration (Same units as X). LR refers to ligand bound to the receptor and the L is the free ligand concentration. Binding data were analyzed using Prism (GraphPad Software Inc., La Jolla, CA). This method is previously mentioned in Chapter 2.

4.2.2.3. Fluorescence-based assay for detecting activity of photoactivatable inhibitors of the 3'-phosphatase activity of PNKP

The assays (100 μ L total volume) were performed in Corning 3573 black, flat bottom 384-well microplates, purchased from Corning Life Sciences (Tewksbury, MA, US), and prepared in 100 mM Tris (pH 7.5), 50 mM NaCl, 10 mM $MgCl_2$, and 1mM DTT. Initially 25 nM PNKP (2.5 μ L) was preincubated with 10 μ M test compound (2 μ L) or DMSO vehicle for 5 -15 min at room temperature (100 μ L total volume). Then HPP (10 μ L) or HPOH (10 μ L) and 80 nM T4 DNA polymerase (4 μ L) were added. For the control reactions, the phosphatase activity of PNKP was monitored by first treating HPP (10 μ L) with 25 nM PNKP (2.5 μ L) to convert all 3'-P to 3'-OH, then adding 80 nM T4 DNA polymerase (4 μ L) to hydrolyse the hairpins substrates. The above assay was previously described in Chapter 2. Fluorescence (320 nm excitation and 405 nm emission) of each well was read in a FLUOstar Optima (BMG Labtech Inc., Guelph, ON, CA). Data were analyzed using Graphpad Prism software.

4.2.2.4. Photocrosslinking of ligand-PNKP mixture

PNKP (30 μ g) was mixed with either 1.5 or 15 μ L of the ligand solution (3 mM) or an equivalent volume of DMSO in the dark at room temperature for 15 min. The mixture was then placed on ice and the photoreaction was initiated by irradiating the mixture with UV light (365 nm) for 60 min.

4.2.2.5. In-solution digestion of ligand-modified PNKP

A reduction buffer consisting of 6-8 M urea and 5 mM DTT/50 mM Tris-HCl (pH 8) was added to the ligand-protein mixture for 1 h at 37°C. Iodoacetamide was added to the mixture to a final concentration 15 mM in the dark at room temperature for 1 h. The concentration of urea was reduced to <1 M by adding 50 mM Tris-HCl (pH 8) before digestion. Trypsin/Lys-C Mix was added to the ligand-protein mixture at a 25:1 protein: trypsin ratio (w/w) overnight at 37°C. The digestion was terminated by adding TFA to a final concentration of 0.5 -1%.

4.2.2.6. Purification of ligand-modified PNKP

Conditioning the Macro Spin C18 column. 400 µL of 100 % acetonitrile was pipetted onto the column and the column was centrifuged for 5 min at 150 x g and the collecting tube was removed. To equilibrate the column, 150 µL of 0.1% TFA was pipetted into the column and centrifuged for 5 min at 150 x g. **Processing the sample.** 150-300 µL of digested sample were added to the column and placed in a new 2 mL centrifuge tube. The sample was centrifuged for 5 min at 150 x g. The sample was then washed with 0.1% TFA 2 x for 3 min at 150 x g. **Eluting the sample.** In a new collecting tube, 150 µL 0.1% TFA and 95% ACN was applied to the column to elute the peptides. This step was repeated twice. After collecting the purified peptide, solvent was reduced to 25-50 µL in a speed-vac.

4.2.2.7. LC-MS/MS analysis

The resultant peptides were subjected to LC-MS/MS analysis using an Easy nanoLC II (Thermo Scientific) system coupled to a Waters Premier QTOF analyzer (Waters, Milford, MA, US). An aliquot of the sample was loaded onto an Acclaim PepMap300, C4, 100 µm

x 2 cm, 5 μm particle size nano trap, (Thermo Scientific, Sunnyvale, CA, US) coupled to an Acclaim PepMap300, C4, 75 μm \times 150 mm, 5 μm particle size nano-analytical column Thermo Scientific, Sunnyvale, CA, US). Desalting on the peptide trap was achieved by flushing the trap with 25 μL of 100% eluent A (0.1% formic acid in water) at a flow rate of 10 $\mu\text{L}/\text{min}$. Peptides were separated at a flow rate of 350 nL/min with a gradient of 1% eluent B (0.1% formic acid in acetonitrile) for 1 minute, 1 to 45% eluent B over 39 minutes, 45 to 98 %B over 5 minutes, kept at 98% eluent B over 4 minutes and back to 1% eluent B over 1 minute. Analysis was performed using Mascot Distiller (Matrix Science, UK) and ProteinScope (Bruker, Bremen, Germany) software packages. Database searches were performed using an in-house Mascot server.

4.3. Results

4.3.1. Measurement of K_d values

The binding constants of the ligands to PNKP were obtained by fluorescence spectroscopy. Since binding of the ligand to PNKP partially quenches the protein Trp fluorescence at 340 nm following excitation at 295 nm, the binding affinity (K_d) can be determined by following fluorescence quenching as a function of ligand concentration. Figure 4.1 shows the fluorescence intensities versus the concentrations of A95B4C50, A95B4C3, and A12B4C67. Nonlinear regression analysis of the binding data revealed unimodal binding with K_d values of $0.14 \pm 0.01 \mu\text{M}$ for A95B4C50, $0.17 \pm 0.01 \mu\text{M}$ for A95B4C3 and $0.23 \pm 0.02 \mu\text{M}$ for A12B4C67.

4.3.2. Biochemical evaluation of the photoaffinity probes

We examined the ability of the photoactivatable PNKP inhibitors to inhibit PNKP 3'-phosphatase activity using the 2-Ap assay described in Chapter 2. As it is evident from

Figure 4.2A, the presence of 10 μM A95B4C50 slightly reduced the expected increase in the fluorescence signal similar to 25 μM A12B4C3 indicating that PNKP phosphatase activity is partially blocked by these two compounds. However, the activity of this ligand was found to be less than its parent derivative A12B4C50. Figure 4.2B, shows that there was no inhibitory effect on the exonuclease activity of T4 pol in the presence of 10 μM A95B4C50. Figures 4.3A and 4.4A, show that both 25 μM A95B4C3 and 25 μM A12B4C67, derivatives of A12B4C3, slightly reduced the expected increase in the fluorescence signal similar to their parent compound A12B4C3, once again, indicating that PNKP phosphatase activity is partially blocked by these compounds. As shown in Figures 4.3B and 4.4B, there was no inhibitory effect on the exonuclease activity of T4 pol in the presence of 25 μM A95B4C3 and A12B4C67, which indicates that the reduced fluorescence signal was indeed due to the inhibition of PNKP only.

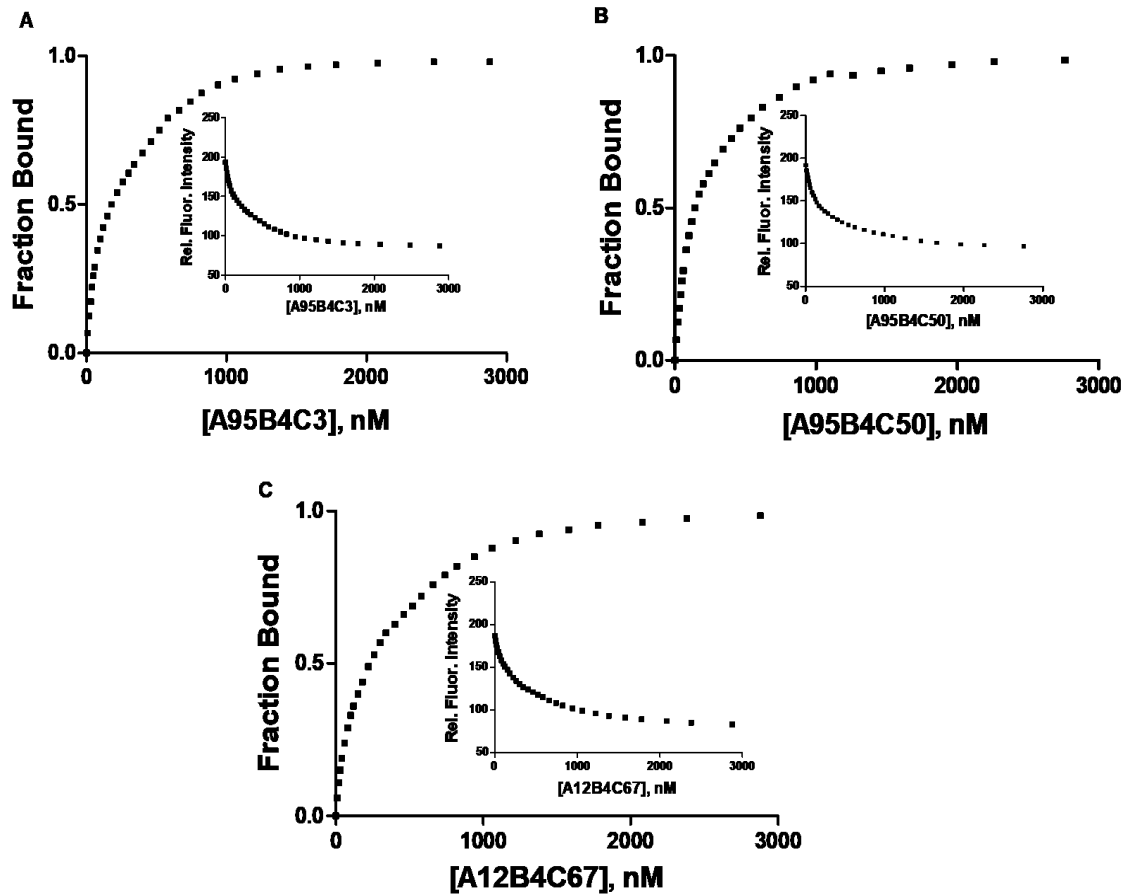


Figure 4.1. A plot of fluorescence intensities of titration of PNKP. (A) A95B4C50, (B) A95B4C3 and (C) A12B4C67. PNKP (0.03 μM) in 50 mM Tris HCl (pH 7.5), 100 mM NaCl, 5 mM MgCl_2 was excited at 295 nm, and fluorescence intensity was monitored at 340 nm. Data presented in this figure were generated by Dr. Rajam Mani.

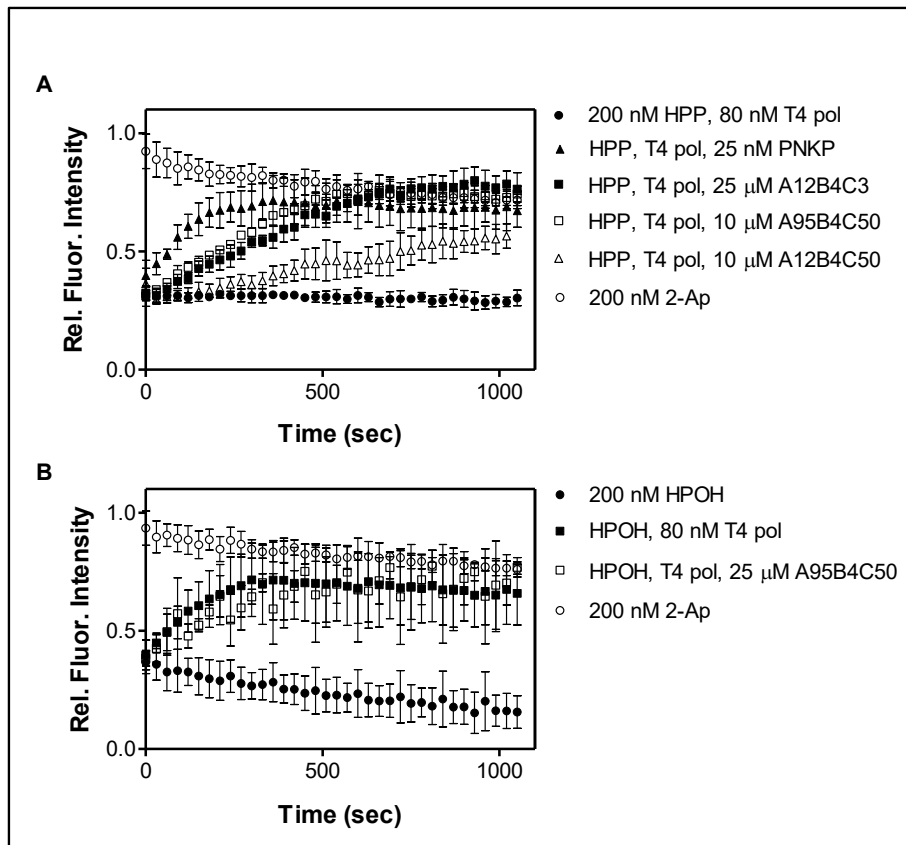


Figure 4.2. The effect of A95B4C50 on PNKP activity. (A) Incubation of hairpin HPP with both PNKP and T4 pol caused an increase in the fluorescence signal (filled triangles), indicating release of 2-ApMP from the hairpin. Open circles represent the fluorescence by 200 nM 2-Ap, which was used as a control for 2-ApMP because the base and mononucleotide display the same fluorescence. In the presence of A95B4C50, the fluorescence signal was partially reduced (open squares), indicating partial inhibition of PNKP phosphatase activity. This response is similar to what was observed with A12B4C3 (filled squares), however, the potency of A95B4C50 is less than its parent compound A12B4C50 (open triangles). (B) There was no reduction of 2-ApMP release from hairpin HPOH in the presence of A95B4C50 (open squares), indicating no inhibition of T4 pol. Each point represents the mean \pm SD ($n = 3$).

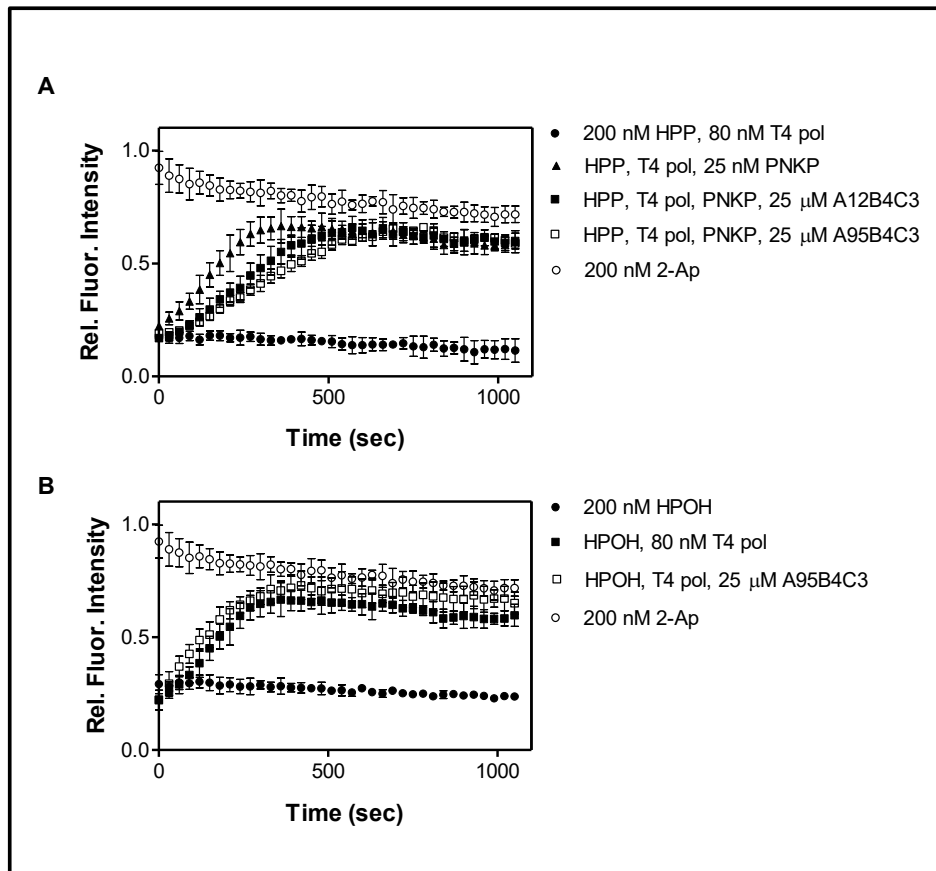


Figure 4.3. The effect of A95B4C3 on PNKP. (A) Incubation of hairpin HPP with both PNKP and T4 pol caused an increase in the fluorescence signal (filled triangles), indicating release of 2-ApMP from the hairpin. In the presence of A95B4C3, the fluorescence signal was partially reduced (open squares), indicating partial inhibition of PNKP phosphatase activity. This response was similar to what was observed with A12B4C3, the parent compound, (filled squares). **(B)** There was no reduction of 2-ApMP release from hairpin HPOH in the presence of A95B4C3 (open squares), indicating no inhibition of T4 pol. Each point represents the mean \pm SD (n = 3).

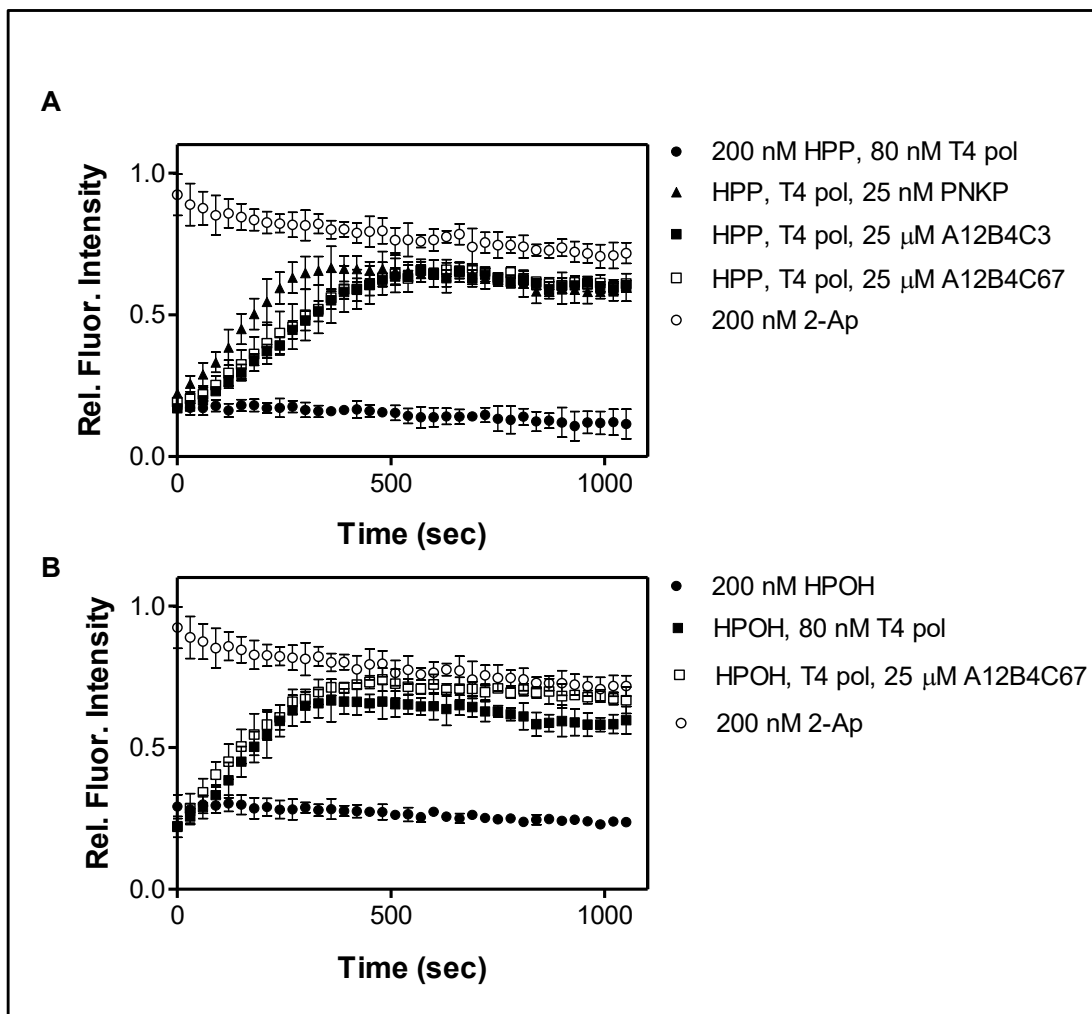


Figure 4.4. The effect of A12B4C67 on PNKP. (A) Incubation of hairpin HPP with both PNKP and T4 pol caused an increase in the fluorescence signal (filled triangles), indicating release of 2-ApMP from the hairpin. In the presence of A12B4C67, the fluorescence signal was partially reduced (open squares), indicating partial inhibition of PNKP phosphatase activity. This response was similar to that observed with A12B4C3, the parent compound, (filled squares). **(B)** There was no reduction of 2-ApMP release from hairpin HPOH in the presence of A12B4C67 (open squares), indicating no inhibition of T4 pol. Each point represents the mean \pm SD ($n = 3$).

4.3.3. Identification of the binding sites by tandem mass spectrometry

Kinetic analysis discussed in Chapter 2 proved that imidopiperidine inhibitors act as non-competitive inhibitors. Therefore, unlike competitive inhibitors, it is not possible to readily predict where the inhibitors bind. To determine the binding sites, photoreactions were conducted between PNKP and the three photoactivatable inhibitors A95B4C50, A95B4C3 and A12B4C67. We digested the complexes formed from the photoreaction with trypsin and analyzed the product mixtures by LC-MS/MS. Below, we discuss the results of reaction with each photoaffinity compound.

4.3.3.1. A95B4C50

A95B4C50 is a photoactivatable form of A12B4C50 (Scheme 4.2), and a more potent derivative of A12B4C3. The digested peptides were loaded onto the LC-MS/MS system and results were analyzed using ProteinScape, a proteomics and data analysis software package ³⁶⁵⁻³⁶⁷. Figure 4.5 shows that the sequence coverage obtained for treated PNKP with A95B4C50 was ~28% compared to 72.9% for untreated PNKP. To identify the modified peptides, we applied ExpASy peptide mass tool. This program computes the masses of the peptides generated by trypsin digestion of a protein sequence from the UniProt Knowledgebase or a user-entered protein sequence ³⁶⁸. We calculated the masses of the expected modified peptides by adding the mass of A95B4C50, i.e. 657 g/mol, to the observed peptide masses of untreated PNKP extracted from LC-MS/MS. Finally, we matched the theoretically calculated peptide masses with the observed peptide masses of PNKP treated with A95B4C50.

A

	10	20	30	40	50	60	70	80	90	100	110	120
MGEVEAPGRL	WLESPPGGAP	PIFLPSDQQA	LVLGRGFLTQ	VTDRKCSRTQ	VELVADPETR	TVAVKQLGVN	PSTTGTQELK	PGLEGLGVG	DTLYLVNGLH	PLTLRWEETR	TPESQPDTPP	
	130	140	150	160	170	180	190	200	210	220	230	240
GTPLVSQDEK	RDALPKKRM	RKSNPGWENL	EKLLVFTAAG	VKPQGVAGF	DLGDLITTR	SGKVPTGPS	DWRILYPEIP	RKLRELEAEG	YKLVIFTNQM	SIGRGKLPAE	EFKAKVEAVV	
	250	260	270	280	290	300	310	320	330	340	350	360
EKLGVPFQVL	VATHAGLYRK	PVTGMMDHLQ	EQANDGTPIS	IGDSIFVQDA	AGRPANWAPG	RKKKDFSCAD	RLFALNLGLP	FATPEEFLK	WPAAGFELPA	FDPRTVSRSG	PLCLPESRAL	
	370	380	390	400	410	420	430	440	450	460	470	480
LSASPEVVVA	VGFPAGKST	FLKKHLVSAG	YVHVNRDTLG	SWQRCVTTCE	TALKQGRVA	IDNTNPDAAAS	FARYVQCARA	AGVPCRCFLF	TATLEQARHN	NRFREMTDSS	HIPVSDMVMY	
	490	500	510	520	530							
GYRKQFEAPT	LAEGFSAILE	IPFRLWVEPR	LGRLYCQFSE	G								

B

	10	20	30	40	50	60	70	80	90	100	110	120
MGEVEAPGRL	WLESPPGGAP	PIFLPSDQQA	LVLGRGFLTQ	VTDRKCSRTQ	VELVADPETR	TVAVKQLGVN	PSTTGTQELK	PGLEGLGVG	DTLYLVNGLH	PLTLRWEETR	TPESQPDTPP	
	130	140	150	160	170	180	190	200	210	220	230	240
GTPLVSQDEK	RDALPKKRM	RKSNPGWENL	EKLLVFTAAG	VKPQGVAGF	DLGDLITTR	SGKVPTGPS	DWRILYPEIP	RKLRELEAEG	YKLVIFTNQM	SIGRGKLPAE	EFKAKVEAVV	
	250	260	270	280	290	300	310	320	330	340	350	360
EKLGVPFQVL	VATHAGLYRK	PVTGMMDHLQ	EQANDGTPIS	IGDSIFVQDA	AGRPANWAPG	RKKKDFSCAD	RLFALNLGLP	FATPEEFLK	WPAAGFELPA	FDPRTVSRSG	PLCLPESRAL	
	370	380	390	400	410	420	430	440	450	460	470	480
LSASPEVVVA	VGFPAGKST	FLKKHLVSAG	YVHVNRDTLG	SWQRCVTTCE	TALKQGRVA	IDNTNPDAAAS	FARYVQCARA	AGVPCRCFLF	TATLEQARHN	NRFREMTDSS	HIPVSDMVMY	
	490	500	510	520	530							
GYRKQFEAPT	LAEGFSAILE	IPFRLWVEPR	LGRLYCQFSE	G								

Figure 4.5. Sequence coverage of PNKP in the presence or absence of A95B4C50 determined by ProteinScope software. (A) Untreated PNKP, after digestion with trypsin, resulted in 72.9% sequence coverage. (B) PNKP treated with A95B4C50 resulted in ~28% sequence coverage after trypsin digestion.

If a hit was found, we further analyzed the modified peptide using ProteinProspector, software that helps to calculate masses resulting from peptide fragmentation, to determine the amino acid in the peptide sequence that has been photolabelled ^{369, 370}. The fragmentations can occur either through C-terminal (y ions), N-terminal (b ions) or both. By conducting analysis with ProteinScape and ExPASy, we were able to find a hit. A95B4C50 was found to induce modification in the peptide PANWAPGR that is located in the region 294-301. The unmodified peptide has a mass, $[M+H]^+$, equal to 868.4 and the counter modified peptide mass, $[M+H]^+$, is 1525.4 (Table 4.1A). By using ProteinProspector software, we obtained the induced fragments of unmodified peptides and by manually adding the weight of the probe to each fragment, we were able to locate the modifications on two different sites. The fragment PANWA is generated from N-terminal fragmentation and R is generated from C-terminal fragmentation (Table 4.1B). This observation was confirmed by the mass spectra of both unmodified peptide PANWAPGR (Figure 4.6A) and its modified counterpart (Figure 4.6B). The mass spectrum of unmodified peptide PANWAPGR confirmed the presence of the fragments 169, 283, 329, 400, 469, 586, 700 and 771 (Table 4.1B). On the other hand, Figure 4.6B shows the presence of a peak corresponding to the mass of the modified PANWAPGR peptide, 1525.4, along with the modified fragments R, 832.35, and PANWA, 1197.35, as was predicted from the analysis shown in Table 4.1B.

Table 4.1. Induced fragments of unmodified and modified peptides after photoreaction with A95B4C50. (A) Hit peptide, 1525.4, was identified among the trypsin fragments following digestion of PNKP treated with A95B4C50. **(B)** Induced fragmentation of both untreated and treated peptide PANWAPGR.

A

<i>Observed peptides of unmodified PNKP</i>	<i>Observed peptides of modified PNKP</i>	
4445.3	4445.4	
3985.7	3985.7	
3704.9	3704.6	
2886.5	2886.5	
868.4	1525.4	Hit peptide: 868.4 + 657
827.5	827.4	
772.4	772.4	

B

Hit peptide: PANWAPGR , a.a : 294 - 301

Sequence ions of unmodified peptide					Sequence ions of modified peptide				
N-terminal		Sequence		C-terminal	N-terminal		Sequence		C-terminal
b				y	b				y
---	1	P	8	---	---	1	P	8	---
169.09	2	A	7	771.38	826.09	2	A	7	1428.38
283.14	3	N	6	700.35	940.14	3	N	6	1357.35
469.21	4	W	5	586.30	1126.21	4	W	5	1243.30
540.25	5	A	4	400.23	1197.25	5	A	4	1057.23
637.30	6	P	3	329.19	1294.30	6	P	3	986.19
694.33	7	G	2	232.14	1351.33	7	G	2	889.14
---	8	R	1	175.11	---	8	R	1	832.11

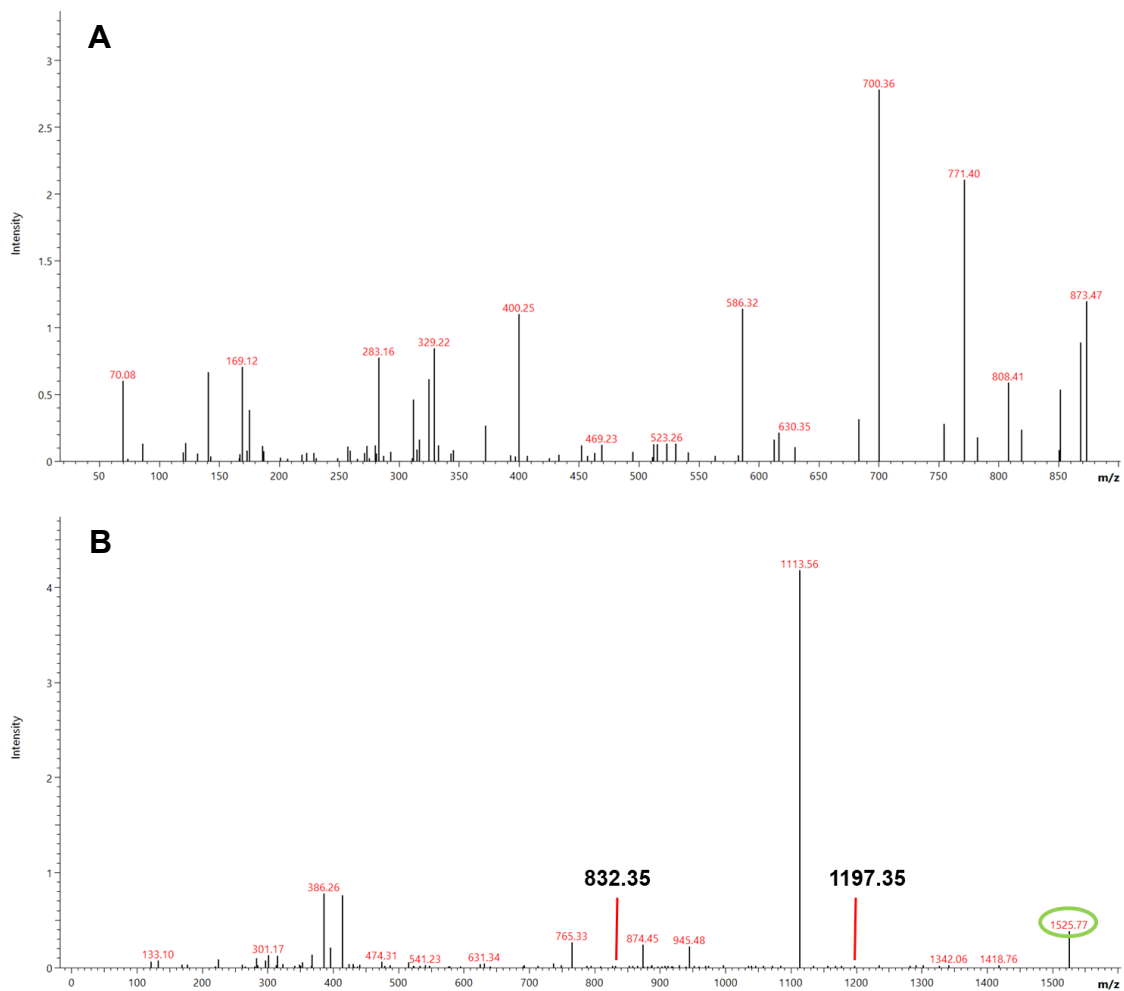


Figure 4.6. Mass spectra of digested-PNKP peptide PANWAPGR. (A) Mass spectrum of unmodified peptide PANWAPGR shows the appearance of peaks related to sequence ions (b & y ions) similar to the one obtained from ProteinProspector (Table 4.1B). **(B)** Mass spectrum of modified peptide PANWAPGR + 657 shows the appearance of peaks related to sequence ions of modified PANWAPGR (1525.7), PANWA (1197.35) and R (832.35) shown in (Table 4.1B).

4.3.3.2. A95B4C3

The same protocol and analysis procedures were conducted for A95B4C3, a modified derivative of A12B4C3. However, we observed a different binding site with this ligand. Figure 4.7 shows that the sequence coverage obtained for PNKP treated with A95B4C3 was ~70.1% compared to 72.9% for untreated PNKP. A modification was observed in the peptide LLVFTAAGVK located at the region 153 -162. According to ProteinScape and ExPASy, the unmodified peptide LLVFTAAGVK has a mass, $[M+H]^+$, equal to 1018.6 and the counter modified peptide mass, $[M+H]^+$, is 1593.2 (Table 4.2A). By using ProteinProspector software, we obtained the induced fragments of unmodified peptides and by manually adding the mass of the probe to each fragment, we were able to locate the modifications on the segment LLVFTA (Table 4.2B). This observation was confirmed by the mass spectrum of the modified peptide LLVFTAAGVK (Figure 4.8). The mass spectrum of unmodified peptide LLVFTAAGVK was not detected by LC-MS/MS. Therefore, another option to confirm the peptide sequence was by measuring the distances between the peaks in the mass spectrum of modified peptide, the distances reflect the mass of amino acids in the sequence. Figure 4.8, shows that by measuring distances between peaks we covered 90% of the sequence LLVFTAAGVK. In addition, Figure 4.8 shows the presence of peaks corresponding to the mass of the modified fragment LLVFTA as was predicted from the analysis shown in Table 4.2B.



Figure 4.7. Sequence coverage of PNKP in the presence or absence of A95B4C3 determined by ProteinScope software. (A) Untreated PNKP, after digestion with trypsin, resulted in 72.9% sequence coverage. (B) PNKP treated with A95B4C3 resulted in 70.1% sequence coverage after trypsin digestion.

Table 4.2. Induced fragments of unmodified and modified peptides after photoreaction with A95B4C3. (A) Hit peptide, 1593.2, was identified among the trypsin-digestion fragments of PNKP treated with A95B4C3. **(B)** Induced fragmentation of both untreated and treated peptide LLVFTAAGVK.

A

<i>Observed peptides of unmodified PNKP</i>	<i>Observed peptides of modified PNKP</i>	
4144.1	4144.1	
3581.7	3581.7	
2863.4	2863.3	
1959.1	1959.1	
1783.9	1783.9	
1018.6	1593.2	Hit peptide: 1018.6+ 574.6
971.5	971.4	

B

Hit peptide : LLVFTAAGVK, a.a : 153 - 162

Sequence ions of unmodified peptide					Sequence ions of modified peptide				
N-terminal		Sequence		C-terminal	N-terminal		Sequence		C-terminal
b				y	b				y
---	1	L	10	---	---	1	L	10	---
227.17	2	L	9	905.54	801.77	2	L	9	1480.14
326.24	3	V	8	792.46	900.84	3	V	8	1367.06
473.31	4	F	7	693.39	1047.91	4	F	7	1267.99
574.35	5	T	6	546.32	1148.95	5	T	6	1120.92
645.39	6	A	5	445.27	1220.00	6	A	5	1019.87
716.43	7	A	4	374.23	1291.03	7	A	4	948.83
773.45	8	G	3	303.20	1348.05	8	G	3	877.80
872.52	9	V	2	246.18	1447.12	9	V	2	820.78
---	10	K	1	147.11	---	10	K	1	721.71

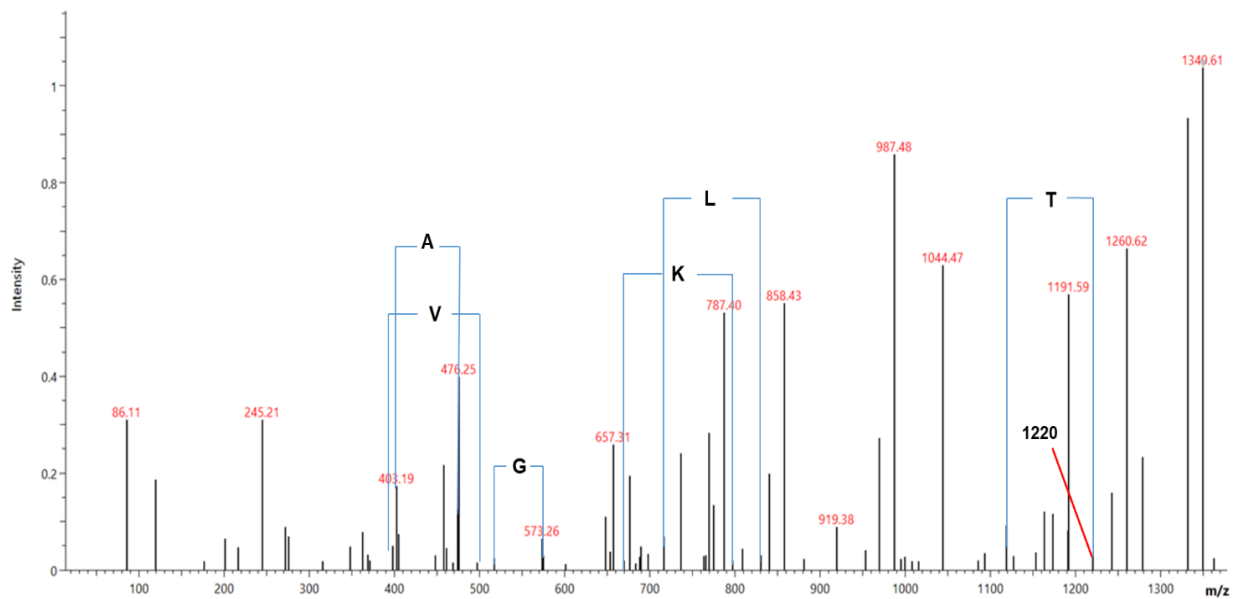


Figure 4.8. Mass spectrum of digested-PNKP peptide LLVFTAAGVK modified by A95B4C3. The mass spectrum of modified peptide shows the appearance of peaks related to the sequence ion LLVFTA (1220) as predicted by ProteinProspector (Table 4.2B). Distance calculated between peaks confirms the presence of 90% of the peptide sequence.

4.3.3.3. A12B4C67

Interaction of PNKP with A12B4C67, another modified derivative of A12B4C3, was also analyzed by the same protocol. Figure 4.9 shows that the sequence coverage obtained for treated PNKP with A12B4C67 was ~72.9%, similar to what was observed for untreated PNKP. By conducting analysis with ProteinScape and ExPASy, we were able to find a hit. A12B4C67 was found to induce modification in the peptide STFLK that is located in the region 379-383. The unmodified peptide has a mass $[M+H]^+$ equal to 595.3 and the counter modified peptide mass $[M+H]^+$ is 1234 (Table 4.3A). By using ProteinProspector software, we obtained the induced fragments of unmodified peptide STFLK and by manually adding the weight of probe to each fragment, we were able to locate the modifications on amino acid K (Table 4.3B). This observation was confirmed by the mass spectra of both unmodified peptide STFLK, Figure 4.10A, and its modified counterpart (Figure 4.10B). The mass spectrum of unmodified peptide STFLK, 595.3, confirmed the presence of the fragments 147.11, 189.08, 260.19, 407.26, 449.23 and 508.31 (Table 4.3B). On the other hand, Figure 4.10B shows the presence of a peak corresponding to the mass of the modified amino acid K, 785.8, as predicted from the analysis shown in Table 4.3B.

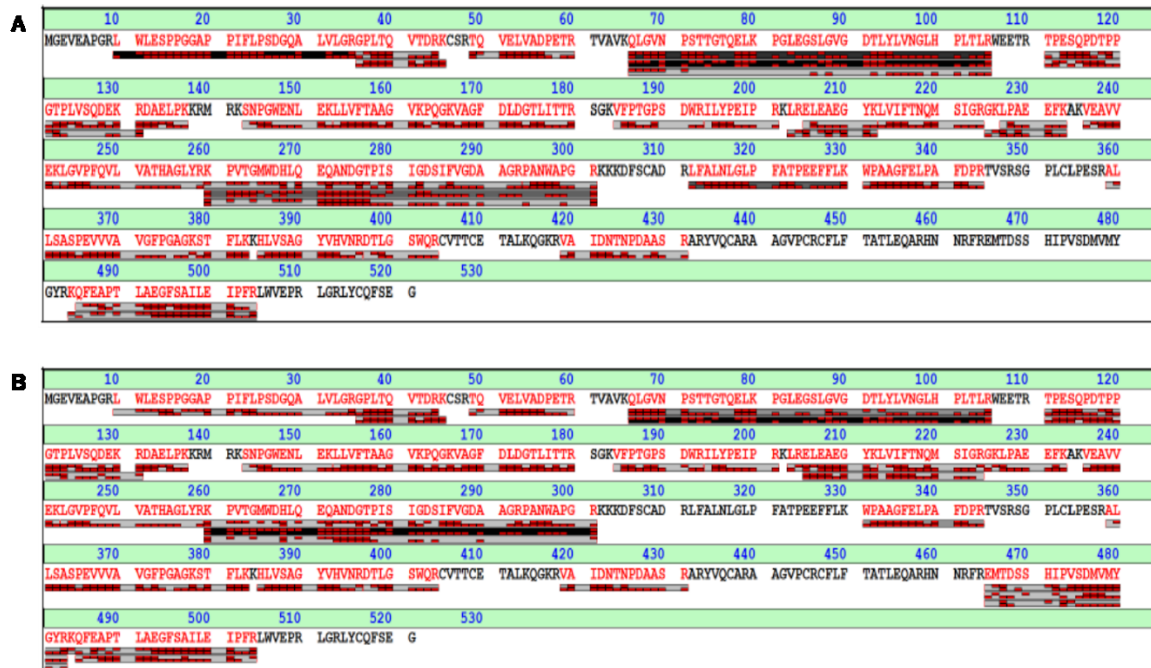


Figure 4.9. Sequence coverage of PNKP in the presence or absence of A12B4C67 determined by ProteinScope software. (A) Untreated PNKP, after digestion with trypsin, resulted in 72.9% sequence coverage. (B) PNKP treated with A12B4C67 also resulted in 72.9% sequence coverage after trypsin digestion.

Table 4.3. Induced fragments of unmodified and modified peptides after photoreaction with A12B4C67. (A) Hit peptide, 1234, was identified among the trypsin-digestion fragments of PNKP treated with A12B4C67. **(B)** Induced fragmentation of both untreated and treated peptide STFLK.

A

<i>Observed peptides of unmodified PNKP</i>	<i>Observed peptides of modified PNKP</i>	
4145.2	4145.1	
2687.4	2687.4	
2364.2	2364.2	
2279.1	2279.1	
2167.1	2167.1	
1573.7	1573.7	
595.3	1234	Hit peptide: 595.3 + 638.7

B

Hit peptide: S T F L K , a.a : 379 - 383

Sequence ions of unmodified peptide					Sequence ions of modified peptide				
N-terminal		Sequence		C-terminal	N-terminal		Sequence		C-terminal
b				y	b				y
---	1	S	5	---	---	1	S	5	---
189.08	2	T	4	508.31	827.78	2	T	4	1147.01
336.15	3	F	3	407.26	974.85	3	F	3	1045.96
449.23	4	L	2	260.19	1087.93	4	L	2	898.89
---	5	K	1	147.11	---	5	K	1	785.81

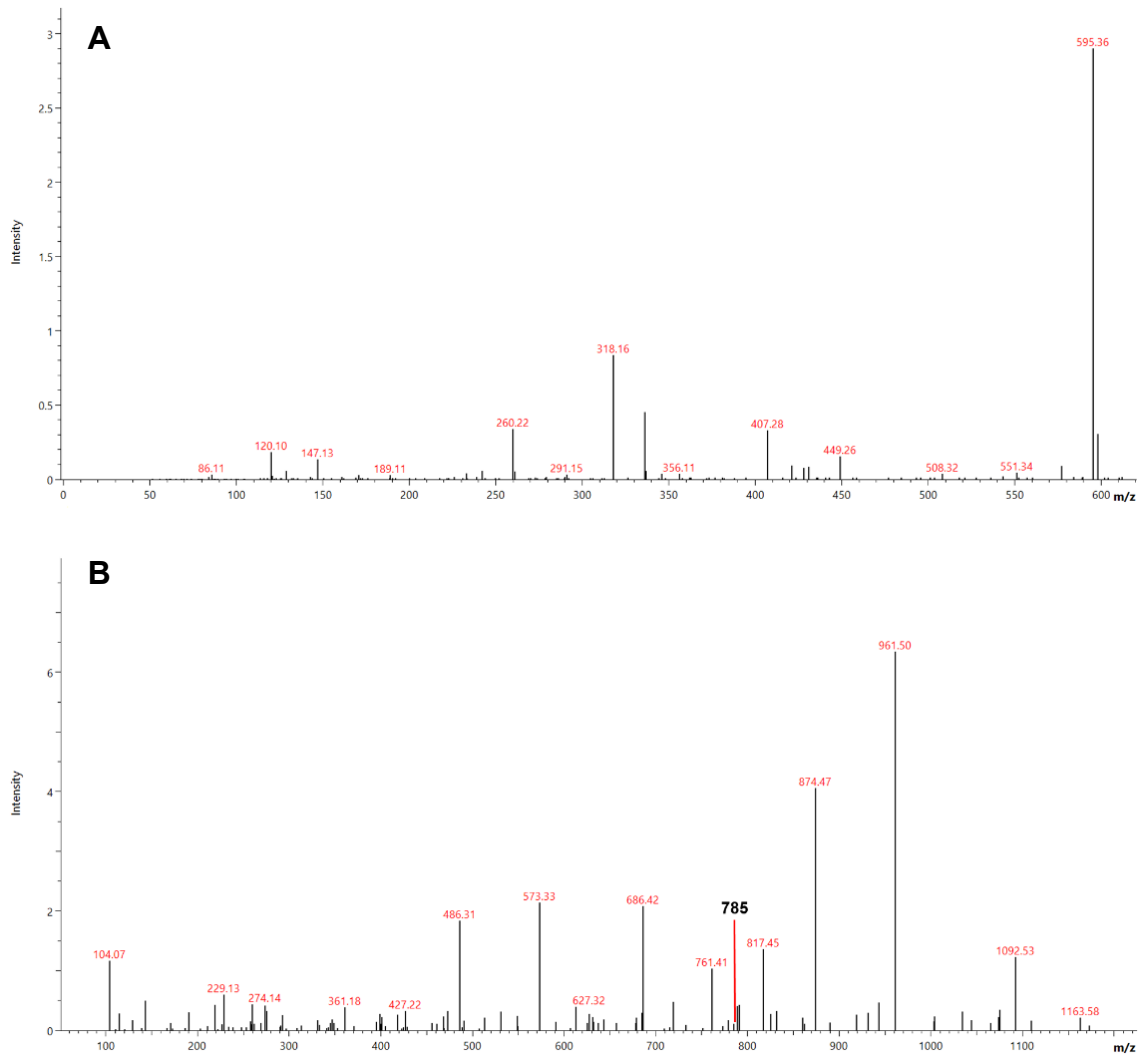


Figure 4.10. Mass spectra of digested-PNKP peptide STFLK. (A) Mass spectrum of unmodified peptide STFLK shows the appearance of peaks related to sequence ions (b & y ions) similar to the one obtained from ProteinProspector (Table 4.3B). **(B)** Mass spectrum of the modified peptide STFLK + 638.7 shows the appearance of peaks related to sequence ion K (785.81) as predicted from the analysis shown in (Table 4.3B).

4.4. Discussion

Characterization of small molecule-protein interaction such as target identification or profiling of the binding site is of high importance in drug discovery research. Benzophenone-based photoaffinity labeling represents a powerful tool to identify small molecule-protein binding sites with high specificity. Benzophenone can be activated at wavelengths >310 nm and can react with macromolecules through free C-H bonds³⁷¹.

In this chapter, we discuss the attachment of the benzophenone functional group directly to PNKP inhibitors A12B4C3 and A12B4C50. Two of the photoaffinity ligands, A95B4C3 and A12B4C67, are derivatives of A12B4C3, while the third ligand is a derivative of A12B4C50. Kinetic analysis was conducted on the photoactivatable ligands to determine their binding efficiency (K_d). K_d values of 0.14 ± 0.01 μM for A95B4C50, 0.17 ± 0.01 μM for A95B4C3 and 0.23 ± 0.02 μM for A12B4C67 were determined. All the K_d values are close to what was determined for their respective parent compounds A12B4C3, 0.37 ± 0.03 μM ,¹⁵⁹ and A12B4C50, 0.09 ± 0.05 μM , (refer to Chapter 2). The photoaffinity ligands were also tested for their ability to inhibit the phosphatase activity of PNKP. Figures 4.2 - 4.4, indicate that all the photoaffinity ligands exert some inhibition of the phosphatase activity of PNKP. A94B4C3 and A12B4C67 have similar potency to their parent compound A12B4C3. However, A95B4C50 showed less activity than its parent compound A12B4C50, but superior activity to A12B4C3.

A95B4C3 and A12B4C67, although both are derived from A12B4C3, show distinct binding sites. A95B4C3 was found to interact with PNKP at the region 153 -163, where the peptide LLVFTAAGVK is located. This peptide is in the phosphatase domain as is shown in Figure 4.11. Further fragmentation of this target peptide lead to the identification

of the LLVFTA segment as the site where the modification occurred. On the other hand, A12B4C67 was found to interact at the region 379 - 383 (STFLK), which surprisingly is located in the kinase domain (Figure 4.11). Induced fragmentations of this peptide resulted in the identification of amino acid lysine (K) as the target of A12B4C67 interaction with this peptide (Table 4.3B).

In an earlier investigation of the potential site of binding of A12B4C3 to PNKP using site-directed mutagenesis, it was shown that there is an interaction between A12B4C3 and Trp402, which lies in the kinase domain of PNKP ¹⁵⁹, suggesting the possibility that the inhibitor binds in the kinase domain without disturbing kinase activity but still inhibiting the phosphatase activity due to the close interaction between the two domains. However, without further analysis, we cannot rule out the possibility that the inhibitors can bind in more than one location and that in some locations the disruption to the protein is insufficient to cause loss of enzymatic function.

A95B4C50 also showed a distinct binding site. Analysis indicated that the interaction between A95B4C50 and PNKP is in the region 294-301, where the peptide, PANWAPGR, is located in the phosphatase domain (Figure 4.11). Induced fragmentation of this peptide resulted in the identification of 2 segments, the amino acid arginine R and PANWA as the targets of A95B4C50 interaction with this peptide (Table 4.1B).

Furthermore, we were able to identify only ~ 28% of PNKP sequence after incubation with A95B4C50. The other identified peptides, 153 - 162 and 379-383, were not or partially identified, respectively. Therefore, A95B4C50 could be binding to PNKP in these regions but we were not able to confirm it due to the low sequence coverage.

Although photolabeling with benzophenone is a powerful tool, conformational flexibility of the photoligand is still a challenge ^{372, 373}. Benzophenone is a bulky group, and its attachment to PNKP inhibitors (mass >500 g/mol) can shift the binding site of the unlabelled inhibitor to areas of PNKP more accommodating to the photoactivatable ligands. Thus, nonspecific labeling is a concern.

Therefore, it is essential to characterize the photolabelled PNKP inhibitors, A95B4C50, A95B4C3 and A12B4C67 by computational and docking analysis and compare it to the parent compounds A12B4C50 and A12B4C3. This will predict where exactly the ketone of the benzophenone is reacting. In addition, performing site directed mutagenesis on the identified target amino acids will further confirm the importance of these locations for the inhibitor to be bound to PNKP.

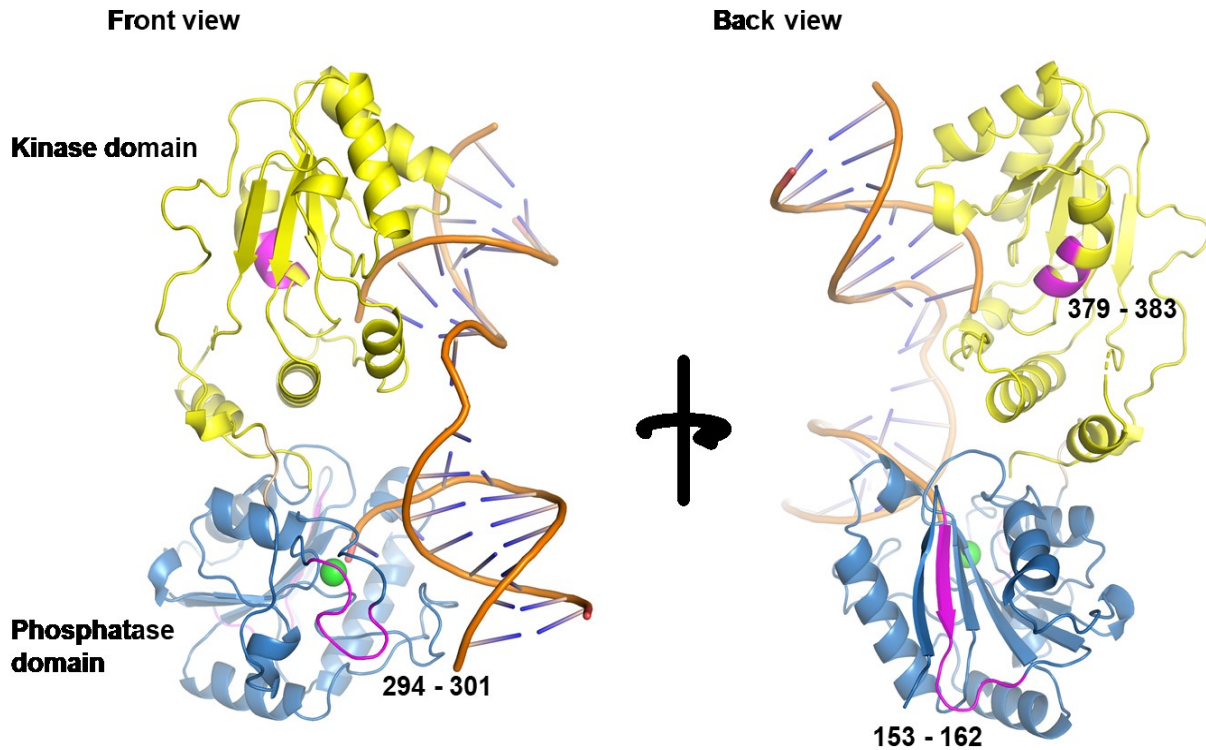


Figure 4.11. The structure of PNKP catalytic domains and the location of the target-binding sites of A95B4C50 (294 - 301), A95B4C3 (153 - 162) and A12B4C67 (379 - 383), highlighted in magenta. **Figure generated by Pymol, courtesy of Dr. Mark Glover (Department of Biochemistry, University of Alberta)**

4.5. Acknowledgments

We thank Bela Reiz, Department of Chemistry (University of Alberta), and Mesfin Fanta, Department of Oncology (University of Alberta) for their technical assistance. We also, thank Dr. Mark Glover, Department of Biochemistry (University of Alberta) for his assistance with PNKP structural analysis. This work was supported by grants funded by the Canadian Institutes of Health Research (MOP 15385) to MW and the Alberta Cancer Foundation Transformative Program Project (26603) to DH, AL and MW.

Chapter 5: Discussion and future work

Overview:

In the last chapter we recap all the data presented in the previous chapters. We also summarize the three main topics discussed in this thesis: (i) the significance of developing small molecule inhibitors of DNA repair enzymes including PNKP, (ii) synthetic lethality and its role in personalized treatment, (iii) targeted delivery of small molecule inhibitors. We also give some suggestions for future experimental procedures required to optimize and complement the work described in this thesis.

5.1. Discussion

5.1.1. The promise of targeted therapy: small molecule inhibitors

The molecular identification and characterization of pathways in different tumors provide us with the knowledge to generate specific therapies that directly target proteins involved in the neoplastic process. Toxic chemotherapeutic agents are being replaced by a new generation of drugs, small molecule inhibitors that recognize specific targets in cancer cells. Although these small molecule inhibitors are challenging to design, they hold the promise of more effective therapies with significantly lower side effects.

Protein phosphorylation regulates many cellular processes, whereas abnormal phosphorylation is a cause or consequence of cancer, such as abnormal proliferation, anti-apoptosis and angiogenesis. Therefore, small molecule inhibitors of protein kinases are proving to be valuable for targeted therapy³⁷⁴. For example, epidermal growth factor receptor (EGFR), a member of ErbB receptor tyrosine kinase family, is activated by mutations, overexpression and autocrine ligand production. Mutations in EGFR can affect cell proliferation, survival, invasion, adhesion and angiogenesis³⁷⁵⁻³⁷⁷. Gefitinib, an EGFR small molecule inhibitor, has been shown to be effective clinically in lung, breast and CRC³⁷⁸⁻³⁸⁰.

Radiation and most conventional chemotherapy cause DNA damage. DNA damage, if not repaired, can lead to cell-cycle arrest or cell death³⁸¹. However, the toxicity of radiation and DNA-damaging drugs is impaired by the effectiveness of several DNA repair pathways. Therefore, DNA repair enzymes have become major targets for novel cancer drugs. For example, NU7441 is a potent and specific inhibitor of DNA-PKcs, which is often overexpressed in non-small cell lung cancer (NSCLC) and is considered to contribute to

radioresistance³⁸². NU7441 has been shown to effectively enhance the effect of ionizing radiation³⁸³. Similarly, inhibitors have been sought for ataxia telangiectasia mutated (ATM), which acts as a sensor of DSBs and activates p53 and other components of the DNA damage response like BRCA1^{384, 385}. Screening of a small molecule inhibitor library led to the identification of KU-55933 as an inhibitor of ATM³⁸⁶. KU-55933 was found to enhance radiosensitivity as well as chemosensitivity to doxorubicin and camptothecin^{386, 387}.

Polynucleotide kinase/phosphatase (PNKP) is a relatively new target in the field of DNA repair inhibition by small molecules. We previously observed that shRNA-mediated depletion of PNKP sensitizes cells to radiation and chemotherapy such as the Top I poison camptothecin¹⁵². The first inhibitor of the DNA 3'-phosphatase activity of PNKP, A12B4C3, was shown to sensitize PC3 cells, AML cells, A549 lung carcinoma and MDA-MB-231 breast cancer cells to γ -radiation, high LET radiation and camptothecin¹⁶⁰⁻¹⁶³. Modifications have been made to A12B4C3 that resulted in the synthesis of A12B4C50 and A83B4C63. These second generation imidopiperidine-based inhibitors have been shown to be more potent than the parent compound (refer to Chapters 2 and 3). Further improvements in potency will be facilitated by unambiguous identification of the binding pocket for this class of inhibitor and rational *in silico* drug design. Through the use of photoactivatable PNKP inhibitors, we observed several binding sites. However, these observations need to be confirmed by site-directed mutagenesis and computational analysis (refer to Chapter 4), and the key site needs to be determined.

Although small molecules are a great advancement in cancer therapy, there remain significant challenges to the treatment of cancer by small molecule inhibitors. 1) In many solid tumors there are many genetic mutations so inhibiting a single pathway may not result in a significant therapeutic effect. 2) The small molecule inhibitors may cause toxic side effects to normal tissues. 3) Factors such as tumor microenvironment heterogeneity and the increased interstitial fluid pressure of tumors make the distribution of therapeutic agents in tumors challenging ³⁸⁸. Suggestions have been proposed to meet challenges such as targeting the tumor microenvironment in combination with therapy regimens using novel delivery approaches ³⁸⁹⁻³⁹¹. Novel approaches employing nanoparticles can aid in delivering higher dosages of anti-cancer drug to tumor tissue and provide longer half-life to establish a more uniform distribution of the drug in tumor tissue ^{392, 393}.

5.1.2. Synthetic lethality, a revolution in the era of personalized treatment

Synthetic lethality can be used to take advantage of cancer cells' dependence on a DNA repair pathway by inhibiting another unrelated pathway, which in turn causes cell death ³⁹⁴. Novel small molecules in pre-clinical and clinical trials combined with individual aberrations in tumors are the focus of cancer treatment today, because this combination should only lead to tumor killing sparing normal cells from toxicity ³⁹⁵. Synthetic lethal screens, by siRNA, the CRISPR/Cas9 system or small molecules, can be used to identify genes or small-molecule compounds to specifically target tumour cells ^{396, 397}. The tumor suppressor PTEN regulates cell migration, survival, growth and DNA damage response ^{398, 399}. PTEN is inactivated in several cancers including 30-50% of CRC cases ⁴⁰⁰⁻⁴⁰². It has been shown that loss of PTEN protein expression is associated with treatment failure by cetuximab, trastuzumab and erlotinib ⁴⁰³⁻⁴⁰⁷. PTEN mutations also affect genome

stability⁴⁰⁸. The C-terminus of PTEN, independent of its phosphatase activity, is important to stabilize the heterochromatin structure⁴⁰⁹. PTEN deficiency causes a defect in DNA DSB repair by HR⁴¹⁰. Therefore, PTEN-deficient tumors should be considered an excellent target for a synthetic lethality approach to treatment. PARP has been shown to be a synthetic lethal partner of PTEN when cells lacking PTEN were found to be sensitive to the PARP inhibitor KU0058948⁴¹⁰.

Similarly, it was confirmed that PNKP inhibition by the small molecule A12B4C3 in PC3 prostate cancer cell line, naturally deficient in PTEN, and HCT116 depleted of PTEN cause synthetic lethality³²⁶. In Chapter 3, we have also demonstrated that the newly found inhibitors A12B4C50 and A83B4C63 exhibit synthetic lethality with PTEN-deficient cells. The mechanism of lethality between PNKP and PTEN has not yet been determined. However, there is a possibility that because PTEN deficiency causes impairment to the HR pathway, the induced inhibition of PNKP by small molecule inhibitors disrupts both SSB repair as well as NHEJ, therefore causing cell death.

Synthetic lethality will provide us with more personalized treatment for each cancer patient. Patients will have their cancer screened to determine major protein or gene deficiencies. With this information it will be possible to match synthetic lethal associations and assign the best personalized treatment. For example, PTEN status in mCRC is a valuable predictive biomarker for monoclonal antibodies targeting epidermal growth factor receptor in chemotherapy as summarized in Figure 5.1⁴¹¹. Similarly, if a CRC patient was found to harbor inactive PTEN the oncologist should design a suitable treatment for the

patient, and potentially this treatment will include the use of PNKP inhibitors as synthetic lethal treatment.

5.1.3. Targeted delivery of small molecule inhibitors

Inhibiting the DNA repair enzyme PNKP by small molecule inhibitors is a challenging problem to normal tissue. We must preserve the DNA repair mechanism in normal tissue, therefore the use of targeted delivery of PNKP small molecule inhibitors is a priority. Nanoparticles, usually smaller than 100 nm, are successfully used in several areas of drug delivery ⁴¹². Small molecule inhibitors can be incorporated into nanoparticles to be targeted to specific tissues, lower the toxicity of the free drug, extend the circulation of drug in the blood, and increase the therapeutic index ⁴¹³. A recent study used a system of self-assembled nanoparticles consisting of conjugates of aptide (high affinity peptide) bound to SN38, the active metabolite of irinotecan, to achieve high drug loading capacity, good solubility and effective tumor growth inhibition in a pre-clinical investigation for SN38 delivery ⁴¹⁴. Similarly, encapsulating the newly found PNKP inhibitors, A12B4C50 and A83B4C63, in PEO-*b*-PCCL and PEO-*b*-PBCL polymeric micelles, respectively, resulted in high efficiency loading, controlled release and effective sensitization of HCT116 cancer cells to radiation and irinotecan. This raises the possibility of co-encapsulation of a PNKP inhibitor with irinotecan or SN38 to improve targeted therapy. In addition, encapsulated PNKP inhibitors can cause synthetic lethality in PTEN-deficient HCT116 cells (Chapter 3).

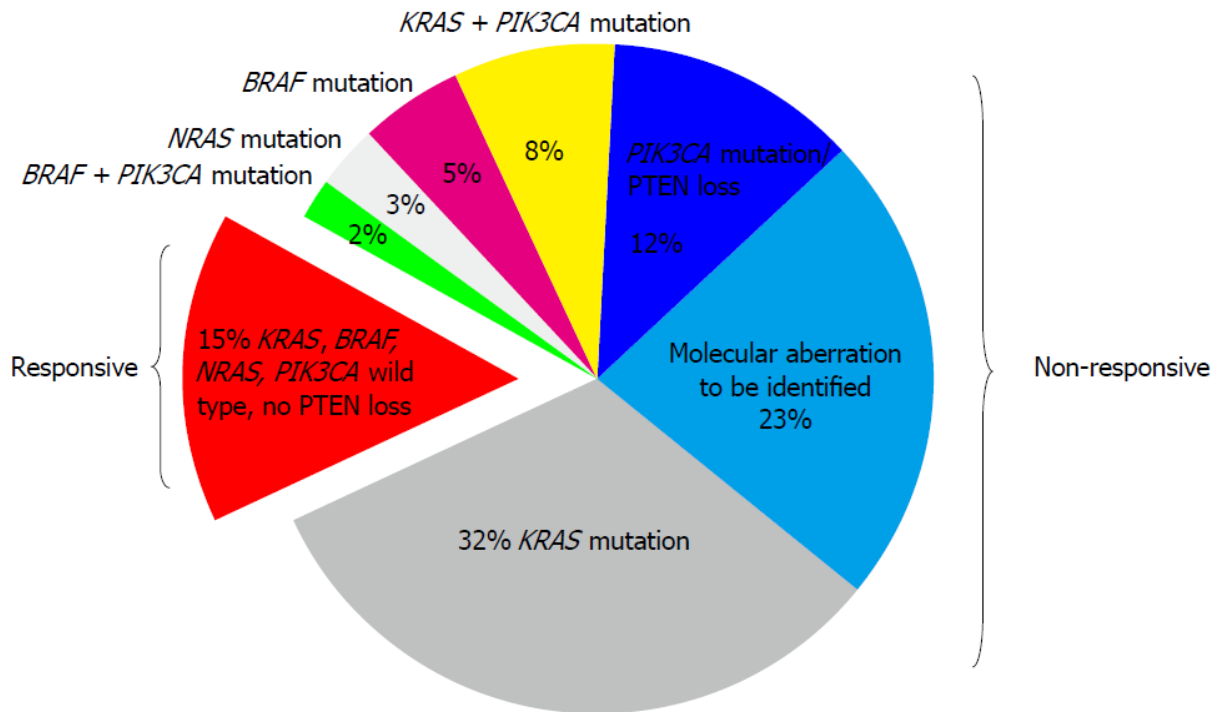


Figure 5.1. PTEN is a predictive biomarker for the outcome of monoclonal antibodies targeting EGFR therapy in mCRC patients. 12% of mCRC patients who did not respond to therapy had loss of expression of PTEN, whereas among the 15% of mCRC patients who were responsive all expressed PTEN. **Luo and Xu. World J Gastroenterol. 2014 Apr 14; 20(14): 3858-3874**

Another issue challenging the efficiency of small molecule inhibitors, is limited penetration into tumor tissues due to the complex tumor microenvironment, therefore, some regions of the tumor may receive lower concentrations of the drug or no drug at all. Targeted nanoparticles with tumor-penetrating peptides enhance the accumulation of poorly penetrating drugs or non-targeted carriers into tumors, as a result the efficacy of the drug is improved ^{415, 416}. Tumor-penetrating peptides enable internalization of drugs to cancer cells by receptor-mediated endocytosis in comparison to the non-targeted drug, which enters passively through the cell membrane ⁴¹⁶. Tumor-internalizing RGD peptide (iRGD) is an example of a tumor-penetrating peptide ⁴¹⁷. A pre-clinical study showed that iRGD-conjugated nanoparticles were able to reduce the level of metastasis of breast cancer in the brain ⁴¹⁸. GE11 peptide has a high affinity for EGFR ⁴¹⁹, and several studies have confirmed the suitability of using GE11 as a targeting moiety to achieve optimum anticancer efficacy ^{420, 421}. We functionalized our nanoparticles with GE11 to target EGFR over-expressing HCT116 cancer cells. Dye-encapsulated GE11-conjugated polymeric micelles showed preferential accumulation in EGFR-overexpressing HCT116 cells compared to minimal internalization observed in SW620 cells, which express no EGFR on their surface. Furthermore, uptake of the functionalized polymeric micelles in HCT116 cells was inhibited by saturation with free GE11 peptide. Together, these data confirm successful internalization of GE11-conjugated polymeric micelles in HCT116 cancer cells through the receptor-mediated process. However, the encapsulation of drugs using nanoparticles also faces limitation such as the nature of the tumor microenvironment, slow release of some nanocarriers that may affect the drug bioavailability, the possibility

of efflux in MDR cells and insufficient stability in the body and fast dissociation of polymeric micelles could lead to premature release of encapsulated drug ⁴²²⁻⁴²⁶.

5.2. Future Work

5.2.1. Optimization of lead compounds, A12B4C50 and A83B4C63

We have demonstrated that A12B4C50 and A83B4C63 are more potent derivatives of A12B4C3. Nevertheless, further modifications to the chemical structure of the second-generation inhibitors are needed to enhance the potency of the inhibitors for *in vivo* applications. A12B4C50 and A83B4C63 have molecular weights equal to 732.8 and 564.6 g/mol, respectively. These masses violate one of the Lipinski's rule of five, i.e. a molecular mass of drug should preferably be less than 500 g/mol ⁴²⁷.

5.2.2. Purification of N12 mixture is needed to identify the active component

We have shown in Chapter 2 that N12 and O7 are the best inhibitors of PNKP phosphatase activity that we obtained from a screening of 200 natural derivative compounds. Unfortunately, these compounds are unstable and decompose easily to other compounds in DMSO (refer to Appendix, Fig. A6). Our next step will be focused on extracting each stable fragment by HPLC. Then, we will test the PNKP phosphatase inhibition activity of each collected fragment. If a hit is found among the fragments, further characterization of the compound by NMR and mass spectrometry will be required to identify the structure of the fragment.

5.2.3. Monitoring the interaction of small molecule inhibitors with PNKP inside living cells

PNKP inhibitors do not further sensitize HCT116-PNKP KO cells to radiation and irinotecan, indicating that in this context these inhibitors are probably specific to PNKP-dependent repair (refer to Chapter 3). However, testing PNKP-inhibitor interaction using purified PNKP does not confirm the binding of the inhibitor to PNKP in living cells. Therefore, it is essential to assess the specificity and efficacy of these inhibitors inside cells. There are several approaches we suggest applying to track the interactions of PNKP inhibitors inside cancer cells. One approach is Fluorescence Resonance Energy Transfer coupled with Fluorescence Lifetime Imaging Microscopy (FRET-FLIM). In this approach a fluorophore is attached to the inhibitor and PNKP is fused with a fluorescent protein. Once the inhibitor is close to PNKP and upon excitation, the donor fluorophore will transfer the energy to the acceptor fluorophore ⁴²⁸. Figure 5.2A shows a schematic illustration of the proposed approach ⁴²⁸.

Another approach is covalently attaching a photoactivatable linker (e.g. azide group) and a biotin substituent to the inhibitors (Figure 5.2B). The modified inhibitor will then bind to the target inside the cell and become covalently attached upon UV activation. Following lysis of the cells, protein-inhibitor complex will be isolated by streptavidin affinity chromatography and subjected to tryptic digestion and mass spectrometry analysis to identify if the bound protein is PNKP and potentially other proteins ⁴²⁸. A similar approach *in vitro* would also allow us to identify the binding site of the inhibitor to the protein under conditions requiring lower concentrations of inhibitor (unlike the large

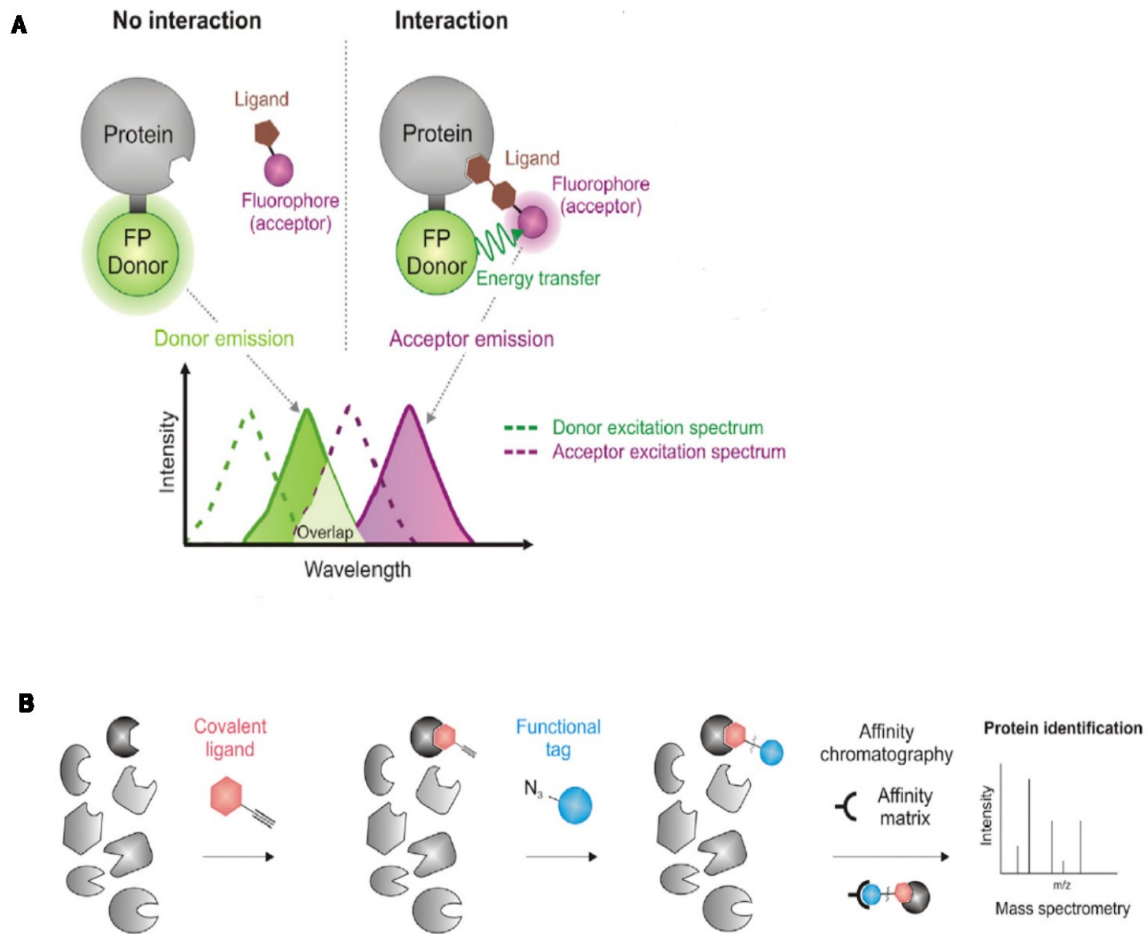


Figure 5.2. Schematic diagram of approaches suggested to monitor PNKP-inhibitor interactions inside living cells. (A) scheme represents FRET-FLIM approach. (B) scheme represents the affinity-based approach for covalently binding inhibitors. Schürmann *et al.* Cell Chem Biol. 2016;23(4):435-41. Re-used with permission from Cell Chemical Biology

excess used in Chapter 4) because it would enable enrichment of the modified protein for the analysis.

5.2.4. Identification of the mechanism responsible of the synthetic lethality partnership between PTEN and PNKP

In Chapter 3, we have shown that a synthetic lethal partnership exists between PTEN and encapsulated-PNKP phosphatase inhibitors. However, the mechanism responsible for this lethality is yet to be determined. A recent study showed the potential of synthetic lethality partnership between PARP1 and PTEN through inhibition of both SSBR and DSBR via HR pathways, respectively ⁴²⁹. Moreover, it was found that PTEN influences the HR pathway by regulating the transcription of Rad51 ¹⁷⁹, although this observation has been challenged ⁴³⁰. Therefore, we propose that the mechanism of synthetic lethality between PNKP and PTEN is also due to the disruption of SSBR, NHEJ and alt-NHEJ (due to PNKP depletion) and HR (due to loss of PTEN). However, Mereniuk *et al.* observed that ectopically expressing Rad51 in the PC3 cell line, which naturally lacks PTEN and Rad51, did not eliminate synthetic lethality when challenged with a PNKP inhibitor, while ectopically expressing wild type PTEN did prevent synthetic lethality ³²⁶. One possibility is that PTEN may also regulate expression of other HR proteins, so simply replacing Rad51 in PC3 cells may not be sufficient to restore HR. We therefore suggest further study of HR in PC3 cells is required. This would entail western blotting for expression of other HR proteins and using a combination of γ -H2AX assay and a homologous recombination assay kit to monitor DSBR in general and HR in particular. We also propose the use of a Rad51 inhibitor, i.e. RI-1, in PTEN-proficient cells in parallel

with a PNKP inhibitor to confirm or eliminate the idea that synthetic lethality is due to disruption of Rad51-mediated HR and SSBR and NHEJ.

5.2.5. Identification of binding sites of inhibitors to PNKP

In Chapter 4, we identified three distinct binding sites of PNKP inhibitors, A95B4C3, A95B4C50 and A12B4C67. Ideally, crystal structures of the PNKP-inhibitor complex would provide the clearest information regarding the binding site of the inhibitors and how they disrupt PNKP structure. Unfortunately, to date no such structures have been obtained (Dr. Mark Glover, personal communication, Department of Biochemistry, University of Alberta).

Another possible way to confirm our photo-crosslinking observations is to apply site-directed mutagenesis to the area of PNKP indicated by photo-crosslinking experiments. The mutations should be designed to prevent the binding of the inhibitor to PNKP (e.g. by altering critical hydrogen bonding or introducing steric factors), but still retain the 3'-phosphatase activity of PNKP. Alternatively, mutations could be designed to mimic the localized disruption of the PNKP structure induced by the inhibitors. In this case the mutated PNKP would lose phosphatase activity. Computational docking analysis of both parent PNKP phosphatase inhibitors, A12B4C3 and A12B4C50, and the corresponding photoactivatable PNKP inhibitors, A12B4C67, A95B4C3 and A95B4C50, will be required to characterize potential interactions of the inhibitors at the identified binding sites. We must confirm that both class of inhibitors are binding in the same region, and that the attachment of the benzophenone group does not alter the chemistry between PNKP and the inhibitors.

5.2.6. Pre-clinical study of PNKP 3'-phosphatase inhibitors: preliminary results and future work

The use of PNKP 3'-phosphatase inhibitors as a combined therapeutic or a monotherapeutic in HCT116 cancer cell lines has shown that they can be potentially effective drugs in the treatment of cancer. Therefore, we need to study the efficacy of the newly identified PNKP 3'-phosphatase inhibitors in xenograft tumor models.

However, before xenografts studies are initiated, the maximum tolerable dose of PNKP 3'-phosphatase inhibitor must be determined. For this, CD-1 mice received doses 2.5, 5, 10, 15, 20, and 50 mg/kg of A83B4C63 free or encapsulated in PEO-*b*-PBCL on day 0, 3, 6 and 9. We monitored body weight, hematology and biochemistry of blood. There was no significant effect on these parameters due to drug exposure, even at the highest dose (data not shown).

We then tested the efficacy of A83B4C63 in inducing synthetic lethality in HCT116-PTEN KO subcutaneous tumors grown in immunocompromised NIH-III mice. Once the tumors had been established from wild type and HCT116-PTEN KO cells, the mice were subjected to 10 mg/kg of free A83B4C63 or PEO-*b*-PBCL-A83B4C63 given IV on day 0, 3 and 6. Our observations (Fig. 5.3) indicated significantly slower growth of the HCT116-PTEN KO tumors in comparison to the wild type HCT116 tumors, which essentially did not respond to treatment with the PNKP inhibitor. Our results also confirm the suitability of polymeric micelles as nano-carriers of A83B4C63 compared to free drug, since it is worth noting that the normalized data in which tumor growth is divided by the original tumor volume appears to indicate no response with free A83B4C63. The general health

of the mice was confirmed by monitoring mice body weight (Fig. 5.4). For future work, optimization of the dose and time of injections is needed to obtain better results. In addition, the pharmacokinetic and pharmacodynamic properties of A83B4C63 need to be determined. It is important to determine the distribution of the drug in other tissues and its rate of clearance from the body. The use of nanoparticles could reduce the non-specific distribution and fast clearance of the free drug. Furthermore, we plan to test the efficacy of PNKP inhibitors as combined therapy with anticancer agents, such as ionizing radiation and irinotecan, to enhance the outcome of these treatments in colorectal cancer and reduce unfavorable effects.

The subcutaneous model provides us with several advantages, including the ease of establishing the tumors and monitoring tumor growth. However, this model lacks the complexity of the colorectal tumor environment. Therefore, as a confirmation of our data with the optimized subcutaneous model, we will need to test the efficacy of A83B4C63 using an orthotopic colorectal tumor model.

Another area that needs to be investigated, is the active targeting of nano-carriers of PNKP inhibitors specifically to colorectal cancer. As mentioned earlier, the size of the polymeric micelles, <100 nm, will direct the nanoparticle to the site of tumor passively. However, the tumor microenvironment is leaky which leads to clearance of the particles from the tumor site. Therefore, we will test a targeting ligand on the surface of the nanoparticles to improve drug accumulation to tumor tissue. We propose to use GE11 peptide to target EGFR, which is overexpressed in colorectal cancer. We will measure

the decrease in tumor volume and the drug concentration from tumor samples to confirm our theory.

5.3. Significance

The focus of this thesis is to overcome resistance of cancer cells to DNA-damaging therapies such as radiation and irinotecan. PNKP 3'-phosphatase inhibitors represent an excellent potential supplement to both therapeutic approaches. Importantly, one of our aims is to advance PNKP 3'-phosphatase inhibitor into a single agent anti-cancer drug. This is possible due to the concept of synthetic lethality which takes advantage of weaknesses that arise in specific types of cancers. Using this approach will help assign personalized treatment regimens specific to the patients' cancer. Another approach we explored in this thesis, and that will help us target DNA repair inhibition specifically to the tumor, is the use of nanoparticles to solubilize and deliver PNKP 3'-phosphatase inhibitors. The use of functionalized nanocarriers to deliver inhibitors to tumors will spare normal tissue from undesirable toxicity and increase the inhibitor's efficacy.

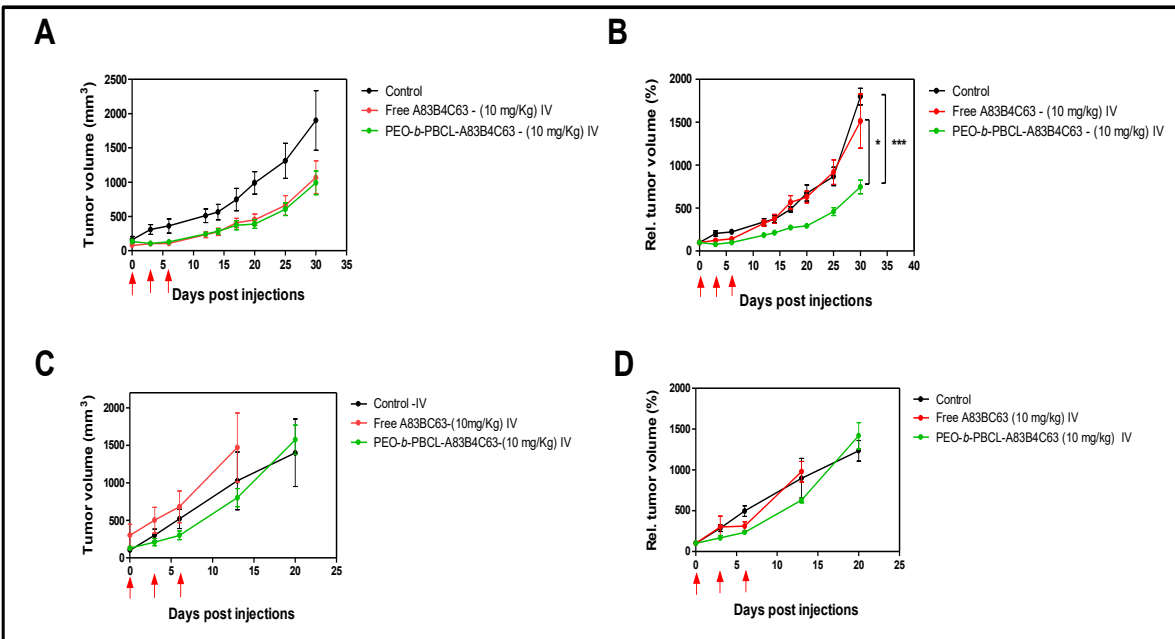


Figure 5.3. Tumor volume curves. (A) The curve shows that the rate of growth of HCT116-PTEN KO grafted tumors in NIH-III mice was significantly reduced when injected with 10 mg/kg of PEO-*b*-PBCL-A83B4C63 and free A83B4C63 compared to that of control groups. The equation used to measure tumor volume is $V = (L \times W \times W)/2$. Days post injection corresponds to the day after the initial injection. (B) Represents the normalized data of (A) obtained by dividing the measured tumor volume by the initial tumor volume and multiplying by 100. (C) The curve showed that the tumor growth of HCT116-PTEN wt grafted in NIH-III mice was not hindered due to injection of 10 mg/kg of either free or PEO-*b*-PBCL-A83B4C63 intravenously. (D) Represents the normalized data of (C). Each point represents mean \pm SD ($n = 5$). Two-tailed unpaired Student's *t*-test was used for statistical comparison, employing GraphPad Prism5 software (La Jolla, CA, USA). Marked points are statistically significant at (* $P \leq 0.05$) and (***) $P \leq 0.001$). **This experiment was carried out in collaboration with Sams Sadat (Faculty of Pharmacy and Pharmaceutical Sciences, University of Alberta)**

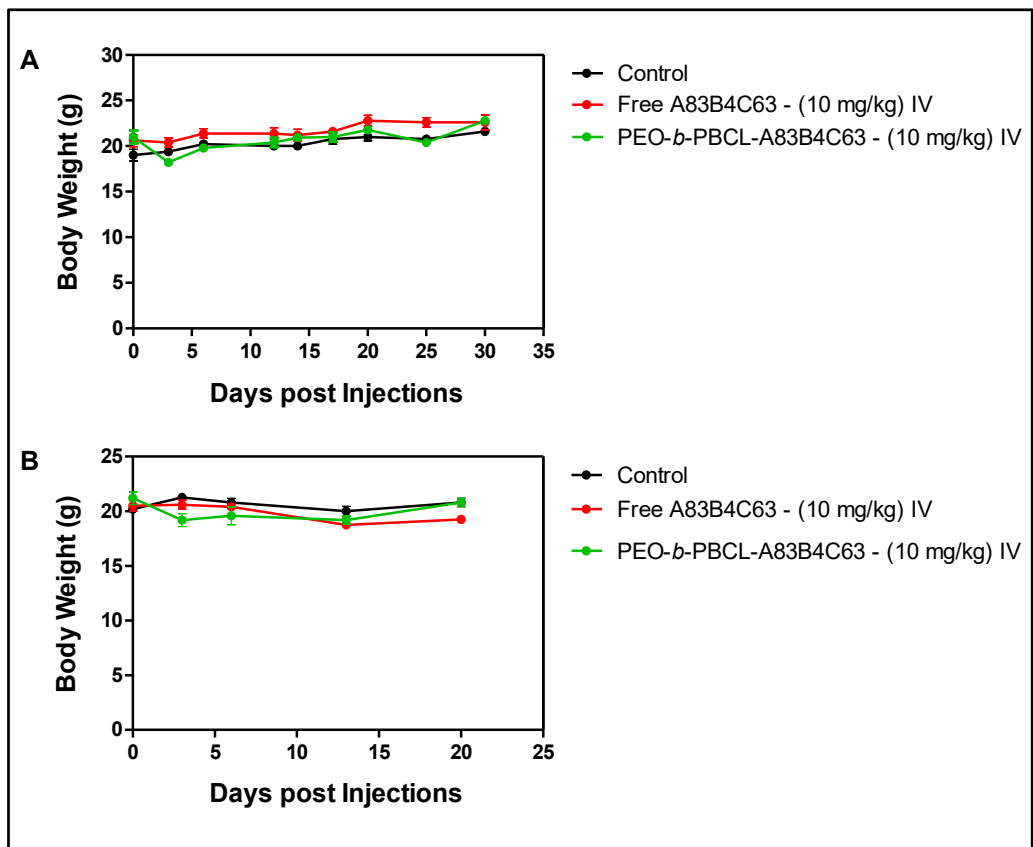


Figure 5.4. Mean body weight–time profile of NIH-III nude mice. The weight of mice was monitored after 3-day consecutive intravenous injection of 5% dextrose, free A83B4C63 and PEO-*b*-PBCL-A83B4C63 at 10 mg/kg in **(A)** NIH-III mice harboring HCT116-PTEN KO cells and **(B)** NIH-III mice harboring HCT116-PTEN wt cells ($n = 5$). This experiment was carried out in collaboration with Sams Sadat (Faculty of Pharmacy and Pharmaceutical Sciences, University of Alberta)

References

- (1) Vindigni, A. and Gonzalo, S. The two faces of DNA repair: disease and therapy. *Mo. Med.* 2013, *110*, 314-319.
- (2) Andres, S.N.; Schellenberg, M.J.; Wallace, B.D.; Tumbale, P.; Williams, R.S. Recognition and repair of chemically heterogeneous structures at DNA ends. *Environ. Mol. Mutagen.* 2015, *56*, 1-21.
- (3) Shire, Z.; Jiang, B.; Abdou, I.; Weinfeld, M. Processing strand break termini in the DNA single-strand break repair pathway, In *The Base excision repair pathway: Molecular Mechanisms and Role in Disease Development and Therapeutic Design*, Wilson III, D.M., Ed.; World Scientific: London, 2017; pp. 281-321.
- (4) Charames, G.S. and Bapat, B. Genomic instability and cancer. *Curr. Mol. Med.* 2003, *3*, 589-596.
- (5) Wilson, D.M.,3rd; Sofinowski, T.M.; McNeill, D.R. Repair mechanisms for oxidative DNA damage. *Front. Biosci.* 2003, *8*, 963.
- (6) Kruman, I.I. and Schwartz, E.I. DNA damage response and neuroprotection. *Front. Biosci.* 2008, *13*, 2504-2515.
- (7) Takagi, M. Erratum to: DNA damage response and hematological malignancy. *Int. J. Hematol.* 2017, *106*, 450-453.

- (8) Ogawa, L.M. and Baserga, S.J. Crosstalk between the nucleolus and the DNA damage response. *Mol. Biosyst* 2017, 13, 443-455.
- (9) Abbotts, R. and Wilson, D.M., 3rd Coordination of DNA single strand break repair. *Free Radic. Biol. Med.* 2017, 107, 228-244.
- (10) Caldecott, K.W. DNA single-strand break repair. *Exp. Cell Res.* 2014, 329, 2-8.
- (11) Wang, J.C. Cellular roles of DNA topoisomerases: a molecular perspective. *Nat. Rev. Mol. Cell Biol.* 2002, 3, 430-440.
- (12) Pommier, Y.; Redon, C.; Rao, V.A.; Seiler, J.A.; Sordet, O.; Takemura, H.; Antony, S.; Meng, L.; Liao, Z.; Kohlhagen, G.; Zhang, H.; Kohn, K.W. Repair of and checkpoint response to topoisomerase I-mediated DNA damage. *Mutat. Res.* 2003, 532, 173-203.
- (13) Das, A.; Wiederhold, L.; Leppard, J.B.; Kedar, P.; Prasad, R.; Wang, H.; Boldogh, I.; Karimi-Busheri, F.; Weinfeld, M.; Tomkinson, A.E.; Wilson, S.H.; Mitra, S.; Hazra, T.K. NEIL2-initiated, APE-independent repair of oxidized bases in DNA: Evidence for a repair complex in human cells. *DNA Repair (Amst)* 2006, 5, 1439-1448.
- (14) Xu, Y. and Her, C. Inhibition of Topoisomerase (DNA) I (TOP1): DNA Damage Repair and Anticancer Therapy. 2015, 5, 1652-1670.
- (15) Weinfeld, M.; Mani, R.S.; Abdou, I.; Aceytuno, R.D.; Glover, J.N. Tidying up loose ends: the role of polynucleotide kinase/phosphatase in DNA strand break repair. *Trends Biochem. Sci.* 2011, 36, 262-271.

- (16) Caldecott, K.W. Single-strand break repair and genetic disease. *Nat. Rev. Genet.* 2008, 9, 619-631.
- (17) Thompson, L.H. and West, M.G. XRCC1 keeps DNA from getting stranded. *Mutat. Res.* 2000, 459, 1-18.
- (18) Caldecott, K.W. Protein ADP-ribosylation and the cellular response to DNA strand breaks. *DNA Repair (Amst)* 2014, 19, 108-113.
- (19) Hanzlikova, H.; Gittens, W.; Krejcikova, K.; Zeng, Z.; Caldecott, K.W. Overlapping roles for PARP1 and PARP2 in the recruitment of endogenous XRCC1 and PNKP into oxidized chromatin. *Nucleic Acids Res.* 2017, 45, 2546-2557.
- (20) Mani, R.S.; Karimi-Busheri, F.; Fanta, M.; Caldecott, K.W.; Cass, C.E.; Weinfeld, M. Biophysical characterization of human XRCC1 and its binding to damaged and undamaged DNA. 2004, 43, 16505-16514.
- (21) Parsons, J.L.; Dianova, I.I.; Boswell, E.; Weinfeld, M.; Dianov, G.L. End-damage-specific proteins facilitate recruitment or stability of X-ray cross-complementing protein 1 at the sites of DNA single-strand break repair. *FEBS J.* 2005, 272, 5753-5763.
- (22) Lu, M.; Mani, R.S.; Karimi-Busheri, F.; Fanta, M.; Wang, H.; Litchfeld, D.W.; Weinfeld, M. Independent mechanisms of stimulation of polynucleotide kinase/phosphatase by phosphorylated and non-phosphorylated XRCC1. *Nucleic Acids Res.* 2010, 38, 510-521.
- (23) Strom, C.E.; Mortusewicz, O.; Finch, D.; Parsons, J.L.; Lagerqvist, A.; Johansson, F.; Schultz, N.; Erixon, K.; Dianov, G.L.; Helleday, T. CK2 phosphorylation of XRCC1

facilitates dissociation from DNA and single-strand break formation during base excision repair. *DNA Repair (Amst)* 2011, 10, 961-969.

(24) Whitehouse, C.J.; Taylor, R.M.; Thistlethwaite, A.; Zhang, H.; Karimi-Busheri, F.; Lasko, D.D.; Weinfeld, M.; Caldecott, K.W. XRCC1 stimulates human polynucleotide kinase activity at damaged DNA termini and accelerates DNA single-strand break repair. 2001, 104, 107-117.

(25) Mani, R.S.; Fanta, M.; Karimi-Busheri, F.; Silver, E.; Virgen, C.A.; Caldecott, K.W.; Cass, C.E.; Weinfeld, M. XRCC1 stimulates polynucleotide kinase by enhancing its damage discrimination and displacement from DNA repair intermediates. *J. Biol. Chem.* 2007, 282, 28004-28013.

(26) Kim, Y.J. and Wilson, D.M., 3rd Overview of base excision repair biochemistry. *Curr. Mol. Pharmacol.* 2012, 5, 3-13.

(27) Caldecott, K.W. Mammalian single-strand break repair: mechanisms and links with chromatin. *DNA Repair (Amst)* 2007, 6, 443-453.

(28) Tomkinson, A.E.; Howes, T.R.; Wiest, N.E. DNA ligases as therapeutic targets. *Transl. Cancer. Res.* 2013, 2, 1219.

(29) Tomkinson, A.E. and Sallmyr, A. Structure and function of the DNA ligases encoded by the mammalian LIG3 gene. 2013, 531, 150-157.

- (30) Simsek, D.; Furda, A.; Gao, Y.; Artus, J.; Brunet, E.; Hadjantonakis, A.K.; Van Houten, B.; Shuman, S.; McKinnon, P.J.; Jasin, M. Crucial role for DNA ligase III in mitochondria but not in Xrcc1-dependent repair. *2011*, *471*, 245-248.
- (31) Liu, Y. and Wilson, S.H. DNA base excision repair: a mechanism of trinucleotide repeat expansion. *Trends Biochem. Sci.* 2012, *37*, 162-172.
- (32) Sykora, P.; Wilson, D.M.,3rd; Bohr, V.A. Base excision repair in the mammalian brain: implication for age related neurodegeneration. *Mech. Ageing Dev.* 2013, *134*, 440-448.
- (33) Hegde, M.L.; Hegde, P.M.; Bellot, L.J.; Mandal, S.M.; Hazra, T.K.; Li, G.M.; Boldogh, I.; Tomkinson, A.E.; Mitra, S. Prereplicative repair of oxidized bases in the human genome is mediated by NEIL1 DNA glycosylase together with replication proteins. *Proc. Natl. Acad. Sci. U. S. A.* 2013, *110*, 3090.
- (34) Sampath, H. Oxidative DNA damage in disease--insights gained from base excision repair glycosylase-deficient mouse models. *Environ. Mol. Mutagen.* 2014, *55*, 689-703.
- (35) Robertson, A.B.; Klungland, A.; Rognes, T.; Leiros, I. DNA repair in mammalian cells: Base excision repair: the long and short of it. *Cell Mol. Life Sci.* 2009, *66*, 981-993.
- (36) Wiederhold, L.; Leppard, J.B.; Kedar, P.; Karimi-Busheri, F.; Rasouli-Nia, A.; Weinfeld, M.; Tomkinson, A.E.; Izumi, T.; Prasad, R.; Wilson, S.H.; Mitra, S.; Hazra, T.K. AP endonuclease-independent DNA base excision repair in human cells. *Mol. Cell* 2004, *15*, 209-220.

- (37) Rosenquist, T.A.; Zaika, E.; Fernandes, A.S.; Zharkov, D.O.; Miller, H.; Grollman, A.P. The novel DNA glycosylase, NEIL1, protects mammalian cells from radiation-mediated cell death. *DNA Repair (Amst)* 2003, 2, 581-591.
- (38) Krokeide, S.Z.; Laerdahl, J.K.; Salah, M.; Luna, L.; Cederkvist, F.H.; Fleming, A.M.; Burrows, C.J.; Dalhus, B.; Bjoras, M. Human NEIL3 is mainly a monofunctional DNA glycosylase removing spiroimindiohydantoin and guanidinohydantoin. *DNA Repair (Amst)* 2013, 12, 1159-1164.
- (39) Noren Hooten, N.; Fitzpatrick, M.; Kompaniez, K.; Jacob, K.D.; Moore, B.R.; Nagle, J.; Barnes, J.; Lohani, A.; Evans, M.K. Coordination of DNA repair by NEIL1 and PARP-1: a possible link to aging. *Aging (Albany NY)* 2012, 4, 674-685.
- (40) Wallace, S.S. DNA glycosylases search for and remove oxidized DNA bases. *Environ. Mol. Mutagen.* 2013, 54, 691-704.
- (41) Mitra, J.; Guerrero, E.N.; Hegde, P.M.; Wang, H.; Boldogh, I.; Rao, K.S.; Mitra, S.; Hegde, M.L. New perspectives on oxidized genome damage and repair inhibition by pro-oxidant metals in neurological diseases. 2014, 4, 678-703.
- (42) Bush, N.G.; Evans-Roberts, K.; Maxwell, A. DNA Topoisomerases. 2015, 6, 2014.
- (43) Lisby, M.; Olesen, J.R.; Skouboe, C.; Krogh, B.O.; Straub, T.; Boege, F.; Velmurugan, S.; Martensen, P.M.; Andersen, A.H.; Jayaram, M.; Westergaard, O.; Knudsen, B.R. Residues within the N-terminal domain of human topoisomerase I play a direct role in relaxation. *J. Biol. Chem.* 2001, 276, 20220-20227.

- (44) Ashour, M.E.; Atteya, R.; El-Khamisy, S.F. Topoisomerase-mediated chromosomal break repair: an emerging player in many games. *Nat. Rev. Cancer*. 2015, *15*, 137-151.
- (45) Pourquier, P.; Ueng, L.M.; Kohlhagen, G.; Mazumder, A.; Gupta, M.; Kohn, K.W.; Pommier, Y. Effects of uracil incorporation, DNA mismatches, and abasic sites on cleavage and religation activities of mammalian topoisomerase I. *J. Biol. Chem.* 1997, *272*, 7792-7796.
- (46) Pourquier, P.; Pilon, A.A.; Kohlhagen, G.; Mazumder, A.; Sharma, A.; Pommier, Y. Trapping of mammalian topoisomerase I and recombinations induced by damaged DNA containing nicks or gaps. Importance of DNA end phosphorylation and camptothecin effects. *J. Biol. Chem.* 1997, *272*, 26441-26447.
- (47) Pommier, Y.; Pourquier, P.; Fan, Y.; Strumberg, D. Mechanism of action of eukaryotic DNA topoisomerase I and drugs targeted to the enzyme. *Biochim. Biophys. Acta* 1998, *1400*, 83-105.
- (48) Hertzberg, R.P.; Caranfa, M.J.; Hecht, S.M. On the mechanism of topoisomerase I inhibition by camptothecin: evidence for binding to an enzyme-DNA complex. 1989, *28*, 4629-4638.
- (49) Porter, S.E. and Champoux, J.J. The basis for camptothecin enhancement of DNA breakage by eukaryotic topoisomerase I. *Nucleic Acids Res.* 1989, *17*, 8521-8532.
- (50) Froelich-Ammon, S.J. and Osheroff, N. Topoisomerase poisons: harnessing the dark side of enzyme mechanism. *J. Biol. Chem.* 1995, *270*, 21429-21432.

- (51) Pommier, Y. Topoisomerase I inhibitors: camptothecins and beyond. *Nat. Rev. Cancer*. 2006, **6**, 789-802.
- (52) Sonderstrup, I.M.; Nygard, S.B.; Poulsen, T.S.; Linnemann, D.; Stenvang, J.; Nielsen, H.J.; Bartek, J.; Brunner, N.; Norgaard, P.; Riis, L. Topoisomerase-1 and -2A gene copy numbers are elevated in mismatch repair-proficient colorectal cancers. *Mol. Oncol*. 2015, **9**, 1207-1217.
- (53) Vaz, B.; Popovic, M.; Newman, J.A.; Fielden, J.; Aitkenhead, H.; Halder, S.; Singh, A.N.; Vendrell, I.; Fischer, R.; Torrecilla, I.; Drobnitzky, N.; Freire, R.; Amor, D.J.; Lockhart, P.J.; Kessler, B.M.; McKenna, G.W.; Gileadi, O.; Ramadan, K. Metalloprotease SPRTN/DVC1 Orchestrates Replication-Coupled DNA-Protein Crosslink Repair. *Mol. Cell* 2016, **64**, 704-719.
- (54) Maskey, R.S.; Flatten, K.S.; Sieben, C.J.; Peterson, K.L.; Baker, D.J.; Nam, H.J.; Kim, M.S.; Smyrk, T.C.; Kojima, Y.; Machida, Y.; Santiago, A.; van Deursen, J.M.; Kaufmann, S.H.; Machida, Y.J. Spartan deficiency causes accumulation of Topoisomerase 1 cleavage complexes and tumorigenesis. *Nucleic Acids Res*. 2017, **45**, 4564-4576.
- (55) Barthelmes, H.U.; Habermeyer, M.; Christensen, M.O.; Mielke, C.; Interthal, H.; Pouliot, J.J.; Boege, F.; Marko, D. TDP1 overexpression in human cells counteracts DNA damage mediated by topoisomerases I and II. *J. Biol. Chem*. 2004, **279**, 55618-55625.
- (56) Allinson, S.L. DNA end-processing enzyme polynucleotide kinase as a potential target in the treatment of cancer. *Future Oncol*. 2010, **6**, 1031-1042.

- (57) Comeaux, E.Q. and van Waardenburg, R.C. Tyrosyl-DNA phosphodiesterase I resolves both naturally and chemically induced DNA adducts and its potential as a therapeutic target. *Drug Metab. Rev.* 2014, 46, 494-507.
- (58) Mehta, A. and Haber, J.E. Sources of DNA double-strand breaks and models of recombinational DNA repair. *Cold Spring Harb Perspect. Biol.* 2014, 6, a016428.
- (59) Lieber, M.R. The mechanism of double-strand DNA break repair by the nonhomologous DNA end-joining pathway. *Annu. Rev. Biochem.* 2010, 79, 181-211.
- (60) Hartlerode, A.J. and Scully, R. Mechanisms of double-strand break repair in somatic mammalian cells. *Biochem. J.* 2009, 423, 157-168.
- (61) Featherstone, C. and Jackson, S.P. DNA double-strand break repair. *Curr. Biol.* 1999, 9, 759.
- (62) Saha, J.; Wang, S.Y.; Davis, A.J. Examining DNA Double-Strand Break Repair in a Cell Cycle-Dependent Manner. *Methods Enzymol.* 2017, 591, 97-118.
- (63) Shibata, A. Regulation of repair pathway choice at two-ended DNA double-strand breaks. *Mutat. Res.* 2017, 803-805, 51-55.
- (64) Karimi-Busheri, F.; Rasouli-Nia, A.; Allalunis-Turner, J.; Weinfeld, M. Human polynucleotide kinase participates in repair of DNA double-strand breaks by nonhomologous end joining but not homologous recombination. *Cancer Res.* 2007, 67, 6619-6625.

- (65) Williams, G.J.; Hammel, M.; Radhakrishnan, S.K.; Ramsden, D.; Lees-Miller, S.P.; Tainer, J.A. Structural insights into NHEJ: building up an integrated picture of the dynamic DSB repair super complex, one component and interaction at a time. *DNA Repair (Amst)* 2014, 17, 110-120.
- (66) Hammel, M.; Yu, Y.; Radhakrishnan, S.K.; Chokshi, C.; Tsai, M.S.; Matsumoto, Y.; Kuzdovich, M.; Remesh, S.G.; Fang, S.; Tomkinson, A.E.; Lees-Miller, S.P.; Tainer, J.A. An Intrinsically Disordered APLF Links Ku, DNA-PKcs, and XRCC4-DNA Ligase IV in an Extended Flexible Non-homologous End Joining Complex. *J. Biol. Chem.* 2016, 291, 26987-27006.
- (67) Rulten, S.L. and Grundy, G.J. Non-homologous end joining: Common interaction sites and exchange of multiple factors in the DNA repair process. *Bioessays* 2017, 39, 10.1002/bies.201600209. Epub 2017 Jan 30.
- (68) Chappell, C.; Hanakahi, L.A.; Karimi-Busheri, F.; Weinfeld, M.; West, S.C. Involvement of human polynucleotide kinase in double-strand break repair by non-homologous end joining. *EMBO J.* 2002, 21, 2827-2832.
- (69) Koch, C.A.; Agyei, R.; Galicia, S.; Metalnikov, P.; O'Donnell, P.; Starostine, A.; Weinfeld, M.; Durocher, D. Xrcc4 physically links DNA end processing by polynucleotide kinase to DNA ligation by DNA ligase IV. *EMBO J.* 2004, 23, 3874-3885.
- (70) Bennardo, N.; Cheng, A.; Huang, N.; Stark, J.M. Alternative-NHEJ is a mechanistically distinct pathway of mammalian chromosome break repair. *PLoS Genet.* 2008, 4, e1000110.

(71) Pannunzio, N.R.; Li, S.; Watanabe, G.; Lieber, M.R. Non-homologous end joining often uses microhomology: implications for alternative end joining. *DNA Repair (Amst)* 2014, 17, 74-80.

(72) Iliakis, G.; Murmann, T.; Soni, A. Alternative end-joining repair pathways are the ultimate backup for abrogated classical non-homologous end-joining and homologous recombination repair: Implications for the formation of chromosome translocations. *Mutat. Res. Genet. Toxicol. Environ. Mutagen.* 2015, 793, 166-175.

(73) Rassool, F.V. and Tomkinson, A.E. Targeting abnormal DNA double strand break repair in cancer. *Cell Mol. Life Sci.* 2010, 67, 3699-3710.

(74) Audebert, M.; Salles, B.; Calsou, P. Involvement of poly(ADP-ribose) polymerase-1 and XRCC1/DNA ligase III in an alternative route for DNA double-strand breaks rejoining. *J. Biol. Chem.* 2004, 279, 55117-55126.

(75) Deriano, L. and Roth, D.B. Modernizing the nonhomologous end-joining repertoire: alternative and classical NHEJ share the stage. *Annu. Rev. Genet.* 2013, 47, 433-455.

(76) Soni, A.; Siemann, M.; Grabos, M.; Murmann, T.; Pantelias, G.E.; Iliakis, G. Requirement for Parp-1 and DNA ligases 1 or 3 but not of Xrcc1 in chromosomal translocation formation by backup end joining. *Nucleic Acids Res.* 2014, 42, 6380-6392.

(77) Simsek, D.; Brunet, E.; Wong, S.Y.; Katyal, S.; Gao, Y.; McKinnon, P.J.; Lou, J.; Zhang, L.; Li, J.; Rebar, E.J.; Gregory, P.D.; Holmes, M.C.; Jasin, M. DNA ligase III

promotes alternative nonhomologous end-joining during chromosomal translocation formation. *PLoS Genet.* 2011, 7, e1002080.

(78) Black, S.J.; Kashkina, E.; Kent, T.; Pomerantz, R.T. DNA Polymerase θ : A Unique Multifunctional End-Joining Machine. 2016, 7, 67.

(79) Hoang TM, Kent T, Pomerantz RT. Modification of 3' Terminal Ends of DNA and RNA Using DNA Polymerase θ Terminal Transferase Activity. 2017, 7,

(80) Audebert, M.; Salles, B.; Weinfeld, M.; Calsou, P. Involvement of polynucleotide kinase in a poly(ADP-ribose) polymerase-1-dependent DNA double-strand breaks rejoining pathway. *J. Mol. Biol.* 2006, 356, 257-265.

(81) Zolner, A.E.; Abdou, I.; Ye, R.; Mani, R.S.; Fanta, M.; Yu, Y.; Douglas, P.; Tahbaz, N.; Fang, S.; Dobbs, T.; Wang, C.; Morrice, N.; Hendzel, M.J.; Weinfeld, M.; Lees-Miller, S.P. Phosphorylation of polynucleotide kinase/ phosphatase by DNA-dependent protein kinase and ataxia-telangiectasia mutated regulates its association with sites of DNA damage. *Nucleic Acids Res.* 2011, 39, 9224-9237.

(82) Karimi-Busheri, F.; Rasouli-Nia, A.; Allalunis-Turner, J.; Weinfeld, M. Human polynucleotide kinase participates in repair of DNA double-strand breaks by nonhomologous end joining but not homologous recombination. *Cancer Res.* 2007, 67, 6619-6625.

- (83) Karimi-Busheri, F. and Weinfeld, M. Purification and substrate specificity of polydeoxyribonucleotide kinases isolated from calf thymus and rat liver. *J. Cell. Biochem.* 1997, *64*, 258-272.
- (84) Jilani, A.; Ramotar, D.; Slack, C.; Ong, C.; Yang, X.M.; Scherer, S.W.; Lasko, D.D. Molecular cloning of the human gene, PNKP, encoding a polynucleotide kinase 3'-phosphatase and evidence for its role in repair of DNA strand breaks caused by oxidative damage. *J. Biol. Chem.* 1999, *274*, 24176-24186.
- (85) Karimi-Busheri, F.; Daly, G.; Robins, P.; Canas, B.; Pappin, D.J.; Sgouros, J.; Miller, G.G.; Fakhrai, H.; Davis, E.M.; Le Beau, M.M.; Weinfeld, M. Molecular characterization of a human DNA kinase. *J. Biol. Chem.* 1999, *274*, 24187-24194.
- (86) Tahbaz, N.; Subedi, S.; Weinfeld, M. Role of polynucleotide kinase/phosphatase in mitochondrial DNA repair. *Nucleic Acids Res.* 2012, *40*, 3484-3495.
- (87) Parsons, J.L.; Khoronenkova, S.V.; Dianova, I.I.; Ternette, N.; Kessler, B.M.; Datta, P.K.; Dianov, G.L. Phosphorylation of PNKP by ATM prevents its proteasomal degradation and enhances resistance to oxidative stress. *Nucleic Acids Res.* 2012, *40*, 11404-11415.
- (88) Edmonds, M.J. and Parsons, J.L. Regulation of base excision repair proteins by ubiquitylation. *Exp. Cell Res.* 2014, *329*, 132-138.

- (89) Dobson, C.J. and Allinson, S.L. The phosphatase activity of mammalian polynucleotide kinase takes precedence over its kinase activity in repair of single strand breaks. *Nucleic Acids Res.* 2006, *34*, 2230-2237.
- (90) Bernstein, N.K.; Williams, R.S.; Rakovszky, M.L.; Cui, D.; Green, R.; Karimi-Busheri, F.; Mani, R.S.; Galicia, S.; Koch, C.A.; Cass, C.E.; Durocher, D.; Weinfeld, M.; Glover, J.N. The molecular architecture of the mammalian DNA repair enzyme, polynucleotide kinase. *Mol. Cell* 2005, *17*, 657-670.
- (91) Karimi-Busheri, F.; Daly, G.; Robins, P.; Canas, B.; Pappin, D.J.; Sgouros, J.; Miller, G.G.; Fakhrai, H.; Davis, E.M.; Le Beau, M.M.; Weinfeld, M. Molecular characterization of a human DNA kinase. *J. Biol. Chem.* 1999, *274*, 24187-24194.
- (92) Jilani, A.; Ramotar, D.; Slack, C.; Ong, C.; Yang, X.M.; Scherer, S.W.; Lasko, D.D. Molecular cloning of the human gene, PNKP, encoding a polynucleotide kinase 3'-phosphatase and evidence for its role in repair of DNA strand breaks caused by oxidative damage. *J. Biol. Chem.* 1999, *274*, 24176-24186.
- (93) Jilani, A. and Ramotar, D. Purification and partial characterization of a DNA 3'-phosphatase from *Schizosaccharomyces pombe*. 2002, *41*, 7688-7694.
- (94) Meijer, M.; Karimi-Busheri, F.; Huang, T.Y.; Weinfeld, M.; Young, D. Pnk1, a DNA kinase/phosphatase required for normal response to DNA damage by gamma-radiation or camptothecin in *Schizosaccharomyces pombe*. *J. Biol. Chem.* 2002, *277*, 4050-4055.

- (95) Bernstein, N.K.; Williams, R.S.; Rakovszky, M.L.; Cui, D.; Green, R.; Karimi-Busheri, F.; Mani, R.S.; Galicia, S.; Koch, C.A.; Cass, C.E.; Durocher, D.; Weinfeld, M.; Glover, J.N. The molecular architecture of the mammalian DNA repair enzyme, polynucleotide kinase. *Mol. Cell* 2005, *17*, 657-670.
- (96) Bernstein, N.K.; Karimi-Busheri, F.; Rasouli-Nia, A.; Mani, R.; Dianov, G.; Glover, J.N.; Weinfeld, M. Polynucleotide kinase as a potential target for enhancing cytotoxicity by ionizing radiation and topoisomerase I inhibitors. *Anticancer Agents Med. Chem.* 2008, *8*, 358-367.
- (97) Bernstein, N.K.; Karimi-Busheri, F.; Rasouli-Nia, A.; Mani, R.; Dianov, G.; Glover, J.N.; Weinfeld, M. Polynucleotide kinase as a potential target for enhancing cytotoxicity by ionizing radiation and topoisomerase I inhibitors. *Anticancer Agents Med. Chem.* 2008, *8*, 358-367.
- (98) Koch, C.A.; Agyei, R.; Galicia, S.; Metalnikov, P.; O'Donnell, P.; Starostine, A.; Weinfeld, M.; Durocher, D. Xrcc4 physically links DNA end processing by polynucleotide kinase to DNA ligation by DNA ligase IV. *EMBO J.* 2004, *23*, 3874-3885.
- (99) Loizou, J.I.; El-Khamisy, S.F.; Zlatanou, A.; Moore, D.J.; Chan, D.W.; Qin, J.; Sarno, S.; Meggio, F.; Pinna, L.A.; Caldecott, K.W. The protein kinase CK2 facilitates repair of chromosomal DNA single-strand breaks. 2004, *117*, 17-28.
- (100) Dobson, C.J. and Allinson, S.L. The phosphatase activity of mammalian polynucleotide kinase takes precedence over its kinase activity in repair of single strand breaks. *Nucleic Acids Res.* 2006, *34*, 2230-2237.

- (101) Karimi-Busheri, F. and Weinfeld, M. Purification and substrate specificity of polydeoxyribonucleotide kinases isolated from calf thymus and rat liver. *J. Cell. Biochem.* 1997, *64*, 258-272.
- (102) Haval-Shahriari, Z.; Weinfeld, M.; Glover, J.N. Characterization of DNA Substrate Binding to the Phosphatase Domain of the DNA Repair Enzyme Polynucleotide Kinase/Phosphatase. 2017, *56*, 1737-1745.
- (103) Leipe, D.D.; Koonin, E.V.; Aravind, L. Evolution and classification of P-loop kinases and related proteins. *J. Mol. Biol.* 2003, *333*, 781-815.
- (104) Garces, F.; Pearl, L.H.; Oliver, A.W. The structural basis for substrate recognition by mammalian polynucleotide kinase 3' phosphatase. *Mol. Cell* 2011, *44*, 385-396.
- (105) Bernstein, N.K.; Hammel, M.; Mani, R.S.; Weinfeld, M.; Pelikan, M.; Tainer, J.A.; Glover, J.N. Mechanism of DNA substrate recognition by the mammalian DNA repair enzyme, Polynucleotide Kinase. *Nucleic Acids Res.* 2009, *37*, 6161-6173.
- (106) Seifried, A.; Schultz, J.; Gohla, A. Human HAD phosphatases: structure, mechanism, and roles in health and disease. *FEBS J.* 2013, *280*, 549-571.
- (107) Coquelle, N.; Haval-Shahriari, Z.; Bernstein, N.; Green, R.; Glover, J.N. Structural basis for the phosphatase activity of polynucleotide kinase/phosphatase on single- and double-stranded DNA substrates. *Proc. Natl. Acad. Sci. U. S. A.* 2011, *108*, 21022-21027.

- (108) Teraoka, H.; Mizuta, K.; Sato, F.; Shimoyachi, M.; Tsukada, K. Polynucleotide kinase from rat-liver nuclei. Purification and properties. *Eur. J. Biochem.* 1975, *58*, 297-302.
- (109) Levin, C.J. and Zimmerman, S.B. A deoxyribonucleic acid kinase from nuclei of rat liver. Purification and properties. *J. Biol. Chem.* 1976, *251*, 1767-1774.
- (110) Shuman, S. and Hurwitz, J. 5'-Hydroxyl polyribonucleotide kinase from HeLa cell nuclei. Purification and properties. *J. Biol. Chem.* 1979, *254*, 10396-10404.
- (111) Tamura, S.; Teraoka, H.; Tsukada, K. Characterization of DNA kinase from calf thymus. *Eur. J. Biochem.* 1981, *115*, 449-453.
- (112) Pfeiffer, B.H. and Zimmerman, S.B. 3'-Phosphatase activity of the DNA kinase from rat liver. *Biochem. Biophys. Res. Commun.* 1982, *109*, 1297-1302.
- (113) Karimi-Busheri, F. and Weinfeld, M. Purification and substrate specificity of polydeoxyribonucleotide kinases isolated from calf thymus and rat liver. *J. Cell. Biochem.* 1997, *64*, 258-272.
- (114) Rasouli-Nia, A.; Karimi-Busheri, F.; Weinfeld, M. Stable down-regulation of human polynucleotide kinase enhances spontaneous mutation frequency and sensitizes cells to genotoxic agents. *Proc. Natl. Acad. Sci. U. S. A.* 2004, *101*, 6905-6910.
- (115) Hegde, M.L.; Mantha, A.K.; Hazra, T.K.; Bhakat, K.K.; Mitra, S.; Szczesny, B. Oxidative genome damage and its repair: implications in aging and neurodegenerative diseases. *Mech. Ageing Dev.* 2012, *133*, 157-168.

- (116) Shen, J.; Gilmore, E.C.; Marshall, C.A.; Haddadin, M.; Reynolds, J.J.; Eyaid, W.; Bodell, A.; Barry, B.; Gleason, D.; Allen, K.; Ganesh, V.S.; Chang, B.S.; Grix, A.; Hill, R.S.; Topcu, M.; Caldecott, K.W.; Barkovich, A.J.; Walsh, C.A. Mutations in PNKP cause microcephaly, seizures and defects in DNA repair. *Nat. Genet.* 2010, *42*, 245-249.
- (117) Reynolds, J.J.; Walker, A.K.; Gilmore, E.C.; Walsh, C.A.; Caldecott, K.W. Impact of PNKP mutations associated with microcephaly, seizures and developmental delay on enzyme activity and DNA strand break repair. *Nucleic Acids Res.* 2012, *40*, 6608-6619.
- (118) Nakashima, M.; Takano, K.; Osaka, H.; Aida, N.; Tsurusaki, Y.; Miyake, N.; Saitsu, H.; Matsumoto, N. Causative novel PNKP mutations and concomitant PCDH15 mutations in a patient with microcephaly with early-onset seizures and developmental delay syndrome and hearing loss. *J. Hum. Genet.* 2014, *59*, 471-474.
- (119) Shimada, M.; Dumitrache, L.C.; Russell, H.R.; McKinnon, P.J. Polynucleotide kinase-phosphatase enables neurogenesis via multiple DNA repair pathways to maintain genome stability. *EMBO J.* 2015, *34*, 2465-2480.
- (120) Jiang, B.; Glover, J.N.; Weinfeld, M. Neurological disorders associated with DNA strand-break processing enzymes. *Mech. Ageing Dev.* 2017, *161*, 130-140.
- (121) Nakashima, M.; Takano, K.; Osaka, H.; Aida, N.; Tsurusaki, Y.; Miyake, N.; Saitsu, H.; Matsumoto, N. Causative novel PNKP mutations and concomitant PCDH15 mutations in a patient with microcephaly with early-onset seizures and developmental delay syndrome and hearing loss. *J. Hum. Genet.* 2014, *59*, 471-474.

- (122) Nair, P.; Hamzeh, A.R.; Mohamed, M.; Saif, F.; Tawfiq, N.; El Halik, M.; Al-Ali, M.T.; Bastaki, F. Microcephalic primordial dwarfism in an Emirati patient with PNKP mutation. *Am. J. Med. Genet. A.* 2016, *170*, 2127-2132.
- (123) Dumitrache, L.C. and McKinnon, P.J. Polynucleotide kinase-phosphatase (PNKP) mutations and neurologic disease. *Mech. Ageing Dev.* 2017, *161*, 121-129.
- (124) Jiang, B.; Glover, J.N.; Weinfeld, M. Neurological disorders associated with DNA strand-break processing enzymes. *Mech. Ageing Dev.* 2017, *161*, 130-140.
- (125) Bras, J.; Alonso, I.; Barbot, C.; Costa, M.M.; Darwent, L.; Orme, T.; Sequeiros, J.; Hardy, J.; Coutinho, P.; Guerreiro, R. Mutations in PNKP cause recessive ataxia with oculomotor apraxia type 4. *Am. J. Hum. Genet.* 2015, *96*, 474-479.
- (126) Chatterjee, A.; Saha, S.; Chakraborty, A.; Silva-Fernandes, A.; Mandal, S.M.; Neves-Carvalho, A.; Liu, Y.; Pandita, R.K.; Hegde, M.L.; Hegde, P.M.; Boldogh, I.; Ashizawa, T.; Koeppen, A.H.; Pandita, T.K.; Maciel, P.; Sarkar, P.S.; Hazra, T.K. The role of the mammalian DNA end-processing enzyme polynucleotide kinase 3'-phosphatase in spinocerebellar ataxia type 3 pathogenesis. *PLoS Genet.* 2015, *11*, e1004749.
- (127) Gao, R.; Liu, Y.; Silva-Fernandes, A.; Fang, X.; Paulucci-Holthauzen, A.; Chatterjee, A.; Zhang, H.L.; Matsuura, T.; Choudhary, S.; Ashizawa, T.; Koeppen, A.H.; Maciel, P.; Hazra, T.K.; Sarkar, P.S. Inactivation of PNKP by mutant ATXN3 triggers apoptosis by activating the DNA damage-response pathway in SCA3. *PLoS Genet.* 2015, *11*, e1004834.

- (128) Pedroso, J.L.; Rocha, C.R.; Macedo-Souza, L.I.; De Mario, V.; Marques, W., Jr; Barsottini, O.G.; Bulle Oliveira, A.S.; Menck, C.F.; Kok, F. Mutation in PNKP presenting initially as axonal Charcot-Marie-Tooth disease. *Neurol. Genet.* 2015, 1, e30.
- (129) Paucar, M.; Malmgren, H.; Taylor, M.; Reynolds, J.J.; Svenningsson, P.; Press, R.; Nordgren, A. Expanding the ataxia with oculomotor apraxia type 4 phenotype. *Neurol. Genet.* 2016, 2, e49.
- (130) Chabner, B.A. and Roberts, T.G., Jr Timeline: Chemotherapy and the war on cancer. *Nat. Rev. Cancer.* 2005, 5, 65-72.
- (131) Delaney, G.; Jacob, S.; Featherstone, C.; Barton, M. The role of radiotherapy in cancer treatment: estimating optimal utilization from a review of evidence-based clinical guidelines. 2005, 104, 1129-1137.
- (132) Baskar, R.; Lee, K.A.; Yeo, R.; Yeoh, K.W. Cancer and radiation therapy: current advances and future directions. *Int. J. Med. Sci.* 2012, 9, 193-199.
- (133) DeVita, V.T., Jr; Young, R.C.; Canellos, G.P. Combination versus single agent chemotherapy: a review of the basis for selection of drug treatment of cancer. 1975, 35, 98-110.
- (134) Kayl, A.E. and Meyers, C.A. Side-effects of chemotherapy and quality of life in ovarian and breast cancer patients. *Curr. Opin. Obstet. Gynecol.* 2006, 18, 24-28.
- (135) Lopez-Jimenez, J.; Martin-Ballesteros, E.; Sureda, A.; Uralburu, C.; Lorenzo, I.; del Campo, R.; Fernandez, C.; Calbacho, M.; Garcia-Belmonte, D.; Fernandez, G.

Chemotherapy-induced nausea and vomiting in acute leukemia and stem cell transplant patients: results of a multicenter, observational study. 2006, *91*, 84-91.

(136) Haider, M.; Hamadah, I.; Almutawa, A. Radiation- and chemotherapy-induced permanent alopecia: case series. *J. Cutan. Med. Surg.* 2013, *17*, 55-61.

(137) Lage, H. An overview of cancer multidrug resistance: a still unsolved problem. *Cell Mol. Life Sci.* 2008, *65*, 3145-3167.

(138) Gibbs, J.B. Mechanism-based target identification and drug discovery in cancer research. *Science* 2000, *287*, 1969-1973.

(139) Imai, K. and Takaoka, A. Comparing antibody and small-molecule therapies for cancer. *Nat. Rev. Cancer.* 2006, *6*, 714-727.

(140) Druker, B.J. STI571 (Gleevec) as a paradigm for cancer therapy. *Trends Mol. Med.* 2002, *8*, 14.

(141) Smith, J.K.; Mamoon, N.M.; Duhe, R.J. Emerging roles of targeted small molecule protein-tyrosine kinase inhibitors in cancer therapy. *Oncol. Res.* 2004, *14*, 175-225.

(142) Herbst, R.S.; Fukuoka, M.; Baselga, J. Gefitinib--a novel targeted approach to treating cancer. *Nat. Rev. Cancer.* 2004, *4*, 956-965.

(143) Madhusudan, S. and Hickson, I.D. DNA repair inhibition: a selective tumour targeting strategy. *Trends Mol. Med.* 2005, *11*, 503-511.

- (144) Madhusudan, S. and Middleton, M.R. The emerging role of DNA repair proteins as predictive, prognostic and therapeutic targets in cancer. *Cancer Treat. Rev.* 2005, 31, 603-617.
- (145) Helleday, T.; Petermann, E.; Lundin, C.; Hodgson, B.; Sharma, R.A. DNA repair pathways as targets for cancer therapy. *Nat. Rev. Cancer.* 2008, 8, 193-204.
- (146) Shen, Y.; Rehman, F.L.; Feng, Y.; Boshuizen, J.; Bajrami, I.; Elliott, R.; Wang, B.; Lord, C.J.; Post, L.E.; Ashworth, A. BMN 673, a novel and highly potent PARP1/2 inhibitor for the treatment of human cancers with DNA repair deficiency. *Clin. Cancer Res.* 2013, 19, 5003-5015.
- (147) McCabe, N.; Hanna, C.; Walker, S.M.; Gonda, D.; Li, J.; Wikstrom, K.; Savage, K.I.; Butterworth, K.T.; Chen, C.; Harkin, D.P.; Prise, K.M.; Kennedy, R.D. Mechanistic Rationale to Target PTEN-Deficient Tumor Cells with Inhibitors of the DNA Damage Response Kinase ATM. *Cancer Res.* 2015, 75, 2159-2165.
- (148) Bixel, K. and Hays, J.L. Olaparib in the management of ovarian cancer. *Pharmacogenomics Pers. Med.* 2015, 8, 127-135.
- (149) Hughes, J.P.; Rees, S.; Kalindjian, S.B.; Philpott, K.L. Principles of early drug discovery. *Br. J. Pharmacol.* 2011, 162, 1239-1249.
- (150) Hoelder, S.; Clarke, P.A.; Workman, P. Discovery of small molecule cancer drugs: successes, challenges and opportunities. *Mol. Oncol.* 2012, 6, 155-176.

- (151) Karimi-Busheri, F.; Lee, J.; Tomkinson, A.E.; Weinfeld, M. Repair of DNA strand gaps and nicks containing 3'-phosphate and 5'-hydroxyl termini by purified mammalian enzymes. *Nucleic Acids Res.* 1998, *26*, 4395-4400.
- (152) Rasouli-Nia, A.; Karimi-Busheri, F.; Weinfeld, M. Stable down-regulation of human polynucleotide kinase enhances spontaneous mutation frequency and sensitizes cells to genotoxic agents. *Proc. Natl. Acad. Sci. U. S. A.* 2004, *101*, 6905-6910.
- (153) Schellenberg, M.J. and Williams, R.S. DNA end processing by polynucleotide kinase/phosphatase. *Proc. Natl. Acad. Sci. U. S. A.* 2011, *108*, 20855-20856.
- (154) Weinfeld, M.; Mani, R.S.; Abdou, I.; Aceytuno, R.D.; Glover, J.N. Tidying up loose ends: the role of polynucleotide kinase/phosphatase in DNA strand break repair. *Trends Biochem. Sci.* 2011, *36*, 262-271.
- (155) Dobson, C.J. and Allinson, S.L. The phosphatase activity of mammalian polynucleotide kinase takes precedence over its kinase activity in repair of single strand breaks. *Nucleic Acids Res.* 2006, *34*, 2230-2237.
- (156) Breslin, C. and Caldecott, K.W. DNA 3'-phosphatase activity is critical for rapid global rates of single-strand break repair following oxidative stress. *Mol. Cell. Biol.* 2009, *29*, 4653-4662.
- (157) Cohen, P. Protein Kinase Inhibitors for the Treatment of Disease: The Promise and the Problems, In *Inhibitors of Protein Kinases and Protein Phosphates*, Anonymous ; Springer Berlin Heidelberg: Berlin, Heidelberg, 2005; 167 ; pp. 1-7.

(158) Freschauf, G.K.; Karimi-Busheri, F.; Ulaczyk-Lesanko, A.; Mereniuk, T.R.; Ahrens, A.; Koshy, J.M.; Rasouli-Nia, A.; Pasarj, P.; Holmes, C.F.; Rininsland, F.; Hall, D.G.; Weinfeld, M. Identification of a small molecule inhibitor of the human DNA repair enzyme polynucleotide kinase/phosphatase. *Cancer Res.* 2009, *69*, 7739-7746.

(159) Freschauf, G.K.; Mani, R.S.; Mereniuk, T.R.; Fanta, M.; Virgen, C.A.; Dianov, G.L.; Grassot, J.M.; Hall, D.G.; Weinfeld, M. Mechanism of action of an imidopiperidine inhibitor of human polynucleotide kinase/phosphatase. *J. Biol. Chem.* 2010, *285*, 2351-2360.

(160) Freschauf, G.K.; Karimi-Busheri, F.; Ulaczyk-Lesanko, A.; Mereniuk, T.R.; Ahrens, A.; Koshy, J.M.; Rasouli-Nia, A.; Pasarj, P.; Holmes, C.F.; Rininsland, F.; Hall, D.G.; Weinfeld, M. Identification of a small molecule inhibitor of the human DNA repair enzyme polynucleotide kinase/phosphatase. *Cancer Res.* 2009, *69*, 7739-7746.

(161) Freschauf, G.K.; Mani, R.S.; Mereniuk, T.R.; Fanta, M.; Virgen, C.A.; Dianov, G.L.; Grassot, J.M.; Hall, D.G.; Weinfeld, M. Mechanism of action of an imidopiperidine inhibitor of human polynucleotide kinase/phosphatase. *J. Biol. Chem.* 2010, *285*, 2351-2360.

(162) Zereshkian, A.; Leyton, J.V.; Cai, Z.; Bergstrom, D.; Weinfeld, M.; Reilly, R.M. The human polynucleotide kinase/phosphatase (hPNKP) inhibitor A12B4C3 radiosensitizes human myeloid leukemia cells to Auger electron-emitting anti-CD123 (1)(1)(1)In-NLS-7G3 radioimmunoconjugates. *Nucl. Med. Biol.* 2014, *41*, 377-383.

(163) Srivastava, P.; Sarma, A.; Chaturvedi, C.M. Targeting DNA repair with PNKP inhibition sensitizes radioresistant prostate cancer cells to high LET radiation. *PLoS One* 2018, *13*, e0190516.

- (164) Lord, C.J.; Tutt, A.N.; Ashworth, A. Synthetic lethality and cancer therapy: lessons learned from the development of PARP inhibitors. *Annu. Rev. Med.* 2015, *66*, 455-470.
- (165) Cairney, C.J.; Godwin, L.S.; Bilsland, A.E.; Burns, S.; Stevenson, K.H.; McGarry, L.; Revie, J.; Moore, J.D.; Wiggins, C.M.; Collinson, R.S.; Mudd, C.; Tsonou, E.; Sadaie, M.; Bennett, D.C.; Narita, M.; Torrance, C.J.; Keith, W.N. A 'synthetic-sickness' screen for senescence re-engagement targets in mutant cancer backgrounds. *PLoS Genet.* 2017, *13*, e1006942.
- (166) Szczurek, E.; Misra, N.; Vingron, M. Synthetic sickness or lethality points at candidate combination therapy targets in glioblastoma. *Int. J. Cancer* 2013, *133*, 2123-2132.
- (167) Brough, R.; Frankum, J.R.; Costa-Cabral, S.; Lord, C.J.; Ashworth, A. Searching for synthetic lethality in cancer. *Curr. Opin. Genet. Dev.* 2011, *21*, 34-41.
- (168) McLornan, D.P.; List, A.; Mufti, G.J. Applying synthetic lethality for the selective targeting of cancer. *N. Engl. J. Med.* 2014, *371*, 1725-1735.
- (169) Kaelin, W.G., Jr The concept of synthetic lethality in the context of anticancer therapy. *Nat. Rev. Cancer.* 2005, *5*, 689-698.
- (170) Sonnenblick, A.; de Azambuja, E.; Azim, H.A., Jr; Piccart, M. An update on PARP inhibitors--moving to the adjuvant setting. *Nat. Rev. Clin. Oncol.* 2015, *12*, 27-41.
- (171) Iglehart, J.D. and Silver, D.P. Synthetic lethality--a new direction in cancer-drug development. *N. Engl. J. Med.* 2009, *361*, 189-191.

- (172) Helleday, T. The underlying mechanism for the PARP and BRCA synthetic lethality: clearing up the misunderstandings. *Mol. Oncol.* 2011, 5, 387-393.
- (173) Amir, E.; Seruga, B.; Serrano, R.; Ocana, A. Targeting DNA repair in breast cancer: a clinical and translational update. *Cancer Treat. Rev.* 2010, 36, 557-565.
- (174) Chalmers, A.J.; Lakshman, M.; Chan, N.; Bristow, R.G. Poly(ADP-ribose) polymerase inhibition as a model for synthetic lethality in developing radiation oncology targets. *Semin. Radiat. Oncol.* 2010, 20, 274-281.
- (175) Dedes, K.J.; Wilkerson, P.M.; Wetterskog, D.; Weigelt, B.; Ashworth, A.; Reis-Filho, J.S. Synthetic lethality of PARP inhibition in cancers lacking BRCA1 and BRCA2 mutations. *Cell. Cycle* 2011, 10, 1192-1199.
- (176) Salmena, L.; Carracedo, A.; Pandolfi, P.P. Tenets of PTEN tumor suppression. 2008, 133, 403-414.
- (177) Song, M.S.; Salmena, L.; Pandolfi, P.P. The functions and regulation of the PTEN tumour suppressor. *Nat. Rev. Mol. Cell Biol.* 2012, 13, 283-296.
- (178) Carracedo, A.; Alimonti, A.; Pandolfi, P.P. PTEN level in tumor suppression: how much is too little? *Cancer Res.* 2011, 71, 629-633.
- (179) Milella, M.; Falcone, I.; Conciatori, F.; Cesta Incani, U.; Del Curatolo, A.; Inzerilli, N.; Nuzzo, C.M.; Vaccaro, V.; Vari, S.; Cognetti, F.; Ciuffreda, L. PTEN: Multiple Functions in Human Malignant Tumors. *Front. Oncol.* 2015, 5, 24.

(180) Gupta, A.; Yang, Q.; Pandita, R.K.; Hunt, C.R.; Xiang, T.; Misri, S.; Zeng, S.; Pagan, J.; Jeffery, J.; Puc, J.; Kumar, R.; Feng, Z.; Powell, S.N.; Bhat, A.; Yaguchi, T.; Wadhwa, R.; Kaul, S.C.; Parsons, R.; Khanna, K.K.; Pandita, T.K. Cell cycle checkpoint defects contribute to genomic instability in PTEN deficient cells independent of DNA DSB repair. *Cell. Cycle* 2009, 8, 2198-2210.

(181) Mendes-Pereira, A.M.; Martin, S.A.; Brough, R.; McCarthy, A.; Taylor, J.R.; Kim, J.S.; Waldman, T.; Lord, C.J.; Ashworth, A. Synthetic lethal targeting of PTEN mutant cells with PARP inhibitors. *EMBO Mol. Med.* 2009, 1, 315-322.

(182) Forster, M.D.; Dedes, K.J.; Sandhu, S.; Frenzas, S.; Kristeleit, R.; Ashworth, A.; Poole, C.J.; Weigelt, B.; Kaye, S.B.; Molife, L.R. Treatment with olaparib in a patient with PTEN-deficient endometrioid endometrial cancer. *Nat. Rev. Clin. Oncol.* 2011, 8, 302-306.

(183) Minami, D.; Takigawa, N.; Takeda, H.; Takata, M.; Ochi, N.; Ichihara, E.; Hisamoto, A.; Hotta, K.; Tanimoto, M.; Kiura, K. Synergistic effect of olaparib with combination of cisplatin on PTEN-deficient lung cancer cells. *Mol. Cancer. Res.* 2013, 11, 140-148.

(184) Mendes-Pereira, A.M.; Martin, S.A.; Brough, R.; McCarthy, A.; Taylor, J.R.; Kim, J.S.; Waldman, T.; Lord, C.J.; Ashworth, A. Synthetic lethal targeting of PTEN mutant cells with PARP inhibitors. *EMBO Mol. Med.* 2009, 1, 315-322.

(185) Zhao, Q.; Guan, J.; Zhang, Z.; Lv, J.; Wang, Y.; Liu, L.; Zhou, Q.; Mao, W. Inhibition of Rad51 sensitizes breast cancer cells with wild-type PTEN to olaparib. *Biomed. Pharmacother.* 2017, 94, 165-168.

(186) McCabe, N.; Hanna, C.; Walker, S.M.; Gonda, D.; Li, J.; Wikstrom, K.; Savage, K.I.; Butterworth, K.T.; Chen, C.; Harkin, D.P.; Prise, K.M.; Kennedy, R.D. Mechanistic Rationale to Target PTEN-Deficient Tumor Cells with Inhibitors of the DNA Damage Response Kinase ATM. *Cancer Res.* 2015, 75, 2159-2165.

(187) Mereniuk, T.R.; Maranchuk, R.A.; Schindler, A.; Penner-Chea, J.; Freschauf, G.K.; Hegazy, S.; Lai, R.; Foley, E.; Weinfeld, M. Genetic screening for synthetic lethal partners of polynucleotide kinase/phosphatase: potential for targeting SHP-1-depleted cancers. *Cancer Res.* 2012, 72, 5934-5944.

(188) Mereniuk, T.R.; El Gendy, M.A.; Mendes-Pereira, A.M.; Lord, C.J.; Ghosh, S.; Foley, E.; Ashworth, A.; Weinfeld, M. Synthetic lethal targeting of PTEN-deficient cancer cells using selective disruption of polynucleotide kinase/phosphatase. *Mol. Cancer. Ther.* 2013, 12, 2135-2144.

(189) Molinari, F. and Frattini, M. Functions and Regulation of the PTEN Gene in Colorectal Cancer. *Front. Oncol.* 2014, 3, 326.

(190) Nassif, N.T.; Lobo, G.P.; Wu, X.; Henderson, C.J.; Morrison, C.D.; Eng, C.; Jalaludin, B.; Segelov, E. PTEN mutations are common in sporadic microsatellite stable colorectal cancer. 2004, 23, 617-628.

(191) Zhou, X.P.; Loukola, A.; Salovaara, R.; Nystrom-Lahti, M.; Peltomaki, P.; de la Chapelle, A.; Aaltonen, L.A.; Eng, C. PTEN mutational spectra, expression levels, and subcellular localization in microsatellite stable and unstable colorectal cancers. *Am. J. Pathol.* 2002, 161, 439-447.

- (192) Goel, A.; Arnold, C.N.; Niedzwiecki, D.; Carethers, J.M.; Dowell, J.M.; Wasserman, L.; Compton, C.; Mayer, R.J.; Bertagnolli, M.M.; Boland, C.R. Frequent inactivation of PTEN by promoter hypermethylation in microsatellite instability-high sporadic colorectal cancers. *Cancer Res.* 2004, *64*, 3014-3021.
- (193) Langlois, M.J.; Bergeron, S.; Bernatchez, G.; Boudreau, F.; Saucier, C.; Perreault, N.; Carrier, J.C.; Rivard, N. The PTEN phosphatase controls intestinal epithelial cell polarity and barrier function: role in colorectal cancer progression. *PLoS One* 2010, *5*, e15742.
- (194) Fan, D.; Lin, X.; Zhang, F.; Zhong, W.; Hu, J.; Chen, Y.; Cai, Z.; Zou, Y.; He, X.; Chen, X.; Lan, P.; Wu, X. MicroRNA 26b promotes colorectal cancer metastasis by down-regulating PTEN and WNT5A. *Cancer. Sci.* 2017,
- (195) Salmena, L.; Carracedo, A.; Pandolfi, P.P. Tenets of PTEN tumor suppression. 2008, *133*, 403-414.
- (196) Sun, Y.; Tian, H.; Wang, L. Effects of PTEN on the proliferation and apoptosis of colorectal cancer cells via the phosphoinositol-3-kinase/Akt pathway. *Oncol. Rep.* 2015, *33*, 1828-1836.
- (197) Bowen, K.A.; Doan, H.Q.; Zhou, B.P.; Wang, Q.; Zhou, Y.; Rychahou, P.G.; Evers, B.M. PTEN loss induces epithelial--mesenchymal transition in human colon cancer cells. *Anticancer Res.* 2009, *29*, 4439-4449.

- (198) Jhawer, M.; Goel, S.; Wilson, A.J.; Montagna, C.; Ling, Y.H.; Byun, D.S.; Nasser, S.; Arango, D.; Shin, J.; Klampfer, L.; Augenlicht, L.H.; Perez-Soler, R.; Mariadason, J.M. PIK3CA mutation/PTEN expression status predicts response of colon cancer cells to the epidermal growth factor receptor inhibitor cetuximab. *Cancer Res.* 2008, *68*, 1953-1961.
- (199) Laurent-Puig, P.; Cayre, A.; Manceau, G.; Buc, E.; Bachet, J.B.; Lecomte, T.; Rougier, P.; Lievre, A.; Landi, B.; Boige, V.; Ducreux, M.; Ychou, M.; Bibeau, F.; Bouche, O.; Reid, J.; Stone, S.; Penault-Llorca, F. Analysis of PTEN, BRAF, and EGFR status in determining benefit from cetuximab therapy in wild-type KRAS metastatic colon cancer. *J. Clin. Oncol.* 2009, *27*, 5924-5930.
- (200) De Roock, W.; De Vriendt, V.; Normanno, N.; Ciardiello, F.; Tejpar, S. KRAS, BRAF, PIK3CA, and PTEN mutations: implications for targeted therapies in metastatic colorectal cancer. *Lancet Oncol.* 2011, *12*, 594-603.
- (201) Cho, K.; Wang, X.; Nie, S.; Chen, Z.G.; Shin, D.M. Therapeutic nanoparticles for drug delivery in cancer. *Clin. Cancer Res.* 2008, *14*, 1310-1316.
- (202) Petros, R.A. and DeSimone, J.M. Strategies in the design of nanoparticles for therapeutic applications. *Nat. Rev. Drug Discov.* 2010, *9*, 615-627.
- (203) Sun, T.; Zhang, Y.S.; Pang, B.; Hyun, D.C.; Yang, M.; Xia, Y. Engineered nanoparticles for drug delivery in cancer therapy. *Angew. Chem. Int. Ed Engl.* 2014, *53*, 12320-12364.

- (204) Danhier, F.; Feron, O.; Preat, V. To exploit the tumor microenvironment: Passive and active tumor targeting of nanocarriers for anti-cancer drug delivery. *J. Control. Release* 2010, *148*, 135-146.
- (205) Perez-Herrero, E. and Fernandez-Medarde, A. Advanced targeted therapies in cancer: Drug nanocarriers, the future of chemotherapy. *Eur. J. Pharm. Biopharm.* 2015, *93*, 52-79.
- (206) Upreti, M.; Jyoti, A.; Sethi, P. Tumor microenvironment and nanotherapeutics. *Transl. Cancer. Res.* 2013, *2*, 309-319.
- (207) Byrne, J.D.; Betancourt, T.; Brannon-Peppas, L. Active targeting schemes for nanoparticle systems in cancer therapeutics. *Adv. Drug Deliv. Rev.* 2008, *60*, 1615-1626.
- (208) Zhong, Y.; Meng, F.; Deng, C.; Zhong, Z. Ligand-directed active tumor-targeting polymeric nanoparticles for cancer chemotherapy. 2014, *15*, 1955-1969.
- (209) Sun, T.; Zhang, Y.S.; Pang, B.; Hyun, D.C.; Yang, M.; Xia, Y. Engineered nanoparticles for drug delivery in cancer therapy. *Angew. Chem. Int. Ed Engl.* 2014, *53*, 12320-12364.
- (210) Khodabandehloo, H.; Zahednasab, H.; Ashrafi Hafez, A. Nanocarriers Usage for Drug Delivery in Cancer Therapy. *Iran. J. Cancer. Prev.* 2016, *9*, 3966. eCollection 2016 Apr.

- (211) Kataoka, K.; Harada, A.; Nagasaki, Y. Block copolymer micelles for drug delivery: design, characterization and biological significance. *Adv. Drug Deliv. Rev.* 2001, 47, 113-131.
- (212) Kedar, U.; Phutane, P.; Shidhaye, S.; Kadam, V. Advances in polymeric micelles for drug delivery and tumor targeting. *Nanomedicine* 2010, 6, 714-729.
- (213) Deshmukh, A.S.; Chauhan, P.N.; Noolvi, M.N.; Chaturvedi, K.; Ganguly, K.; Shukla, S.S.; Nadagouda, M.N.; Aminabhavi, T.M. Polymeric micelles: Basic research to clinical practice. *Int. J. Pharm.* 2017, 532, 249-268.
- (214) Aliabadi, H.M. and Lavasanifar, A. Polymeric micelles for drug delivery. *Expert Opin. Drug Deliv.* 2006, 3, 139-162.
- (215) Duncan, R. The dawning era of polymer therapeutics. *Nat. Rev. Drug Discov.* 2003, 2, 347-360.
- (216) Kwon, G.S. Polymeric micelles for delivery of poorly water-soluble compounds. *Crit. Rev. Ther. Drug Carrier Syst.* 2003, 20, 357-403.
- (217) Sutton, D.; Nasongkla, N.; Blanco, E.; Gao, J. Functionalized micellar systems for cancer targeted drug delivery. *Pharm. Res.* 2007, 24, 1029-1046.
- (218) Gong, J.; Chen, M.; Zheng, Y.; Wang, S.; Wang, Y. Polymeric micelles drug delivery system in oncology. *J. Control. Release* 2012, 159, 312-323.

- (219) Xu, W.; Ling, P.; Zhang, T. Polymeric micelles, a promising drug delivery system to enhance bioavailability of poorly water-soluble drugs. *J. Drug Deliv.* 2013, *2013*, 340315.
- (220) Aliabadi, H.M.; Shahin, M.; Brocks, D.R.; Lavasanifar, A. Disposition of drugs in block copolymer micelle delivery systems: from discovery to recovery. *Clin. Pharmacokinet.* 2008, *47*, 619-634.
- (221) Gaucher, G.; Dufresne, M.H.; Sant, V.P.; Kang, N.; Maysinger, D.; Leroux, J.C. Block copolymer micelles: preparation, characterization and application in drug delivery. *J. Control. Release* 2005, *109*, 169-188.
- (222) Aliabadi, H.M.; Elhasi, S.; Mahmud, A.; Gulamhusein, R.; Mahdipoor, P.; Lavasanifar, A. Encapsulation of hydrophobic drugs in polymeric micelles through co-solvent evaporation: the effect of solvent composition on micellar properties and drug loading. *Int. J. Pharm.* 2007, *329*, 158-165.
- (223) Adams, M.L.; Lavasanifar, A.; Kwon, G.S. Amphiphilic block copolymers for drug delivery. *J. Pharm. Sci.* 2003, *92*, 1343-1355.
- (224) Feng, R.; Zhu, W.; Teng, F.; Liu, N.; Yang, F.; Meng, N.; Song, Z. Poly(ethylene glycol) amphiphilic copolymer for anticancer drugs delivery. *Anticancer Agents Med. Chem.* 2015, *15*, 176-188.
- (225) Kim, S.Y.; Shin, I.G.; Lee, Y.M.; Cho, C.S.; Sung, Y.K. Methoxy poly(ethylene glycol) and epsilon-caprolactone amphiphilic block copolymeric micelle containing

indomethacin. II. Micelle formation and drug release behaviours. *J. Control. Release* 1998, 51, 13-22.

(226) Aliabadi, H.M.; Mahmud, A.; Sharifabadi, A.D.; Lavasanifar, A. Micelles of methoxy poly(ethylene oxide)-b-poly(epsilon-caprolactone) as vehicles for the solubilization and controlled delivery of cyclosporine A. *J. Control. Release* 2005, 104, 301-311.

(227) Mahmud, A.; Xiong, X.B.; Lavasanifar, A. Development of novel polymeric micellar drug conjugates and nano-containers with hydrolyzable core structure for doxorubicin delivery. *Eur. J. Pharm. Biopharm.* 2008, 69, 923-934.

(228) Molavi, O.; Ma, Z.; Mahmud, A.; Alshamsan, A.; Samuel, J.; Lai, R.; Kwon, G.S.; Lavasanifar, A. Polymeric micelles for the solubilization and delivery of STAT3 inhibitor cucurbitacins in solid tumors. *Int. J. Pharm.* 2008, 347, 118-127.

(229) Xiong, X.B.; Uludag, H.; Lavasanifar, A. Biodegradable amphiphilic poly(ethylene oxide)-block-polyesters with grafted polyamines as supramolecular nanocarriers for efficient siRNA delivery. 2009, 30, 242-253.

(230) Shahin, M. and Lavasanifar, A. Novel self-associating poly(ethylene oxide)-b-poly(epsilon-caprolactone) based drug conjugates and nano-containers for paclitaxel delivery. *Int. J. Pharm.* 2010, 389, 213-222.

(231) Garg, S.M.; Vakili, M.R.; Lavasanifar, A. Polymeric micelles based on poly(ethylene oxide) and alpha-carbon substituted poly(varepsilon-caprolactone): An in vitro study on

the effect of core forming block on polymeric micellar stability, biocompatibility, and immunogenicity. *Colloids Surf. B Biointerfaces* 2015, 132, 161-170.

(232) Mahmud, A.; Xiong, X.B.; Aliabadi, H.M.; Lavasanifar, A. Polymeric micelles for drug targeting. *J. Drug Target.* 2007, 15, 553-584.

(233) Xiong, X.B.; Falamarzian, A.; Garg, S.M.; Lavasanifar, A. Engineering of amphiphilic block copolymers for polymeric micellar drug and gene delivery. *J. Control. Release* 2011, 155, 248-261.

(234) Herbst, R.S. Review of epidermal growth factor receptor biology. *Int. J. Radiat. Oncol. Biol. Phys.* 2004, 59, 21-26.

(235) Navolanic, P.M.; Steelman, L.S.; McCubrey, J.A. EGFR family signaling and its association with breast cancer development and resistance to chemotherapy (Review). *Int. J. Oncol.* 2003, 22, 237-252.

(236) Barber, T.D.; Vogelstein, B.; Kinzler, K.W.; Velculescu, V.E. Somatic mutations of EGFR in colorectal cancers and glioblastomas. *N. Engl. J. Med.* 2004, 351, 2883.

(237) Paez, J.G.; Janne, P.A.; Lee, J.C.; Tracy, S.; Greulich, H.; Gabriel, S.; Herman, P.; Kaye, F.J.; Lindeman, N.; Boggon, T.J.; Naoki, K.; Sasaki, H.; Fujii, Y.; Eck, M.J.; Sellers, W.R.; Johnson, B.E.; Meyerson, M. EGFR mutations in lung cancer: correlation with clinical response to gefitinib therapy. *Science* 2004, 304, 1497-1500.

(238) Sok, J.C.; Coppelli, F.M.; Thomas, S.M.; Lango, M.N.; Xi, S.; Hunt, J.L.; Freilino, M.L.; Graner, M.W.; Wikstrand, C.J.; Bigner, D.D.; Gooding, W.E.; Furnari, F.B.; Grandis,

J.R. Mutant epidermal growth factor receptor (EGFRvIII) contributes to head and neck cancer growth and resistance to EGFR targeting. *Clin. Cancer Res.* 2006, 12, 5064-5073.

(239) Yarden, Y. The EGFR family and its ligands in human cancer. signalling mechanisms and therapeutic opportunities. *Eur. J. Cancer* 2001, 37 Suppl 4, 3.

(240) Lage, A.; Crombet, T.; Gonzalez, G. Targeting epidermal growth factor receptor signaling: early results and future trends in oncology. *Ann. Med.* 2003, 35, 327-336.

(241) Flynn, J.F.; Wong, C.; Wu, J.M. Anti-EGFR Therapy: Mechanism and Advances in Clinical Efficacy in Breast Cancer. *J. Oncol.* 2009, 2009, 526963.

(242) Harandi, A.; Zaidi, A.S.; Stocker, A.M.; Laber, D.A. Clinical Efficacy and Toxicity of Anti-EGFR Therapy in Common Cancers. *J. Oncol.* 2009, 2009, 567486.

(243) Deeks, E.D. Neratinib: First Global Approval. 2017, 77, 1695-1704.

(244) Loree, J.M. and Kopetz, S. Recent developments in the treatment of metastatic colorectal cancer. *Ther. Adv. Med. Oncol.* 2017, 9, 551-564.

(245) Mazza, V. and Cappuzzo, F. Treating EGFR mutation resistance in non-small cell lung cancer - role of osimertinib. *Appl. Clin. Genet.* 2017, 10, 49-56.

(246) Mamot, C.; Ritschard, R.; Kung, W.; Park, J.W.; Herrmann, R.; Rochlitz, C.F. EGFR-targeted immunoliposomes derived from the monoclonal antibody EMD72000 mediate specific and efficient drug delivery to a variety of colorectal cancer cells. *J. Drug Target.* 2006, 14, 215-223.

- (247) Lee, P.C.; Chiou, Y.C.; Wong, J.M.; Peng, C.L.; Shieh, M.J. Targeting colorectal cancer cells with single-walled carbon nanotubes conjugated to anticancer agent SN-38 and EGFR antibody. 2013, *34*, 8756-8765.
- (248) Ladner, R.C.; Sato, A.K.; Gorzelany, J.; de Souza, M. Phage display-derived peptides as therapeutic alternatives to antibodies. *Drug Discov. Today* 2004, *9*, 525-529.
- (249) Li, Z.; Zhao, R.; Wu, X.; Sun, Y.; Yao, M.; Li, J.; Xu, Y.; Gu, J. Identification and characterization of a novel peptide ligand of epidermal growth factor receptor for targeted delivery of therapeutics. *FASEB J.* 2005, *19*, 1978-1985.
- (250) Krumpe, L.R. and Mori, T. Potential of phage-displayed peptide library technology to identify functional targeting peptides. *Expert Opin. Drug Discov.* 2007, *2*, 525.
- (251) Ahmed, S.; Mathews, A.S.; Byeon, N.; Lavasanifar, A.; Kaur, K. Peptide arrays for screening cancer specific peptides. *Anal. Chem.* 2010, *82*, 7533-7541.
- (252) Abourbeh, G.; Shir, A.; Mishani, E.; Ogris, M.; Rodl, W.; Wagner, E.; Levitzki, A. PolyIC GE11 polyplex inhibits EGFR-overexpressing tumors. *IUBMB Life* 2012, *64*, 324-330.
- (253) Colzani, B.; Speranza, G.; Dorati, R.; Conti, B.; Modena, T.; Bruni, G.; Zagato, E.; Vermeulen, L.; Dakwar, G.R.; Braeckmans, K.; Genta, I. Design of smart GE11-PLGA/PEG-PLGA blend nanoparticulate platforms for parenteral administration of hydrophilic macromolecular drugs: synthesis, preparation and in vitro/ex vivo characterization. *Int. J. Pharm.* 2016, *511*, 1112-1123.

(254) Grunwald, G.K.; Vetter, A.; Klutz, K.; Willhauck, M.J.; Schwenk, N.; Senekowitsch-Schmidtke, R.; Schwaiger, M.; Zach, C.; Wagner, E.; Goke, B.; Holm, P.S.; Ogris, M.; Spitzweg, C. EGFR-Targeted Adenovirus Dendrimer Coating for Improved Systemic Delivery of the Theranostic NIS Gene. *Mol. Ther. Nucleic Acids* 2013, 2, e131.

(255) Cheng, L.; Huang, F.Z.; Cheng, L.F.; Zhu, Y.Q.; Hu, Q.; Li, L.; Wei, L.; Chen, D.W. GE11-modified liposomes for non-small cell lung cancer targeting: preparation, ex vitro and in vivo evaluation. *Int. J. Nanomedicine* 2014, 9, 921-935.

(256) Xu, W.W.; Liu, D.Y.; Cao, Y.C.; Wang, X.Y. GE11 peptide-conjugated nanoliposomes to enhance the combinational therapeutic efficacy of docetaxel and siRNA in laryngeal cancers. *Int. J. Nanomedicine* 2017, 12, 6461-6470.

(257) Torre, L.A.; Bray, F.; Siegel, R.L.; Ferlay, J.; Lortet-Tieulent, J.; Jemal, A. Global cancer statistics, 2012. *CA Cancer. J. Clin.* 2015, 65, 87-108.

(258) Marmol, I.; Sanchez-de-Diego, C.; Pradilla Dieste, A.; Cerrada, E.; Rodriguez Yoldi, M.J. Colorectal Carcinoma: A General Overview and Future Perspectives in Colorectal Cancer. *Int. J. Mol. Sci.* 2017, 18, 10.3390/ijms18010197.

(259) Pino, M.S. and Chung, D.C. The chromosomal instability pathway in colon cancer. 2010, 138, 2059-2072.

(260) Tariq, K. and Ghias, K. Colorectal cancer carcinogenesis: a review of mechanisms. *Cancer. Biol. Med.* 2016, 13, 120-135.

- (261) Jiricny, J. and Marra, G. DNA repair defects in colon cancer. *Curr. Opin. Genet. Dev.* 2003, 13, 61-69.
- (262) Ashktorab, H. and Brim, H. DNA Methylation and Colorectal Cancer. *Curr. Colorectal Cancer. Rep.* 2014, 10, 425-430.
- (263) Wright, M.; Beaty, J.S.; Ternent, C.A. Molecular Markers for Colorectal Cancer. *Surg. Clin. North Am.* 2017, 97, 683-701.
- (264) Chawla, A.K.; Kachnic, L.A.; Clark, J.W.; Willett, C.G. Combined modality therapy for rectal and colon cancer. *Semin. Oncol.* 2003, 30, 101-112.
- (265) Mayer, A.; Tsiompanou, E.; Flynn, A.A.; Pedley, R.B.; Dearling, J.; Boden, R.; Begent, R.H. Higher dose and dose-rate in smaller tumors result in improved tumor control. *Cancer Invest.* 2003, 21, 382-388.
- (266) Rullier, E. and Laurent, C. Advances in surgical treatment of rectal cancer. *Minerva Chir.* 2003, 58, 459-457.
- (267) Marques, R.P.; Duarte, G.S.; Sterrantino, C.; Pais, H.L.; Quintela, A.; Martins, A.P.; Costa, J. Triplet (FOLFOXIRI) versus doublet (FOLFOX or FOLFIRI) backbone chemotherapy as first-line treatment of metastatic colorectal cancer: A systematic review and meta-analysis. *Crit. Rev. Oncol. Hematol.* 2017, 118, 54-62.
- (268) Wang, J.; Luo, L.; Wang, D.; Guo, B.; Li, J.; Yang, Z.; Tang, D. Combination adjuvant chemotherapy with targeted drugs for treatment of colorectal cancer: A network meta-analysis. *J. Cell. Biochem.* 2018, 119, 1521-1537.

(269) Landry, J.C.; Feng, Y.; Cohen, S.J.; Staley, C.A.; Whittington, R.; Sigurdson, E.R.; Nimeiri, H.; Verma, U.; Prabhu, R.S.; Benson, A.B. Phase 2 study of preoperative radiation with concurrent capecitabine, oxaliplatin, and bevacizumab followed by surgery and postoperative 5-fluorouracil, leucovorin, oxaliplatin (FOLFOX), and bevacizumab in patients with locally advanced rectal cancer: ECOG 3204. 2013, *119*, 1521-1527.

(270) Morganti, A.G.; Cellini, F.; Mignogna, S.; Padula, G.D.; Caravatta, L.; Deodato, F.; Picardi, V.; Macchia, G.; Cilla, S.; Buwenge, M.; Lullo, L.D.; Gambacorta, M.A.; Balducci, M.; Mattiucci, G.C.; Autorino, R.; Valentini, V. Low-dose radiotherapy and concurrent FOLFIRI-bevacizumab: a Phase II study. 2016, *12*, 779-787.

(271) Fink, D.; Nebel, S.; Aebi, S.; Zheng, H.; Cenni, B.; Nehme, A.; Christen, R.D.; Howell, S.B. The role of DNA mismatch repair in platinum drug resistance. *Cancer Res.* 1996, *56*, 4881-4886.

(272) Leguisamo, N.M.; Gloria, H.C.; Kalil, A.N.; Martins, T.V.; Azambuja, D.B.; Meira, L.B.; Saffi, J. Base excision repair imbalance in colorectal cancer has prognostic value and modulates response to chemotherapy. 2017, *8*, 54199-54214.

(273) Buti, S.; Ricco, M.; Chiesa, M.D.; Copercini, B.; Tomasello, G.; Brighenti, M.; Passalacqua, R. Oxaliplatin-induced hemolytic anemia during adjuvant treatment of a patient with colon cancer: a case report. *Anticancer Drugs* 2007, *18*, 297-300.

(274) Spanos, C.P.; Mamopoulos, A.; Tsapas, A.; Syrakos, T.; Kiskinis, D. Female fertility and colorectal cancer. *Int. J. Colorectal Dis.* 2008, *23*, 735-743.

(275) Gonfloni, S. Targeting DNA damage response: threshold, chromatin landscape and beyond. *Pharmacol. Ther.* 2013, *138*, 46-52.

(276) Sankaranarayanan, K.; Taleei, R.; Rahmanian, S.; Nikjoo, H. Ionizing radiation and genetic risks. XVII. Formation mechanisms underlying naturally occurring DNA deletions in the human genome and their potential relevance for bridging the gap between induced DNA double-strand breaks and deletions in irradiated germ cells. *Mutat. Res.* 2013, *753*, 114-130.

(277) Adachi, N.; Suzuki, H.; Iizumi, S.; Koyama, H. Hypersensitivity of nonhomologous DNA end-joining mutants to VP-16 and ICRF-193: implications for the repair of topoisomerase II-mediated DNA damage. *J. Biol. Chem.* 2003, *278*, 35897-35902.

(278) Riballo, E.; Kuhne, M.; Rief, N.; Doherty, A.; Smith, G.C.; Recio, M.J.; Reis, C.; Dahm, K.; Fricke, A.; Krempler, A.; Parker, A.R.; Jackson, S.P.; Gennery, A.; Jeggo, P.A.; Lobrich, M. A pathway of double-strand break rejoining dependent upon ATM, Artemis, and proteins locating to gamma-H2AX foci. *Mol. Cell* 2004, *16*, 715-724.

(279) Pitcher, R.S.; Green, A.J.; Brzostek, A.; Korycka-Machala, M.; Dziadek, J.; Doherty, A.J. NHEJ protects mycobacteria in stationary phase against the harmful effects of desiccation. *DNA Repair (Amst)* 2007, *6*, 1271-1276.

(280) Karimi-Busheri, F.; Daly, G.; Robins, P.; Canas, B.; Pappin, D.J.; Sgouros, J.; Miller, G.G.; Fakhrai, H.; Davis, E.M.; Le Beau, M.M.; Weinfeld, M. Molecular characterization of a human DNA kinase. *J. Biol. Chem.* 1999, *274*, 24187-24194.

(281) Caldecott, K.W. Mammalian DNA single-strand break repair: an X-ra(y)ted affair. *Bioessays* 2001, 23, 447-455.

(282) Zhu, W.; Zhao, Z.; Li, Z.; Jiang, J.; Shen, G.; Yu, R. A graphene oxide platform for the assay of DNA 3'-phosphatases and their inhibitors based on hairpin primer and polymerase elongation. *J. Mater. Chem. B* 2013, 1, 361-367.

(283) Parsons, J.L.; Khoronenkova, S.V.; Dianova, I.I.; Ternette, N.; Kessler, B.M.; Datta, P.K.; Dianov, G.L. Phosphorylation of PNKP by ATM prevents its proteasomal degradation and enhances resistance to oxidative stress. *Nucleic Acids Res.* 2012, 40, 11404-11415.

(284) Kashkina, E.; Qi, T.; Weinfeld, M.; Young, D. Polynucleotide kinase/phosphatase, Pnk1, is involved in base excision repair in *Schizosaccharomyces pombe*. *DNA Repair (Amst)* 2012, 11, 676-683.

(285) O'Connor, M.J.; Martin, N.M.; Smith, G.C. Targeted cancer therapies based on the inhibition of DNA strand break repair. 2007, 26, 7816-7824.

(286) Mereniuk, T.R.; Maranchuk, R.A.; Schindler, A.; Penner-Chea, J.; Freschauf, G.K.; Hegazy, S.; Lai, R.; Foley, E.; Weinfeld, M. Genetic screening for synthetic lethal partners of polynucleotide kinase/phosphatase: potential for targeting SHP-1-depleted cancers. *Cancer Res.* 2012, 72, 5934-5944.

(287) Song, C.; Zhang, C.; Zhao, M.P. Development of a high-throughput screening platform for DNA 3'-phosphatases and their inhibitors based on a universal molecular beacon and quantitative real-time PCR. *Chem. Asian J.* 2010, 5, 1146-1151.

(288) Mani, R.S.; Karimi-Busheri, F.; Fanta, M.; Cass, C.E.; Weinfeld, M. Spectroscopic studies of DNA and ATP binding to human polynucleotide kinase: evidence for a ternary complex. 2003, 42, 12077-12084.

(289) Reha-Krantz, L.J.; Nonay, R.L.; Stocki, S. Bacteriophage T4 DNA polymerase mutations that confer sensitivity to the PPI analog phosphonoacetic acid. *J. Virol.* 1993, 67, 60-66.

(290) Toure, B.B.; Hoveyda, H.R.; Tailor, J.; Ulaczyk-Lesanko, A.; Hall, D.G. A three-component reaction for diversity-oriented synthesis of polysubstituted piperidines: solution and solid-phase optimization of the first tandem aza[4+2]/allylboration. *Chemistry* 2003, 9, 466-474.

(291) An, J. and Carmichael, W.W. Use of a colorimetric protein phosphatase inhibition assay and enzyme linked immunosorbent assay for the study of microcystins and nodularins. *Toxicon* 1994, 32, 1495-1507.

(292) Hariharan, C.; Bloom, L.B.; Helquist, S.A.; Kool, E.T.; Reha-Krantz, L.J. Dynamics of nucleotide incorporation: snapshots revealed by 2-aminopurine fluorescence studies. 2006, 45, 2836-2844.

- (293) Reha-Krantz, L.J.; Hariharan, C.; Subuddhi, U.; Xia, S.; Zhao, C.; Beckman, J.; Christian, T.; Konigsberg, W. Structure of the 2-aminopurine-cytosine base pair formed in the polymerase active site of the RB69 Y567A-DNA polymerase. 2011, *50*, 10136-10149.
- (294) Song, C.; Zhang, C.; Zhao, M. Rapid and sensitive detection of DNA polymerase fidelity by singly labeled smart fluorescent probes. *Biosens. Bioelectron.* 2011, *26*, 2699-2702.
- (295) Ma, C.; Liu, H.; Du, J.; Chen, H.; He, H.; Jin, S.; Wang, K.; Wang, J. Quencher-free hairpin probes for real-time detection of T4 polynucleotide kinase activity. *Anal. Biochem.* 2016, *494*, 1-3.
- (296) Fidalgo da Silva, E.; Mandal, S.S.; Reha-Krantz, L.J. Using 2-aminopurine fluorescence to measure incorporation of incorrect nucleotides by wild type and mutant bacteriophage T4 DNA polymerases. *J. Biol. Chem.* 2002, *277*, 40640-40649.
- (297) Coquelle, N.; Haval-Shahriari, Z.; Bernstein, N.; Green, R.; Glover, J.N. Structural basis for the phosphatase activity of polynucleotide kinase/phosphatase on single- and double-stranded DNA substrates. *Proc. Natl. Acad. Sci. U. S. A.* 2011, *108*, 21022-21027.
- (298) Derbyshire, V.; Grindley, N.D.; Joyce, C.M. The 3'-5' exonuclease of DNA polymerase I of *Escherichia coli*: contribution of each amino acid at the active site to the reaction. *EMBO J.* 1991, *10*, 17-24.

- (299) Song, C.; Zhang, C.; Zhao, M.P. Development of a high-throughput screening platform for DNA 3'-phosphatases and their inhibitors based on a universal molecular beacon and quantitative real-time PCR. *Chem. Asian J.* 2010, *5*, 1146-1151.
- (300) Chen, F.; Zhao, Y.; Qi, L.; Fan, C. One-step highly sensitive fluorescence detection of T4 polynucleotide kinase activity and biological small molecules by ligation-nicking coupled reaction-mediated signal amplification. *Biosens. Bioelectron.* 2013, *47*, 218-224.
- (301) Lin, L.; Liu, Y.; Yan, J.; Wang, X.; Li, J. Sensitive nanochannel biosensor for T4 polynucleotide kinase activity and inhibition detection. *Anal. Chem.* 2013, *85*, 334-340.
- (302) Palmer, T. and Bonner, P.L.R. *Enzymes : biochemistry, biotechnology and clinical chemistry*. Woodhead Publishing: Oxford, 2011; pp. 126–152.
- (303) Seifried, A.; Knobloch, G.; Duraphe, P.S.; Segerer, G.; Manhard, J.; Schindelin, H.; Schultz, J.; Gohla, A. Evolutionary and structural analyses of mammalian haloacid dehalogenase-type phosphatases AUM and chronophin provide insight into the basis of their different substrate specificities. *J. Biol. Chem.* 2014, *289*, 3416-3431.
- (304) Weinfeld, M.; Mani, R.S.; Abdou, I.; Aceytuno, R.D.; Glover, J.N. Tidying up loose ends: the role of polynucleotide kinase/phosphatase in DNA strand break repair. *Trends Biochem. Sci.* 2011, *36*, 262-271.
- (305) Adams, M.L.; Lavasanifar, A.; Kwon, G.S. Amphiphilic block copolymers for drug delivery. *J. Pharm. Sci.* 2003, *92*, 1343-1355.

(306) Perez-Herrero, E. and Fernandez-Medarde, A. Advanced targeted therapies in cancer: Drug nanocarriers, the future of chemotherapy. *Eur. J. Pharm. Biopharm.* 2015, 93, 52-79.

(307) Houdaihed, L.; Evans, J.C.; Allen, C. Overcoming the Road Blocks: Advancement of Block Copolymer Micelles for Cancer Therapy in the Clinic. *Mol. Pharm.* 2017, 14, 2503-2517.

(308) Matsumura, Y. Polymeric micellar delivery systems in oncology. *Jpn. J. Clin. Oncol.* 2008, 38, 793-802.

(309) Lu, Y. and Park, K. Polymeric micelles and alternative nanonized delivery vehicles for poorly soluble drugs. *Int. J. Pharm.* 2013, 453, 198-214.

(310) Nishiyama, N.; Matsumura, Y.; Kataoka, K. Development of polymeric micelles for targeting intractable cancers. *Cancer. Sci.* 2016, 107, 867-874.

(311) Yousefpour Marzbali, M. and Yari Khosroushahi, A. Polymeric micelles as mighty nanocarriers for cancer gene therapy: a review. *Cancer Chemother. Pharmacol.* 2017, 79, 637-649.

(312) Zhang, Y.; Ren, T.; Gou, J.; Zhang, L.; Tao, X.; Tian, B.; Tian, P.; Yu, D.; Song, J.; Liu, X.; Chao, Y.; Xiao, W.; Tang, X. Strategies for improving the payload of small molecular drugs in polymeric micelles. *J. Control. Release* 2017, 261, 352-366.

(313) Honary, S. and Lavasanifar, A. The effect of self-assembly conditions on the size of di- and tri-block copolymer micelles: solicitation from response surface methodology. *Pharm. Dev. Technol.* 2015, 20, 957-65.

(314) Talelli, M.; Barz, M.; Rijcken, C.J.; Kiessling, F.; Hennink, W.E.; Lammers, T. Core-Crosslinked Polymeric Micelles: Principles, Preparation, Biomedical Applications and Clinical Translation. *Nano Today* 2015, 10, 93-117.

(315) Srinivasan, M.; Rajabi, M.; Mousa, S.A. Multifunctional Nanomaterials and Their Applications in Drug Delivery and Cancer Therapy. *Nanomaterials (Basel)* 2015, 5, 1690-1703.

(316) Dai, W.; Wang, X.; Song, G.; Liu, T.; He, B.; Zhang, H.; Wang, X.; Zhang, Q. Combination antitumor therapy with targeted dual-nanomedicines. *Adv. Drug Deliv. Rev.* 2017, 115, 23-45.

(317) Hsu, J.L. and Hung, M.C. The role of HER2, EGFR, and other receptor tyrosine kinases in breast cancer. *Cancer Metastasis Rev.* 2016, 35, 575-588.

(318) Hung, M.S.; Chen, I.C.; Lin, P.Y.; Lung, J.H.; Li, Y.C.; Lin, Y.C.; Yang, C.T.; Tsai, Y.H. Epidermal growth factor receptor mutation enhances expression of vascular endothelial growth factor in lung cancer. *Oncol. Lett.* 2016, 12, 4598-4604.

(319) Marmol, I.; Sanchez-de-Diego, C.; Pradilla Dieste, A.; Cerrada, E.; Rodriguez Yoldi, M.J. Colorectal Carcinoma: A General Overview and Future Perspectives in Colorectal Cancer. *Int. J. Mol. Sci.* 2017, 18, 10.3390/ijms18010197.

(320) Tang, H.; Chen, X.; Rui, M.; Sun, W.; Chen, J.; Peng, J.; Xu, Y. Effects of surface displayed targeting ligand GE11 on liposome distribution and extravasation in tumor. *Mol. Pharm.* 2014, *11*, 3242-3250.

(321) Colzani, B.; Speranza, G.; Dorati, R.; Conti, B.; Modena, T.; Bruni, G.; Zagato, E.; Vermeulen, L.; Dakwar, G.R.; Braeckmans, K.; Genta, I. Design of smart GE11-PLGA/PEG-PLGA blend nanoparticulate platforms for parenteral administration of hydrophilic macromolecular drugs: synthesis, preparation and in vitro/ex vivo characterization. *Int. J. Pharm.* 2016, *511*, 1112-1123.

(322) Hu, D.; Mezghrani, O.; Zhang, L.; Chen, Y.; Ke, X.; Ci, T. GE11 peptide modified and reduction-responsive hyaluronic acid-based nanoparticles induced higher efficacy of doxorubicin for breast carcinoma therapy. *Int. J. Nanomedicine* 2016, *11*, 5125-5147.

(323) Fan, M.; Yang, D.; Liang, X.; Ao, J.; Li, Z.; Wang, H.; Shi, B. Design and biological activity of epidermal growth factor receptor-targeted peptide doxorubicin conjugate. *Biomed. Pharmacother.* 2015, *70*, 268-273.

(324) Nijman, S.M. Synthetic lethality: general principles, utility and detection using genetic screens in human cells. *FEBS Lett.* 2011, *585*, 1-6.

(325) Leung, A.W.; de Silva, T.; Bally, M.B.; Lockwood, W.W. Synthetic lethality in lung cancer and translation to clinical therapies. *Mol. Cancer.* 2016, *15*, 61.

(326) Mereniuk, T.R.; El Gendy, M.A.; Mendes-Pereira, A.M.; Lord, C.J.; Ghosh, S.; Foley, E.; Ashworth, A.; Weinfeld, M. Synthetic lethal targeting of PTEN-deficient cancer

cells using selective disruption of polynucleotide kinase/phosphatase. *Mol. Cancer. Ther.* 2013, 12, 2135-2144.

(327) Liu, Y.; Hu, X.; Han, C.; Wang, L.; Zhang, X.; He, X.; Lu, X. Targeting tumor suppressor genes for cancer therapy. *Bioessays* 2015, 37, 1277-1286.

(328) Jackson, R.A. and Chen, E.S. Synthetic lethal approaches for assessing combinatorial efficacy of chemotherapeutic drugs. *Pharmacol. Ther.* 2016, 162, 69-85.

(329) Fanta, M.; Zhang, H.; Bernstein, N.; Glover, M.; Karimi-Busheri, F.; Weinfeld, M. Production, characterization, and epitope mapping of monoclonal antibodies against human polydeoxyribonucleotide kinase. 2001, 20, 237-242.

(330) Lee, C.; Kim, J.S.; Waldman, T. PTEN gene targeting reveals a radiation-induced size checkpoint in human cancer cells. *Cancer Res.* 2004, 64, 6906-6914.

(331) Aliabadi, H.M.; Mahmud, A.; Sharifabadi, A.D.; Lavasanifar, A. Micelles of methoxy poly(ethylene oxide)-b-poly(epsilon-caprolactone) as vehicles for the solubilization and controlled delivery of cyclosporine A. *J. Control. Release* 2005, 104, 301-311.

(332) Mahmud, A. and Lavasanifar, A. The effect of block copolymer structure on the internalization of polymeric micelles by human breast cancer cells. *Colloids Surf. B Biointerfaces* 2005, 45, 82-89.

(333) Mahmud, A.; Xiong, X.-.; Lavasanifar, A. Novel self-associating POly(ethylene oxide)-block-poly(e-caprolactone) block copolymers with functional side groups on the polyester block for drug delivery. 2006, 39, 9419-9428.

(334) Garg, S.M.; Vakili, M.R.; Lavasanifar, A. Polymeric micelles based on poly(ethylene oxide) and alpha-carbon substituted poly(varepsilon-caprolactone): An in vitro study on the effect of core forming block on polymeric micellar stability, biocompatibility, and immunogenicity. *Colloids Surf. B Biointerfaces* 2015, 132, 161-170.

(335) Xiong, X.B.; Mahmud, A.; Uludag, H.; Lavasanifar, A. Conjugation of arginine-glycine-aspartic acid peptides to poly(ethylene oxide)-b-poly(epsilon-caprolactone) micelles for enhanced intracellular drug delivery to metastatic tumor cells. 2007, 8, 874-884.

(336) Mathews, A.S.; Ahmed, S.; Shahin, M.; Lavasanifar, A.; Kaur, K. Peptide modified polymeric micelles specific for breast cancer cells. *Bioconjug. Chem.* 2013, 24, 560-570.

(337) Shahin, M.; Ahmed, S.; Kaur, K.; Lavasanifar, A. Decoration of polymeric micelles with cancer-specific peptide ligands for active targeting of paclitaxel. 2011, 32, 5123-5133.

(338) Lavasanifar, A.; Samuel, J.; Kwon, G.S. The effect of fatty acid substitution on the in vitro release of amphotericin B from micelles composed of poly(ethylene oxide)-block-poly(N-hexyl stearate-L-aspartamide). *J. Control. Release* 2002, 79, 165-172.

(339) Aliabadi, H.M. and Lavasanifar, A. Polymeric micelles for drug delivery. *Expert Opin. Drug Deliv.* 2006, 3, 139-162.

(340) Balin-Gauthier, D.; Delord, J.P.; Rochaix, P.; Mallard, V.; Thomas, F.; Hennebelle, I.; Bugat, R.; Canal, P.; Allal, C. In vivo and in vitro antitumor activity of oxaliplatin in

combination with cetuximab in human colorectal tumor cell lines expressing different level of EGFR. *Cancer Chemother. Pharmacol.* 2006, *57*, 709-718.

(341) Curtin, N.J. Inhibiting the DNA damage response as a therapeutic manoeuvre in cancer. *Br. J. Pharmacol.* 2013, *169*, 1745-1765.

(342) Ulbrich, K.; Hola, K.; Subr, V.; Bakandritsos, A.; Tucek, J.; Zboril, R. Targeted Drug Delivery with Polymers and Magnetic Nanoparticles: Covalent and Noncovalent Approaches, Release Control, and Clinical Studies. *Chem. Rev.* 2016, *116*, 5338-5431.

(343) Stover, E.H.; Konstantinopoulos, P.A.; Matulonis, U.A.; Swisher, E.M. Biomarkers of Response and Resistance to DNA Repair Targeted Therapies. *Clin. Cancer Res.* 2016, *22*, 5651-5660.

(344) Brown, J.S.; O'Carrigan, B.; Jackson, S.P.; Yap, T.A. Targeting DNA Repair in Cancer: Beyond PARP Inhibitors. *Cancer. Discov.* 2017, *7*, 20-37.

(345) Srivas, R.; Shen, J.P.; Yang, C.C.; Sun, S.M.; Li, J.; Gross, A.M.; Jensen, J.; Licon, K.; Bojorquez-Gomez, A.; Klepper, K.; Huang, J.; Pekin, D.; Xu, J.L.; Yeerna, H.; Sivaganesh, V.; Kollenstart, L.; van Attikum, H.; Aza-Blanc, P.; Sobol, R.W.; Ideker, T. A Network of Conserved Synthetic Lethal Interactions for Exploration of Precision Cancer Therapy. *Mol. Cell* 2016, *63*, 514-525.

(346) Gavande, N.S.; VanderVere-Carozza, P.S.; Hinshaw, H.D.; Jalal, S.I.; Sears, C.R.; Pawelczak, K.S.; Turchi, J.J. DNA repair targeted therapy: The past or future of cancer treatment? *Pharmacol. Ther.* 2016, *160*, 65-83.

- (347) Hsiang, Y.H.; Hertzberg, R.; Hecht, S.; Liu, L.F. Camptothecin induces protein-linked DNA breaks via mammalian DNA topoisomerase I. *J. Biol. Chem.* 1985, *260*, 14873-14878.
- (348) Ward, J.F. The yield of DNA double-strand breaks produced intracellularly by ionizing radiation: a review. *Int. J. Radiat. Biol.* 1990, *57*, 1141-1150.
- (349) Olive, P.L. The role of DNA single- and double-strand breaks in cell killing by ionizing radiation. *Radiat. Res.* 1998, *150*, 42.
- (350) Hegde, M.L.; Hazra, T.K.; Mitra, S. Early steps in the DNA base excision/single-strand interruption repair pathway in mammalian cells. *Cell Res.* 2008, *18*, 27-47.
- (351) Karimi-Busheri, F.; Lee, J.; Tomkinson, A.E.; Weinfeld, M. Repair of DNA strand gaps and nicks containing 3'-phosphate and 5'-hydroxyl termini by purified mammalian enzymes. *Nucleic Acids Res.* 1998, *26*, 4395-4400.
- (352) Chappell, C.; Hanakahi, L.A.; Karimi-Busheri, F.; Weinfeld, M.; West, S.C. Involvement of human polynucleotide kinase in double-strand break repair by non-homologous end joining. *EMBO J.* 2002, *21*, 2827-2832.
- (353) Schellenberg, M.J. and Williams, R.S. DNA end processing by polynucleotide kinase/phosphatase. *Proc. Natl. Acad. Sci. U. S. A.* 2011, *108*, 20855-20856.
- (354) Andres, S.N.; Schellenberg, M.J.; Wallace, B.D.; Tumbale, P.; Williams, R.S. Recognition and repair of chemically heterogeneous structures at DNA ends. *Environ. Mol. Mutagen.* 2015, *56*, 1-21.

- (355) Dorman, G. and Prestwich, G.D. Benzophenone photophores in biochemistry. 1994, 33, 5661-5673.
- (356) Olszewski, J.D.; Dorman, G.; Elliott, J.T.; Hong, Y.; Ahern, D.G.; Prestwich, G.D. Tethered benzophenone reagents for the synthesis of photoactivatable ligands. *Bioconjug. Chem.* 1995, 6, 395-400.
- (357) Prestwich, G.D.; Dorman, G.; Elliott, J.T.; Marecak, D.M.; Chaudhary, A. Benzophenone photoprobes for phosphoinositides, peptides and drugs. *Photochem. Photobiol.* 1997, 65, 222-234.
- (358) Weber, P.J. and Beck-Sickinger, A.G. Comparison of the photochemical behavior of four different photoactivatable probes. *J. Pept. Res.* 1997, 49, 375-383.
- (359) Dorman, G. Estimation of the binding site of drugs by means of new types of photoactive ligands. *Acta Pharm. Hung.* 1998, 68, 95-105.
- (360) Dorman, G. and Prestwich, G.D. Using photolabile ligands in drug discovery and development. *Trends Biotechnol.* 2000, 18, 64-77.
- (361) Robinette, D.; Neamati, N.; Tomer, K.B.; Borchers, C.H. Photoaffinity labeling combined with mass spectrometric approaches as a tool for structural proteomics. *Expert Rev. Proteomics* 2006, 3, 399-408.
- (362) Hepperle, M.; Eckert, J.; Gala, D. Sequential mono-N-arylation of piperazine nitrogens. Part 1: A simplified method and its application to the preparation of a key N,N'-biaryl piperazine antifungal intermediate. 1999, 40, 5655-5659.

(363) Budke, B.; Kalin, J.H.; Pawlowski, M.; Zelivianskaia, A.S.; Wu, M.; Kozikowski, A.P.; Connell, P.P. An optimized RAD51 inhibitor that disrupts homologous recombination without requiring Michael acceptor reactivity. *J. Med. Chem.* 2013, *56*, 254-263.

(364) COTTER, R.J.; SAUERS, C.K.; WHELAN, J.M. The Synthesis of N-Substituted Isomaleimides. 1961, *26*, 10-15.

(365) Chamrad, D.C.; Koerting, G.; Gobom, J.; Thiele, H.; Klose, J.; Meyer, H.E.; Blueggel, M. Interpretation of mass spectrometry data for high-throughput proteomics. *Anal. Bioanal Chem.* 2003, *376*, 1014-1022.

(366) Thiele, H.; Glandorf, J.; Hufnagel, P. Bioinformatics strategies in life sciences: from data processing and data warehousing to biological knowledge extraction. *J. Integr. Bioinform* 2010, *7*, 141.

(367) Mayer, G.; Stephan, C.; Meyer, H.E.; Kohl, M.; Marcus, K.; Eisenacher, M. ProCon - PROteomics CONversion tool. *J. Proteomics* 2015, *129*, 56-62.

(368) Wilkins, M.R.; Lindskog, I.; Gasteiger, E.; Bairoch, A.; Sanchez, J.C.; Hochstrasser, D.F.; Appel, R.D. Detailed peptide characterization using PEPTIDEMASS--a World-Wide-Web-accessible tool. 1997, *18*, 403-408.

(369) Baliban, R.C.; Dimaggio, P.A.; Plazas-Mayorca, M.D.; Garcia, B.A.; Floudas, C.A. PILOT_PROTEIN: identification of unmodified and modified proteins via high-resolution mass spectrometry and mixed-integer linear optimization. *J. Proteome Res.* 2012, *11*, 4615-4629.

- (370) Yu, F.; Li, N.; Yu, W. PIPI: PTM-Invariant Peptide Identification Using Coding Method. *J. Proteome Res.* 2016, *15*, 4423-4435.
- (371) Prestwich, G.D.; Dorman, G.; Elliott, J.T.; Marecak, D.M.; Chaudhary, A. Benzophenone photoprobes for phosphoinositides, peptides and drugs. *Photochem. Photobiol.* 1997, *65*, 222-234.
- (372) Kotzyba-Hibert, F.; Kapfer, I.; Goeldner, M. Recent Trends in Photoaffinity Labeling. 1995, *34*, 1296-1312.
- (373) Kawamura, A.; Hindi, S.; Mihai, D.M.; James, L.; Aminova, O. Binding is not enough: flexibility is needed for photocrosslinking of Lck kinase by benzophenone photoligands. *Bioorg. Med. Chem.* 2008, *16*, 8824-8829.
- (374) Knight, Z.A. and Shokat, K.M. Features of selective kinase inhibitors. *Chem. Biol.* 2005, *12*, 621-637.
- (375) Jorissen, R.N.; Walker, F.; Pouliot, N.; Garrett, T.P.; Ward, C.W.; Burgess, A.W. Epidermal growth factor receptor: mechanisms of activation and signalling. *Exp. Cell Res.* 2003, *284*, 31-53.
- (376) Mendelsohn, J. and Baselga, J. Status of epidermal growth factor receptor antagonists in the biology and treatment of cancer. *J. Clin. Oncol.* 2003, *21*, 2787-2799.
- (377) Han, S.W.; Hwang, P.G.; Chung, D.H.; Kim, D.W.; Im, S.A.; Kim, Y.T.; Kim, T.Y.; Heo, D.S.; Bang, Y.J.; Kim, N.K. Epidermal growth factor receptor (EGFR) downstream

molecules as response predictive markers for gefitinib (Iressa, ZD1839) in chemotherapy-resistant non-small cell lung cancer. *Int. J. Cancer* 2005, *113*, 109-115.

(378) Koizumi, F.; Kanzawa, F.; Ueda, Y.; Koh, Y.; Tsukiyama, S.; Taguchi, F.; Tamura, T.; Saijo, N.; Nishio, K. Synergistic interaction between the EGFR tyrosine kinase inhibitor gefitinib ("Iressa") and the DNA topoisomerase I inhibitor CPT-11 (irinotecan) in human colorectal cancer cells. *Int. J. Cancer* 2004, *108*, 464-472.

(379) Yanase, K.; Tsukahara, S.; Asada, S.; Ishikawa, E.; Imai, Y.; Sugimoto, Y. Gefitinib reverses breast cancer resistance protein-mediated drug resistance. *Mol. Cancer. Ther.* 2004, *3*, 1119-1125.

(380) Singh, M. and Jadhav, H.R. Targeting non-small cell lung cancer with small-molecule EGFR tyrosine kinase inhibitors. *Drug Discov. Today* 2017,

(381) Helleday, T.; Petermann, E.; Lundin, C.; Hodgson, B.; Sharma, R.A. DNA repair pathways as targets for cancer therapy. *Nat. Rev. Cancer.* 2008, *8*, 193-204.

(382) Xing, J.; Wu, X.; Vaporciyan, A.A.; Spitz, M.R.; Gu, J. Prognostic significance of ataxia-telangiectasia mutated, DNA-dependent protein kinase catalytic subunit, and Ku heterodimeric regulatory complex 86-kD subunit expression in patients with nonsmall cell lung cancer. 2008, *112*, 2756-2764.

(383) Yu, L.; Shang, Z.F.; Hsu, F.M.; Zhang, Z.; Tumati, V.; Lin, Y.F.; Chen, B.P.; Saha, D. NSCLC cells demonstrate differential mode of cell death in response to the combined treatment of radiation and a DNA-PKcs inhibitor. 2015, *6*, 3848-3860.

(384) Banin, S.; Moyal, L.; Shieh, S.; Taya, Y.; Anderson, C.W.; Chessa, L.; Smorodinsky, N.I.; Prives, C.; Reiss, Y.; Shiloh, Y.; Ziv, Y. Enhanced phosphorylation of p53 by ATM in response to DNA damage. *Science* 1998, *281*, 1674-1677.

(385) Ball, L.G. and Xiao, W. Molecular basis of ataxia telangiectasia and related diseases. *Acta Pharmacol. Sin.* 2005, *26*, 897-907.

(386) Hickson, I.; Zhao, Y.; Richardson, C.J.; Green, S.J.; Martin, N.M.; Orr, A.I.; Reaper, P.M.; Jackson, S.P.; Curtin, N.J.; Smith, G.C. Identification and characterization of a novel and specific inhibitor of the ataxia-telangiectasia mutated kinase ATM. *Cancer Res.* 2004, *64*, 9152-9159.

(387) Tian, X.; Lara, H.; Wagner, K.T.; Saripalli, S.; Hyder, S.N.; Foote, M.; Sethi, M.; Wang, E.; Caster, J.M.; Zhang, L.; Wang, A.Z. Improving DNA double-strand repair inhibitor KU55933 therapeutic index in cancer radiotherapy using nanoparticle drug delivery. 2015, *7*, 20211-20219.

(388) Tredan, O.; Galmarini, C.M.; Patel, K.; Tannock, I.F. Drug resistance and the solid tumor microenvironment. *J. Natl. Cancer Inst.* 2007, *99*, 1441-1454.

(389) Zhang, B.; Hu, Y.; Pang, Z. Modulating the Tumor Microenvironment to Enhance Tumor Nanomedicine Delivery. *Front. Pharmacol.* 2017, *8*, 952.

(390) Lv, Y.; Xu, C.; Zhao, X.; Lin, C.; Yang, X.; Xin, X.; Zhang, L.; Qin, C.; Han, X.; Yang, L.; He, W.; Yin, L. Nanoplatform Assembled from a CD44-Targeted Prodrug and Smart

Liposomes for Dual Targeting of Tumor Microenvironment and Cancer Cells. *ACS Nano* 2018,

(391) Shen, S.; Zhang, Y.; Chen, K.G.; Luo, Y.L.; Wang, J. Cationic Polymeric Nanoparticle Delivering CCR2 siRNA to Inflammatory Monocytes for Tumor Microenvironment Modification and Cancer Therapy. *Mol. Pharm.* 2018,

(392) Cun, X.; Chen, J.; Ruan, S.; Zhang, L.; Wan, J.; He, Q.; Gao, H. A Novel Strategy through Combining iRGD Peptide with Tumor-Microenvironment-Responsive and Multistage Nanoparticles for Deep Tumor Penetration. *ACS Appl. Mater. Interfaces* 2015, 7, 27458-27466.

(393) Cao, D.; Liang, L.; Xu, Y.; Sun, J.; Lei, M.; Wang, M.; Wei, Y.; Sun, Z. Tumor associated macrophages and angiogenesis dual-recognizable nanoparticles for enhanced cancer chemotherapy. *Nanomedicine* 2018,

(394) Shaheen, M.; Allen, C.; Nickoloff, J.A.; Hromas, R. Synthetic lethality: exploiting the addiction of cancer to DNA repair. 2011, *117*, 6074-6082.

(395) Fang, B. Development of synthetic lethality anticancer therapeutics. *J. Med. Chem.* 2014, *57*, 7859-7873.

(396) Chan, D.A. and Giaccia, A.J. Harnessing synthetic lethal interactions in anticancer drug discovery. *Nat. Rev. Drug Discov.* 2011, *10*, 351-364.

(397) Dhanjal, J.K.; Radhakrishnan, N.; Sundar, D. Identifying synthetic lethal targets using CRISPR/Cas9 system. *Methods* 2017,

(398) Tamura, M.; Gu, J.; Matsumoto, K.; Aota, S.; Parsons, R.; Yamada, K.M. Inhibition of cell migration, spreading, and focal adhesions by tumor suppressor PTEN. *Science* 1998, 280, 1614-1617.

(399) Keniry, M. and Parsons, R. The role of PTEN signaling perturbations in cancer and in targeted therapy. 2008, 27, 5477-5485.

(400) Li, J.; Yen, C.; Liaw, D.; Podsypanina, K.; Bose, S.; Wang, S.I.; Puc, J.; Miliaresis, C.; Rodgers, L.; McCombie, R.; Bigner, S.H.; Giovanella, B.C.; Ittmann, M.; Tycko, B.; Hibshoosh, H.; Wigler, M.H.; Parsons, R. PTEN, a putative protein tyrosine phosphatase gene mutated in human brain, breast, and prostate cancer. *Science* 1997, 275, 1943-1947.

(401) Salmena, L.; Carracedo, A.; Pandolfi, P.P. Tenets of PTEN tumor suppression. 2008, 133, 403-414.

(402) Sawai, H.; Yasuda, A.; Ochi, N.; Ma, J.; Matsuo, Y.; Wakasugi, T.; Takahashi, H.; Funahashi, H.; Sato, M.; Takeyama, H. Loss of PTEN expression is associated with colorectal cancer liver metastasis and poor patient survival. *BMC Gastroenterol.* 2008, 8, 56.

(403) Nagata, Y.; Lan, K.H.; Zhou, X.; Tan, M.; Esteva, F.J.; Sahin, A.A.; Klos, K.S.; Li, P.; Monia, B.P.; Nguyen, N.T.; Hortobagyi, G.N.; Hung, M.C.; Yu, D. PTEN activation contributes to tumor inhibition by trastuzumab, and loss of PTEN predicts trastuzumab resistance in patients. *Cancer. Cell.* 2004, 6, 117-127.

(404) Frattini, M.; Saletti, P.; Romagnani, E.; Martin, V.; Molinari, F.; Ghisletta, M.; Camponovo, A.; Etienne, L.L.; Cavalli, F.; Mazzucchelli, L. PTEN loss of expression predicts cetuximab efficacy in metastatic colorectal cancer patients. *Br. J. Cancer* 2007, 97, 1139-1145.

(405) Loupakis, F.; Pollina, L.; Stasi, I.; Ruzzo, A.; Scartozzi, M.; Santini, D.; Masi, G.; Graziano, F.; Cremolini, C.; Rulli, E.; Canestrari, E.; Funel, N.; Schiavon, G.; Petrini, I.; Magnani, M.; Tonini, G.; Campani, D.; Floriani, I.; Cascinu, S.; Falcone, A. PTEN expression and KRAS mutations on primary tumors and metastases in the prediction of benefit from cetuximab plus irinotecan for patients with metastatic colorectal cancer. *J. Clin. Oncol.* 2009, 27, 2622-2629.

(406) Sos, M.L.; Koker, M.; Weir, B.A.; Heynck, S.; Rabinovsky, R.; Zander, T.; Seeger, J.M.; Weiss, J.; Fischer, F.; Frommolt, P.; Michel, K.; Peifer, M.; Mermel, C.; Girard, L.; Peyton, M.; Gazdar, A.F.; Minna, J.D.; Garraway, L.A.; Kashkar, H.; Pao, W.; Meyerson, M.; Thomas, R.K. PTEN loss contributes to erlotinib resistance in EGFR-mutant lung cancer by activation of Akt and EGFR. *Cancer Res.* 2009, 69, 3256-3261.

(407) Mao, C.; Liao, R.Y.; Chen, Q. Loss of PTEN expression predicts resistance to EGFR-targeted monoclonal antibodies in patients with metastatic colorectal cancer. *Br. J. Cancer* 2010, 102, 940.

(408) Gupta, A.; Yang, Q.; Pandita, R.K.; Hunt, C.R.; Xiang, T.; Misri, S.; Zeng, S.; Pagan, J.; Jeffery, J.; Puc, J.; Kumar, R.; Feng, Z.; Powell, S.N.; Bhat, A.; Yaguchi, T.; Wadhwa, R.; Kaul, S.C.; Parsons, R.; Khanna, K.K.; Pandita, T.K. Cell cycle checkpoint defects

contribute to genomic instability in PTEN deficient cells independent of DNA DSB repair. 2009, 8, 2198-2210.

(409) Gong, L.; Govan, J.M.; Evans, E.B.; Dai, H.; Wang, E.; Lee, S.; Lin, H.; Lazar, A.J.; Mills, G.B.; Lin, S. Nuclear PTEN tumor-suppressor functions through maintaining heterochromatin structure. 2015, 14, 2323-2332.

(410) Mendes-Pereira, A.M.; Martin, S.A.; Brough, R.; McCarthy, A.; Taylor, J.R.; Kim, J.S.; Waldman, T.; Lord, C.J.; Ashworth, A. Synthetic lethal targeting of PTEN mutant cells with PARP inhibitors. *EMBO Mol. Med.* 2009, 1, 315-322.

(411) Luo, H.Y. and Xu, R.H. Predictive and prognostic biomarkers with therapeutic targets in advanced colorectal cancer. *World J. Gastroenterol.* 2014, 20, 3858-3874.

(412) LaVan, D.A.; McGuire, T.; Langer, R. Small-scale systems for in vivo drug delivery. *Nat. Biotechnol.* 2003, 21, 1184-1191.

(413) Khawar, I.A.; Kim, J.H.; Kuh, H.J. Improving drug delivery to solid tumors: priming the tumor microenvironment. *J. Control. Release* 2015, 201, 78-89.

(414) Kim, H.; Lee, Y.; Kang, S.; Choi, M.; Lee, S.; Kim, S.; Gujrati, V.; Kim, J.; Jon, S. Self-assembled nanoparticles comprising aptide-SN38 conjugates for use in targeted cancer therapy. 2016, 27, 4484/27/48/48LT01. Epub 2016 Nov 2.

(415) Kurrikoff, K.; Gestin, M.; Langel, Ü Recent in vivo advances in cell-penetrating peptide-assisted drug delivery. 2016, 13, 373-387.

- (416) Ruoslahti, E. Tumor penetrating peptides for improved drug delivery. *Adv. Drug Deliv. Rev.* 2017, 110-111, 3-12.
- (417) Yin, H.; Yang, J.; Zhang, Q.; Yang, J.; Wang, H.; Xu, J.; Zheng, J. iRGD as a tumorpenetrating peptide for cancer therapy (Review). *Mol. Med. Rep.* 2017, 15, 2925-2930.
- (418) Hamilton, A.M.; Aidoudi-Ahmed, S.; Sharma, S.; Kotamraju, V.R.; Foster, P.J.; Sugahara, K.N.; Ruoslahti, E.; Rutt, B.K. Nanoparticles coated with the tumor-penetrating peptide iRGD reduce experimental breast cancer metastasis in the brain. *J. Mol. Med. (Berl)* 2015, 93, 991-1001.
- (419) Li, Z.; Zhao, R.; Wu, X.; Sun, Y.; Yao, M.; Li, J.; Xu, Y.; Gu, J. Identification and characterization of a novel peptide ligand of epidermal growth factor receptor for targeted delivery of therapeutics. *FASEB J.* 2005, 19, 1978-1985.
- (420) Pi, J.; Jiang, J.; Cai, H.; Yang, F.; Jin, H.; Yang, P.; Cai, J.; Chen, Z.W. GE11 peptide conjugated selenium nanoparticles for EGFR targeted oridonin delivery to achieve enhanced anticancer efficacy by inhibiting EGFR-mediated PI3K/AKT and Ras/Raf/MEK/ERK pathways. *Drug Deliv.* 2017, 24, 1549-1564.
- (421) Xu, W.W.; Liu, D.Y.; Cao, Y.C.; Wang, X.Y. GE11 peptide-conjugated nanoliposomes to enhance the combinational therapeutic efficacy of docetaxel and siRNA in laryngeal cancers. *Int. J. Nanomedicine* 2017, 12, 6461-6470.

(422) Chavanpatil, M.D.; Patil, Y.; Panyam, J. Susceptibility of nanoparticle-encapsulated paclitaxel to P-glycoprotein-mediated drug efflux. *Int. J. Pharm.* 2006, *320*, 150-156.

(423) Manzoor, A.A.; Lindner, L.H.; Landon, C.D.; Park, J.Y.; Simnick, A.J.; Dreher, M.R.; Das, S.; Hanna, G.; Park, W.; Chilkoti, A.; Koning, G.A.; ten Hagen, T.L.; Needham, D.; Dewhirst, M.W. Overcoming limitations in nanoparticle drug delivery: triggered, intravascular release to improve drug penetration into tumors. *Cancer Res.* 2012, *72*, 5566-5575.

(424) Miller, T.; Breyer, S.; van Colen, G.; Mier, W.; Haberkorn, U.; Geissler, S.; Voss, S.; Weigandt, M.; Goepferich, A. Premature drug release of polymeric micelles and its effects on tumor targeting. *Int. J. Pharm.* 2013, *445*, 117-124.

(425) Song, G.; Darr, D.B.; Santos, C.M.; Ross, M.; Valdivia, A.; Jordan, J.L.; Midkiff, B.R.; Cohen, S.; Nikolaishvili-Feinberg, N.; Miller, C.R.; Tarrant, T.K.; Rogers, A.B.; Dudley, A.C.; Perou, C.M.; Zamboni, W.C. Effects of tumor microenvironment heterogeneity on nanoparticle disposition and efficacy in breast cancer tumor models. *Clin. Cancer Res.* 2014, *20*, 6083-6095.

(426) Yhee, J.Y.; Jeon, S.; Yoon, H.Y.; Shim, M.K.; Ko, H.; Min, J.; Na, J.H.; Chang, H.; Han, H.; Kim, J.H.; Suh, M.; Lee, H.; Park, J.H.; Kim, K.; Kwon, I.C. Effects of tumor microenvironments on targeted delivery of glycol chitosan nanoparticles. *J. Control. Release* 2017, *267*, 223-231.

(427) Lipinski, C.A. Lead- and drug-like compounds: the rule-of-five revolution. *Drug Discov. Today Technol.* 2004, *1*, 337-341.

(428) Schurmann, M.; Janning, P.; Ziegler, S.; Waldmann, H. Small-Molecule Target Engagement in Cells. *Cell. Chem. Biol.* 2016, 23, 435-441.

(429) Zhao, Q.; Guan, J.; Zhang, Z.; Lv, J.; Wang, Y.; Liu, L.; Zhou, Q.; Mao, W. Inhibition of Rad51 sensitizes breast cancer cells with wild-type PTEN to olaparib. *Biomed. Pharmacother.* 2017, 94, 165-168.

(430) Fraser, M.; Zhao, H.; Luoto, K.R.; Lundin, C.; Coackley, C.; Chan, N.; Joshua, A.M.; Bismar, T.A.; Evans, A.; Helleday, T.; Bristow, R.G. PTEN deletion in prostate cancer cells does not associate with loss of RAD51 function: implications for radiotherapy and chemotherapy. *Clin. Cancer Res.* 2012, 18, 1015-1027.

Appendix: Supplementary material

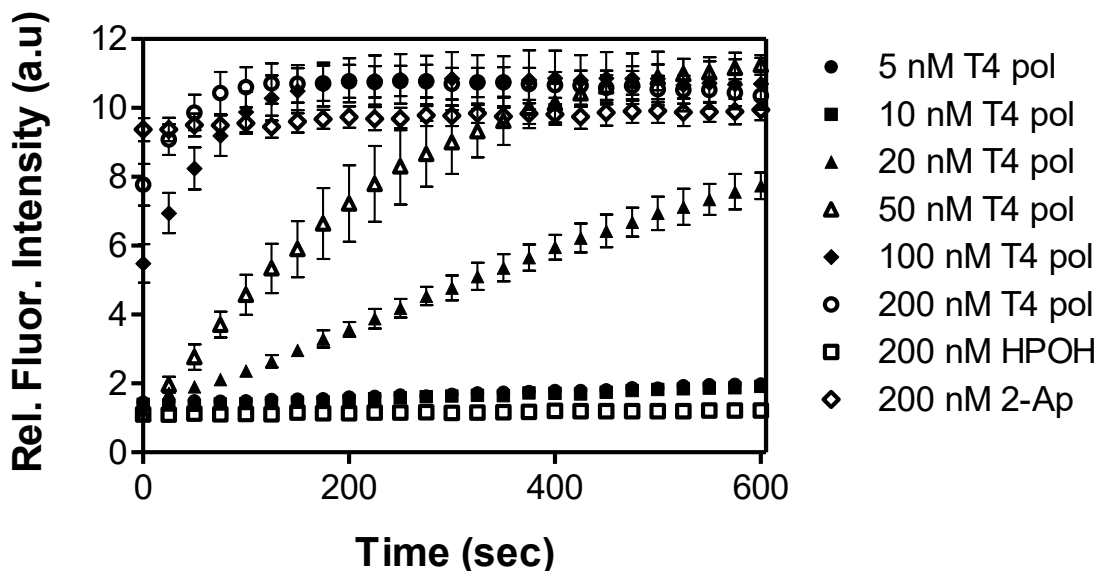


Figure A1. Time course for monitoring the activity of T4 DNA polymerase (T4 pol) by varying the concentration of enzyme from 0.005 to 0.2 μM . The reactions were carried out in 100 mM HEPES (pH 7.5), 50 mM NaCl, 10 mM MgCl_2 , and 1mM DTT. The constituents of each test assay were 5 - 100 nM T4 pol and 0.2 μM of the HPOH probe. The protocol of this assay is described in detail in section 2.3.1. Each data point (mean \pm SD) is an average of three replicate measurements.

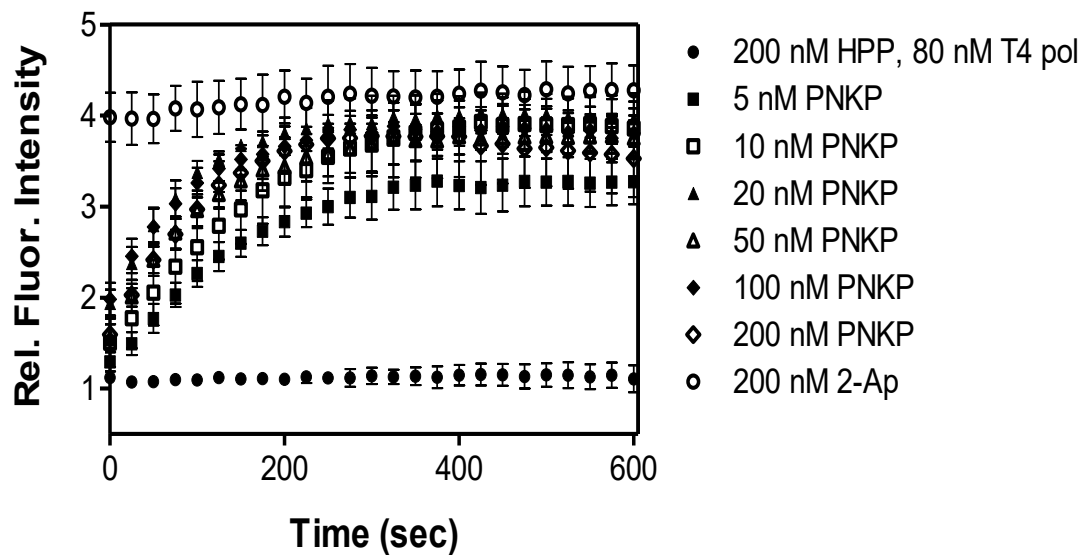


Figure A2. Time course for monitoring the activity of PNKP by varying the concentration of enzyme from 0.005 to 0.2 μ M. The assays were performed in 100 mM HEPES (pH 7.5), 50 mM NaCl, 10 mM MgCl₂, and 1mM DTT. The constituents of each test assay included 5 - 100 nM PNKP, 80 nM T4 pol and 0.2 μ M of the HPP probe. The protocol of this assay is described in detail in section 2.3.1. Each data point (mean \pm SD) is an average of three replicate measurements.

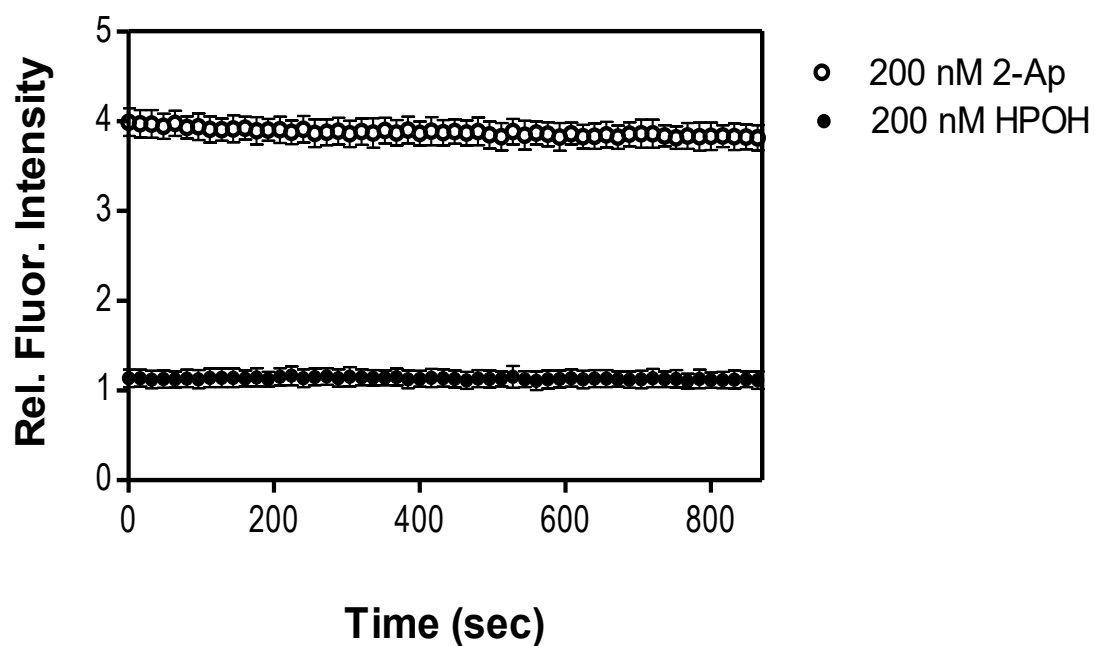


Figure A3. Fluorescence Intensities of 200 nM 2-Ap (open circles) and 200 nM HPOH (filled circles). Data were analyzed using Graphpad Prism software. Each data point (mean \pm SD) is an average of three replicate measurements.

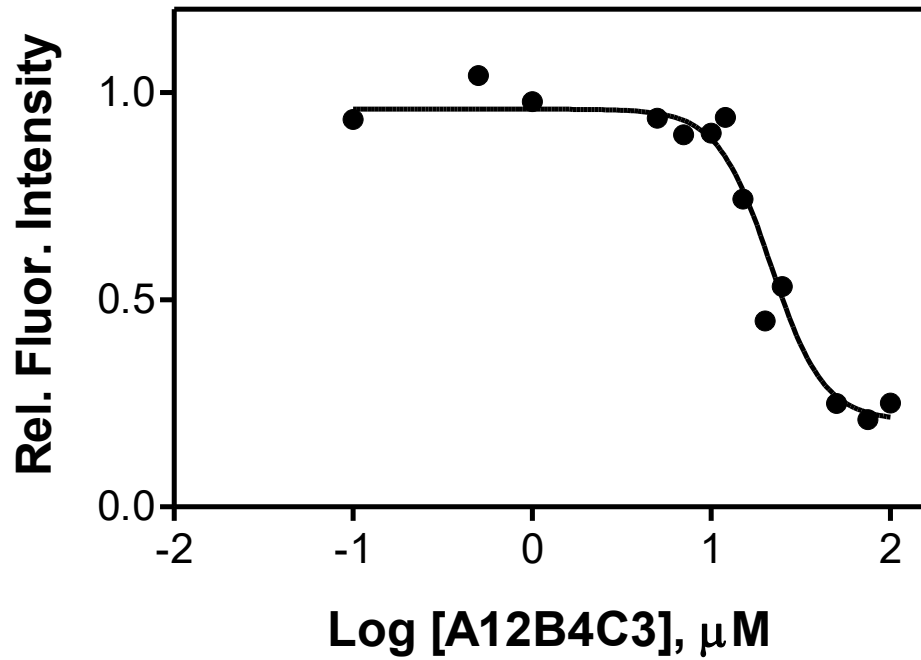


Figure A4. Dose dependent inhibition of PNKP by inhibitor A12B4C3. Each data point is an average of three replicate measurements. IC₅₀ value is calculated using GraphPad prism software and is equal to 22 μM.

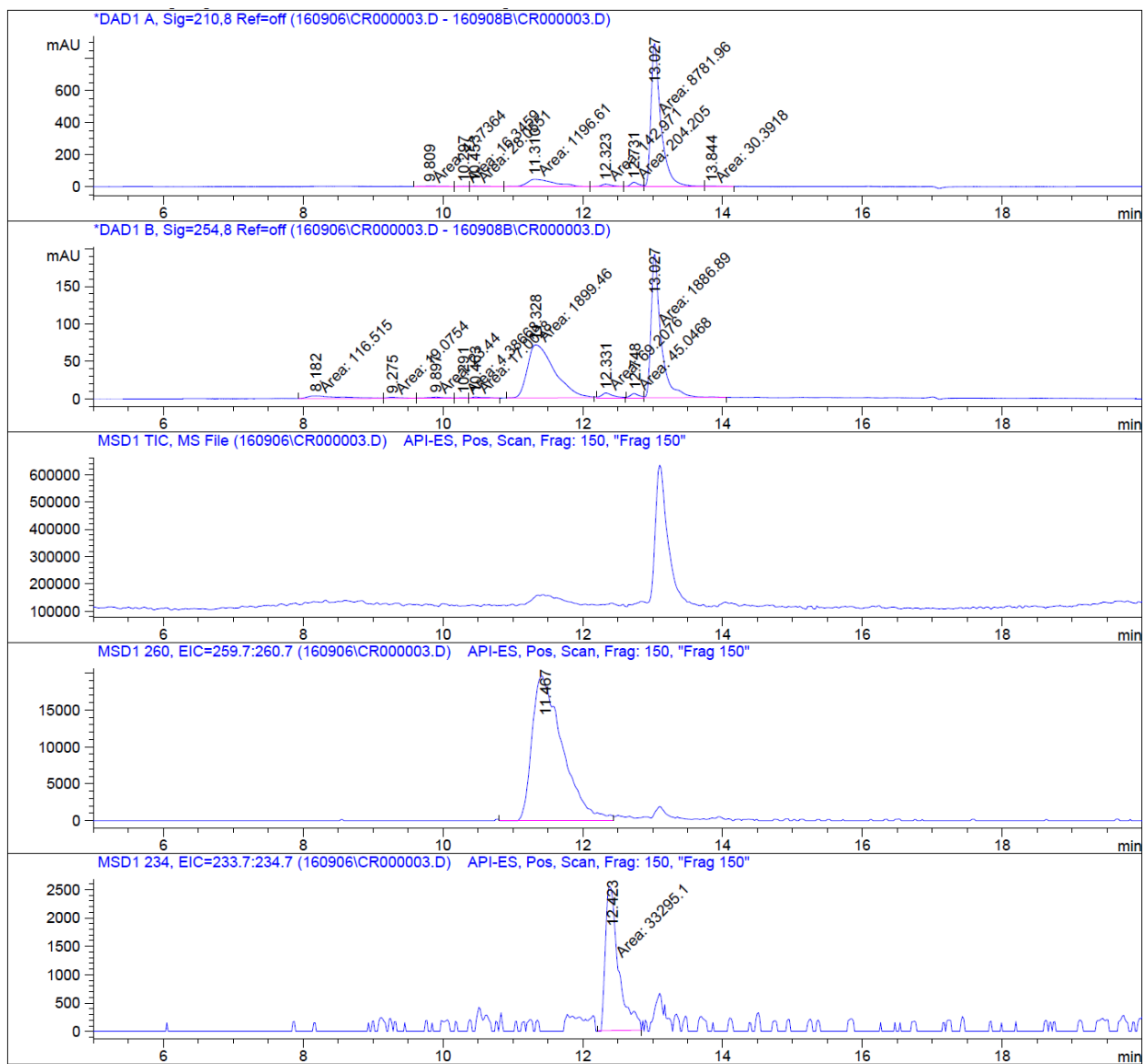
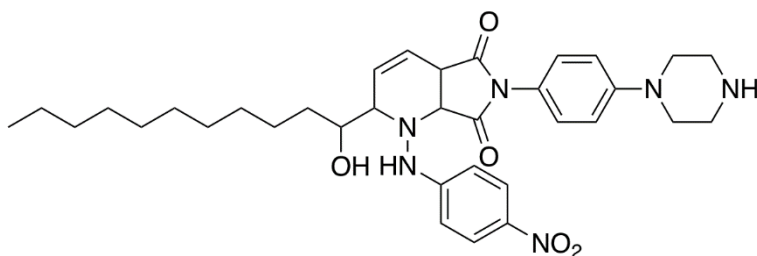


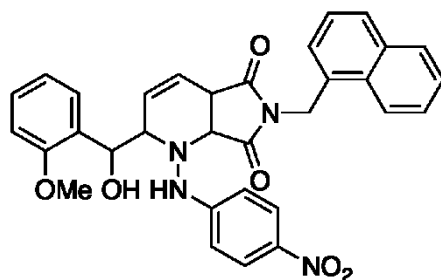
Figure A5. Chromatogram of N12 dissolved in DMSO under storage at room temperature. The data indicate that this compound is not stable in DMSO and it converts to other compounds.



A12B4C50

2-(1-hydroxyundecyl)-1-[(4-nitrophenyl)amino]-6-[4-(piperazin-1-yl)phenyl]-

2H,4aH,7aH-pyrrolo[3,4-b]pyridine-5,7-dione: ^1H NMR (500 MHz; CD_3OD): δ 8.01 (d, $J = 9.1$, 2H), 7.15-7.13 (m, 2H), 7.07 (d, $J = 9.1$, 2H), 6.89-6.84 (m, 2H), 6.18-6.14 (m, 1H), 6.07 (dt, $J = 10.3$, 2.1, 1H), 4.00-3.98 (m, 1H), 3.85-3.82 (m, 1H), 3.68-3.65 (m, 1H), 3.50-3.48 (m, 1H), 3.46-3.43 (m, 4H), 3.36-3.33 (m, 4H), 1.63-1.57 (m, 2H), 1.42-1.38 (m, 2H), 1.34-1.25 (m, 4H), 1.22-1.15 (m, 10H), 0.88 (t, $J = 7.1$, 3H); ^{13}C NMR (125 MHz; CD_3OD): δ 176.8, 174.8, 156.1, 151.4, 139.6, 129.1, 128.5, 126.9, 126.0, 120.5, 117.8, 111.5, 71.5, 68.7, 63.9, 47.4, 44.6, 43.4, 33.0, 32.7, 30.66, 30.65, 30.62, 30.45, 30.44, 27.2, 23.7, 19.3, 14.4; IR (microscope, cm^{-1}): 3292.42 (br), 3050.96, 2924.75, 2853.00, 1713.48, 1598.98, 1517.12, 1456.24, 1376.98, 1323.37; HRMS (ESI) for $\text{C}_{34}\text{H}_{47}\text{N}_6\text{O}_5$: calcd. 619.3602; found 619.3600.



A83B4C63

2-[hydroxy(2-methoxyphenyl)methyl]-6-(naphthalen-1-ylmethyl)-1-[(4-

nitrophenyl)amino]-2H,4aH,7aH-pyrrolo[3,4-b]pyridine-5,7-dione: ¹H NMR (700 MHz; C₆D₆): δ 8.64 (d, *J* = 7.8, 1H), 7.95 (d, *J* = 8.2, 2H), 7.85 (d, *J* = 6.3, 1H), 7.60 (d, *J* = 8.1, 1H), 7.55 (d, *J* = 8.2, 1H), 7.45 (d, *J* = 0.5, 1H), 7.23 (dd, *J* = 9.1, 5.1, 2H), 7.00 (t, *J* = 7.4, 1H), 6.80 (s, 1H), 6.33 (d, *J* = 7.8, 1H), 5.64 (br s, 1H), 5.11 (ddd, *J* = 10.2, 4.6, 1.9, 1H), 5.02 (br s, 1H), 4.92 (d, *J* = 14.3, 1H), 4.66 (dd, *J* = 8.1, 4.1, 1H), 3.75 (br s, 1H), 2.95 (s, 3H), 2.71 (br s, 1H); ¹³C NMR (125 MHz; CDCl₃): δ 174.3, 156.0, 140.1, 134.1, 133.8, 133.5, 131.4, 130.2, 129.19, 129.17, 128.7, 127.7, 127.2, 126.7, 126.1, 125.9, 125.2, 123.6, 121.0, 111.5, 110.5, 55.1, 50.9, 40.6, 29.7; IR (microscope, cm⁻¹): 3523.28 (br), 3291.61 (br), 3191.27, 3046.49, 2936.94, 2837.33, 2624.75, 2430.88, 1779.09, 1701.45, 1593.84, 1497.17, 1477.38, 1465.04, 1437.71, 1397.43, 1375.38, 1319.38; HRMS (ESI): for C₃₂H₂₈N₄O₆: calcd. 563.1936; found 563.1937.

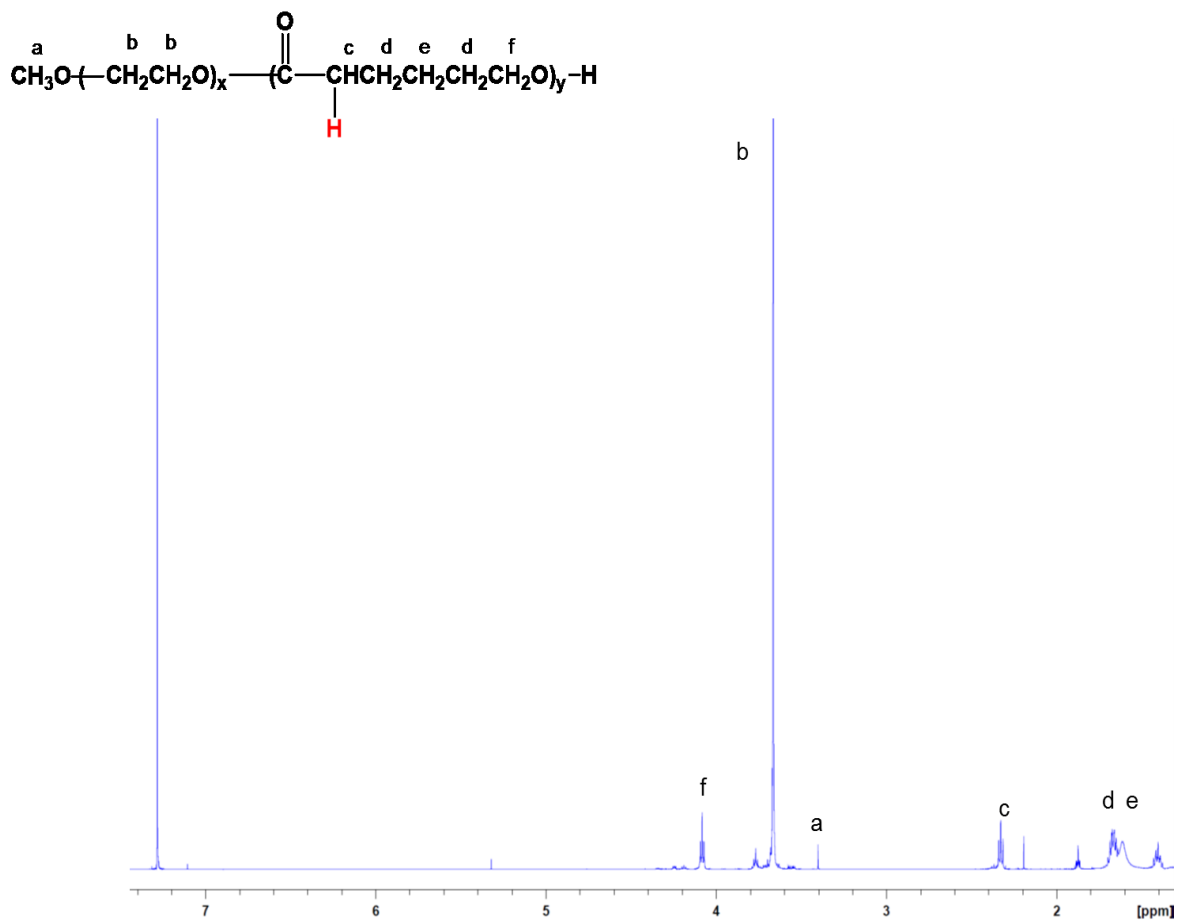


Figure A8. ¹H NMR spectrum of PEO-*b*-PCL block copolymer in CDCl₃ and peak assignments.

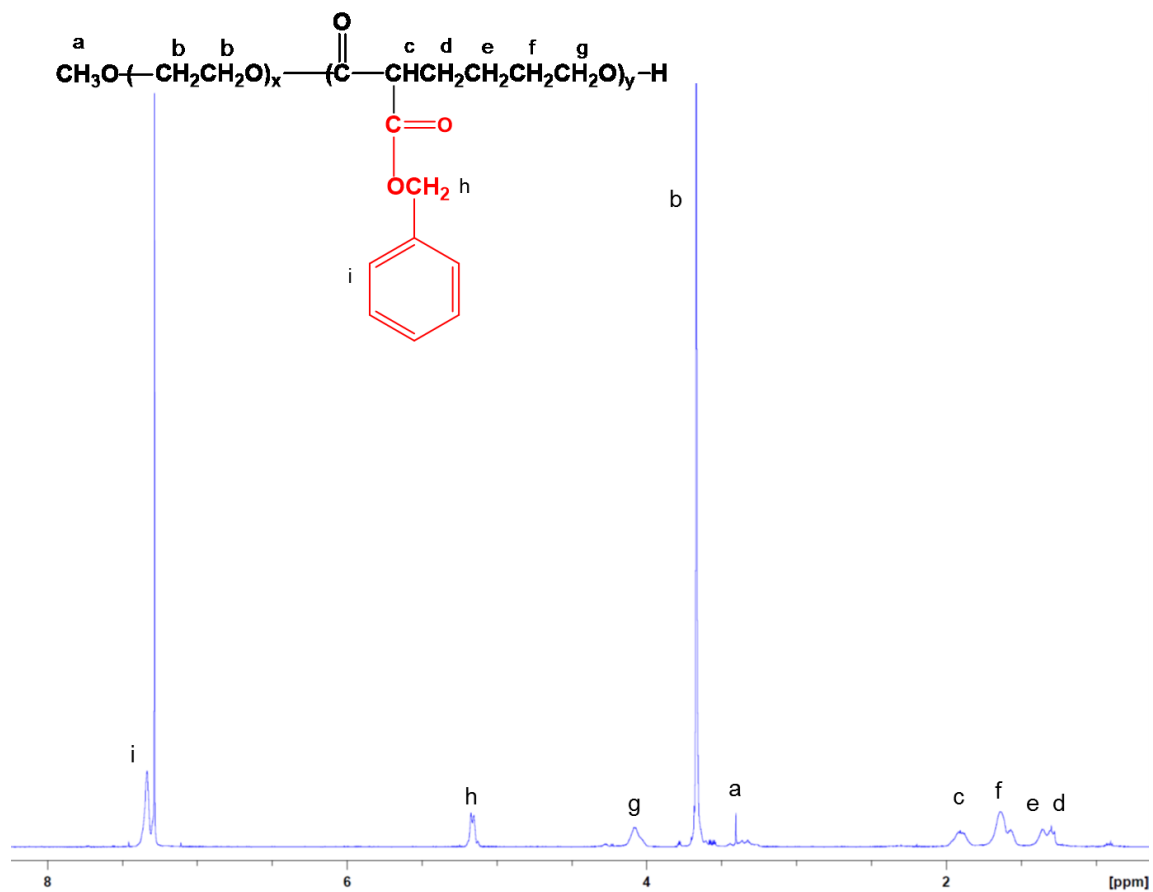


Figure A9. ¹H NMR spectrum of PEO-*b*-PBCL block copolymer in CDCl₃ and peak assignments.

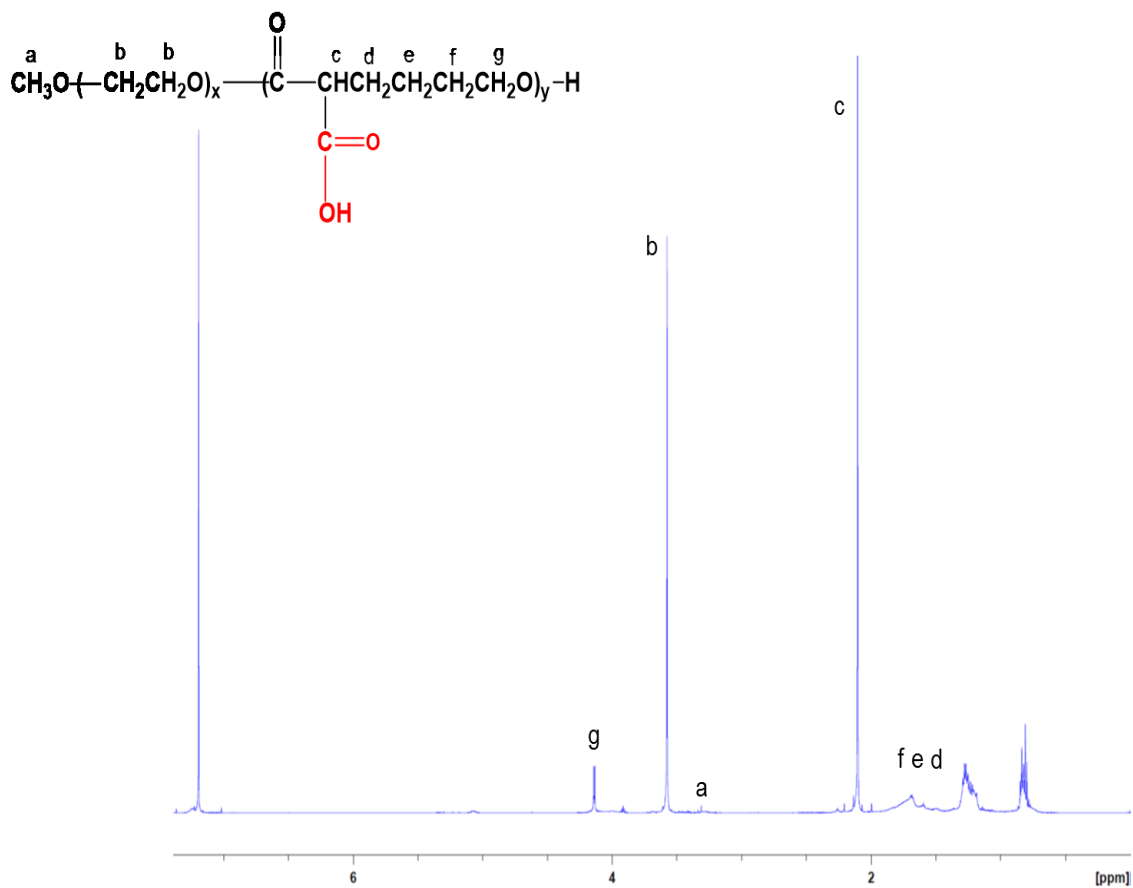


Figure A10. ¹H NMR spectrum of PEO-*b*-PCCL block copolymer in CDCl₃ and peak assignments.

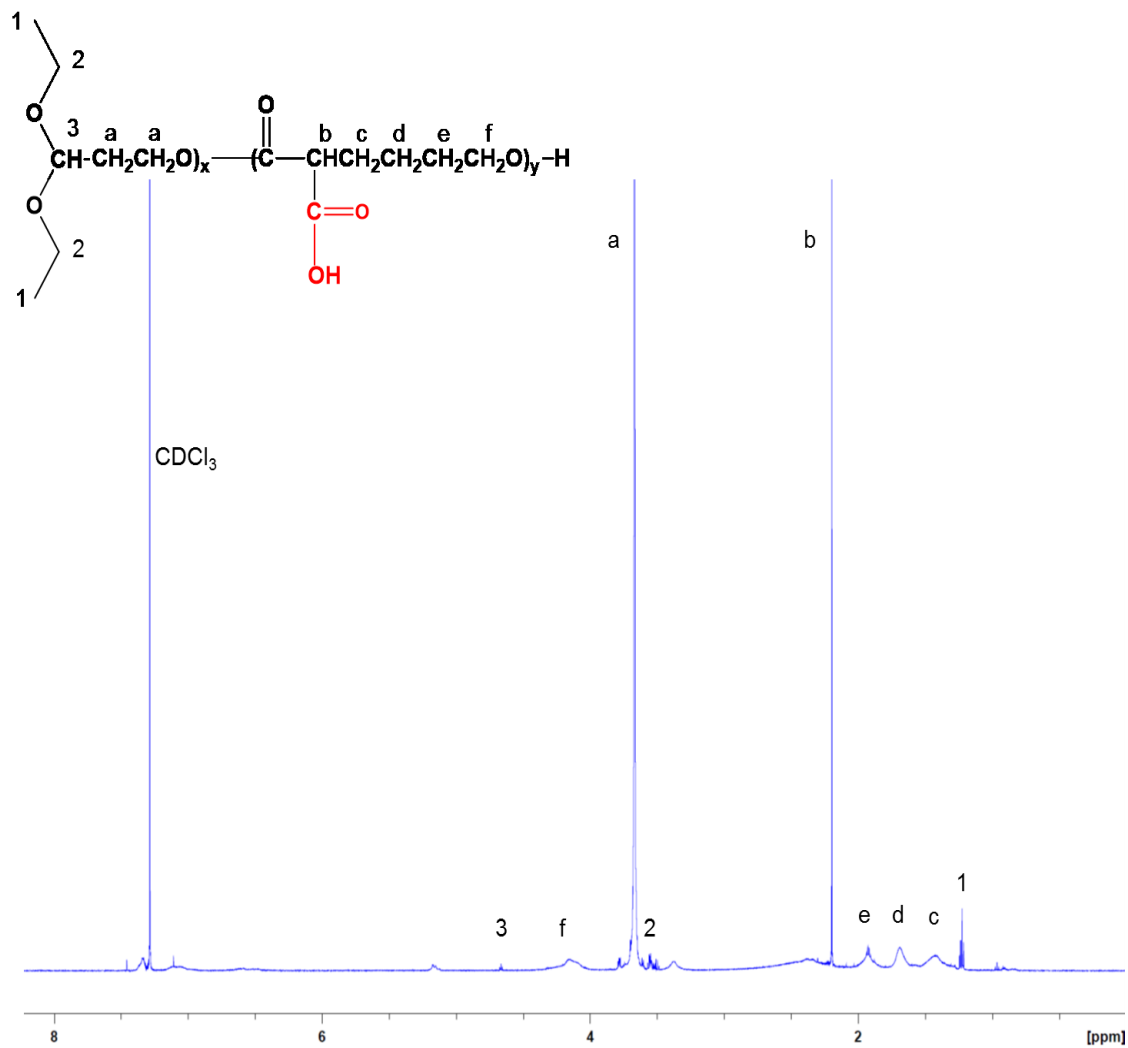


Figure A11. ¹H NMR spectrum of act-PEO-*b*-PCCL block copolymer in CDCl₃ and peak assignments.

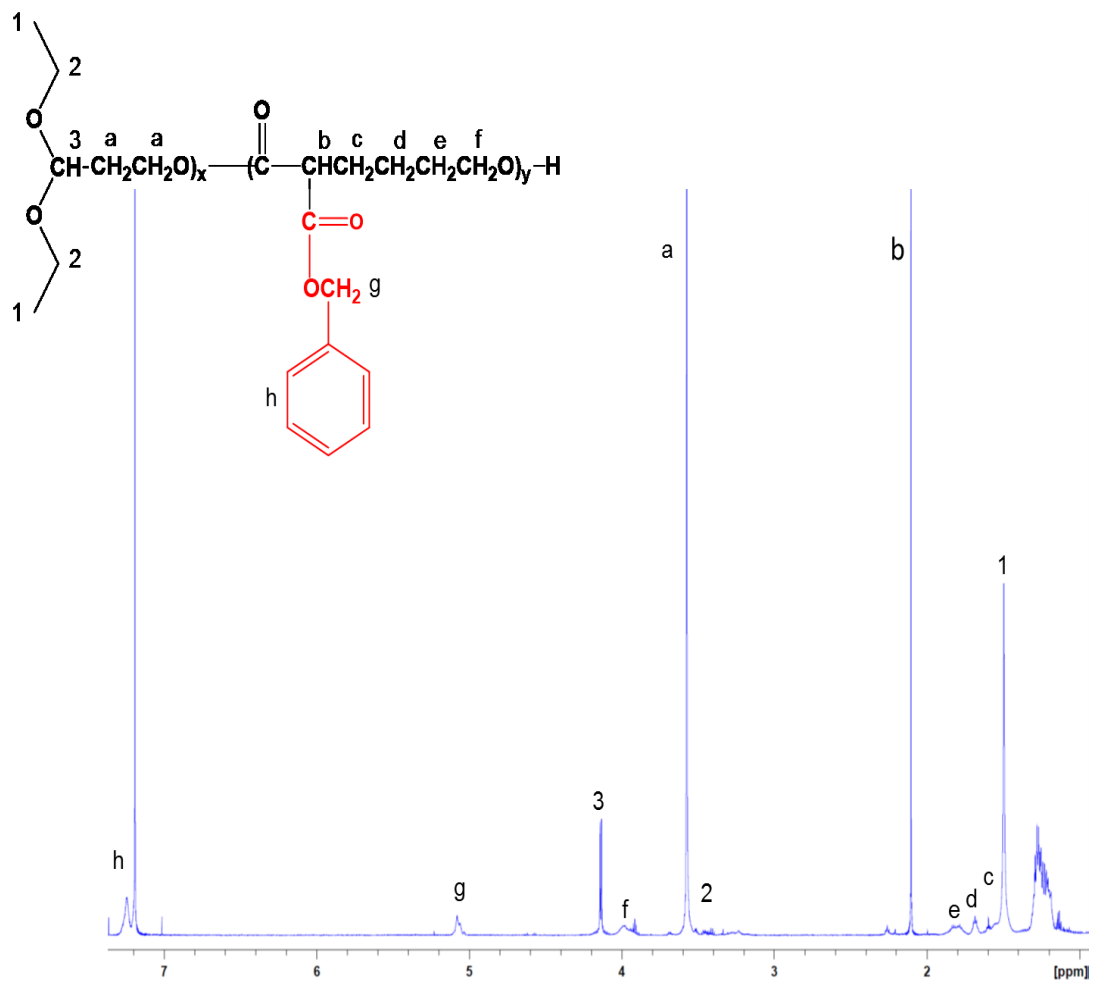


Figure A12. ¹H NMR spectrum of act-PEO-*b*-PBCL block copolymer in CDCl₃ and peak assignments.

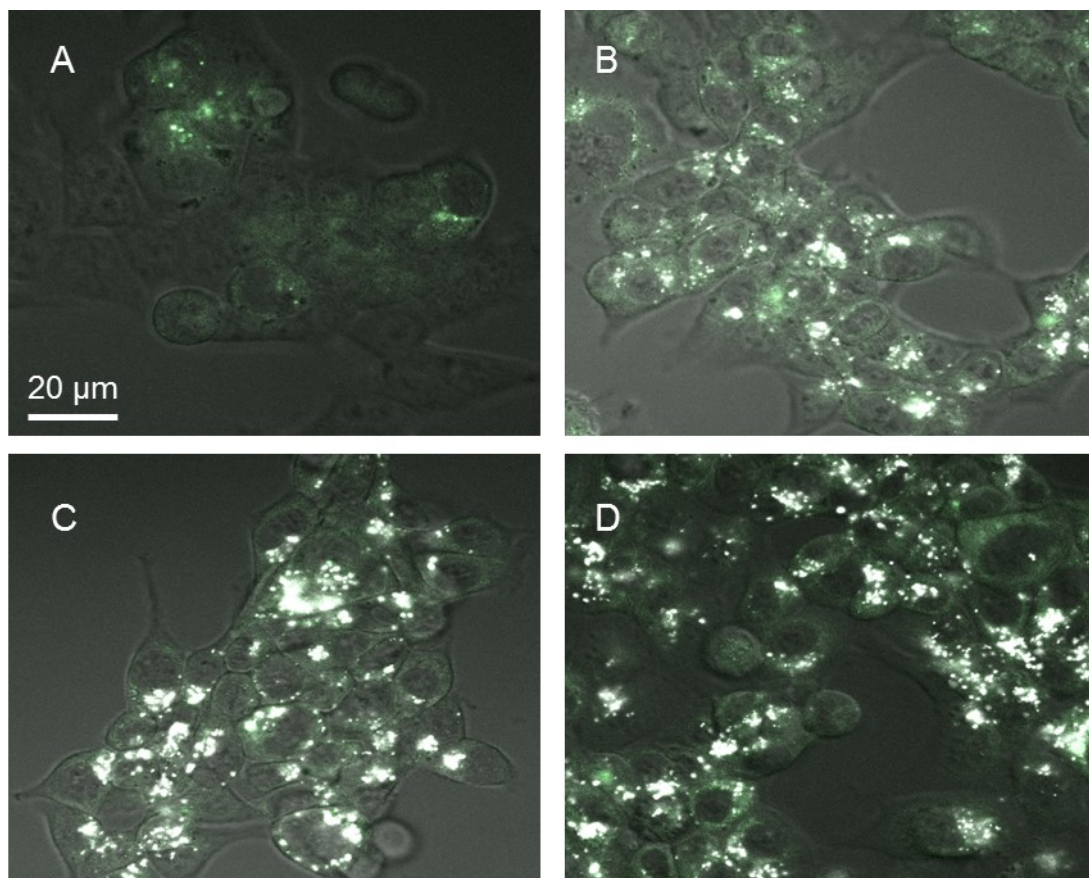


Figure A13. Live cell fluorescence microscopy images of A12B4C50 (4 μ M) accumulation in HCT116 after 4 h incubation. **(A)** Control cells. **(B)** Free A12B4C50. **(C)** PEO-*b*-PCCL-A12B4C50. **(D)** GE11-PEO-*b*-PBCL-A12B4C50. Bright signals indicate fluorescence of A12B4C50 (excitation wavelength 380 nm and emission wavelength 405 nm).

Permission to re-use content

Licensee: Zahra Shire. License date: September 15, 2017. License number: 4190460869896. Journal: DNA repair. Title: Mammalian single-strand break repair: Mechanisms and links with chromatin. Type of reuse: Reuse in thesis/dissertation

Licensee: Zahra Shire. License date: September 15, 2017. License number: 3682631436534. Journal: Molecular Cell. Title: The Molecular Architecture of the Mammalian DNA Repair Enzyme, Polynucleotide Kinase. Type of reuse: Reuse in thesis/dissertation

Licensee: Zahra Shire. License date: September 18, 2017. License number: 4192030037829. Journal: Gastroenterology. Title: The Chromosomal Instability Pathway in Colon Cancer. Type of reuse: Reuse in thesis/dissertation

Licensee: Zahra Shire. License date: September 20, 2017. License number: 4193240705034. Journal: Cellular and Molecular Life Sciences. Title: An overview of cancer multidrug resistance: a still unsolved problem. Type of reuse: Reuse in thesis/dissertation

Licensee: Zahra Shire. License date: September 24, 2017. License number: 4195431394074. Journal: J Control Release. Title: To exploit the tumor microenvironment: Passive and active tumor targeting of nanocarriers for anti-cancer drug delivery. Type of reuse: Reuse in thesis/dissertation

Licensee: Zahra Shire. License date: September 24, 2017. License number: 4195431394074. Journal: Angewandte Chemie International Edition. Title: Engineered Nanoparticles for Drug Delivery in Cancer Therapy. Type of reuse: Reuse in thesis/dissertation

Licensee: Zahra Shire. License date: September 30, 2017. License number: 4199030618857. Journal: European Journal of Pharmaceutics and Biopharmaceutics. Title: Advanced targeted therapies in cancer: Drug nanocarriers, the future of chemotherapy. Type of reuse: Reuse in thesis/dissertation

Licensee: Zahra Shire. License date: September 30, 2017. License number: 4198881492300. Journal: International Journal of Radiation Oncology*Biophysics. Title: Review of epidermal growth factor receptor biology. Type of reuse: Reuse in thesis/dissertation

Licensee: Zahra Shire. License date: October 3, 2017. License number: 4201600999690. Journal: International Journal of Pharmaceutics. Title: Design of smart GE11-PLGA/PEG-PLGA blend nanoparticulate platforms for parenteral administration of hydrophilic macromolecular drugs: synthesis, preparation and in vitro/ex vivo characterization. Type of reuse: Reuse in thesis/dissertation

Licensee: Zahra Shire. License date: October 4, 2017. License number: 4201930565810. Journal: Nature Reviews Clinical Oncology. Title: An update on PARP inhibitors [mdash] moving to the adjuvant setting. Type of reuse: Reuse in thesis/dissertation

Licensee: Zahra Shire. License date: October 5, 2017. License number: 4202560490208.
Journal: Nature Reviews Molecular Cell Biology. Title: The functions and regulation of the PTEN tumour suppressor. Type of reuse: Reuse in thesis/dissertation

Licensee: Zahra Shire. License date: October 5, 2017. License number: 4202571297773.
Journal: Molecular Cancer Therapeutics. Title: Synthetic Lethal Targeting of PTEN-Deficient Cancer Cells Using Selective Disruption of Polynucleotide Kinase/Phosphatase.
Type of reuse: Reuse in thesis/dissertation

Licensee: Zahra Shire. License date: November 16, 2017. License number: 4230980399307. Journal: BioEssays. Title: Non-homologous end joining: Common interaction sites and exchange of multiple factors in the DNA repair process. Type of reuse: Reuse in thesis/dissertation

Licensee: Zahra Shire. License date: December 23, 2017. License number: 4254860317274. Journal: Cell Chemical Biology. Title: Small-Molecule Target Engagement in Cells. Type of reuse: Reuse in thesis/dissertation

Licensee: Zahra Shire. License date: December 30, 2017. License number: 4258911504028. Journal: Trends in Biochemical Sciences. Title: DNA-Protein Crosslink Proteolysis Repair. Type of reuse: Reuse in thesis/dissertation